Investigations on structural interaction of cold-formed steel roof purlin-sheet system

by

Congxiao Zhao

A thesis submitted to the

University of Birmingham

for the degree of

DOCTOR OF PHILOSOPHY

School of Civil Engineering

College of Engineering and Physical Sciences

University of Birmingham

March 2014

ABSTRACT

Cold-formed steel (CFS) sections are commonly used in modern building construction. When used as secondary roof purlins, CFS sections are often attached to trapezoidal sheets through self-drilling or self-tapping screws to form a complete roofing system. Most purlin members are of thin-walled open cross section, which means that they are susceptible to buckling when subjected to roof loading at the top flange in either an upward or a downward direction. The presence of roof sheet and the screw connections tend to stabilise the purlin by providing a lateral and rotational restraining effect, and thus enhance their load-carrying capacity. The load application points, where the sheeting/purlin connections are located, are often eccentric to the shear centre, and thus inevitably generate a torsional moment that will induce twisting and/or warping deformations in addition to bending deflection. This type of complexity associated with the loading conditions will be exacerbated by the occurrence of single- or mixed-mode buckling (e.g. overall, distortional and local buckling) due to compression flanges tending to move sideways. The connections between purlin and roof sheeting provide a restraining effect on purlin members by preventing such lateral and twisting movements, and thus have a beneficial effect on their load-carrying capacity. In design practice, this effect should be taken into account from a design-efficiency perspective.

In this thesis investigations on the interactional behaviour of CFS purlin-sheeting system have been carried out through a series of steps. Firstly, a rotational restraint test (F-test) was carried out on unit-length Z- and Σ-purlin sections with sheet attachment to measure the rotational stiffness at the connections, followed by an engineering-orientated model for quantifying the rotational stiffness developed by author. In that model, the rotation was deemed to be primarily caused by the localised deformation of the roof sheeting and the distortional deformation of the purlin flange. The rotation caused by the separation of connection was found to be negligible. The model was

validated by the experimental test results. Secondly, a set of full-scaled multiple-point loading tests on Z- roof system and a set of UDL loading tests on Σ- roof system have been conducted to investigate the load-carrying capacity and buckling behaviour of purlin-sheeting system, as well as the impact of rotational stiffness on the system's overall structural performance. Thirdly, finite element simulations of the existing tests have been carried out and successfully validated. A full model and a simplified model have been respectively generated using FEM. Whereas the full model can be specifically used to study the buckling modes of the system and shows better precision to the flexural stiffness and ultimate load; the simplified model is simpler, easier to use and hence more cost-effective for engineering applications. Finally, extensive numerical parametric studies have been established to further investigate the factors that could affect the rotational stiffness, such as various purlin geometries, screw spacings, sheeting types and thicknesses.

The ultimate aim of this thesis is to reveal that numerical models can be solely used for studying the performance of cold-formed purlin-sheeting system including rotational stiffness, flexural stiffness, bending behaviour as well as load-carrying capacity, without the reference of theoretical and experimental data.

KEYWORDS: Cold-Formed Steel; thin-walled structures; rotational stiffness; connections; local failure; trapezoidal sheet; single-span; experimental studies; analytical model; Z- purlin; Σ- purlin; purlin-sheeting system; numerical model; finite element method; parametric studies.

ACKNOWLEDGEMENT

AUTHOR'S PUBLICATIONS

Journal Publications:

1. Zhao, C.X., Yang, J., Wang F.L., Chan, A.H.C.(2014), "**Rotational stiffness of cold-formed steel roof purlin-sheeting connections**", *Engineering Structures*, 59 (284-297)

2. Zhao, C.X., Yang, J., Wang F.L., Chan, A.H.C. (2014), "**Effect of sheeting on the behaviour of Σ- purlin systems numerical parametric studies**", *Engineering Structures* (under review).

Conference Publications:

1. Zhao, C.X., Yang, J., Chan, A.H.C. (2011), "**Experimental investigation into cold-formed sigma steel purlins and roof sheeting interaction**", *Proceeding of 3rd International Postgraduate Conference on Infrastructure and Environment*, Hong Kong, China.

2. Zhao, C.X., Yang, J., Chan, A.H.C. (2011), "**Investigation into the rotational stiffness of cold-formed steel purlin-sheeting connection**", *10th International Conference on Advances in Steel Concrete Composite and Hybrid Structures*, Singapore

CONTENTS

LIST OF FIGURES

Figure 5-44: Deformed shape under uplift loading

LIST OF TABLES

LIST OF DEFINITIONS

AISC	American Institute of Steel Construction
AISI	American Iron and Steel Institute
AS	Australia Standard
BSI	British Standards Institution
b_T	The breadth of roof sheet single trough;
C_D	Rotational stiffness of purlin with attached sheet
$C_{D,A}$	Rotational stiffness at purlin-sheeting connection
CFS	Cold-formed Steel
D	Flexural rigidity, $Et^3/12(1-v^2)$
DB	Distortional buckling
DSM	Direct Strength Method
DSMB	Direct Strength Method for Beams
E	Young's Modulus
EPDM	Ethylene-Propylene-Diene Monomer
EWM	Effective Width Method
FD	Face-down position; to replicate purlin under uplift loading condition
FEA	Finite Element Analysis
FEM	Finite Element Method
FSM	Finite Strip Method
FU	Face-up position; to replicate purlin under gravity loading condition
F_u	Ultimate load capacity
GBT	Generalised Beam Theory

I_s, I_p	the Second moment of areas of sheet and purlin;
K	Equivalent elastic stiffness at purlin free flange
K_o	Plate-buckling coefficient
LB	Local buckling
LTB	Lateral-torsional buckling
$LVDT$	Linear Variable Differential Transformer
$M_{c,Rd}$	Design moment resistance of a cross section
M_{cr}	Critical elastic buckling moment of a flexural member
M_n	Nominal moment of a flexural member
M_y	First yield moment of a cross section
NAS	North American Specification
NZS	New Zealand Standard
R	Reduction factor introduced in AISI
RHS	Rectangular Hollow Section
S	The screw distance
UDL	Uniformly Distributed Load
v	Poisson's ratio
VDL	Variable Distributed Load
W_{eff}	Effective section modulus at the yield stress level
θ_k	The rotation angle due to the separation between the roof sheet and the purlin flange at the screw connection;
θ_l	The rotation angle associated with the localised deformation of the sheet at the screw connection;
θ_p	The rotation angle due to the purlin flange bending;

θ_s The rotation angle of the cantilever sheet at the screw connection;

Chapter 1: Introduction

1.1. Background of cold-formed steel sections

There are two major types of steel used in steel construction. Hot-rolled steel, which rolled into final dimensions under significant high scaling temperatures (i.e., over 900 C^o); and the other type, cold-formed steel, which is composed of sections made from flat steel coils or steel plates at ambient temperature into structural elements, under a cold-forming process.

Fabricated by means of folding, roll-forming or press braking (Figs. 1-1 & 1-2), cold-formed elements can be made into various shapes with thickness ranging from 0.9mm to 8mm, and are widely used in manufactures, i.e. car bodies, railway coaches, highway products and etc (Martin and Purkiss, 2007).

Figure 1-1: Press braking   Figure 1-2: Cold rolling

(source from http://www.coldrollingmills.com/pcat-gifs/products-small/cold-rolling-mills.jpg)

Due to the significant growth in structural construction in recent years, high strength cold-formed elements of up to 550 MPa can now be produced. In general, cold-formed steel has the following advantages when compared to conventional hot-rolled steel elements:

1. High strength-to-weight ratio: cold-formed members are generally lighter and stronger when compared to hot-rolled counterparts. Fig. 1-3 shows a typical stress-strain curve for cold-formed steel material. As seen, the curve does not exhibit an obvious yield point with a yield plateau, as a result of cold-forming processing which generates a strain-hardening effect, and the yield strength can be increased by 15%-30%.
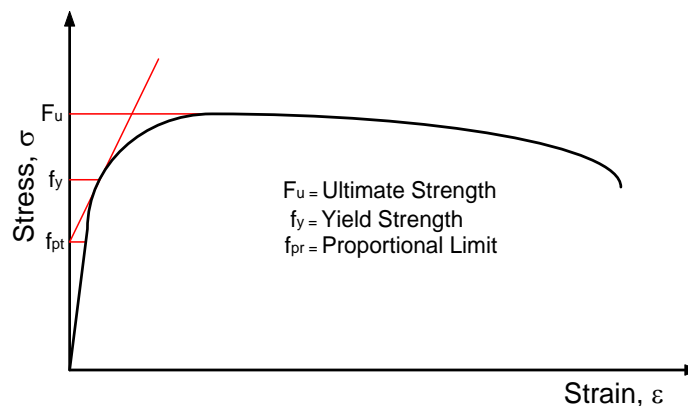
Figure 1-3: Typical stress-strain curve of cold-formed steels

2. Ease of handling and transportation. These cold-formed members are light and nestable, making it a cost effective material in erection and delivery.

3. Versatility of fabrication and mass production. Cold-forming makes the steel production flexible in varieties and quantities. Even unusual sectional configurations can be produced economically.

4. Flexibility in design. Cold-formed sections can be use as anti-sag bars, beams and ties and sheets can be used as a diaphragm members or external reinforcement of concrete slabs.

1.2. Application in modern construction

The use of cold-formed steel started in both UK and America in 1850s but had not been widely

used until 1940s. Cold-formed steel elements, usually having thin-walled and open cross section, have a major use as purlins, cladding rails, or other secondary members between the main structural frame and the corrugated roof or wall sheeting. Commonly used shapes include channel sections (C), Z- sections (Z), Σ- sections, Hat sections and I sections. Fig.1-4 below gives an overview of the commonly used cross sections.
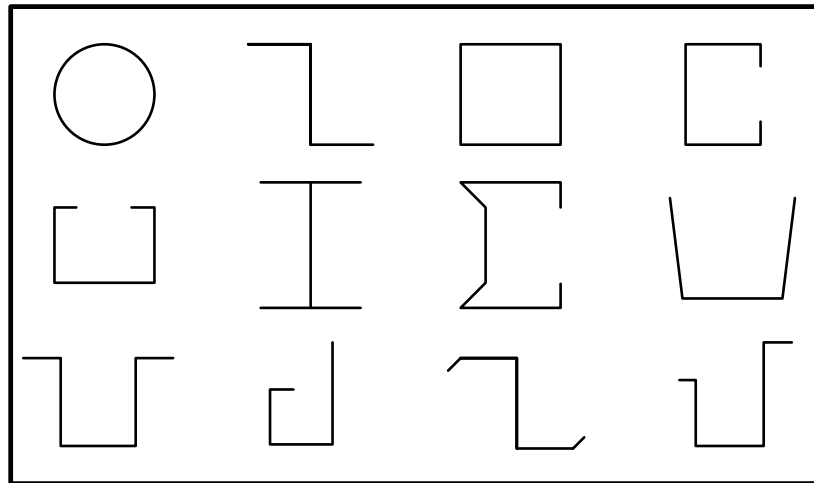
Figure 1-4: Cold-formed steel sections

Although cold-formed thin-walled sections are becoming increasingly popular in construction field, there are a few of problems associated with it. Firstly, thin-walled members normally have low stiffness due to their open and thin geometry. For singly symmetric or diagonally symmetric sections such as C- and Z-, the low flexural rigidity in constituent elements or entire cross section gives it a high tendency to localised and overall failure; in addition, while the yield strength of steel coil is increased under cold forming, the ductility will be reduced. Careful design considerations are required for seismic actions and robustness; lastly, due to its thin wall nature in cross section, most cold-formed members are seen as 'slender', which means that their buckling strength is lower than yield strength so they are unlikely to reach their full strength (Rhodes and Seah, 1992).

There are three basic modes of buckling for cold-formed members. A) Local buckling, a mode

involving plate flexure alone without transverse deformation of the line or lines of intersection of adjoining plates; B) distortional buckling, a mode of buckling involving buckling of flange and web at same wavelength, resulting a change in cross-sectional shape excluding local buckling; and C) flexural-torsional buckling, sometimes also called torsional-flexural, a mode in which compression members can bend and twist simultaneously without change of cross-sectional shape. Fig. 1-5 reveals the difference of these three buckling modes under compression and bending, and Fig. 1-6, derived from BS EN 1993-1-3 (EC3) indicates a comparison of these buckling modes by means of critical buckling stresses and halve-wavelength.
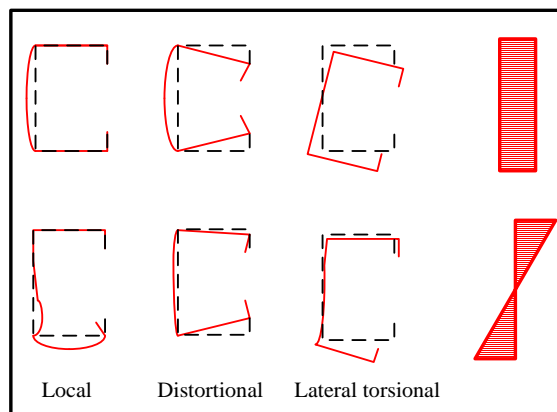
Figure 1-5: Different buckling modes under compression and bending
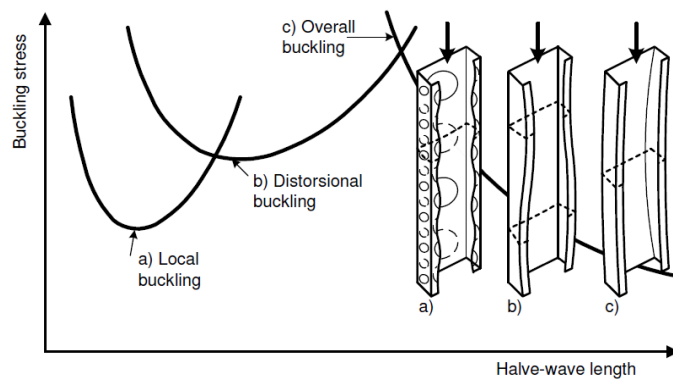
Figure 1-6: Relationship between elastic critical stress and halve-wavelength for local, distortional and flexural (overall) buckling (BS EN 1993-1-3)

1.3. Interaction of purlin-sheeting system

Cold-formed steel purlin sections are commonly used in roof constructions. Purlins are a type of secondary structural member transferring loads from roof sheets to primary frame structures. When used as purlins or cladding rails, cold-formed elements are connected with corrugated sheeting or cladding by means of screw or weld. The sheeting can provide certain degree of lateral and torsional restraints to the supporting purlins, thus to reduce the liability of suffering buckling. Most of purlin sections are of thin-walled open cross section. When experiencing roof loading at the top flange in either upward or downward direction, the load application points are often off the shear centre, and thus inevitably induce torsional moment, which will develop twisting and/or warping deformations in addition to the bending deflection. This will be aggravated by the occurrence of buckling (e.g. overall, distortional and local buckling) due to compression flanges tending to move sideways.

The connections between purlin sections and roof sheets will provide restraining effect preventing such types of lateral and twisting movements and thus have a beneficial effect on the load-carrying capacity of purlin members. In design practice, this effect should be taken into account. It has become a common view that there exist strong interactions between purlin and sheeting through connections when experiencing loading, so the study of purlin and corrugated sheeting should be carried out by treating them as an integral system.

1.4. Research need for determining rotational stiffness of purlin-sheet system

All these studies have come to an agreement on the fact that roof sheets provide both lateral and rotational restraints to purlins. While the lateral restraint is usually considered to be fully effective, the rotational one is rather variable and plays a significant role in determining the behaviour of the purlins, i.e. higher rotational stiffness can lead to a reduced buckling length in the

5

compression zone and a reduced stress in the free flange, therefore a higher load resistance (Vrany, 2007).

Special considerations of the performance of the purlin-sheeting system have been implemented into national standards such as EC3, The North American Specification (NAS from AISI) and Australian/New Zealand standard (AS/NZS 4600). Numerous studies have been carried out in this field to improve the standards of cold-formed purlin-sheeting design.

In UK the most commonly used guidance on CFS section design is provided in BS EN 1993-1-3 or referred to as EC3 (BSI, 2006). The design is based on the 'effective width' and the 'effective thickness' method for calculating the post-buckling strength of purlin; and an elastic model created by Pekoz and Soroushian (1982) was adopted for purlin-sheeting design, involving both of the lateral deflection and rotational movement that are analysed by means of an idealised sub-structure utilizing the theory of a beam-column on an elastic foundation, as illustrated in Fig. 1-7.
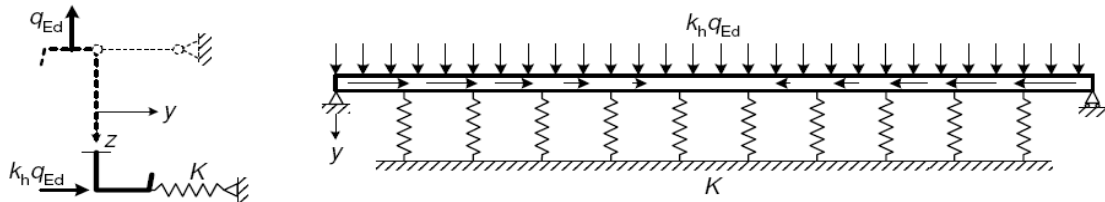
Figure 1-7: Analytical model for purlin restrained by sheeting in EC3

The rotational stiffness, C_D, given to the purlin by sheeting at connection is assumed to contain both effect of flexural stiffness of the sheeting and the connection at screw point. The formula considered effect of loading, geometry of sheet and purlin as well as type of connection. This is expressed in EC3 calculation with:

$$C_D = \frac{1}{\left(\dfrac{1}{C_{D,A}} + \dfrac{1}{C_{D,C}}\right)}$$ Equation (1-1)

where rotational stiffness at connection is stated as an empirical formula as:

$$C_{D,A} = C_{100} \cdot k_{ba} \cdot k_t \cdot k_{bR} \cdot k_A \cdot k_{bT}$$
Equation (1-2)

Despite providing a general design approach, current design specifications like EC3 was proven to be a complicated and conservative approach when calculating the potential buckling modes and the critical bending strength for the roof system (Toma and Wittemann 1994) , and the problems are raised mainly in the following aspects:

1. The design of compression elements is based on the assumption that the beam is fully restrained at both longitudinal and transverse directions so that it only experiences in-plane pure bending. However in practical case, full restrained is impossible to achieve so that the beam may be bent asymmetrically. (Ye *et al.* 2004)

2. The interaction between purlin and attached sheeting has a complex nature and any related parameters can be difficult to qualify in design respect. For example the rotational stiffness, in particular, varies for different sheeting types, connection configuration, purlin geometry and loading directions. EC3 has simplified the problem by making assumptions but led to over-conservative outcomes. (Vrany 2002)

3. Current methods used in EC3 emphasizes mainly on C and Z sections. However with the increasing use of thinner material stabilised by more numbers of folds such as Σ-sections, there is a potential need to develop a more comprehensive design specification in the basis of EC3.

1.5. Aims and objectives

The principal aim of this report is to investigate the structural interaction behaviour of CFS roof purlins with attached sheets when subject to external loading by means of experimental, theoretical and numerical simulation. This is achieved through the following objectives:

1. To measure the rotational restraint stiffness at the connection of purlin-sheet system via experimental and numerical approaches. Find out how important of this stiffness and the factors that may affect it, such as the screw spacing, variable purlin section geometries, loading condition and connection details.

2. To develop a design model for predicting the rotational stiffness at connection. The model should be applicable to purlin-sheeting system regardless of purlin profile, sheet profile and loading directions. Experimental data and numerical simulations can be used for validation purposes.

3. To characterize the interactional behaviour of the purlin-sheeting system under gravity loading when only partial restraint is provided. This objective can be achieved via experimental approach followed by numerical validation. The generated buckling mode, ultimate load and the flexural stiffness of the structures are to be investigated.

4. To characterize the interactional behaviour of the purlin-sheeting system under both gravity and uplift loadings when full lateral restraint is provided. This objective can be achieved via experimental approach followed by numerical validation. The generated buckling modes, ultimate load as well as the flexural stiffness of the structure are to be investigated.

5. Based on the above results, to investigate the effect of rotational stiffness on overall performance of purlin-sheeting system by carrying out an extensive series of parametric studies. The ultimate objective is to generate a complete system to learn and design the interactional performance of CFS roofing system solely by numerical approach.

1.6. Research methodology and thesis layout

All the above-mentioned aims and objectives will be achieved through experimental,

analytical and numerical approaches. The layout of this thesis is summarised as follows:

Chapter 1 presents an introduction of cold-formed steel sections, the manufacturing procedure of cold-formed steel, the research background and a brief history of cold-formed steel, design codes and specifications and main features of cold-formed steel sections. Aims and objectives are highlighted in this chapter, too.

Chapter 2 provides a comprehensive literature review about the state-of-art research findings in Cold-formed steel purlin sections. Special attention is drawn to the field of purlin under transverse loading and its integrated performance with attached roof sheeting. Short-come of current research has also been mentioned, knowledge gaps have been identified that lead to the aims and objectives of this study.

Chapter 3 describes the experimental investigation of rotational stiffness at connection of purlin-sheeting system, i.e. F-test. This section provides detailed information for test apparatus, procedure and results. The results are analysed and discussed in comparison with EC3 prediction. An analytical model based on plate theory and one-way beam theory is established, which the model takes account of the effects of sheet localised deformation and purlin distortion at the connection point. The predictions are verified using test data.

Chapter 4 further extends chapter 3 by generating a replicated model to the test using a finite element method. Model establishment, boundary conditions, material properties and solution schemes of the FEM model are introduced and results are compared with test data. Parametric studies are carried out to investigate the impact of variables such as sheet thickness and connection type to the rotational stiffness.

Chapter 5 investigates the loading capacity of CFS purlin-sheeting system by conducting two series of experiments. One is four-point load bending test of Z- purlin sections with

dis-continuoued sheet attachment, the other is uniformly distributed load bending test of Σ- purlin sections with continuoued sheet attachment. Results of load capacity, initial buckling mode and failure buckling mode are studied. FEM is adopted to simulate both tests.

Chapter 6 presents a conclusion summary for the hitherto research findings of this study, as well as recommendations for the future work.

Chapter 2: Literature Review

2.1. Introduction

As a result of the growing application of CFS sections in the building and construction industries, research on the structural performance of CFS purlin and purlin-sheet system has become an academic focus. This chapter presents a critical literature review encompassing the fundamental principles established by various researchers on CFS purlin sections, and their key findings. Special attention is drawn to the CFS purlin under transverse loading and its integrated performance with an attached roof sheet. The literature review will be divided into the following sub-sections: In Section 2.2, research on the structural behaviour of the CFS purlin as flexural members under transverse loading; Due to their instabilities, Section 2.3 lists researches on the performance of the purlin restrained by the attached sheet, including studies focusing on the individual behaviour of sheet and screw connections; In Section 2.4, discusses the existing design codes for purlin-sheet systems and their shortcomings; and in Section 2.5 presents key research on the FEM and its application on analysing purlin-sheet system performance.

2.2. The structural behavior of flexural members

Due to the nature of thin-walled CFS members, the thin plate cross-section is usually open and has a relatively low flexural rigidity when comparing to heavy steel sections. Together with the resulting benefit of cold-forming process (i.e. accuracy of profile, high strength to weight ratios and manufacturing flexibility), the nature of the CFS cross section may lead to different type of deformation under transverse loading, especially when insufficient restraint is applied to the flexural member. In this section, key studies regarding to the structural behaviour of CFS beam members are reviewed in aspects of pre-buckling, buckling as well as post-buckling and failure.

11

2.2.1.   Pre-buckling

In early research, effect of pre-buckling deformation is neglected in the theoretical works of Timoshenko (1953) and Bleich (1952). However later investigations by Vacharajittiphan et al (1974) suggested that ignoring this pre-buckling effect would lead to significant mis-estimation of buckling loads in some cases. Von Karman et al (1932) discovered that for a simply-supported compression plate, a uniformly distributed stress (less than critical stress) in the pre-buckling stage will be redistributed into a non-uniform stress (exceed critical stress) in post-buckling stage, as illustrated in Fig.2-1. ('Effective width method' was developed based on this theory, which will be introduced with detail in sub-section 2.4.1). As a result, the structure is able to carrying more loads and thus has an increased strength.

(a) Pre-buckling   (b) Post-buckling
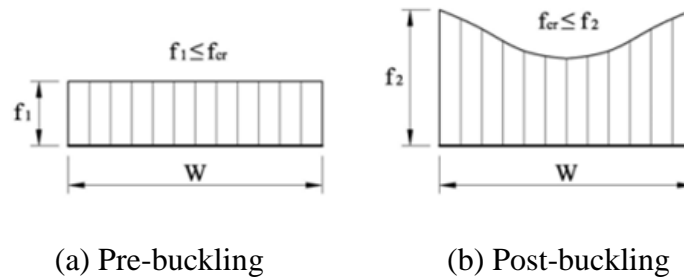
Figure 2-1: Stress distribution in a simply supported compression plate (Von Karmen et al, 1932)

Trahair (1996) stated that the pre-buckling deformation in the plane of the beam could increase the buckling resistance of the beam, as the concave curvature of the deformed beam behaves like an 'arch' that could increases its buckling resistance. He then came up with an assumption that, capacity of beams with high slenderness can be approximately equal to elastic buckling capacity based on the offset of the weakening effects of the geometrical imperfections and the strengthening effects of the pre-buckling deformations. This point will be applied when considering purlin-sheeting behaviour in finite element (FE) models in this research, geometrical imperfection can be seen negligible when pre-buckling (or cold-forming) deformation is

considered in the numerical model.

The corresponding bending stress in the pre-buckling state, calculated from the bending moment using a classical bending theory of beams, varies not only with the cross-sectional coordinates but also with the longitudinal coordinate of the beam. The variation of pre-buckling stresses along the beam axis is often referred to as the stress gradient or moment gradient. Chu et al (2006) investigated the influence of stress gradient on the elastic distortional buckling stress of Z-section beams using a semi-analytical method. Their numerical results showed that stress gradient has significant influence on the distortional buckling, but the influence decreases with the increase of the beam length.

Chen and Li (2009) found that if the member had an infinite length, the pre-buckling stress in the central wave would be almost constant. Therefore, the buckling of the central wave zone of the member with parabolic pre-buckling stress distribution will be the same as that of the member with a constant pre-buckling stress distribution.

In one sentence, pre-buckling can have impact on determining the buckling strength, buckling mode as well as post-buckling behavior of a CFS beam. Therefore the aim of all these studies of pre-buckling of CFS beams is to have a better understanding of the buckling and post-buckling behavior of CFS members under transverse loadings.

According to Trahair (1993), buckling can be defined as the section suddenly deforming in a plane different to the original plane of loading under compression. Based on the difference in half-wavelength of the order of magnitude of individual plate element, buckling of CFS members can be categorised into local, distortional and lateral-torsional (Euler) buckling (Fig.2-2). (The figure presents an elastic buckling analysis of a Z- section under pure bending; the values were derived from finite strip method but are for illustration only in this case. It shows possible

deformation of Z- member under each buckling mode and a relationship between half-wavelength and its critical load factor M_{cr}/M_y, where M_{cr} represents the critical elastic buckling moment, M_y is the yielding moment of the beam about major axis.
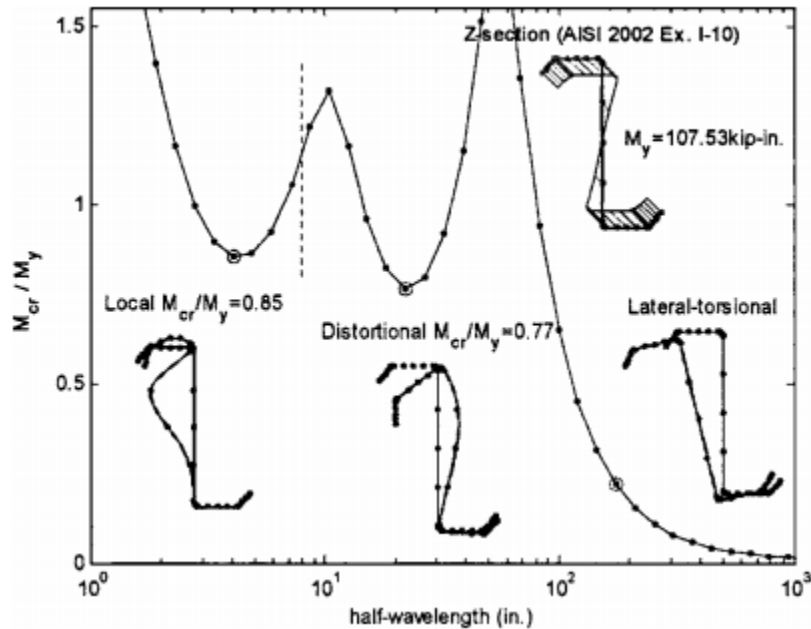
Figure 2-2: Relationship between buckling modes and half-wavelength for local, distortional and lateral-torsional (flexural) buckling of a CFS Z- section (AISI, 2007)

2.2.2. *Local buckling (LB)*

Local buckling involves ripples of cross section geometry without overall lateral displacement or twist. It experiences a relatively short half-wavelength of the buckling deflection curve (i.e. generally less than the width of the compressive element (Macdonald et al, 2008), and can be further divided into flange buckling (i.e. where only the purlin flange buckles), partial web buckling (i.e. where only part of the web buckles) and coupled local buckling (i.e. where the flange and web buckle together) (Roberts and Jhita, 1983). During this deformation, the sectional corner junctions remain straight (Figs. 2-3 and 2-4).
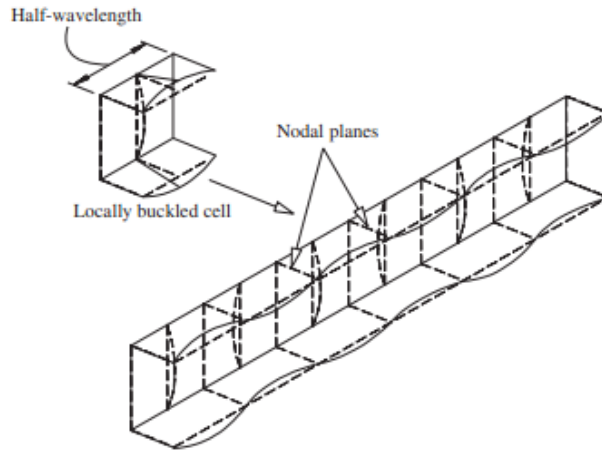
Figure 2-3: Local buckling of CFS C section (Bambach, 2006)
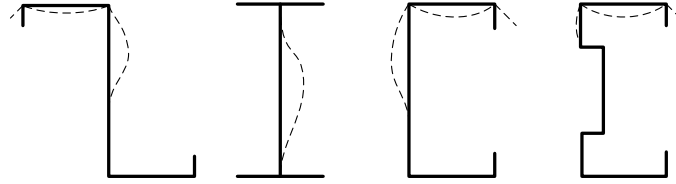
Figure 2-4: Local buckling of different cross sections

For a simply supported rectangular plate, local buckling is resisted by the plate's flexural rigidity $Et^3/12(1-v^2)$; the plate may buckle if it is subjected to in-plane compressive loading of its middle surface. A well-developed equation for calculating the local buckling elastic critical stress under compression, bending and shear is of the form:

$$\sigma_{cr,p} = \frac{K_o \pi^2 E}{12(1-v^2)} \left(\frac{t}{b}\right)^2 \qquad \text{(Equation 2-1)}$$

where E is the Young's modulus, b is the width of the plate, v is Poisson's ratio and K_o is the plate-buckling coefficient. The equation was initially developed by Bryan (1891) for a rectangular plate. Several studies have focused on the determination and refinement of K_o value. Gerard and Becker (1957) suggested that K_o may approach to a constant value following the increase in the

plate's aspect ratio. Bijlaard and Fisher (1953) studied the web flange interaction in prediction of the local buckling stress and developed a relationship for the flange local plate buckling coefficient in terms of cross-section dimensions, flexural rigidity of flange and half-wavelength of the buckled shape. Bulson (1970) developed a number monographs in his literature and determined the K_o values as a function of stress gradient. Hancock (1978) and Seif and Schafer (2010) investigate this issue by adopting Finite Strip Method (FSM). Based on extensive previous researches and adjustments, the equation is now adopted in several major design codes, either in calculations form (EC3) or empirical expression (AISC).

When local buckling occurs, the CFS member does not fail but can continue to bear additional loading beyond its initial buckling range. This is due to the redistribution of the longitudinal stresses within the member, from the weaker part to stiffer part of the component plates. Bambach (2006) found that in unstiffened elements of CFS sections, where local buckling is likely to occur, the stress redistribution in some cases may develop tensile stresses in axially compressed elements. Thus the load-carrying capacity is associated with the purlin's post-buckling behaviour. von Karmen et al (1932) defined the term 'effective width' to resolve the stress redistribution problem, which was later further developed by Winter (1947) as the Effective Width Method (EWM) for structural members under compression. This method is now incorporated into major design codes for Cold-formed steel structures in EC3 (2006), AISI (2007), AS/NZS (2005). Detail of EWM is to be discussed in section 2.4.1.1.

Research studies focusing on the behaviour of CFS sections under local buckling include Peköz (1986), developed a unified approach to extending the application to all types of cross sections under uniform compression. Cohen and Pekoz (1987) have carried out studies on stiffened plate elements under pure compression and stress gradients; while Bambach and Rasmussen (2004)

conducted a series of tests to study the local buckling resistance on unstiffened elements with consideration of uniform compression and stress gradient, and developed a different effective width equation to the stifferened cases. Yu and Schafer (2003) carried out a series of experiment to investigate the local buckling resistance of lipped sections; bracings were provided to eliminate distortional and lateral-torsional buckling. The tests focused on the performance of the web in the compression zone, with a validated FE model presented in a later study (Yu and Schafer, 2007). Alinia and Moosavi (2008) studied the local buckling of web plates under both shear and in-plane bending using FE modelling. The presence of longitudinal stiffener results in a significant increase in the critical stress. Another FE study by Lee et al. (1996) looked at the local buckling behaviour of 'I' sections with web stiffeners under shear. It was found that the flange-to-web thickness ratio has an impact on the web buckling stress.

So far local buckling of CFS beam members have been thoroughly investigated for traditional sections, study on new developed sections is still scarce. In this research emphasis will be placed on the local buckling of Σ- sections, especially when restrained with roof sheet.

2.2.3. *Distortional buckling (DB)*

This is a mode of buckling involving buckling of flange and web at the same wavelength, resulting in a change in cross-sectional shape which excludes local buckling. The term 'distortional buckling' was originally coined by Hancock (1985) and is found more commonly with the presence of the edge stiffeners in CFS sections. Because these stiffeners (i.e. lips) reduce the occurrence of local buckling of beam members by eliminating out-plane deflection at the flange-lip junction, but, instead, distortional buckling is triggered, which has a longer half-wavelength curve than that of the local buckling (i.e. 3-6 times longer than LB). Examples of distortional buckling in different shapes are illustrated in Fig. 2-5.
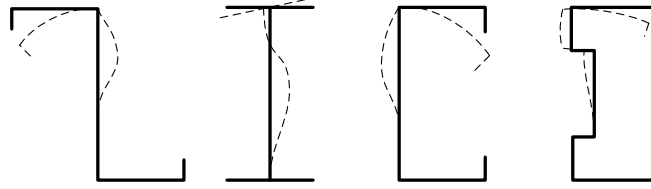
Figure 2-5: Example of cross-sectional distortional buckling

Previous research has systematically investigated the strength and performance of CFS members under distortional buckling. Lau and Hancock (1987) provided a formula for calculating distortional buckling for columns based on the model shown in Fig. 2-6. The restraining effect of the flange-web junction can be simplified into two spring elements: the rotational spring stiffness k_ϕ represents the flexural restraint provided by the web which is in pure compression, and the translational spring stiffness k_x represents the resistance to translational movement of the section in the buckling mode. And later Hancock (1997) modified this model for estimating elastic distortional buckling stress for flexural members under a constant bending moment, with particular attention to the rotational stiffness k_ϕ due to different ways of web deflection as compressive and flexural member. This model laid the foundation for CFS distortional buckling analysis and was later incorporated into the Australia/New Zealand design manual (AS/NZS, 2005).
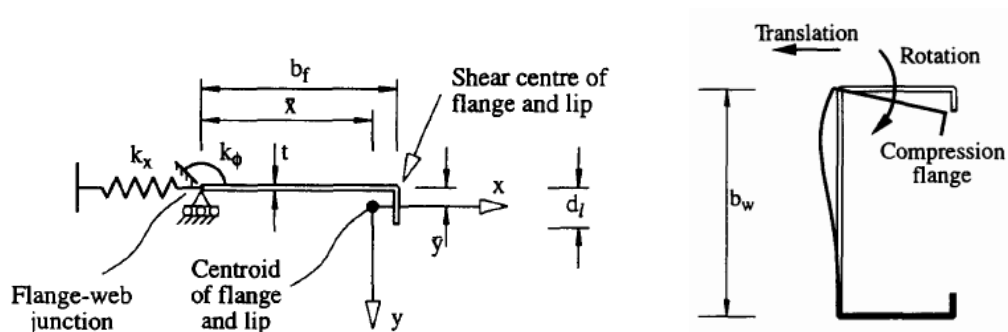
Figure 2-6: Hancock's simple flange distortional buckling model (Lau and Hancock, 1987)

In EC3 (BSI, 2006), a calculation method is provided in EN 1993-1-3 to determine the elastic distortional buckling stress of CFS plane elements with intermediate or edge stiffeners (Fig. 2-7). The model assumes that the stiffener behaves as a compression member with continuous partial restraint, with a spring stiffness K_d that should be determined by applying a unit load per unit length u, as:

$$K_d = \frac{1}{\delta} = \frac{Et^3}{4(1-v^2)b_1^2(b_1+h_p)}$$ (Equation 2-2)

where δ is the deflection caused by the unit load, b_1 is the horizontal distance from the web line to the load and h_p is the web depth. E is Young's modulus, v is Poisson's ratio and t is the sectional core thickness.
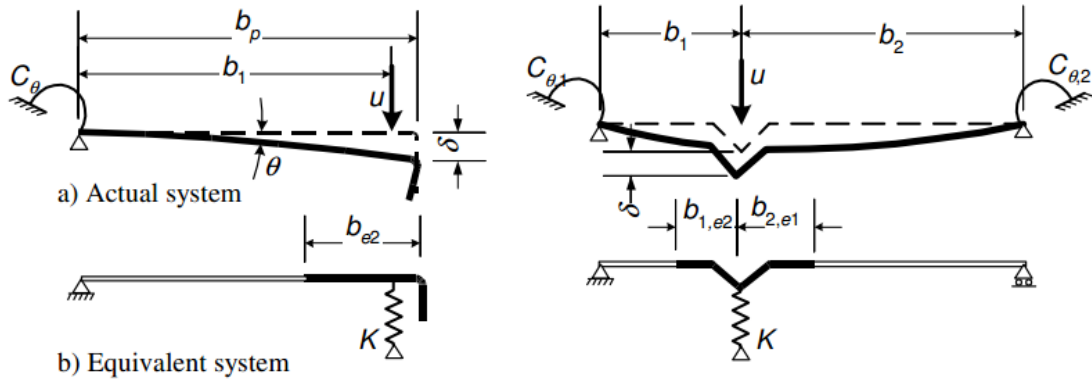
Figure 2-7: Distortional buckling calculation mode used in EC3 (BSI, 2006)

The critical stress of DB is calculated as

$$\sigma_{cr,d} = \frac{2\sqrt{K_d EI_s}}{A_s}$$ (Equation 2-3)

where I_s and A_s represent the effective second moment of inertia and effective area due to local buckling. The design strength of DB is thus calculated by applying a reduction factor χ_d to the initial effective cross-section of the stiffener. This reduction factor can be calculated based on the

value $\sigma_{cr,d}$.

This calculation model in EC3 allows for the interactional effect of local and distortional buckling, which is the most common effect for flexural members under bending. However, the shortcoming is that this model ignores the stiffness reduction due to the compressive stress in the web as stated in Hancock's (1997) model; and is not suitable to apply to cases where LB and DB do not interact or simultaneously occur.

On the basis of Hancock's previous work, Schafer and Pekӧz (1999) extended the model to investigate the distortional buckling initiates in the web. They used an interaction-buckling model between the web and flange. By doing so, the stress-dependent portion (geometric stiffness) of both the flange and the web can be predicted with a greater accuracy. This model was later adopted into the North American Design Standards (AISI-S100-07). Silverstre and Camotim (2004a, 2004b) have supplied another analytical solution for elastic distortional buckling based on Generalised Beam Theory (GBT) (the principle of GBT is discussed in details in section 2.5.3). Li and Chen (2008) developed an analytical model that combines Hancock's and the EC3 model by applying the stiffness spring at the centroid of a compression flange and lip system. In this way, both the stiffness reduction due to the in-plane stress in web and the flexural stiffness in the web and the compression flange can be taken into account (Fig. 2-8). The model also considered the elastic distortional buckling stress of Σ- sections in particular, since the rotational spring at the flange-web junction as well as the buckling stress in the web is different from Z- and C- sections, because of the extra folds presented in web.
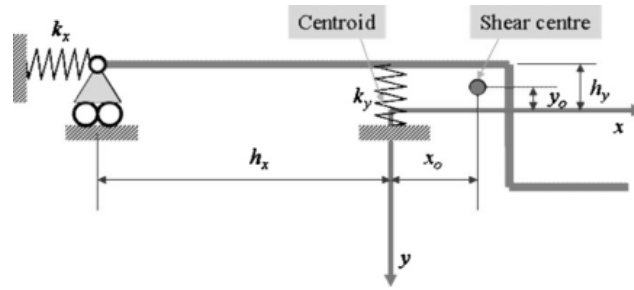
Figure 2-8: Distortional buckling analytical model (Li and Chen, 2008)

In addition to the above-mentioned analytical models, there are several researchers who have looked at the problem using numerical or experimental methods, including distortional buckling of a single purlin as well as purlin with attached roof claddings. Key studies include Yu and Schafer (2007), who used the FSM to investigate the elastic distortional buckling behaviour of C- and Z-purlin sections under moment gradient. Yu and Schafer (2006) conducted a series of tests to measure the purlin-sheet system strength capacity under distortional buckling. Jiang and Davies (1998) investigated the distortional buckling of CFS section in roof system by exploring a modified model and using it in a compression member with the assumption that a rigid translational restraint was applied to the purlin top flange. Both downward and uplift loading conditions were considered.

For post-buckling DB strength, Sridharan (1982) indicates that soon after distortional buckling takes place, yielding occurs in the lip either at the tip or the flange junction depending on the direction of the flange and lip move. On the contrary, experimental results from Kwon and Hancock (1992) reveal substantial post-buckling reserve in distortional buckling, even when the lip has yielded and developed local plastic mechanisms. Yang and Hancock (2004) spotted the difference in distortional buckling strength when the lip stiffener was deformed either inward (I-I mode) or outward (O-O mode). The report by Yap and Hancock (2006) established a numerical study on the post-buckling performance using ABAQUS.

21

Like the shortcomings mentioned in the previous sub-section, the DB behaviour of CFS flexural members are rarely focused on Σ- sections. In addition, when the purlin is attached with the sheet, its buckling behaviour may be very different from when the beam is presented on its own. This problem will be studied in this research.

2.2.4. Lateral-torsional buckling (LTB)

Lateral-torsional buckling, also called flexural-torsional buckling involves a beam bending about its major axis would suddenly bending about its minor axis, with a degree of twist, without change of cross-sectional shape of the compressive member. For opened, thin-wall CFS beam sections, LTB is a common cause of failure if the compressive members are not effectively restrained, as a result of its low torsional flexibility. As illustrated in Fig. 2-9, the LTB has a half-wavelength in the order of the length between effective supports, which is the longest deflection length when compared to local and distortional buckling behaviour (Yu, 2000).
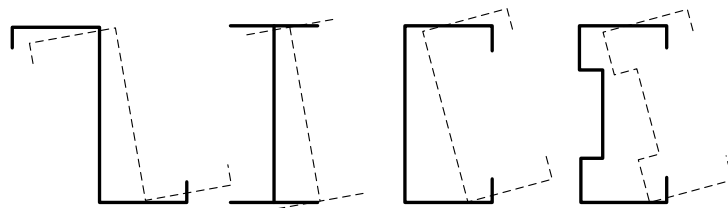
Figure 2-9: Lateral-torsional buckling of CFS sections

Credit was given to Michell (1899) for producing the first theoretical studies on the lateral buckling of beams with long narrow rectangular sections. Timoshenko (1910) then derived the fundamental differential equation of torsion of symmetrical I-beams and applied it onto the investigation of the lateral buckling of transversely loaded deep I-beams. After Timoshenko and Gere (1961), a general form of critical elastic LTB moment for a doubly symmetric beam with loading acting at the shear centre can be expressed as:

$$M_{cr} = \alpha \frac{\pi}{l} \left[\sqrt{EI_y \left(GK_T + \frac{EI_w \pi^2}{l^2} \right)} \right]$$ (Equation 2-4)

where l, E, G, K_T, I_y and I_w represent respectively the length of beam, elastic modulus, shear modulus, torsion constant, second moment of inertia about minor axis, and warping constant, respectively. α is the moment gradient coefficient related to loading conditions, which is 1.0 for uniform bending, 1.13 for a uniformly distributed load (UDL) and 1.36 for a concentrated load at beam mid-span. Trahair (1993) provided a summary table containing a range of α values under various loading conditions, shown in Fig. 2-10 below.
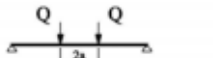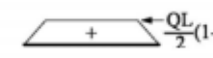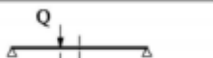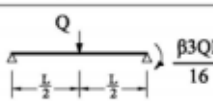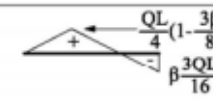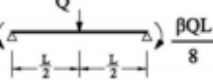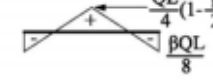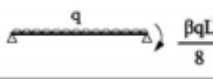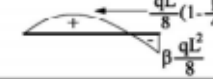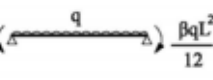
Beam Segment	Moment Distribution	α_m	Range
M $\overset{\longrightarrow}{}$ βM	M $+$ βM	$1.75+1.05\beta+0.3\beta^2 \ngtr 2.5$	$-1<\beta<1$
Q Q, $2a$	$+$ $-\frac{QL}{2}(1-\frac{2a}{L})$	$1.0+0.35(1.0-2a/L)^2$	$0<2a/L<1$
Q, a	$+$ $-\frac{QL}{4}(1-\frac{4a^2}{L^2})$	$1.35+0.4(2a/L)^2$	$0<2a/L<1$
Q $\overset{\longrightarrow}{}$ $\beta\frac{3QL}{16}$, $\frac{L}{2}$ $\frac{L}{2}$	$+$ $-\frac{QL}{4}(1-\frac{3\beta}{8})$ $\beta\frac{3QL}{16}$	$1.35+0.15\beta$ $-1.2+3.0\beta$	$0<\beta<0.89$ $0.89<\beta<1$
$\frac{\beta QL}{8}$ $\overset{Q}{\longrightarrow}$ $\frac{\beta QL}{8}$, $\frac{L}{2}$ $\frac{L}{2}$	$+$ $-\frac{QL}{4}(1-\frac{\beta}{2})$ $\frac{\beta QL}{8}$	$1.35+0.36\beta$	$0<\beta<1$
q $\overset{\longrightarrow}{}$ $\frac{\beta qL^2}{8}$	$+$ $-\frac{qL^2}{8}(1-\frac{\beta}{4})^2$ $\beta\frac{qL^2}{8}$	$1.13+0.10\beta$ $-1.25+3.5\beta$	$0<\beta<0.7$ $0.7<\beta<1$
$\frac{\beta qL^2}{12}$ $\overset{q}{\longrightarrow}$ $\frac{\beta qL^2}{12}$	$+$ $\frac{qL^2}{8}(1-\frac{2\beta}{3})$ $\beta\frac{qL^2}{12}$	$1.13+0.12\beta$ $-2.38+4.8\beta$	$0<\beta<0.75$ $0.75<\beta<1$

Figure 2-10: Moment factor for doubly symmetric beams (Trahair, 1993)

Salvadori (1955) and Vlasov (1961) have shown that Eqn. (2-4) can also be made valid for different boundary conditions, which are to extend the effective-length concept used in columns to beam buckling. Galambos (1968) listed a series of values of the effective-length factor for several

combinations of end conditions; Salvadori (1955) modified Eqn. (2-4) to account for moment gradient between lateral brace points. Kirby and Nethercot (1979) proposed a closed-form expression considering various shapes of moment diagrams within an unbraced segment, which was later incorporated into AISC specifications (AISC, 2010):

$$\alpha = C_b = \frac{12.5M_{max}}{2.5M_{max} + 3M_A + 4M_B + 3M_C} \leq 3.0 \qquad \text{(Equation 2-5)}$$

where M_{max} is the maximum moment, M_A, M_B, M_C are the absolute values of the moment at 1/4 point, 1/2 point and 3/4 point, respectively (Fig. 2-11). This equation is applicable to non-linear moment gradient.
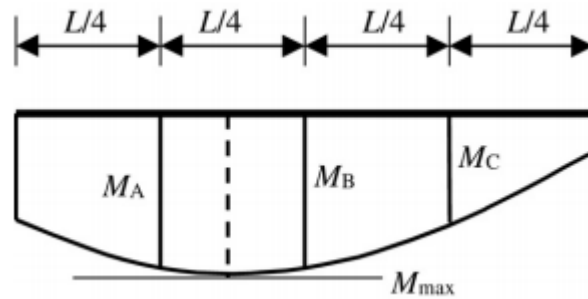
Figure 2-11: Moment diagram for Equation 2-5

However it is worth noting that in AISC, the theory presumes the beam always has the same degree of prevention for lateral bending as for warping at each of its support, regardless of the value C_b (Serna, 2006). This assumption has been incorporated by Lim et al (2003) using FEM, into I-beam elastic buckling problem with the linear moment diagrams.

In EC3, LTB of beams is designed under ultimate limit state related to member buckling resistance. The buckling resistance is obtained by multiplying the resistance of the cross-section by a reduction factor χ_{LT}. This reduction factor is a function of two other parameters: the imperfection factor α and the non-dimensional slenderness $\bar{\lambda}_{LT}$ (Serna, 2006).

Whilst slenderness is associated with beam cross section and dimension, imperfection is another important factor when LTB takes place. Imperfection is defined as the initial deviation of a practical member from an idealised geometry. Because of the nature of thin-walled sections, the appearance of imperfection is unavoidable and can be significant. Both the magnitude and the pattern of imperfection will have a great impact in determining the moment strength of LTB. With the lack of flatness, the out-of-plane bending and twist of LTB increases plate deformation from the onset of loading. The effect of imperfection as well as residual stresses is best studied through numerical approaches, such as those of (Dubina and Ungureanu, 2002) has revealed that both deflection and twist imperfections are significant in the case of LTB of thin-walled beams. Boissonnade et al (2012) suggested a "Type 1" imperfection as the most appropriate form to analyse LTB performance using the FEM, with the features of parabolic residual stress distribution and a constant initial torsional twist equal to L/(2000h) with no local geometrical imperfection (Fig.2-12). Other studies including Bailey (1996), Vila Real et al (2004) and Kankanamge and Mahendran (2011) have focused on the unrestrained LTB beam with imperfections under fire conditions, which is not within the scope of this thesis and hence is not discussed.
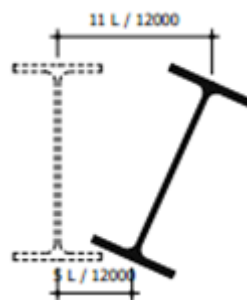
Figure 2-12: Initial geometrical imperfection shape type (Boissonnade, 2012)

Other representative studies consist of experiments conducted by Put et al (1999a and 1999b) who performed lateral buckling tests of simply supported and unbraced cold-formed steel lipped

channel beams subjected to mid-span loading. Zhao et al (1995) conducted lateral buckling tests of CFS rectangular hollow section (RHS) beams. Lateral buckling test for both C and Z section beams is available in Pi et al (1998 & 1999). The experimental investigations are very limited on this topic since it is technically difficult to measure the lateral-torsional buckling separately without the interference of local and distortional buckling.

It is noted from previous studies that the length of unbraced CFS members is always limited because little post-buckling reserve of strength can be gained in LTB mode (Timoshenko, 1945; Vlasov, 1961; and Trahair, 1993). In modern design CFS beam with greater length, the member is often strengthened using lateral restraints (i.e. cladding, floor or interval bracing/anti-sag bars) to form a composite systems. In this way, the likelihood of LTB is reduced when it is subjected to positive flexure, and hence maximising the structural capacity of CFS members. However the composite structure may cause one of two problems: (a) if the diaphragm attached to the beam is not strong enough, i.e. cladding provides partial restraints instead of full restraint to the beam, then it is possible for the beam to become unstable and this may even cause buckling mode interaction (Ye, 2002); and (b) the connection, either bolted or screw fastened, between the beam and the diaphragm may lead to complexity for analyse. Whilst the former case has been widely investigated, the latter case has remained as an issue that very scarce literatures have been focused on. Therefore (b) will be the research emphasise of this study and will be discussed in more detail in the following chapters.

2.2.5. *Buckling interactions*

In the previous sub-sections, the literature has been categorised into individual buckling modes, but this does not mean that each of the buckling mode takes place independently. Quite the opposite in reality: the buckling modes may interact with each other and reduce the strength of the

structure, which may need to be studied and considered in cold-formed steel design. It is suggested from (Schafer, 2008) that this interactional effect can reduce the resistance of the members that is governed by a single buckling mode. Of greatest importance in this respect is the interaction of local buckling with the other buckling modes.

For the interaction of local and overall buckling, Lindner and Aschinger (1994) proposed alternative design procedures to address the load capacity of CFS beams subjected to both lateral-torsional buckling and local plate buckling effects. Trahair (1994) stated that the local buckling of a thin compression flange may precipitate a nonlinear interaction between local and lateral buckling by reducing the beam minor axis bending and warping torsion contributions to the resistance to overall lateral buckling. This nonlinear interaction is relatively unimportant for a cold-formed beam with non-uniform bending moment, since local buckling occurs only in the high moment region and therefore has little effect on over-all lateral buckling. Batista (2010) developed a design method called "effective section method" to encounter local-global buckling interaction of CFS beams/columns.

Due to the presence of edge stiffeners, the occurrence of local buckling is reduced at the expense of distortional buckling, as mentioned earlier in section 2.2.3. This gives rise to the possibility of a local/distortional buckling interaction for lipped sections, and local buckling in general induces distortional buckling at a slightly lower load than that would have occurred in the absence of local buckling (Mcdonalds et al, 2008). The LB/DB interactions of compressive members have been studied using experimental approaches by Kwon and Hancock (1992) and Yang and Hancock, (2004). The FEM is adopted to investigate the LB/DB interaction with the application of various initial imperfections on simply supported channel columns (Dinis et al, 2007) and beams (Dinis et al, 2010), indicating that initial imperfection and the position of

initiated buckling on the cross section has a significant effect on the post-buckling strength and failure mechanism of the beams. For design guidance, only BS EN 1993-1-3 (BSI, 2006) provides assessments and reliable estimations of this behaviour. It is suggested by Natalia Kutanova (2009) that for local/distortional buckling, the post-buckling strength may be different when the initiated buckling mode is local or distortional buckling. Therefore there is a need to investigate distortional initiated LB/DB buckling interaction in terms of its deformation and strength, which is carried out by the author via both experiments and numerical approach for Z- sections, detail can be reviewed in Zhao et al (2014).

Other interactional behaviour includes a numerical study by Pi et al (1998) to investigate the elastic lateral-distortional buckling, inelastic behaviour and strengths of CFS beams and developed improved design rules for lateral-distortional buckling.

Bambach (2009) uses photogrammetry to measure the buckling modes and interactions in edge-stiffened C-sections. Nandini and Kalyanaraman (2010) developed a modified method combined with LTB and direct strength method for beams (DSMB) based on extensive FEA parametric studies and test data, to predict beam strength under interaction of all three buckling modes.

2.2.6. *Combined bending and torsion*

CFS members normally have an open section where the shear centre and centroid do not coincide. This means that in most cases transverse load would apply away from the shear centre of the member and therefore causes torque. For beam members under combined effect of bending and torsion, lateral-torsional buckling can become the failure mode if the beam is unbraced or only partially braced.

Barsoum and Gallagher (1970) introduced the first derivative of the rotation in FEM, as the

seventh degree of freedom at each node, representing warping deformation. The method is used to analyse stability problem of symmetric sections using linear expression. Laudiero and Zaccaria (1988) conducted a linear analysis of structures on asymmetric members of thin-walled open section. Geometric effects were included. Recent improvement was found in Ronagh et al (2000) to extend the application to various cross sections.

Kavanagh and Ellifrit (1994) examined unsheeted channel sections with loading applied on the web centreline via experiment. The braces were used with various quantity and positions. It was found that in general the strengths of the C- sections increased as the amount of bracing increased. The impact of bending stress and torsion stress would have different impact on a beam, of which becomes the main effect depends on the number of bracings and the beam span. It is worth noting that analytical method was used to compare with the test results, hence factors such as initial imperfection or residual stresses is not considered.

Put et al. (1999) presented a series of bending and torsion test on C- beams. The tests show that the beam strengths decrease as the load eccentricity increases and that the strength is higher when the load acts on the centroid side of the shear centre than when it acts on the side away from the shear centre. Regarding to large torsion, Mohri et al. (2008) produced a FE formulation without any assumption on the torsion angle amplitude. In their method, shortening effect, pre-buckling deflections and flexural–torsional coupling effects can be included.

Based on the above-mentioned literature, both linear and nonlinear investigations on the combined bending and torsion on CFS beams are generally successful, but it can be seen that unbraced CFS beams can always generate stability problem. When used as in roof or floor system, CFS beams are fastened to diaphragm which acts like a restraining bracing to the member. With the lateral and torsional restraints provided by these profiles, structural performance of purlin can

29

be increased but its deformation may behave differently. The following section lists the key studies regarding to the CFS purlin attached with sheet when used in roofing system, which will be the main concern in this research.

2.3. Purlin-sheeting system

When CFS sections are adopted as purlins, metal trapezoidal sheets are normally screw-fastened to the purlins to form a complete structure. The presence of the sheet enhances the load resistance of purlins by providing it with a certain degree of lateral and rotational restraint. Normally the two sections are seen as an integrated system during the design process (Yang and Liu, 2012). Researches regarding to the performance of purlin-sheet system is always a hotspot and can date back as far as 1960s up to the present time. The general performance of purlin-sheeting system consists of the interaction of the trapezoidal sheeting, CFS purlin, as well as the self-tapping/self-drilling screw at connection point. The most accurate and direct approach to investigate this behaviour is via experimental test programmes. As the emphasis of this thesis, background knowledge of previous literatures is to be reviewed in the following sections: 2.3.1 lists the several major research on roof sheet and its behaviour under loading; 2.3.2 lists some findings on the purlin-sheeting connection- the screw fasteners, including its different types of failure modes; 2.3.3 provides studies for the performance of overall purlin-sheeting system, and finally 2.3.4 focuses on the interaction of purlin-sheeting system at connection area, which is the research emphasis of this thesis. The advantages and limitations of these literatures will be discussed.

2.3.1. *Investigation of roof sheets*

Xu and Reardon (1993) conducted a series of static test on different types of roof sheets with different profiles to investigate their structural behaviour. They found that the failure mode and

ultimate strength of the sheet varies significantly with profile shape. It was also suggested that the use of cyclone washers, i.e. EPDM washers, together with screw fasteners would increase sheet load-carrying capacity by reducing local plastic deformation. Mahendran (1990) investigated the effects of roofing spans and fastener spacing on the structural behaviour of an 'arc-tangent' type roofing sheet (illustrated in Fig. 2-13). It is suggested that the local plastic buckling load, i.e. taken as internal reaction per fastener, is not affected by roofing spans. However, the failure load is closely related to the way of use of cyclone washers.
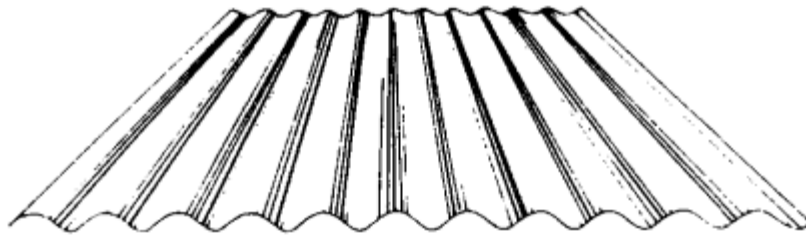
Figure 2-13: Profile of an arc-tangent roof sheet, (Xu and Reardon, 1993)

Chung (1996) carried out an experimental investigation of the restraining factors associated with thick-insulated roof systems, such as the thickness of insulation, types of seam connection and screw fixing, and construction detail. It was found that insufficient restraint would occur with increased thickness in panel insulation, this may trigger lateral-torsional buckling and result the system to fail at a much lower load capacity. Also a fast fixing method such as 'clip fixing' may reduce labour cost but also lead to premature structural failure if it is not set up properly.

Gebremedhin and Price (1999) spent three years producing a full-scale diaphragm test programme on post-frame building and derived an extensive amount of test data related to purlin, cladding, end walls and the interaction behaviour within them. They drew the conclusion that continuity of roof sheet can be treated as one diaphragm as a result of the support provided by purlins and trusses; purlin at different position of the frame exhibited distinguished behaviour, i.e.

31

the edge purlin showed more shear characteristics, the middle purlin showed more flexural characteristics, and the intermediate ones showed more of a hybrid of both.

From a slightly different angle, a study from Prevatt and Schiff (1996) that carried out testing of the standing seam roof and found that seam-clipped connection is a weak spot under wind suctioning pressure (Fig. 2-14). A pressure chamber was used to apply uniform static uplift load to sheet panels. The impact of the clip on the seam roof is investigated and validated using a FEA model. It was noted that the distribution of the relative horizontal displacement and rotations between the upper edges of panels was uneven along the seams with peak values at the clip locations.

(small image is from http://www.metalstandingseamroof.com/standing-seam-type/snap-on-cap-with-clips-metal-roof-type/)
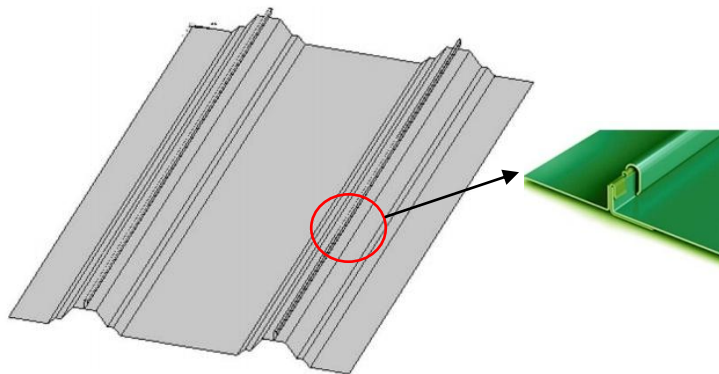
Figure 2-14: Section of standing seam roof (Damatty et al, 2003)

Limitation of the above studies include: (a) Studies regarding to individual cases of roof sheets with various geometrical shapes and properties. The outcome is not general to apply to design codes; and (b) Structural behaviour of single sheet would be very different from when it is fastened to purlin sections. The presence of purlin would provide a restraining effect to the sheet, both at the purlin-sheeting contact and connection point, which will be investigated in this research.

2.3.2. Investigation of screw fasteners

As a mean of connection in purlin-sheeting system, self-drilling or self-tapping screws are the

primary means of fastening cold-formed steel members in construction. Self-drilling screw is externally threaded fastener that can drill its own hole when inserted by using screw guns and stabilised the structure without the need for nuts. Therefore the initial applied pressure, the size and shape of screw head, the shaft and the type of thread, as well as the mechanical property of neoprene washer would all have an impact on the rotational restraint for CFS purlin-sheeting system.

At the location where the screws are positioned, severe localised deformation is often suffered by the roof sheet due to stress concentration, causing severe damage to the entire structure. One major type of this phenomenon is a pull-through or pull-over (Fig.2-15), where the sheet experiences substantial deformation or tear to allow the head passes through completely when the screw is under tensile force. Mahendran (1994) and Back and Stevens (1979) investigated the problem on crest-fixed corrugated roof sheets under uplift loading by experiment. They observed that localised plastic deformation at the crest is followed by global buckling and yielding at the crest with increase in loading. Mahendran (1998) later conducted another experimental investigation to determine the pull-through strength of sheet cladding system under cyclic uplift loading, using different steel thicknesses and grades. Misiek (2010) carried out a series of pull-through tests on steel and aluminium, trapezoidal and corrugated, single and sandwiched roof sheet system. It was concluded that the load-bearing behaviour and capacity can differ greatly with the use of different components and fixings. Therefore different test set-ups should be selected depending on individual cases.
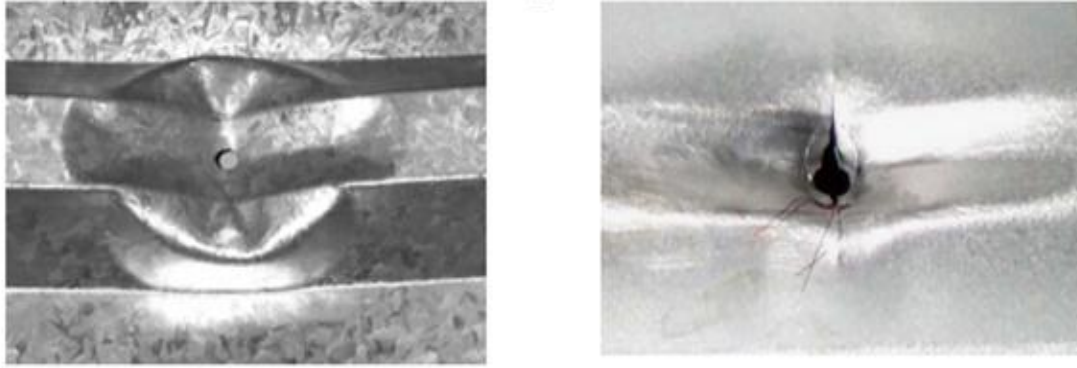
Figure 2-15: A pull-over failure of screw connection (Mahaarachchi, 2003)

Another typical failure mode involves the screw fasteners being 'pulled out' of the sheet under uplift loading and results in a separation of the roof system and a rapid decrease in the load-carrying capacity. It is called the pull-out failure of screw connections (Fig.2-16). With the tendency of using thin high-strength steel sheet and purlins, this kind of local failure has become more common and can be critical in a similar manner to pull-through behaviour (Mahaarachchi, 2003).
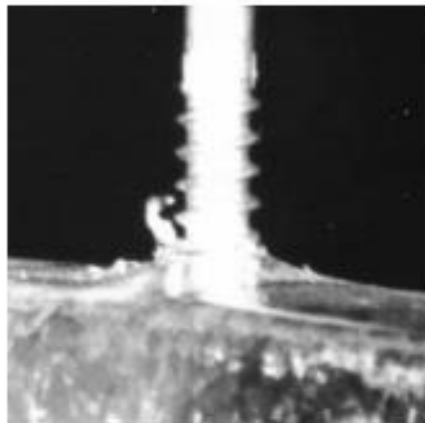
Figure 2-16: A pull-out failure of screw connection (Mahaarachchi, 2003)

The investigation of screw fasteners is not the emphasis of this thesis, however it is important to have a clear understanding of it, such as its possible type of deformation, failure types and mechanisms, so that when studying the performance of purlin-sheeting system, the impact of

fasteners can be split off from other interactional factors.

2.3.3.   *Investigations of purlin-sheeting system*

Yu and Schafer (2003) carried out a test on the local buckling behaviour of purlins. Bracings were provided to eliminate distortional and lateral-torsional buckling and specimens were positioned in pairs in opposing fashion to ensure that extra restriction was given to prevent distortion. The results suggested that the ratio of moment capacity M_{test}/M_y has an impact on post-buckling behaviour and failure mechanisms of the purlins. A similar test on the distortional buckling behaviour of C- and Z- purlins was also presented by Yu and Schafer (2006). It was found that when the compression flange was not restrained sufficiently, distortional buckling may be the predominant failure mode and can cause larger strength reduction than localised failure. Even in the case when the elastic critical value of distortional buckling is greater than local buckling, it still has a tendency to fail due to its low post-buckling strength reserve. Sokol (1996) has mainly focused on the lateral torsional buckling of purlins restrained by sheets and developed a semi-analytical method including the effects of an anti-sag bar and the moment gradient.

Analysis of partially restrained CFS purlin includes: a study from Ye et al (2002) which discussed the impact of the restraining effect of roof sheet on purlin buckling modes using finite strip method; Ye et al (2004) on developing an analytical model for predicting purlin strength under partial restraint; an analytical method developed by Li (2004) for determining the lateral-torsional buckling strength of a partially restrained CFS purlin, the critical buckling strengths were derived from energy methods. The method was then further improved by Chu et al (2004), to include factors affecting the lateral-torsional buckling strength, such as moment gradient, warping stress, loading direction and positions as well as the presence of anti-sag bars are discussed.

A study conducted by TNO Building and Construction Research involved single span tests (Kip and Tomà, 1986). A series of 4-6m long C-, Z- and Σ- sections were carried out using a vacuum chamber to simulate uniformly distributed gravity and uplift loading. Lateral spring stiffness was taken into account. However the More vacuum rig tests have been carried out. Table 2-1 gives a summary of the experimental results performed at the University of Sydney over the past 10 years.

Table 2-1: Summary of Vacuum Rig Tests carried out in University of Sydney (Pham and Hancock, 2009)

Series	Loading	Span*	Bridging[+]	Sheeting Type	Rafter Fixing
S1	Uplift	3-span lapped	0, 1, 2	Screw fastened	Cleats
S2	Uplift	2-span lapped	0, 1, 2	Screw fastened	Cleats
S3	Uplift	Simply supported	0, 1, 2	Screw fastened	Cleats
S4	Gravity	3-span lapped	0, 1	Screw fastened	Cleats
S5	Uplift	Simply supported	0, 1, 2	Concealed fastened	Cleats
S6	Uplift	3-span lapped	1	Concealed fastened	Cleats
S7	Uplift	Simply supported	0, 1, 2	Screw fastened	Cleats
S8	Uplift	Simply supported 3-span lapped	1, 2	Screw fastened	Cleats

*3X7.0 m spans with 900 mm laps between bolt centres for 3-span lapped configuration; 2x10.5 m spans with 1500 mm laps between bolt centres for 2-span lapped configuration; 1x7.0 m spans for simply supported configuration; [+]0: Zero rows of bridging in each span; 1: One rows of bridging in each span; 2: Single and double spans: Two rows of bridging in each span; Triple spans: Two rows of bridging in the end spans, one row in the central span

It was found that under uplift, purlins tend to fail in localised deformation at the junctions of the free flange-web corner, lip-stiffeners or across the full width of the free flange. Toma and Wittemann (1994) reported a test which studied single span purlins with relatively large corner radii under uplift loading. The Cornell test was set up to involve the initial rotation in the purlin induced by sheeting during loading. The results were found to be on average 19.5% lower than

EC3 calculations. Rousch and Hancock (1997) conducted a test on single span C- and Z-purlin-sheeting system under UDL uplift loads. The study focused on the nonlinear behaviour of the structure with measurements of its lateral displacement and stress distribution across the purlin span. Li. et al (2012) have presented an analytical method for predicting the behaviour of Z-purlins under an uplift load when they are partially restrained by roof sheets. The model adopts the classic asymmetrical beam theory by considering both bending and twisting effects. Vieira et al. (2010) developed an empirical formula to calculate the stress distribution of partially restrained C-sections under uplift loads; validation of numerical model was also provided. There is only a very limited literature on Σ- purlin and, in one of them, Yang and Liu (2012) reported an experiment to measure the load-carrying capacity and failure modes of a single span Σ- purlin-sheeting system under udl gravity and uplift loading. It was found that both ultimate load and buckling modes are different from Z- and C- counterpart sections.

When used in practical case, sheeted purlin sections normally require more than one span in order to complete a roof structure. Large-scale tests on purlin-sheeting system have been carried out to simulate the behaviour of double span and multiple span purlin-sheeting systems. Laine and Tuomala (1999) studied the effect of support reaction at internal support for continuous purlins using double span tests; whereas Zhang and Tong (2008) focus on multi-span cold-formed elements and the effect of different connection configuration by examining the moment resistance and flexural rigidity.

Moore (1988) conducted a series of double-span roof structure loading experiment under variable distributed load (VDL) and uniformly distributed load (UDL) with Σ-purlin sections. The test involves both working load as well as a 24-hour long-term static load prior to failure to compare the displacement and rotation of the structure. A detailed comparison of the structural

performance under VDL and UDL was presented. It was concluded that the difference caused by using VDL and UDL is negligible, and the rotation of purlin was small. It can be criticised that the test has following limitations: (a) UDL was applied as dead weight, which may cause possible stress concentration or moment gradient that made the results similar to VDL, in ideal condition the two should not be considered same; (b) purlin rotation is small because the structure was only under gravity load, condition can be significantly different when under uplift load; and (c) the test is too general, interactional effect was not investigated particularly. However the author pointed out that the structure continued to carry excessive load even when the structure was "badly distorted", which may due to the membrane action of the purlin and attached sheet. In this research, this membrane action will be specifically studied.

2.3.4.   Purlin-sheeting system at connection

The roof sheets provide both lateral and rotational restraints to purlins, the lateral restraint is usually considered to be fully effective, whereas the rotational one is rather variable and plays a significant role in determining the behaviour of the purlins, i.e. higher rotational stiffness can lead to a reduced buckling length in the compression zone and a reduced stress in the free flange, and therefore a higher load resistance (Vrany, 2007). The effect of rotational restraint in purlin-sheeting system is associated with a variety of factors, such as the shape and the thickness of the sheeting, the cross-section of the purlin, the number of screws per unit length, the type of screws and their applied locations. Ye et al (2002, 2004) investigated the effect of magnitude and location of rotational restraints on the buckling resistance and buckling mode of purlins. The study by Schafer (2008) found that an adequate rotational restraint from roof sheets can partially or even fully eradicate distortional buckling failure mode. Katnam et al. (2007a, 2007b) presented a nonlinear FE model to quantify the rotational stiffness from both single-skin and insulated sandwich

sheeting. Vrany (2002) used a flexibility method to predict the rotational stiffness. The calculation model took account of most major factors, and hence it became overly complicated and the derivations of some coefficients were unclear. The semi-analytical model developed by Gao and Moen (2012) is the latest and to date the most accurate method of predicting rotational stiffness at connection. The model considers the rotation at connections generated by both localised deformation of panel and the bending of the restrained purlin flange. The model distinguishes between C- and Z- sections and provides results with less than 11% deviation in comparison to experiment and FE simulation. However, the method has some shortcomings: The method assumes only one way of contact for Z- and C- sections under the uplift loading. It has proved valid for C- sections since the torsional moment caused by shear flows bring the section into contact with the roof sheet at its flange-lip junction line. However, according to Vrany (2007), there are two possible deformation modes for Z-sections. Depending on the eccentricity of loading, the purlin may contact the attached sheets at either flange-web or flange-lip junction line, and this will lead to a difference in the resulting rotational stiffness.

The method introduces a rather simplified FE model while neglecting the purlin-sheet interaction at screw points; hence it is not a pure analytical method.

Validations show that this model is not suitable for specimens outside the given range, which suggests that the panel's local flexural rigidity provided in the report may be calibrated for the tested specimens only.

In this study, a different and more accurate formula is established by the author to predict the rotational stiffness of CFS purlin-sheeting system at connection. The method is general to apply to all kind of single sheet roof system disregard to purlin and sheet geometry, connection type and loading directions.

2.4. Design specification for CFS purlin and system

In this section the main design methods for CFS purlin (2.4.1) as well as purlin with sheet (2.4.2) are introduced. In 2.4.1 introduces effective width method used in EC3, and Direct strength method used in AISI. In 2.4.2, introduces calculation procedures adopted in EC3 and reduction factor method adopted in AISI. Comparisons are made between different code specifications.

2.4.1.   Design methods of flexural section

Two major approaches in determining the ultimate strength of single flexural CFS section are considered herein. **Effective Width Method (EWM)** was initially introduced by van Karmen et al (1932) and has now been well-established and adopted in design specifications such as EC3 (BSI, 2006), North American Specification (AISI, 2007) as well as Australian and New Zealand standard (Standards Australia, 2006). Another relatively recent concept, **Direct Strength Method (DSM)** was developed by Schafer and Peköz (1998) and recently included as an alternative procedure in AISI (2007) and Standards Australia (2006) for strength determination. In following sections, both of the methods are to be critically evaluated for their strengths and weaknesses in CFS member analysis.

2.4.1.1. Effective Width Method (EWM)

EWM for beams came after similar expressions for columns and was initiated by an extensive experimental programme (LaBoube and Yu, 1982). The traditional approach by Peköz (1987) considers the effective width for compression flanges and average stress for webs. As illustrated in Fig. 2-17(a), the stress distribution is uniform for a uniformly compressed rectangular plate prior to buckling load. When the plate starts to buckle, it deflects laterally and experiences a stress gradient, with the mid-portion no longer efficient under loading although areas close to the edge supports continue to carry increasing load (Fig. 2-17(b)). This stress distribution for the

post-buckling range is complex in nature and difficult to quantify in practice since the variation for individual members can be significantly different. Instead, this loss in plate effectiveness can be treated as an approximate means to account for equilibrium of stress applied on partial width of the plate, namely 'the effective width' (Fig.2-17 (c)).
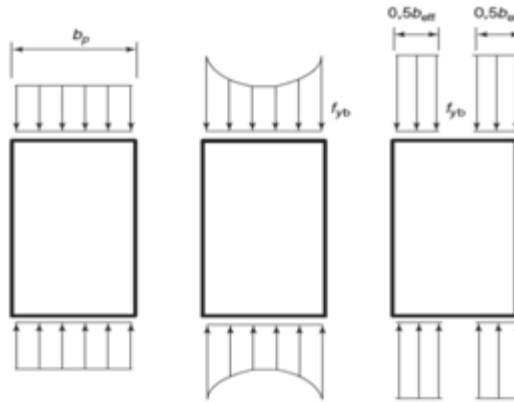
Left to right: (a) Stress distribution up to buckling; (b) stress distribution at failure; and (c) stress distribution at effective width

Figure 2-17: Concept of effective width method (Martin & Purkiss, 2007)
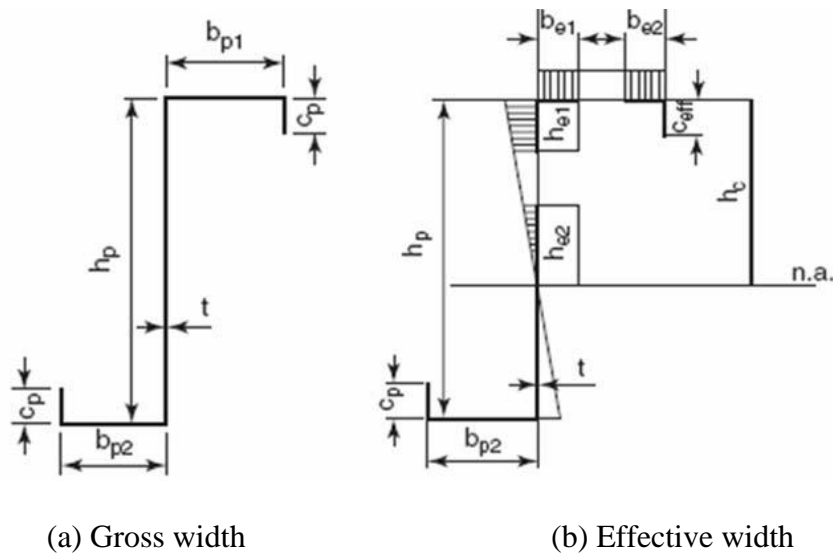
(a) Gross width   (b) Effective width

Figure 2-18: Gross and effective width of a CFS Z- section (Martin and Purkiss 2007)

The unified EWM in design codes includes effective width for both compression flanges and web when the section is under local buckling (Fig.2-18). For distortional buckling, EC3 considers this effect on the basis of local buckling by extending the theory of EWM to a 'reduced thickness' of edge or intermediate stiffeners. It has suggested that EWM has advantages such as: (a) it provides a clear model for CFS cross-section where the material is ineffective in carrying load; (b) it considers the interactional effect of local-distortional buckling as well as the interaction of individual elements by using iteration equations; and (c) it clearly leads to the notion of neutral axis shift in the section due to local-buckling, because once effective widths have been introduced into all the plate elements, the gross neutral axis is unlikely to be at the same location as the effective neutral axis (Schafer, 2008) and (Ziemian, 2010); (c) it provides unconservative results in predicting the ultimate strength of CFS sections. However, there are shortcomings for EWM: because of the consideration of this neutral axis shift, the effective width of the web is a function of the neutral axis location, EWM equations leads to complication with the requirement of iteration (Ziemian, 2010). In addition, EWM ignores inter-element (i.e. between the flange and the web) equilibrium and compatibility in determining the elastic buckling behaviour; with the development of complex shapes such as additional folds and stiffeners added to the sections, the calculation process becomes cumbersome.

2.4.1.2. Direct Strength Method (DSM)

In the meantime, an alternative method devised by Schafer and Pekoz (1998) examined the buckling strength by separating each mode, called Direct Strength Method (DSM). The fundamental principle of DSM is to determine all three of the elastic instability modes, i.e. local (M_{nl}), distortional (M_{nd}), and lateral-torsional buckling strength (M_{ne}) of thin-walled member by using elastic linear buckling solutions for the gross cross sections instead of effective ones, the

three main equations are listed below (Schafer and Pekoz, 2008):

(a) The nominal lateral-torsional buckling moment capacity for gross section:

$$M_{ne} = \begin{cases} M_{cr,e} & for & M_{cr,e} < 0.56M_y \\ \dfrac{10}{9}M_y\left(1-\dfrac{10M_y}{36M_{cr,e}}\right) & for & 2.78 \geq M_{cr,e} \geq 0.56M_y \\ M_y & for & M_{cr,e} > 2.78M_y \end{cases} \qquad \text{(Equation 2-6)}$$

where $M_{cr,e}$ is the critical elastic lateral-torsional buckling moment, and M_y is the first yield moment of the gross cross section.

(b) The nominal local buckling moment capacity:

$$M_{nl} = \begin{cases} M_{ne} & for & slenderness\ \lambda_l \leq 0.776 \\ \left[1-0.15\left(\dfrac{M_{cr,l}}{M_{ne}}\right)^{0.4}\right]\left(\dfrac{M_{cr,l}}{M_{ne}}\right)^{0.4}M_{ne} & for & slenderness\ \lambda_l > 0.776 \end{cases} \qquad \text{(Equation 2-7)}$$

where $M_{cr,l}$ is the elastic critical moment capacity of local buckling and λ_l is the non-dimensional slenderness $\sqrt{M_{ne}/M_{ol}}$.

(b) The nominal distortional buckling moment capacity M_{nd}:

$$M_{nd} = \begin{cases} M_y & for & slenderness\ \lambda_l \leq 0.673 \\ \left[1-0.22\left(\dfrac{M_{cr,d}}{M_y}\right)^{0.5}\right]\left(\dfrac{M_{cr,d}}{M_y}\right)^{0.5}M_y & for & slenderness\ \lambda_l > 0.673 \end{cases} \qquad \text{(Equation 2-8)}$$

where $M_{cr,d}$ is the elastic critical moment capacity of distortional buckling (Pham and Hancock, 2009).

In the case of beams not fully braced and locally unstable, DSM considers the problem by the summation of the lateral-torsional buckling strength without any reduction for local buckling (M_{cre}) and the strength considering local-global interaction (M_{crl}). Whilst in the case of a restrained beam

experiencing distortional buckling, the strength is calculated with comparison to yield strength M_y instead of M_{cre}, as shown in Eqn. (2-8). This is based on the assumption that distortional buckling failures are independent of LTB, which suggests that the effect of distortional-global buckling interaction is negligible in DSM (AISI, 2007). The DSM can be generalised as a function of all the above-mentioned moment strengths. A reduction factor can be applied to the gross-sectional strength for buckling interaction. A detailed calculation of mentioned variables can be accomplished by using a numerical method (Schafer and Ádány, 2006).

Major advantages of adopting DSM include: (a) it provides an equivalent level of accuracy for predicting CFS member capacity when compared to EWM with a simpler calculation procedure, especially for complicated cross-section geometry, since DSM does not require the determination of the stress for each individual element within the member; (b) it allows a visualisation with separation of the buckling mode and its minimum critical load and/or bending moment; (c) it gives the access to computational tools to obtain buckling strength capacity, such as studies in Shafer and Adany (2006) and Bebiano et al (2008).

However limitations also exist for DSM such as the fact that by separating buckling mode, it ignores the effect of the LB/DB and DB/LTB, as well as the LB/DB/LTB interaction. This may provide unsafe design values. And neglecting inter-element interaction may lead to over-conservatism for simple profiled sections.

Both EWM and DSM offer a simplified solution to an originally complicated nonlinear problem with CFS beams so that designers have a working reference without the need to test every individual section. However, it is important to realise that neither EWM nor DSM is totally correct since the formulae provided are empirical, i.e. factors and coefficients based on extensive yet limited experimental test data. As a result of a significant development of new cross sections and

dimensions of thin-walled members over recent decades are verified indisputably, it is suggested by Schafer (2008) that a fully nonlinear computational simulation may be the optimum solution in the long term for structural analysis of CFS members. In this research, emphasis will be drawn to the numerical modelling, experimental methods are used to validate the FEA models and their comparisons are to be discussed.

2.4.2. Design method for purlin-sheeting system

2.4.2.1. BSI: Design of steel structures (EC3)

The behaviour of purlin with attached sheeting has been widely considered in various codes of practice. In the UK the most commonly used guidance on CFS section design is provided in EC3 (BSI, 2006). For cases of purlin under uplift loading case, the design is based on an elastic model adopted from (Pekoz and Soroushian 1982), involving both lateral deflection and rotational movement which are analysed by means of an idealised sub-structure utilizing the theory of a beam-column on an elastic foundation.
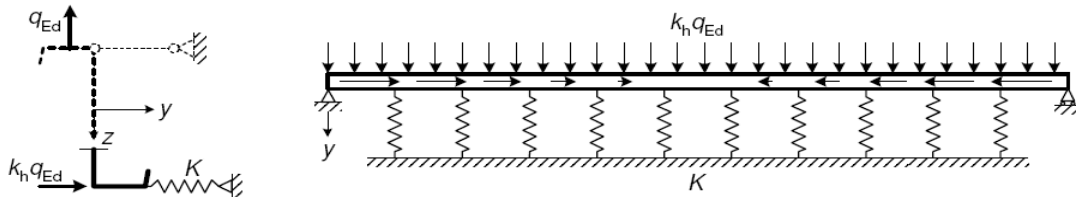
Figure 2-19: Design model for purlin restrained by sheeting in EC3 (BSI, 2006)

As illustrated in Fig.2-19, for a single laterally braced purlin under uplift loading, the rotational restraint provided to the purlin flange can be simplified into an equivalent lateral spring acting at the free purlin flange. This can be seen as a purlin beam acting on an elastic foundation, with the elastic stiffness of K. The relationship between K and rotational stiffness C_D is (EC3, 2006):

$$\frac{1}{K} = \frac{4\left(1-v^2\right)h^2\left(h_d + b_{\text{mod}}\right)}{Et^3} + \frac{h^2}{C_D}$$
(Equation 2-9)

where K is determined from: $\frac{1}{K} = \frac{1}{K_A} + \frac{1}{K_B} + \frac{1}{K_C}$ and K consists of: the stiffness due to sheet

bending, the purlin distortion and the localised deformation at the connection point. The empirical

equations consist of factors based on experimental tests.

Despite providing a general design approach, current design specifications like EC3 was

proven to provide a complicated and conservative approach for calculating the potential buckling

modes and the critical bending strength for the roof system (Toma and Wittemann, 1994). This

comment is proved by author based on test/EC3 comparison provided in later section of this thesis.

2.4.2.2. North American Specification for the design of cold-formed steel structural members (AISI)

An R-factor approach is adopted by the North American Specification (AISI S100-07 W,

2007), for predicting sheeted purlin capacity under wind uplift. The approach is based on the use of

reduction factors (R-factors) to account for the nonlinear twisting and flexural-torsional behaviour

of purlins when screw-fastened with sheeting. The nominal flexural strength M_n of a section (C- or

Z-) under parallel loading to the web can be calculated using Eqn.(2-10):

$$M_n = RS_cF_y$$
(Equation 2-10)

where S_c is the effective section modulus and F_y is the yield stress. The reduction factor R is

determined based on tests performed on purlin sheeting systems manufactured in the USA and

their determination has been reported by LaBoube (1990); some typical values of R is presented in

Table 2-2 below.

Table 2-2: Typical R values from AISI specification (AISI, 2007)

Depth Range, in (mm)	Profile	*R* value
$d{\leq}6.5$ (165)	C or Z	0.70
6.5(165) $<d{\leq}8.5$(216)	C or Z	0.65
8.5(216) $<d{\leq}11.5$(292)	Z	0.50
8.5(216) $<d{\leq}11.5$(292)	C	0.40

This design method is relatively easy to apply, but the detailed deduction procedure for corresponding R-factors is unclear. It is also worth noting that AISI only considers the use of this method for Z- and C- sheeted purlins and hence has limited applicability.

2.5. Numerical methods

With the dramatic development of computers and software in the past few decades, numerical analysis has become a powerful tool for studying complex structural system such as the CFS purlin-sheeting interaction. The vast majority of research studies have revealed an obvious superiority that numerical method can offer to the traditional physical experiments in studying thin-walled steel structures, especially for extensive parametric studies (Lucas, 1997a, 1997b; Yu and Schafer, 2007; Trahair, 2002). Nowadays, with the diversity of CFS sections and an increasing degree of complexity in their geometrical variations, the numerical method is an efficient tool for investigating purlin-sheeting behaviour in a systematic way.

Common numerical methods used in research into CFS structures include Finite Strip Method (FSM), Finite Element Method (FEM) and the relatively new approach of Generalised Beam Theory (GBT). These methods are explained and related literatures are summarised in the following sub-sections.

2.5.1. *Finite Strip Method (FSM)*

Finite Strip Method (FSM) was originally developed by Cheung (1976) and pioneered by

Hancock et al. (2001) and Schafer (1998) in the use of stability analysis specifically for cold-formed steel sections. The core idea is to mesh the member only in the cross-sectional direction so that the member is divided into a number of strips (Fig.2-20). FSM was used particularly to study thin-walled prismatic structures. In this approach it is assumed that the deformation pattern of a structure in one direction can be evaluated analytically and the structure could be discretised into strips to examine CFS sections under longitudinal stress. Compared to FEM, FSM generates a less accurate but efficiently acceptable prediction for section elastic buckling strength (i.e. critical load versus half-wavelength) as well as cross section buckling mode shapes. Schafer (2002) developed a program based on FSM that can identify local, distortional and lateral-torsional buckling of purlin-sheeting system and can carry out post-buckling analysis that allows for buckling mode interactions. Ye et al. (2002 & 2004) discussed the influences of rotational and partial lateral restraints provided by sheeting on the pre-buckling stress and buckling analysis of CFS purlin sections under uniformly distributed uplift loads, using FSM. Limitation of FSM is mainly used in analysing post-buckling behavior of CFS members, related studies include Lau and Hancock (1989), Dawe and Wang (1996), and later Schafer and his colleague (Schafer and Adany, 2006; Adany and Schafer 2006a, 2006b). However when analysing ultimate strength and post-failure behaviour of members, FEM is more advantageous because of its finer mesh.
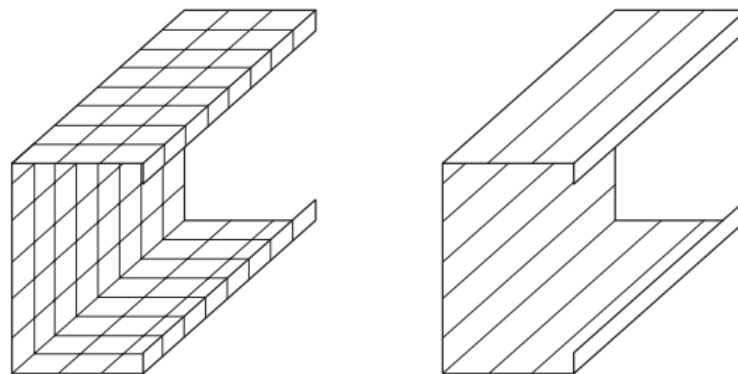
Figure 2-20: Mesh pattern of FEM versus FSM (Martin and Purkiss, 2007)

2.5.2. Finite Element Method (FEM)

With the development of computer tools, the majority of later-established numerical studies on purlins-sheeting systems are using FEM, because of its higher accuracy. The process of FEM begins with dividing the domain into discrete regions, named finite elements, which are interconnected at nodal points. In other words, FEM replaces continuous functions by these pieces-wise approximations defined on polygons and solves the problem using partial differential equations (see Yu, 2005). The manner of finite elements distribution, or mesh, is dependent on the geometry of the structure as well as required accuracy of the solution. FEM hence solves the problem by using polynomial approximations so that the problems can be reduced into a set of linear equations. In structures, the most commonly used method is the displacement-based finite element analysis (FEA), which the basic principle is to establish a set of functions that are chosen so that they uniquely define the state of displacement within each element in terms of its nodal values. In this way the number of degrees of freedom becomes finite, and any other displacement within an element can be approximated by interpolation using so called shape functions and the known nodal values. By solving these equilibrium equations, the displacement of each nodal point could be derived.

Generally, a finer mesh leads to more accurate results but requires proportionally longer analysing time, where the analysis in the case of a coarse mesh would take less time to run, but the results would be less reliable. The objective is to have as few elements as possible in order to reduce the analysis run time, but to refine the mesh at locations where the stress concentrations occur to give an accurate result.

FEM is able to achieve large-quantity and high-accuracy simulations of the real- world behaviour of thin-walled structures without performing physical tests. With the combined use of

iteration schemes, FEM is able to study the CFS-sectional performance at all stages (i.e. elastic buckling, plastic buckling and post failure behaviour). Lucas et al (1997a, 1997b) established a FE model incorporating a rectangular thin-walled plate element initially generated by Chin et al (1994). The full model, where the connection between sheet and purlin was modelled using nodal constrained equations, and later the simplified model, where the effect of sheeting was substituted by spring elements, were used to evaluate the structural performance of purlin-sheeting system under uniformly distributed loads. However, not all modelling information was presented in the publication, e.g. the material property, boundary condition at supports and meshing details, hence the model is difficult to reproduce. Laine & Tuomala (1999) presented a numerical study for continuous purlin-sheeting system. They emphasised the shear force of sheeted purlin section at internal support. The presence of the sheet is simplified with nodal displacement restraint on the purlin. Yu and Schafer (2007) generated a nonlinear FE model to simulate their previous tests on local buckling and distortional buckling of Z- and C- purlin-sheeting systems. With the consideration of initial imperfection and moment gradient, the model produced good agreement with test data, and the extension outside the tested range are also corresponded well with the Direct Strength Method (DSM). However, the numerical model is developed to simulate test condition as well as to validate DSM, so buckling modes are considered separately. This may lead to a limited practical significance for engineering problems. Ren et al (2012) presented a validated FE model to describe the bending and twisting behaviour of C-section purlin partially restrained by sheeting. The effect of sheet was simplified into spring elements at the restrained purlin flange. By altering the beam lengths and stiffness values, it was found that both factors can make a noticeable difference to the moment correction factor, K_R. Vieira (2010) investigated the longitudinal stress distribution of C- purlin cross-section, assuming full lateral-restraint and partial rotational restraint

is provided by sheet under wind load, the restraint is determined based on a F-test and also applied as restraint in replacement with the real sheet.

Since the majority of the numerical studies have focused on the general performance of the integrated system, FE investigation on specified restraint at the connection point and how the variation of this factor affect the overall stiffness and ultimate load of the structure is very scarce. Katnam et al (2007a, 2007b) presented a non-linear FE model to quantify the rotational stiffness of both single-skin and insulated sandwich sheeting. The model considered interactional behaviour of both sheet and purlin and the influence of screws with neoprene washers on the rotational stiffness at connection. The results may have made good agreement with test data because of the great amount of detail considered in the FE model, on the other hand, they made the study over-specific and therefore led to difficulty in its application to other cases. Fan et al (1997) developed a FEM to simulate the structural behaviour of single lap screw connection connected with roof sheet under static shear, the part of a single screw, including screw shaft, head and neoprene washer are considered as a continuous body by assuming that linking and interaction of these elements do not affect the behaviour of a connection. Pre-stress when tightening the screw was also modelled.

FEMs are used in vast amount of literatures, which that have all shown the successful application in validating thin-walled beams with high level of accuracy (when compared to test results). However the use of FEM particularly on the Σ-purlin-sheeting connection is still very scarce. In this research, since the ultimate load of purlin-sheeting system is considered, FEM method is used to investigate the behaviour of Σ-section, with emphasis on screw positions.

2.5.3. *Generalised Beam Theory (GBT)*

Generalised Beam Theory (GBT), developed by Schardt (1983), involves the general mechanical behaviour of the prismatic structures by using deformation resultant functions for axial

stress, bending, distortion and torsion. The method was later extended by Davies et al (1994a, 1994b) to investigate the stability behaviour of both linear (first-order) and nonlinear (second-order) thin-walled steel members. The fundamental (first-order) beam equation of GBT is:

$$E\,{}^{k}C\,{}^{k}V''' - G\,{}^{k}D\,{}^{k}V'' + {}^{k}B\,{}^{k}V = {}^{k}q \qquad \text{(Equation 2-11)}$$

where E is the Young's modulus, G is the shear modulus, ${}^{k}C$, ${}^{k}D$ and ${}^{k}B$ is the section properties for each deformation mode, ${}^{k}V$ and ${}^{k}q$ are the deformation and distributed load to corresponding mode, respectively. The second-order equation, meanwhile, has an additional term considering the effect of warping stress:

$$E\,{}^{k}C\,{}^{k}V''' - G\,{}^{k}D\,{}^{k}V'' + {}^{k}B\,{}^{k}V + \sum_{i=1}^{n}\sum_{j=1}^{n} {}^{ijk}K_{\sigma}({}^{i}W\,{}^{j}V)'' - {}^{ijk}K_{\tau}\left(2\,{}^{ij}W\,{}^{j}V' + {}^{i}W''\,{}^{j}V\right) = {}^{k}q$$

$$\text{(Equation 2-12)}$$

In this way, GBT is able to decompose the member deformation (buckling modes) into a linear relationship of cross sectional deformation modes. It is able to take account for the geometry imperfection and nonlinearity. The ability to separate different buckling modes makes the method especially amenable to design methods. Davies and Jiang (1996, 1998) extended the implementation of GBT into the distortional behaviour of open sections with pinned and free-to-warp end conditions. Silvestre and Camotim (2004a, 2004b) have developed a code and a followed numerical programme specifically to study the pre- and post-buckling behaviour of plain channel members; it has been validated by them as a useful tool for predicting the elastic stability of CFS sections.

2.6. Knowledge gap and methodology

A detailed literature review has been presented in this chapter. Method adopted in design codes as well as some main findings from researchers are introduced. Although there are extensive findings are available from previous studies, there are still some problems that are deeded to be solved or improved. The following knowledge gaps were found and solutions are provided in this thesis:

1. The CFS flexural member under transverse loading at its elastic stage only have been investigated in design codes based on the assumption that the beam is fully restrained at both longitudinal and lateral directions, so that it experiences only in-plane pure bending. In practical case, full restraint is impossible to achieve, so that the beam may be bended asymmetrically. Therefore numerical simulation would be a more appropriate approach when compared to analytical prediction.

2. The CFS purlin-sheeting system has a complex nature as a result of its interacting behaviour and any related parameters can be difficult to quantify in design respect. For example the rotational stiffness, in particular, varies between different sheeting types, connection configuration, purlin geometry and loading directions. Most design methods have simplified the problem by making assumptions, but this has led to either over-conservative or unsafe outcomes. A simple but sound analytical method for predicting rotational stiffness is needed.

3. The design codes and majority of studies have looked at the behaviour of purlin with and without sheeting in Z- and C- sections. Studies on Σ- sections are yet still scarce. Since Σ- has additional stiffeners presented in the web, it is suggested that it has different buckling behaviour and ultimate load than conventional C- and Z- sections, due to its increased

flexural and torsional stiffness. Further investigation of the Σ- purlins is needed.

4. There are many studies focused on the structural performance of CFS purlin-sheeting system. The effect of the sheet is, in most studies, replaced by equivalent springs. This substitution may be used for design process but can be over-conservative for analytical purposes. FEM can be introduced to simulate the integrated system to provide results with a higher level of accuracy.

2.7. Summary

The literature review critically considers the current up-to-date specification codes used for CFS purlin flexural members and purlin-sheeting system along with their limitations. The review also summarises the key findings of previous researchers using the approaches of experiment, numerical simulation and analytical prediction. The review can be further divided into:

1. Investigation of elastic buckling of CFS flexural members, including local, distortional and lateral-torsional buckling modes and mode interactions;

2. Investigation of the purlin-sheeting system with regard to the behaviour of roof sheets, and screw fasteners as well as the integrated system. The importance of an accurate determination of the rotational stiffness of connections is highlighted.

3. Design methods including EMW and DSM are introduced and comparisons and limitations are provided in detail;

4. Numerical methods including FSM, FEM and GBT are introduced and comparisons and limitations are provided in detail;

5. The knowledge gap and methodology for research and development of structural behaviour are identified.

Chapter 3 Rotational stiffness at purlin-sheeting connection

3.1. Introduction

Under external loading, the roof sheet will strengthen the attached purlin by providing it with a considerable amount of lateral and rotational restraints. Many researchers have studied this interactional behaviour by simplifying the effect of sheet into two spring elements: lateral spring and rotational spring. It has been widely accepted that the lateral spring stiffness is relatively large when compared to rotational spring and can always be treated as rigid, in other words, the stiffness is equals to infinity; whereas the rotational spring is always flexible and its stiffness can make a significant impact on the performance of a purlin-sheeting system, i.e. higher rotational stiffness can lead to a reduced buckling length in the compression zone and a reduced stress in the free flange, and thus a higher load resistance (Vrany, 2007). The rotational stiffness is dependent on many factors such as the shape and the thickness of sheeting, the cross-section of the purlin, the number of screws per unit length, the type of screws and their applied locations, and can therefore be difficult to quantify.

Previous studies determining this rotational stiffness of a purlin-sheeting system are very limited, and are mainly based on experimental and numerical approaches. More details on the related publications can be found in section 2.3.4.

Whilst experiments and numerical simulations are able to achieve accurate results, they are not entirely suitable for design purposes. A simple but sound analytical method is required for use in practical applications. EC3 introduces empirical formulae for predicting the overall rotational stiffness. The formulae are derived from test results and are only applicable to sections/connections that are within the given range. The EC3 method for predicting rotational stiffness has been criticised over the last decades for its poor accuracy (Vrany, 2002; Katnam

2007a & 2007b; Gao and Moen, 2012) and hence improvement are needed. EC3 may as well have realised its own limitation, by introducing a combined method of test and calculation model as an alternative approach for deriving the rotational stiffness. This test method is adapted in the following section for measuring the rotational stiffness at purlin-sheeting connection only, and its results are compared with the results of empirical formulae in EC3.

Among other analytical method, the semi-analytical model developed by Gao & Moen (2012) is to date the latest and most accurate method in predicting rotational stiffness. The model considers the rotation at connections generated by both localised deformation of a panel and the bending of a restrained purlin flange. The model distinguishes between channel and Z- sections and provides results of less than 11% deviation in comparison to experimental studies and FE simulations. However, the method has some limitations:

1. The method assumes only one type of contact for Z- and C- sections under the uplift loading condition. It is valid for channel sections since the torsional moment caused by the eccentric applied load brings the section into contact with the roof sheet at its flange-lip junction line. However, according to Vrany (2007), there are two possible deformation modes for Z- sections. Depending on the direction of the eccentric load, the purlin may be in contact with the attached sheet at either the flange-web or the flange-lip junction line. Therefore, this will lead to different behaviour patterns in the resulting rotational stiffness.

2. The method utilises a rather simplified FE model that neglects purlin-sheeting interaction at the screw points; hence in order to obtain results, engineers need to have access to computer programs.

3. Validation shows that this model is not suitable for specimens outside the specified range,

which suggests that the panel's local flexural rigidity as described in the paper may be calibrated for the tested specimens only.

In this chapter a thorough investigation is conducted to determine the rotational stiffness at CFS purlin-sheeting connection, parametric studies are carried out to find the impact of each factor on the value of the rotational stiffness. The targets are realised through the following steps:

1. A rotational restraint test (or F-test) is carried out to measure the rotational stiffness of CFS Z- and Σ- sections with attached single sheet;

2. A pure analytical model is proposed to predict the rotational stiffness, and its outcome is validated by comparing it to both the F- test results and EC3 predictions;

3. A series of parametric studies are performed to assess how the rotational stiffness is affected by: different loading conditions; purlin geometries; sheeting thickness and different screw positions.

4. On the basis of the above findings, provide appropriate suggestions for design purposes.

3.2. Experimental investigation into rotational stiffness at purlin-sheet connection

3.2.1. Test set-up

EC3 Section 10 introduces a rotational restraint test (or F-test) to characterise overall rotational restraint provided by sheet to purlin, by measuring the equivalent vertical displacement at the free flange of purlin (Fig. 3-1). In this study, instead of the overall stiffness, the rotational stiffness only at the connection is required. For this purpose, a series of F-test have been conducted for single Σ- and Z- sections attached to first generation single roof sheet, to measure the rotational stiffness of purlin-sheeting system under both uplift and downward loading conditions.
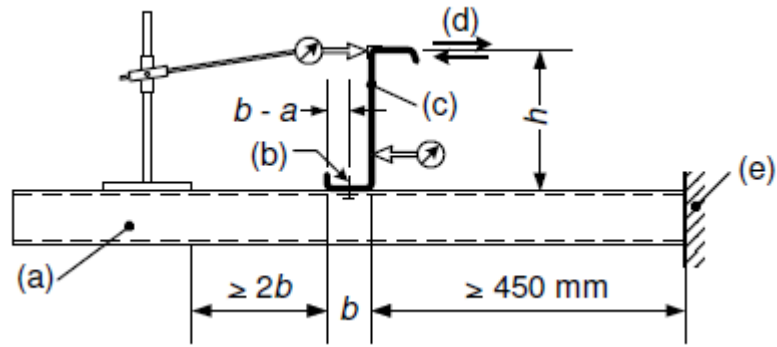
Figure 3-1: F-test set-up introduced in EC3

The test set-up is adapted based on BS EN 1993-1-3-2006 (A 5.3). The test set-up is illustrated in Figure 3-2: the trapezoidal sheet is fixed onto a channel section with two bolts on the mid line of each trough/crest clamped with timber blocks and steel plates. The sheet formed a rigidly supported cantilever plate. The distance between the line of connection to the support end is no less than 450mm, as required by EC3 specification (this is to ensure that sufficient cantilever deformation can take place). The direction of the purlins is positioned to simulate gravity and uplift load as in a practical situation. For instance, the purlin would be facing down under uplift loading so that it contacts the sheet at flange lip corner, and facing up under gravity loading so that it contacts the sheet at flange-web corner (Fig. 3-3 and 3-4). The CFS Σ- purlin section is connected onto the sheet at the mid-point of every trough using self-drilling Tek screws (Fig. 3-5).
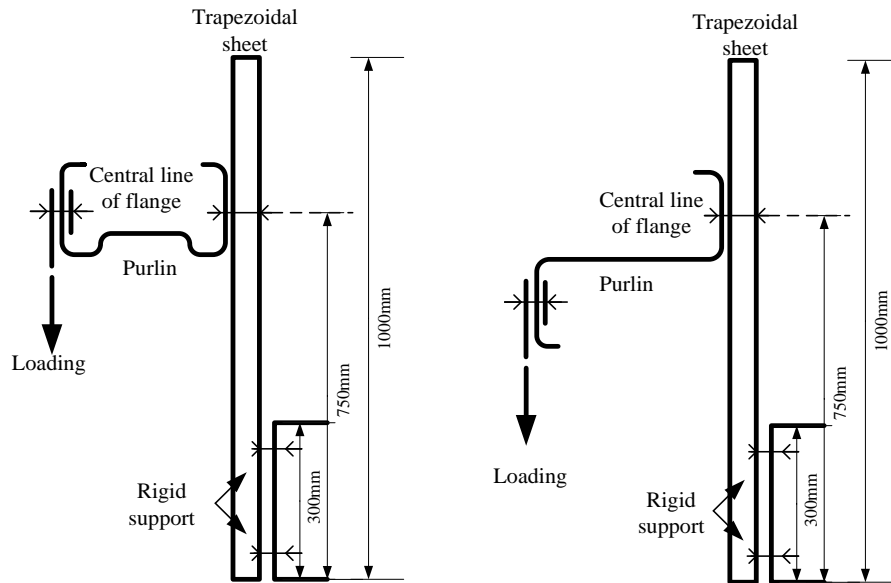
(a) Face-up
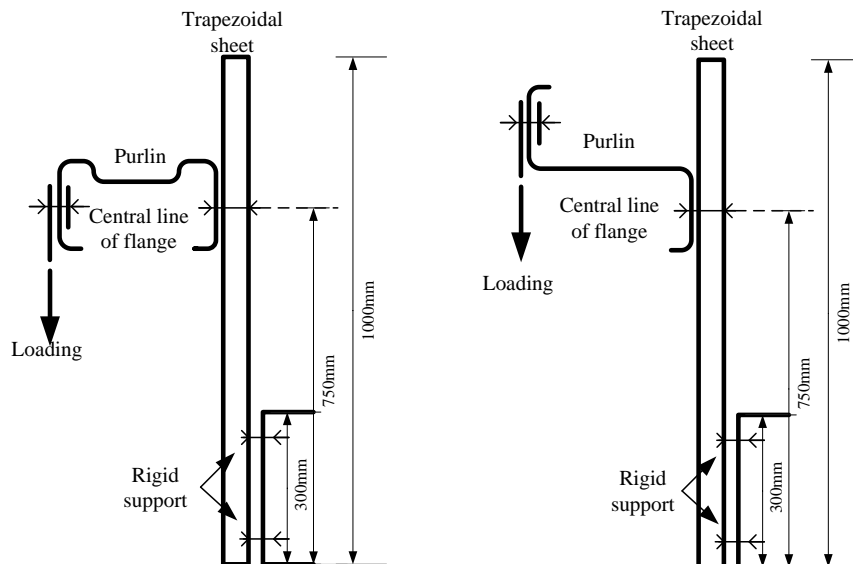
(b) Face-down

Figure 3-2: F-test arrangement for Σ- and Z- sections

Purlin section geometry is summarised in Tables 3-1 and 3-2 for each of the test set-up. The nominal yield stress of the tested specimen is 450 N/mm². The true stress-strain relationship is determined via material tensile coupon test. The detail of the coupon test is provided in Appendix

A.1 along with the test results. In this test programme, each specimen is assigned with a unique three-part ID indicating the purlin type, cross-sectional dimensions (represent the web depth and the thickness) and purlin directions ("facing down" or "facing up" represents the uplift and gravity loading conditions and are hereafter denoted as FD or FU, respectively). For example, specimen Σ20025FD indicates a Σ- section with a web depth of 200mm and cross sectional thickness of 2.5 mm, which is fixed in a "facing down" manner.

Table 3-1: Properties of test specimens for Z- sections
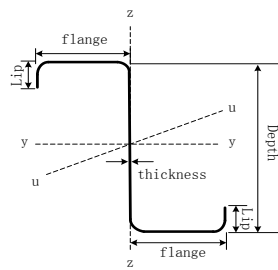
(y-y is geometric axis u-u is principal axis of cross section)

Specimen	Thickness (mm)	Depth (mm)		Width (mm)	Length (mm)
	Average	Top flange	Bottom flange	Web	Longitudinal
14614-FD-T1	1.56	62	62.0	147	999.5
14614-FU-T1	1.54	64	61.5	145	999.0
14618-FD-T1	1.78	63	59.0	145	998.5
14618-FU-T1	1.78	62	61.0	147	999.0
20617-FD-T1	1.71	66	66.5	200	1000.0
20617-FU-T1	1.71	66.5	65.5	202	1000.0
30720-FD-T1	2.08	76.5	76.0	299	1000.0
30720-FU-T1	2.08	75.5	76.5	300	1000.0

Table 3-2: Properties of test specimens for Σ- sections
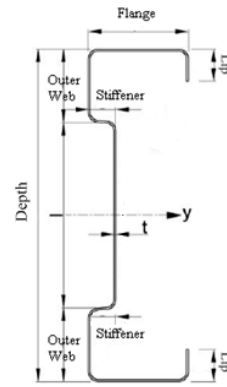
（y-y is geometric axis of cross section）

| Specimen | Thickness (mm) | Depth (mm) | | Width (mm) | | | Length (mm) |
	Average	Top flange	Bottom flange	Web	Stiffener	Outer web	Longitudinal
20012-FD	1.26	59.0	58.5	202.5	16	45	995.0
20012-FU	1.23	59.0	61.5	201.0	16	45	998.5
20016-FD	1.63	61.0	62.0	201.0	16	45	1000.0
20016-FU	1.58	62.0	60.5	200.5	16	45	998.5
20025-FD	2.40	61.0	61.5	200.0	16	45	991.0
20025-FU	2.42	61.5	61.0	198.0	16	45	993.0
24015-FD	1.54	63.5	62.0	239.0	16	50	999.0
24015-FU	1.52	62.5	63.0	239.0	16	50	1000.0
24023-FD	2.25	61.5	62.0	240.0	16	50	1002.0
24023-FU	2.19	62.5	62.0	240.5	16	50	1004.5
24030-FD	3.02	63.5	63.0	241.0	16	50	998.0
24030-FU	3.09	61.5	62.0	239.5	16	50	996.0
30018-FD	1.78	74.5	77.5	300.5	16	60	998.5
30018-FU	1.79	75.0	76.5	301.0	16	60	999.5
30025-FD	2.37	73.0	75.5	300.0	16	60	997.0
30025-FU	2.29	75.5	74.5	301.0	16	60	996.5
30030-FD	2.99	75.0	75.0	301.5	16	60	1000.0
30030-FU	3.04	74.5	76.0	300.5	16	60	988.5

Figure 3-3: Face-down position (Uplift)

Figure 3-4: Face-up position (Gravity)

Figure 3-5: Rear view of the set-up

3.2.2. *Test specimen and apparatus*

The apparatus required for each rotational restraint test is listed as following;

- A single skinned trapezoidal CFS sheet (size: 1060mm $\times$ 1000mm $\times$ 0.7mm   Fig.3-6, profile shape is shown in Fig. 3-7).

- A single CFS Z- or Σ- purlin with approximate length of 1000mm.

- 5 timber blocks (300mm $\times$ 115mm $\times$ 20mm, Fig.3-8) and 4 small steel plates (250mm $\times$ 20mm $\times$ 10mm, Fig. 3-9) for fixed support fixing.

- 2 large steel plates with 7 holes for load transfer (Fig.3-10):

    1) Dimensions: 100mm $\times$ 800mm $\times$ 10mm, weight: 61N

    2) Dimensions: 50mm $\times$ 800mm $\times$ 10mm, weight: 30N

- 5.5$\times$32mm self-drilling screws for purlin and sheeting connection (Fig. 3-11).

- 25 Grade M8.8 bolts for support fixing.

- 9 dial gauges with 0.01mm accuracy for displacement measurement.

- 2 digital inclinometers with accuracy of 0.1 degree to measure the rotation/distortion of purlin.

Figure 3-6: Sheeting with dimensions 1060mm $\times$ 1000mm $\times$ 0.7mm
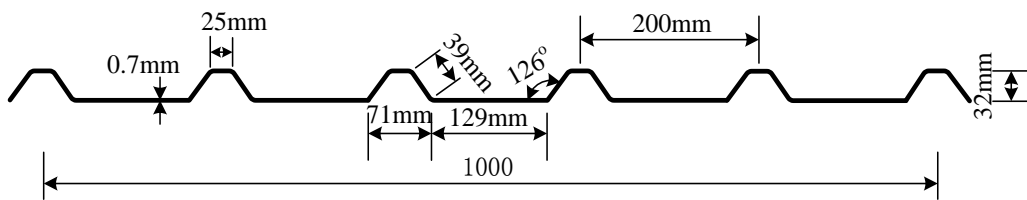
Figure 3-7: Dimensions of sheet profile

Figure 3-8: Timber block with dimensions 300mm $\times$ 115mm $\times$ 20mm

Figure 3-9: Four steel plates with dimensions 250mm $\times$ 20mm $\times$ 10mm

Figure 3-10: Steel plate with dimensions 100mm $\times$ 800mm $\times$ 10mm and

50mm $\times$ 800mm $\times$ 10mm

Figure 3-11: 5.5 $\times$ 32mm Tek screws and self-drilling machine

3.2.3. *Test procedure*

A stiff steel plate was bolted to the free flange of the purlin, by using several bolts to model

the load distribution; weights were applied to this steel plate through a hook (Fig. 3-12). As a

result of such a loading arrangement, the load applied by weights was always in the plumb direction. Weights were applied in increment until the occurrence of the plastic deformation in the roof sheet. The vertical deflections at several locations were recorded at each loading increment by using dial gauges, which were placed at the purlin's outer webs and free flange (Fig. 3-13a). The rotational angles near both restrained and free flanges were monitored by using two digital inclinometers, with an accuracy of 0.1 degree, placed at the outer webs as close to the web-flange junction lines as possible. The lateral displacements of sheet and purlin due to bending were recorded (Fig. 3-13b).

Figure 3-12: Multiple-point loads to simulate the uniformly distributed load

(a)Dial gauges placed at the rear side of the roof sheet
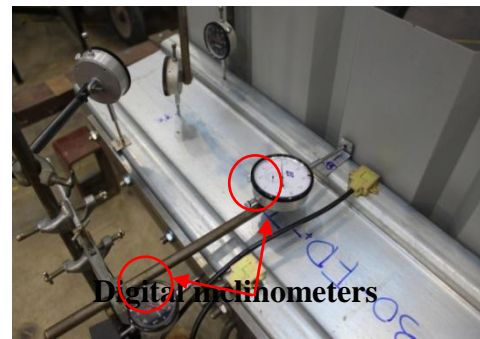
(b) Dial gauges and inclinometers attached to purlin

Figure 3-13: Measurement of displacements

3.2.4. *Test results and discussion*

Tests were continued until the yield failure of the roof sheeting occurred. The applied load and deflections were recorded at each loading increment, from which a complete moment-against-rotation relationship for each screw connection can be established. Table 3-3 presents a summary for the actual sizes of test specimens, the loads that cause the vertical deflection of the free flange of the purlin equal to approximately 1/10 of the purlin web depth, and the rotation and vertical deformation measured at this load level. The rotational stiffness $C_{D,A}$ of each specimen was determined by dividing the moment induced at connection due to that vertical load by the corresponding rotation captured, and is presented in the same table. This approach to calculating the rotational stiffness is in accordance with the requirement of EC3 (BSI, 2006).

Table 3-3: F-test results

Specimen ID	Measured web depth, mm	Purlin thickness, mm	Load*,N	Rotation, Radian	Vertical deformation, mm	$C_{D,A}$Nm/rad/mm
Σ20012FD	203	1.26	141	0.072	21.5	394
Σ20012FU	201	1.23	151	0.054	19.5	502
Σ20016FD	200	1.58	201	0.070	21.5	622
Σ20016FU	200	1.62	241	0.070	21.7	691
Σ20025FD	200	2.40	328	0.073	21.8	895
Σ20025FU	198	2.42	384	0.075	20.8	1024
Σ24015FD	239	1.58	151	0.063	23.4	593
Σ24015FU	241	1.58	151	0.052	24.5	696
Σ24023FD	241	2.17	301	0.085	24.0	848
Σ24023FU	241	2.20	301	0.072	23.6	1009
Σ24030FD	240	2.95	385	0.091	22.7	909
Σ24030FU	241	2.99	381	0.087	22.6	1047
Σ30018FD	301	1.81	201	0.082	30.9	735
Σ30018FU	301	1.79	171	0.068	29.8	753
Σ30025FD	300	2.37	241	0.079	30.8	921
Σ30025FU	301	2.31	301	0.084	29.5	1078
Σ30030FD	301	3.04	341	0.105	30.8	977
Σ30030FU	302	2.99	381	0.096	30.5	1191
Z14614FD	147	1.56	302	0.086	14.2	512
Z14614FU	145	1.54	331	0.061	13.5	762
Z14618FD	145	1.78	404	0.080	14.9	730
Z14618FU	147	1.78	444	0.078	14.9	820
Z20617FD	200	1.80	261	0.077	21.3	680
Z20617FU	202	1.71	320	0.073	19.3	876
Z30720FD	299	2.08	221	0.084	31.2	791
Z30720FU	300	2.08	261	0.082	29.5	955

* These recorded loads cause the vertical deflection of the free flange of the purlin equal to approximately 1/10 of the purlin web depth.

Typical complete moment-rotation curves recorded for specimen Σ20012 are presented in Fig. 3-14 for both FU and FD arrangements; similar curves for other specimens are presented in Fig. 3-28 (later in the chapter) in comparison to the theoretical prediction results. A common feature of these curves is that they remain almost linear during the entire loading range. In all cases, the test result showed a higher $C_{D,A}$ under gravity load (FU) than under uplift load (FD). The possible reason that caused this may due to the resultant moment generated: when the load P is applied at the purlin's free flange, a coupled moment is generated at the connection, which is equivalent to the reaction force P acting at the line of contact between purlin and sheeting, multiplied by the distance from the line of contact to connections. Under gravity load (FU), the purlin attached the sheets at its flange-lip corner, which tends to deflect under loading and thus the distance s is reduced. With the moment remains constant, the applied load is increased with an increased rotated angle, resulting in a reduction in rotational stiffness, $C_{D,A}$ (Fig. 3-15). The degree of deflection of the sheet caused by the purlin angle was monitored and proved this cause as shown in Fig. 3-16 & Fig. 3-17. When loaded under the same loading level with the same purlin sections, the sheet deformation is always more severe under uplift load (FD case) than that under gravity load case (FU case). This difference agrees by Chung and StQuinton (1996), since full restraint to the purlins is known to be achieved under gravity loading. Vrany (2006) has also pointed out that gravity loading tends to increase the rotational stiffness, whilst uplift loading decreases it. It was suggested that when under compression, the free flange is under tension which tends to stabilize the cross-section.
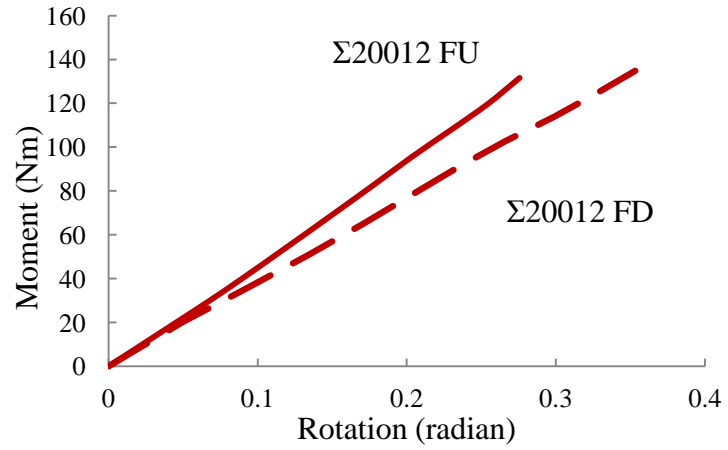
Figure 3-14: A typical moment-rotation curve of Σ20012
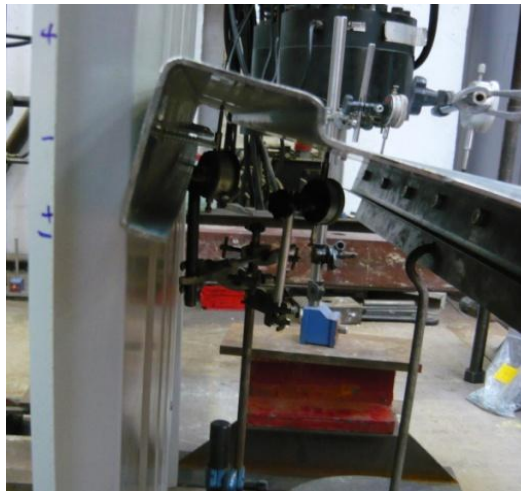
Figure 3-15: Σ- section line of contact between purlin and sheeting (FD test)
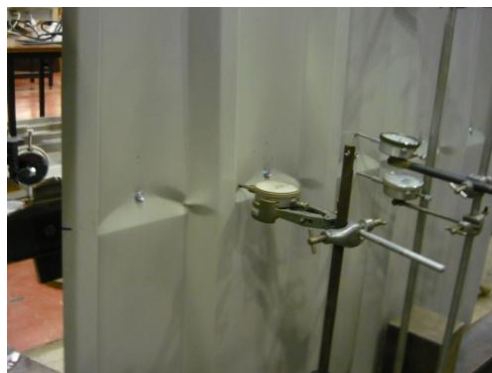
Figure 3-16: Local sheet deformation (FD)

Figure 3-17: Local sheet deformation (FU)

Failed specimens were unloaded and dismounted and the permanent deformations were revealed. It can be seen from Fig.3-18 that at the end of loading, localised plastic deformation occurs at each screw connection point, as evidenced by noticeable yield lines formed along the contact line, and two lines linking the screw point to both ends of the contact line. In all tests, the purlin sections have a greater thickness than the roof sheet. Distortional deformation of the purlin can only be clearly observed at the time the plastic yield line is about to be formed. Typical deformation modes of the tested purlin-sheeting system observed during tests are presented in Fig. 3-19 for both face-down and face-up tests.
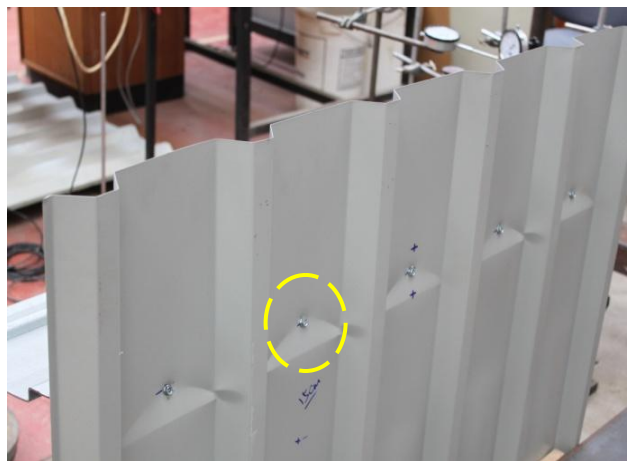
Figure 3-18: Local plastic deformation of sheet
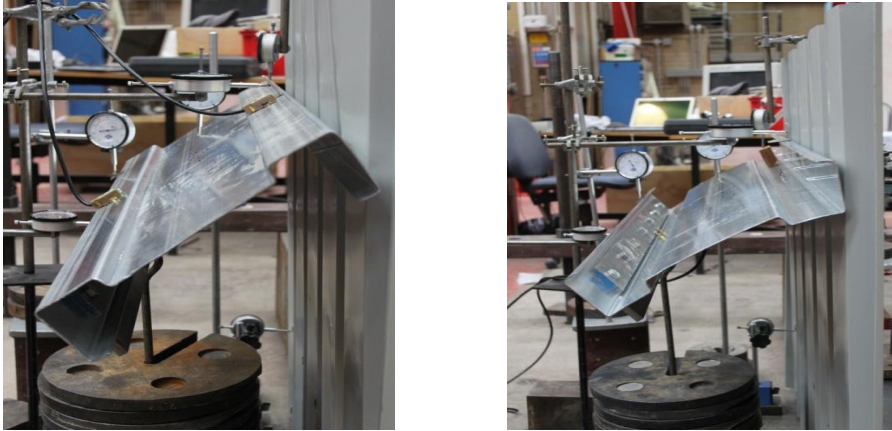
Figure 3-19: Deformation modes for both FD and FU specimens

3.3. Analytical model for predicting rotational stiffness at purlin-sheet connection

3.3.1.   Introduction

Design method from EC3 is the most commonly used model for predicting rotational stiffness for a CFS purlin-sheeting system. However because of its assumptions made in order to simplify the calculation process, it has been criticised either unsafe or conservative for some cases, and is only applicable for a limited range of purlin and sheet sections. The model will be explained in detail in section 3.2.2, followed by a working example in Appendix A.2.

In order to improve the current design model, a pure analytical method is developed and the details are provided in section 3.2.3. It is seen that the rotational stiffness can be derived from the general moment/rotation ratio, from which the rotation is further divided into 4 components. Each component is explained and analysed, and its corresponding rotation is then summed up to predict the rotational stiffness. A working example is presented in Appendix A.3. A comparison between the test results with both EC3 and analytical prediction is provided in section 3.3, discussions and conclusions are then made.

3.3.2. EC3 design method

In the EC3 design code, the rotational stiffness C_D given to the purlin by the sheeting can be calculated as:

$$C_D = \cfrac{1}{\left(\cfrac{1}{C_{D,A}} + \cfrac{1}{C_{D,C}}\right)}$$
(Equation 3-1)

where $C_{D,A}$ is the rotational stiffness of the connection between the sheeting and the purlin; and $C_{D,C}$ is the rotational stiffness corresponding to the flexural stiffness of the sheeting. Since the flexural stiffness of the sheet in most case is large, the latter term can therefore be treated as negligible and only $C_{D,A}$ is considered.

The empirical formula for calculating $C_{D,A}$ provided in EC3 is given:

$$C_{D,A} = C_{100} \cdot k_{ba} \cdot k_t \cdot k_{bR} \cdot k_A \cdot k_{bT}$$
(Equation 3-2)

assuming the sheet-to-purlin fasteners are positioned at the mid-point of the purlin flange. The factors are derived from extensive test data, as illustrated in Fig. 3-20.

$$k_{ba} = (b_a / 100)^2 \qquad \text{if } b_a < 125\text{mm};$$
$$k_{ba} = 1{,}25(b_a / 100) \qquad \text{if } 125\text{mm} \le b_a < 200\text{mm};$$

$$k_t = (t_{nom} / 0{,}75)^{1{,}1} \qquad \text{if } t_{nom} \ge 0{,}75\text{mm}; \text{ positive position;}$$
$$k_t = (t_{nom} / 0{,}75)^{1{,}5} \qquad \text{if } t_{nom} \ge 0{,}75\text{mm}; \text{ negative position;}$$
$$k_t = (t_{nom} / 0{,}75)^{1{,}5} \qquad \text{if } t_{nom} < 0{,}75\text{mm};$$

$$k_{bR} = 1{,}0 \qquad \text{if } b_R \le 185\text{mm};$$
$$k_{bR} = 185 / b_R \qquad \text{if } b_R > 185\text{mm};$$

for gravity load:
$$k_A = 1{,}0 + (A - 1{,}0) \cdot 0{,}08 \qquad \text{if } t_{nom} = 0{,}75\text{mm}; \text{ positive position;}$$
$$k_A = 1{,}0 + (A - 1{,}0) \cdot 0{,}16 \qquad \text{if } t_{nom} = 0{,}75\text{mm}; \text{ negative position;}$$
$$k_A = 1{,}0 + (A - 1{,}0) \cdot 0{,}095 \qquad \text{if } t_{nom} = 1{,}00\text{mm}; \text{ positive position;}$$
$$k_A = 1{,}0 + (A - 1{,}0) \cdot 0{,}095 \qquad \text{if } t_{nom} = 1{,}00\text{mm}; \text{ negative position;}$$

- linear interpolation between $t = 0{,}75$ and $t = 1{,}0$ mm is allowed
- for $t < 0.75$ mm the formula is not valid;
- for $t > 1$ mm, the formula needs to be used with $t = 1$ mm

for uplift load:
$$k_A = 1{,}0;$$
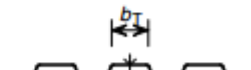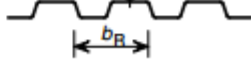
$$k_{bT} = \sqrt{\frac{b_{T,max}}{b_T}} \qquad \text{if } b_T > b_{T,max}, \text{ otherwise } k_{bT} = 1;$$

$A[\text{kN/m}] \le 12\text{kN/m}$ load introduced from sheeting to beam;

where:

b_a is   the width of the purlin flange [in mm];

b_R is   the corrugation width [in mm];

b_T is   the width of the sheeting flange through which it is fastened to the purlin;

$b_{T,max}$ is   given in Table 10.3;

C_{100} is   a rotation coefficient, representing the value of $C_{D,A}$ if $b_a = 100$ mm.

Table 10.3: Rotation coefficient C_{100} for trapezoidal steel sheeting

Positioning of sheeting		Sheet fastened through		Pitch of fasteners		Washer diameter [mm]	C_{100}	$b_{T,max}$
Positive 1)	Negative1)	Trough	Crest	$e = b_R$	$e = 2b_R$		[kNm/m]	[mm]
For gravity loading:								
×		×		×		22	5,2	40
×		×			×	22	3,1	40
	×		×	×		K_a	10,0	40
	×		×		×	K_a	5,2	40
	×	×		×		22	3,1	120
	×	×			×	22	2,0	120
For uplift loading:								
×		×		×		16	2,6	40
×		×			×	16	1,7	40

Key:

b_R is the corrugation width;

b_T is the width of the sheeting flange through which it is fastened to the purlin.

K_a indicates a steel saddle washer as shown below with $t \geq 0,75$ mm

Sheet fastened:

- through the trough:

- through the crest:

The values in this table are valid for:

- sheet fastener screws of diameter: $\phi = 6,3$ mm;

- steel washers of thickness: $t_w \geq 1,0$ mm.

1) The position of sheeting in positive when the narrow flange is on the purlin and negative when the wide flange is on the purlin.

Figure 3-20: Typical values of C_{100} for trapezoidal steel sheeting (BSI, 2006)

3.3.3. Analytical model to predict rotational stiffness at connection

An analytical model is developed and presented here for predicting the rotational stiffness of the purlin specimen at connection points under the applied loads as seen in the test. The purlin is connected to the roof sheet with self-drilling screws at one flange, but is free to move at the other.

The total rotation angle captured near the junction line between the connected flange and the adjacent outer web or flange lips should comprise the following 4 components, illustrated in Fig. 3-21 and summarised as follows:

(1) θ_s, the rotation angle of the cantilever sheet under a row of concentred moments generated at screw connection points;

(2) θ_l, the rotation angle associated with the localised deformation of the sheet under the pulling force in each screw;

(3) θ_k, the rotation angle due to the separation between the roof sheet and the purlin flange at the connection point; and

(4) θ_p, the rotation angle due to the purlin flange bending.
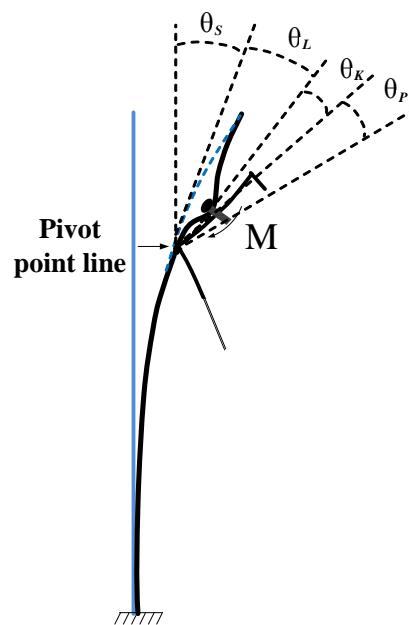
Figure 3-21: Rotation developed during the F-test

3.3.3.1. Rotation angle of the cantilever sheet, θ_S

During the F-test, the trapezoidal sheet is rigidly fixed at the base and free at the top, behaving

as a one-way cantilever plate. The loaded purlin section transfers the load to the sheet in the form of a row of concentred moments, which produces rotation angle θ_s (Fig.3-22). The magnitude of θ_s depends on the geometric configuration and the fixing arrangement of the sheet and the applied moment. Therefore the rotation stiffness associated with this component varies with actual construction details and should be considered separately. In this case, it will be excluded from the overall rotation angle measured using inclinometers. It is anticipated that the real rotation of the cantilever sheet should be very close to the theoretical calculation based on the cantilever theory. To confirm this, a dial gauge was horizontally placed at 200mm below the screw point to measure the lateral deflection (point A in Fig. 3-22). The measured deflections at point A were then compared with the calculated ones based on the one-way cantilever plate. The comparison of an example of Σ24015FU is presented in Fig. 3-23, which shows a reasonably close agreement. The calculation follows $\theta_S = ML_1 / D$, where L_1 is the vertical distance between the fixed support and the point A, and EI_s is the flexural rigidity of the sheet trough plate. The comparison of an example of Σ24015FU is presented in Fig. 3-23, which shows a reasonably agreement with slight discrepancy. This is because a concentrated line load induced by the contact line between the purlin flange and roof sheeting. This load produces a localised deformation in the sheet, which opposes the cantilever deflection. The deflection recorded at Point A, therefore, will be smaller than the pure cantilever case. However, since the rotation caused by this effect is insignificant compared to other components, it is deemed that the proposed theoretical prediction is acceptable.
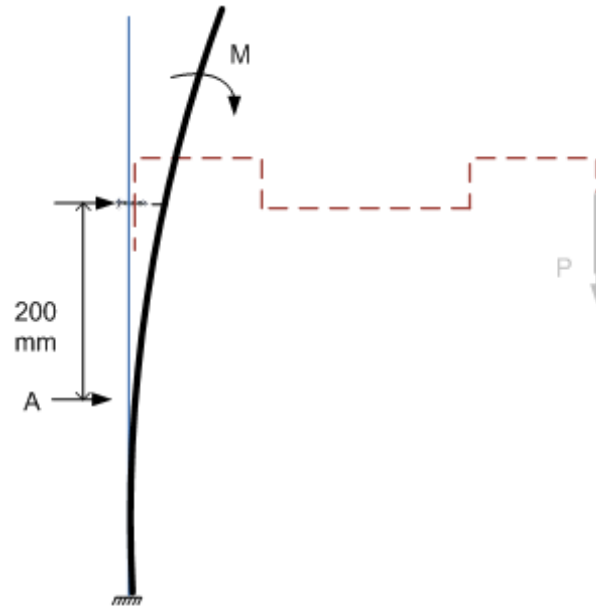
Figure 3-22: Cantilever sheet in the test and the calculation model
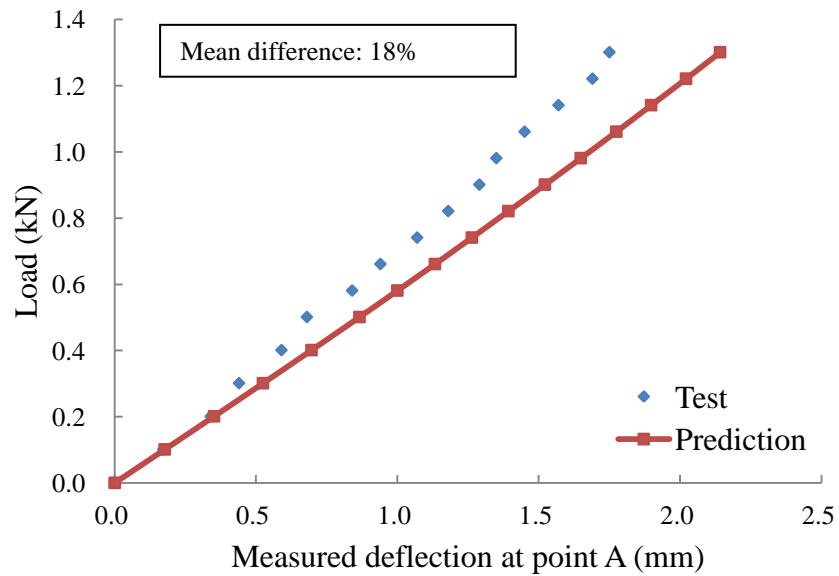
Figure 3-23: Comparison of the load-deflection between test and prediction (Σ24015FU)

3.3.3.2. Rotation angle caused by the sheet local deformation at connection, θ_l

In order to maintain the moment equilibrium, a couple is generated at each purlin-sheeting connection point, with two opposite forces acting at the screw point and the line of contact,

respectively. While the reaction force at the line of contact is supported by the webs of roof sheet, the pulling force from the screw will produce a localised deformation in the sheet in the surrounding area, and the rotation angle due to this local deflection is defined as θ_l (Fig. 3-24).
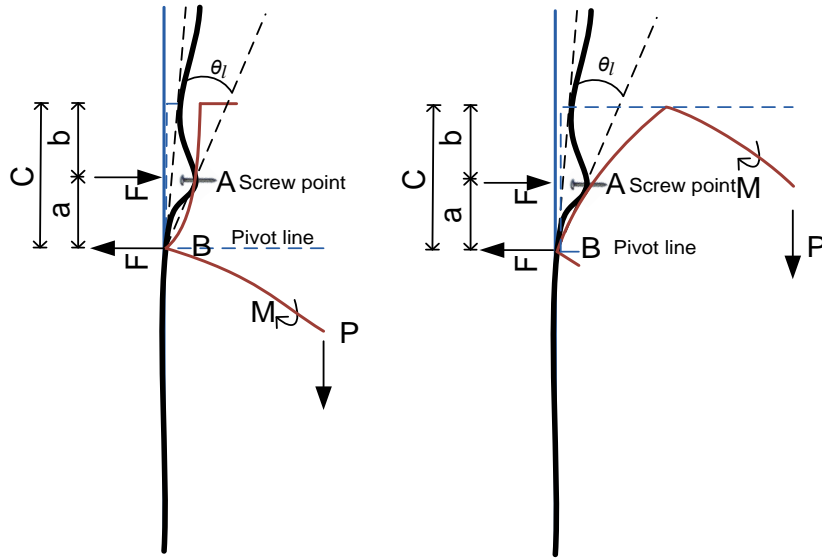
(a) Contact at flange-web line   (b) Contact at flange-lip line

Figure 3-24: Purlin-sheet interaction at a connection point

The screw force F under the applied load P can be calculated as $F = M / na$, where M is the applied moment, a is the distance between the screw and the line of contact and n is the number of screws. In this case, since the screw is located at the mid-point of purlin flange, a equals the half flange width, C. This load causes the roof sheet to deform locally around the screw point. Assuming the force at each screw point is identical, the deformation of the sheet at every trough can be treated as a thin rectangular plate subjected to a concentrated load (Fig.3-25). By adopting the classic Kirchhoff thin plate theory, the governing equation can be expressed as:

$$\left(\partial^2 / \partial x^2 + \partial^2 / \partial y^2 \right)^2 w = Q(x) / D \qquad \text{(Equation 3- 3)}$$

where w is the deflection of plate; $Q(x)$ is the applied force function depended on the loading condition, i.e. for centrally loading case, $Q(x) = F.\delta(x - h_T/2, y)$, where F is the magnitude of the point load; D is the flexural rigidity, i.e. $Et_s^3/12(1-v^2)$; E is the Young's modulus of the plate material, t_s is the thickness of the roof sheet.

In line with the deformation pattern, the boundary conditions can be set as follows: two vertical folding lines of the sheet are considered as simply supported (S). The pivot line is considered as the fixed (C) edge as a result of the observation of a very early occurrence of plastic hinge under the applied load. A hypothetic line is chosen at a zero deflection location as the forth line, also considered as fixed. Therefore the final boundary condition together with the dimension symbols are illustrated in Fig.3-25, where b_T is the sheet trough width; and h_T is the height of the plate where fixed edges are located; in this case it can be assumed equal to the purlin flange width C.
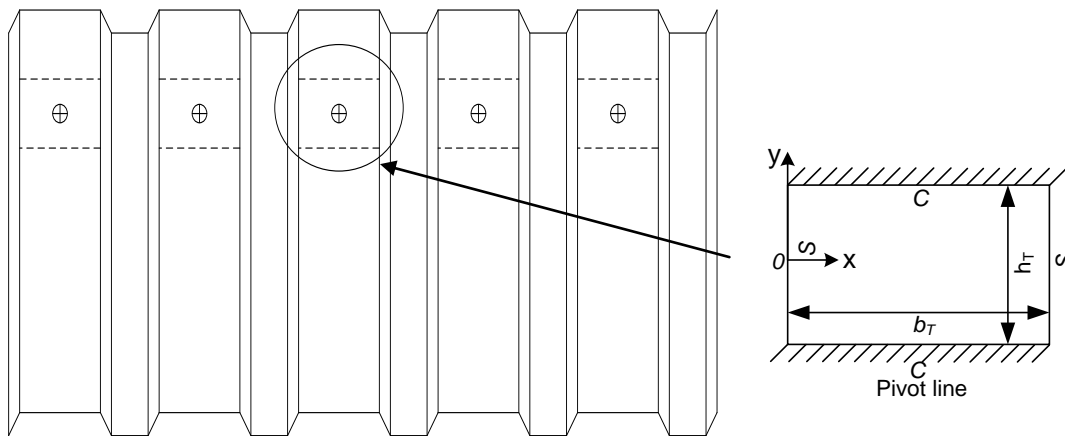
Figure 3-25: Plate model for predicting rotation due to the localised sheet deformation

$$w = \sum_{m=1}^{\infty} Y_m \sin\left(\frac{m\pi x}{b_T}\right) \qquad \text{(Equation 3-4)}$$

where $m=1,3,5...,n$, and

$$Y_m = A_m \cosh\left(\frac{m\pi y}{b_T}\right) + B_m\left(\frac{m\pi y}{b_T}\right)\sinh\left(\frac{m\pi y}{b_T}\right) + C_m \sinh\left(\frac{m\pi y}{b_T}\right) + D_m\left(\frac{m\pi y}{b_T}\right)\cosh\left(\frac{m\pi y}{b_T}\right)$$

(Equation 3-5)

For a plate with two opposite edges simply supported and the other two fixed (*S-C*-S-C), the constants can be solved as:

$$A_m = \frac{b_T F(-1)^{\frac{m+1}{2}}\left[-4b_T^2\cosh\left(\frac{m\pi h_T}{2b_T}\right)^2 + m^2\pi^2 h_T^2 + 4b_T^2\right]}{4\left[m\pi h_T + 2b_T\sinh\left(\frac{m\pi h_T}{2b_T}\right)\cosh\left(\frac{m\pi h_T}{2b_T}\right)\right]m^3\pi^3 D}$$

$$B_m = \frac{b_T^3 F(-1)^{\frac{m+1}{2}}\left[1-\cosh\left(\frac{m\pi h_T}{2b_T}\right)^2\right]}{\left[m\pi h_T + 2b_T\sinh\left(\frac{m\pi h_T}{2b_T}\right)\cosh\left(\frac{m\pi h_T}{2b_T}\right)\right]m^3\pi^3 D}$$

$$C_m = \frac{b_T^2 F(-1)^{\frac{m+1}{2}}}{m^3\pi^3 D} - \left\{H(y) - \frac{\left[2b_T\sinh\left(\frac{m\pi h_T}{2b_T}\right)\cosh\left(\frac{m\pi h_T}{2b_T}\right)+m\pi h_T\right]}{2\left[m\pi h_T + 2b_T\sinh\left(\frac{m\pi h_T}{2b_T}\right)\cosh\left(\frac{m\pi h_T}{2b_T}\right)\right]}\right\}$$

$$D_m = \frac{b_T^2 F(-1)^{\frac{m+1}{2}}}{m^3\pi^3 D} - \left\{\frac{1}{2} - H(y)\right\}$$

(Equation 3-6)

For engineering applications, $m=5$ can be deemed to produce sufficiently accurate results. $H(y)$ represents the Heaviside function, ie. $H(y)=0$ for $y< 0$ and $H(y)=1$ for $y \geq 0$. The resolved constants can be substituted into Eq. (3-4) to calculate the deflection caused by local sheet

deformation. To facilitate the engineering application, the equation can be simplified into the following form:

$$\theta_L = \frac{w}{a} = \frac{\beta F h_T^2}{E t_s^3 a} = \frac{\beta M h_T^2}{n E t_s^3 a^2} \qquad\qquad \text{(Equation 3-7)}$$

where the coefficient β depends on the b_T/h_T ratio and the location of screw in relation to the trough panels. For ease of design purpose, some common values of β are presented in Table 3-4.

To validate this model, the horizontal displacement at points A and B were also measured (see Fig.3-24).We calculate the differential displacements between these two points and compare them with the calculation results. A comparison of specimen Σ30018 FU is presented in Fig.3-26 with total applied load against horizontal difference between point A and B, which shows a close agreement.

Table 3-4: Typical values of coefficient β

Screw location in the trough	b_T/h_T ratio							Empirical equations
	1.0	1.2	1.4	1.5	1.6	1.8	2.0	
At centre	0.077	0.078	0.078	0.078	0.078	0.077	0.077	$\beta = 0.078$
At 1/3 trough width	0.057	0.055	0.051	0.049	0.046	0.042	0.037	$\beta = -0.003\dfrac{b_T}{h_T} + 0.061$
At 1/4 trough width	0.043	0.040	0.035	0.032	0.029	0.024	0.020	$\beta = -0.004\dfrac{b_T}{h_T} + 0.047$
At 1/5 trough width	0.034	0.031	0.026	0.024	0.022	0.017	0.014	$\beta = -0.003\dfrac{b_T}{h_T} + 0.038$
At 1/10 trough width	0.017	0.015	0.012	0.010	0.009	0.006	0.004	$\beta = -0.002\dfrac{b_T}{h_T} + 0.019$

(*Note: the values derived in Table 3-4 are for t_s of 0.7mm, for different thickness use $\beta' = \frac{\beta t^3}{0.7^3}$)
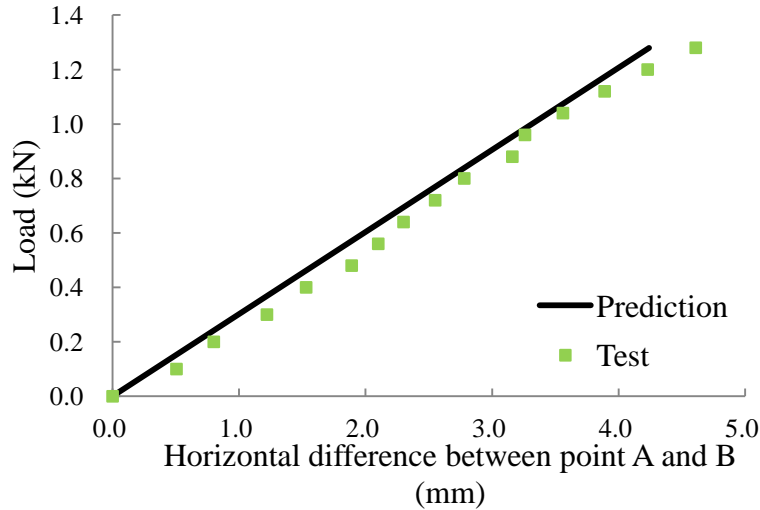
Figure 3-26: Comparison of load-localised deflection between test and prediction for specimen

Σ30018 FU

3.3.3.3. Rotation angle caused by the separation of connection, θ_k

Under the applied load, the purlin profile tends to separate from the sheet because of the resilience of the sealing washer. In our tests, it has been found that during the linear stage, the rotation associated with this effect is relatively small when compared to the other components. Therefore, this component is neglected in the calculation model.

3.3.3.4. Rotation angle caused by the deformation of purlin flange, θ_p

The deformation of purlin flange and web is calculated with the bending theory for one way slabs. By rotating Fig. 3-24 by 90 degrees, the flange panel between the pivot line and screw point, as illustrated in Fig. 3-27, can be assumed as a simply supported one-way slab with a moment applied at one end. Thus the maximum rotation can be expressed in Eqn. (3-8) or (3-9) depending on the contact:

$$\theta_P = \frac{Ma}{3D} \qquad \text{(Equation 3- 8)}$$

$$\theta_P = \frac{Ma}{3D} + \frac{Mb}{D} \qquad\qquad \text{(Equation 3- 9)}$$

where a is the vertical distance between the screw point and the line of contact, and

$D = Et_p^3/12(1-v^2)$ is the flexural rigidity of the purlin flange panel. It has been suggested (BSI,

2006) that the contact condition under different loading directions can be determined for C- and Σ-

sections, i.e. a flange-web junction line contact for the gravity load and a flange-lip junction line

contact for the uplift load. However, for Z- sections under a specified loading direction, the purlin

flange may contact with the sheet in either way, depending on factors such as the screw position,

purlin geometry and loading magnitude.
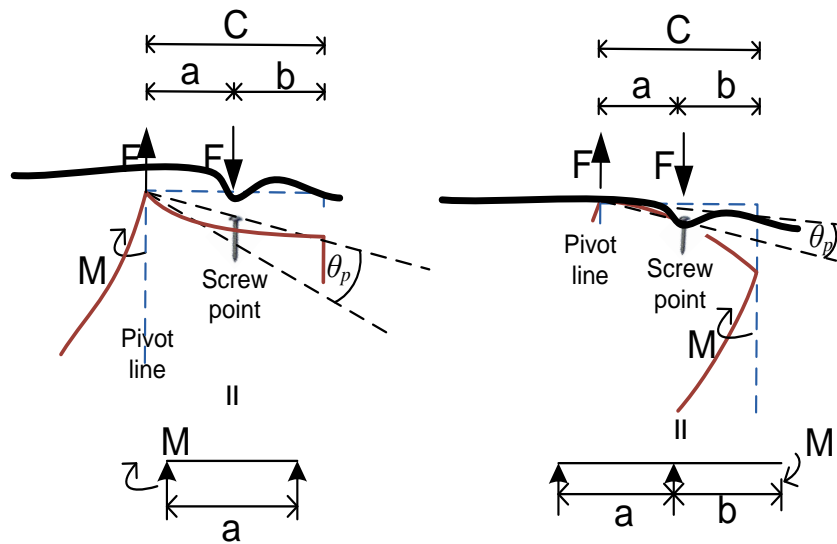
(a) Contact at purlin's

flange-web junction line

(b) Contact at purlin's

flange-lip junction line

Figure 3-27: Analytical model of rotation angle caused by purlin flange bending

Based on the abovementioned assumptions and validations, it can be suggested that only the

terms of θ_l and θ_p are considered in our analytical model.The term of θ_s should be determined

based on the actual construction design details and by using the one-way slab theory. The term of

θ_k are deemed to be negligible.

The final rotational stiffness per unit length run at each connection, i.e. $C_{D,A}$, with a unit of N .m/rad, can be expressed as:

When the contact is at flange-web junction line:

$$C_{D,A} = \frac{M}{\theta_L + \theta_P} = \frac{M}{\left(\dfrac{\beta M h_{\mathrm{T}}^2}{nEt_S^3 a^2} + \dfrac{Ma}{3EI_P}\right)} = \frac{E}{\left(\dfrac{\beta h_{\mathrm{T}}^2}{nt_S^3 a^2} + \dfrac{a}{3I_P}\right)} \qquad \text{(Equation 3-10)}$$

When the contact is at flange-lip junction line:

$$C_{D,A} = \frac{M}{\theta_L + \theta_P} = \frac{M}{\left(\dfrac{\beta M h_{\mathrm{T}}^2}{nEt_S^3 a^2} + \dfrac{Ma}{3EI_P} + \dfrac{Mb}{EI_P}\right)} = \frac{E}{\left(\dfrac{\beta h_{\mathrm{T}}^2}{nt_S^3 a^2} + \dfrac{a}{3I_P} + \dfrac{b}{I_P}\right)} \qquad \text{(Equation 3-11)}$$

3.4. Overall rotation and comparison to experimental data

The results recorded from the F-tests have been used to validate the analytical model presented above. Typical moment-rotation curves from both the test results and analytical predictions are presented in Fig. 3-28. As seen, most curves show a notable linear feature during the entire loading range except for Z30720FD. This suggests that a constant rotation stiffness employed for the purlin-sheeting interaction design is essentially valid. The analytical result of the rotational stiffness is compared with the experiment/EC3 values summarised in Table 3-5. It is worth noting that the inclinometers used to measure the rotation angles are fixed near the flange-web corner. Although in the test, they were fixed closest to the corner, it is inevitable that an offset distance e between the centre and corner would take place. To allow for that, in calculating $C_{D,A}$, the additional angle developed between the corner and inclinometer centre is allowed by taking into account with an term of e/I_p to the denominator in both Eqns. (3-8) and (3-9).

Table 3-5: Comparisons of rotational stiffness between test and analytical predictions

Specimen Name	$C_{D,A}$ prediction, Nm/rad/mm	$C_{D,A}$ test Nm/rad/mm	$C_{D,A}$ EC3 Nm/rad/mm	Test/prediction ratio	Test/EC3 ratio	Average Test C_D	FD/FU ratio
Σ20012 FD	403	394	470	0.98	0.84	399	
Σ20012 FU	508	502	970	0.99	0.52	505	0.79
Σ20016 FD	607	622	470	1.02	1.32	615	
Σ20016 FU	772	691	970	0.89	0.71	732	0.78
Σ20025 FD	930	895	470	0.96	1.90	913	
Σ20025 FU	1048	1024	970	0.98	1.06	1036	0.89
Σ24015 FD	588	593	470	1.01	1.26	591	
Σ24015 FU	731	696	970	0.95	0.72	714	0.80
Σ24023 FD	860	848	470	0.99	1.80	854	
Σ24023 FU	987	1009	970	1.02	1.04	998	0.87
Σ24030 FD	939	909	470	0.97	1.93	924	
Σ24030 FU	1090	1047	970	0.96	1.08	1069	0.86
Σ30018 FD	672	735	677	1.09	1.09	704	
Σ30018 FU	805	753	1397	0.94	0.54	779	0.83
Σ30025 FD	883	921	677	1.04	1.36	902	
Σ30025 FU	1002	1078	1397	1.08	0.77	1040	0.88
Σ30030 FD	1023	977	677	0.96	1.44	1000	
Σ30030 FU	1108	1191	1397	1.07	0.85	1150	0.92
Z14614 FD	557	512	470	0.92	1.09	535	
Z14614 FU	717	762	970	0.94	0.79	740	0.72
Z14618 FD	723	730	470	1.01	1.55	727	
Z14618 FU	889	820	970	0.92	0.85	855	0.81
Z20617 FD	674	680	508	1.01	1.34	677	
Z20617 FU	868	876	1050	1.01	0.83	872	0.78
Z30720 FD	810	791	677	0.98	1.17	801	
Z30720 FU	958	955	1397	1.00	0.68	957	0.85
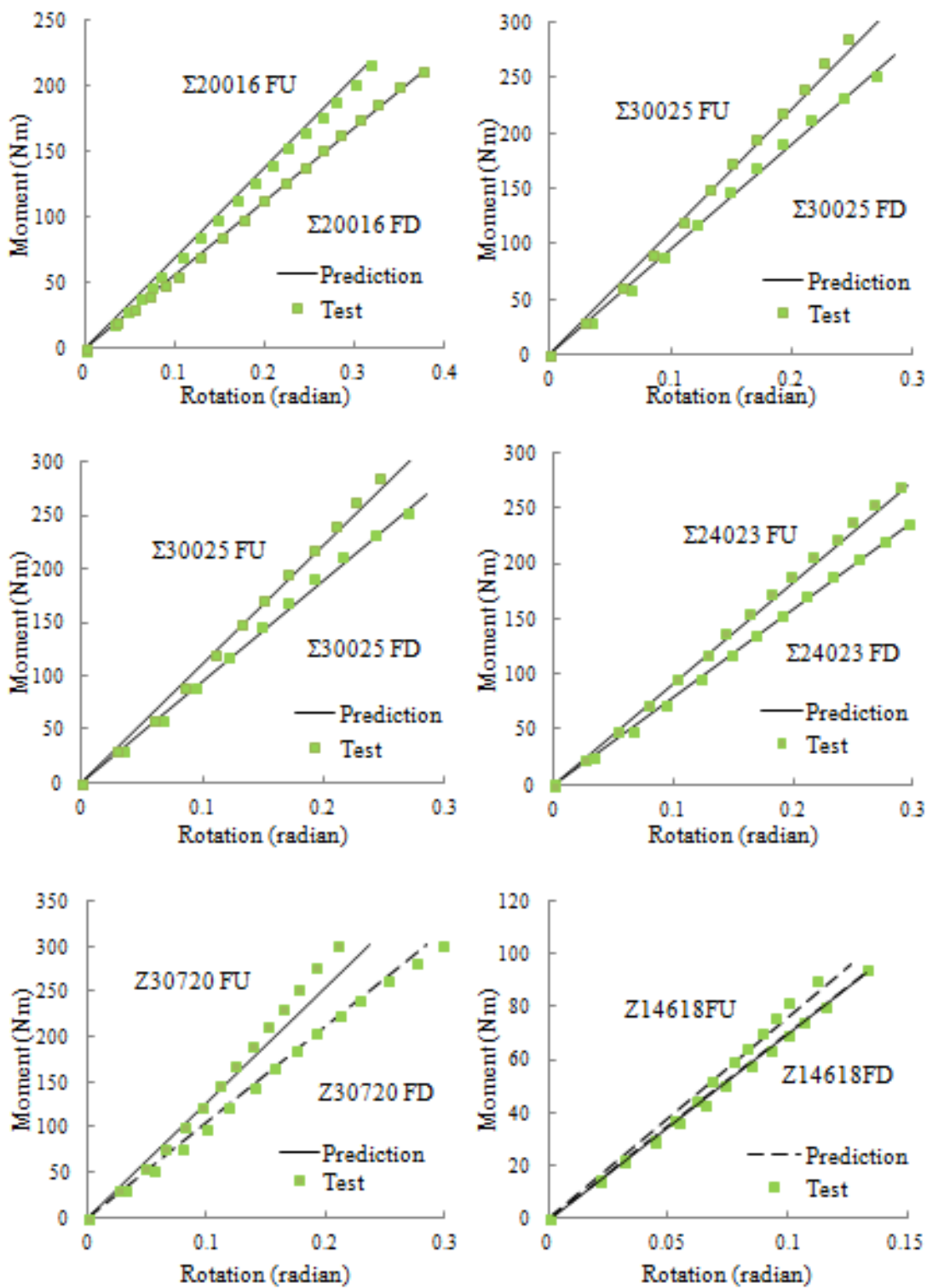
Figure 3-28: Moment-rotation relationships between test results and analytical predictions

It can be seen that $C_{D,A}$ from test and EC3 shows a noticeable variation, Test/EC3 ratio ranges from 0.52 to 1.93 (i.e. maximum difference 93%), with an standard deviation of 0.40. The difference does not have a direct relationship with purlin geometry or loading direction, and none of the sections has a significantly better EC3 result than the analytical prediction (Specimen Σ 30018 FD has almost same value for analytical and EC3 prediction values). Hence it is suggested that EC3 shows a lack of accuracy, which can either be unsafe or over-conservative, when used as a design tool for predicting rotational stiffness of purlin-sheeting connections.

For analytical prediction, consistently good agreement is achieved between the test and prediction results, which suggest that the analytical model can provide sufficiently accurate results for rotational stiffness. It is noted that the analytical model is a linear model, as can be seen from the derivation process. The test/prediction ratios from Table 3-5 have a standard deviation of 0.05and a maximum difference of 11%.

The last column in Table 3-5 shows the ratio of rotational stiffness between FU and FD, and it can be seen that the rotational stiffness in the FU condition is greater than that in the FD condition in all cases, regardless of the purlin's geometry.   The FD/FU ratio ranges from 0.72 to 0.92. This trend also agrees with the results based on the EC3 model. The cause of this trend can be easily explained by the additional term in the analytical model, i.e., Eqn. (3-8) and Eqn. (3-9). The term that causes the difference is $b/\mathrm{E}I_p$, which indicates that a purlin with a smaller b value or a larger thickness is likely to produce a notable difference under FD and FU conditions.
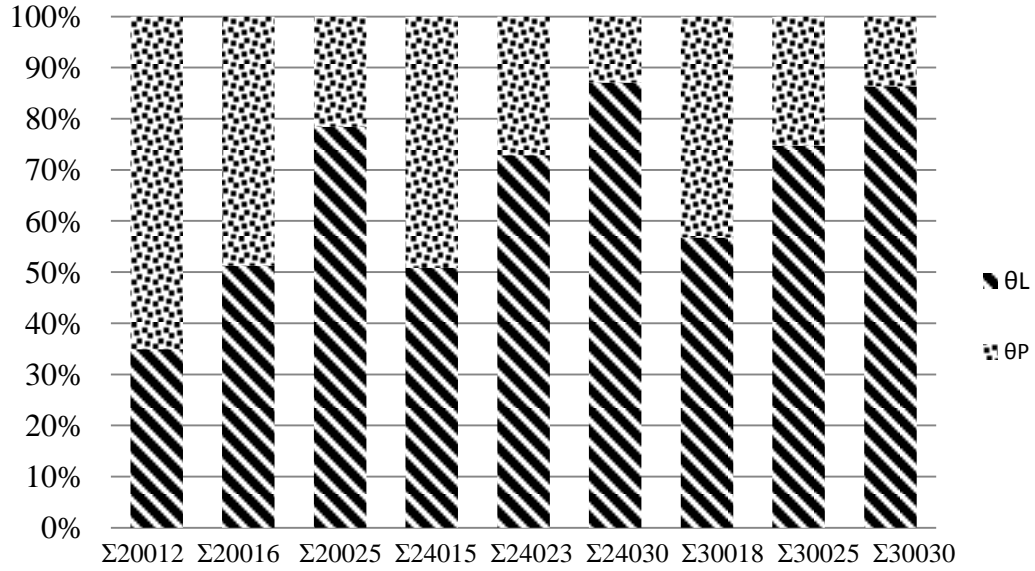
Figure 3-29: Proportion of θ_l and θ_p in overall rotation under FD for Σ- sections
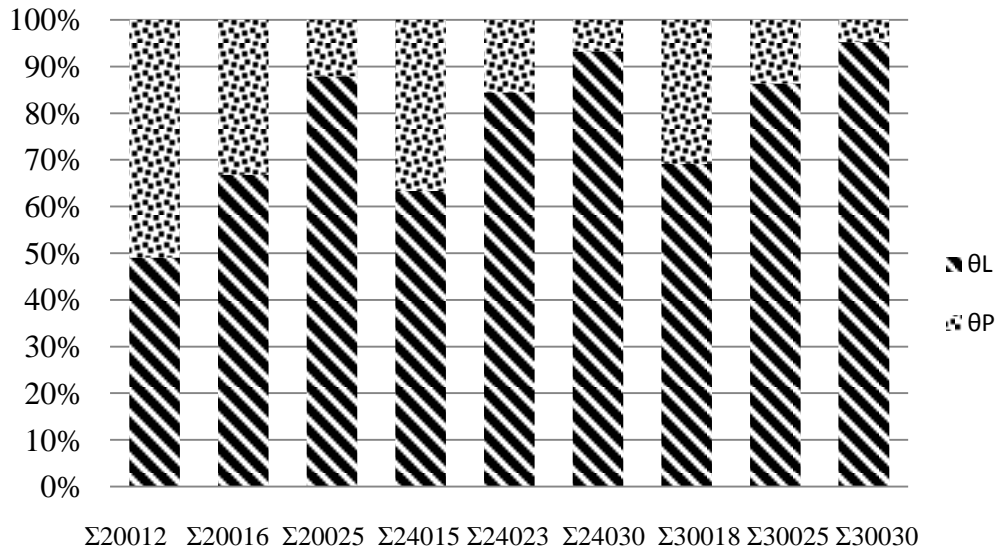
Figure 3-30: Proportion of θ_l and θ_p in overall rotation under FU for Σ- sections

Figure 3-31: Proportion of θ_l and θ_p in overall rotation under FD for Z- sections
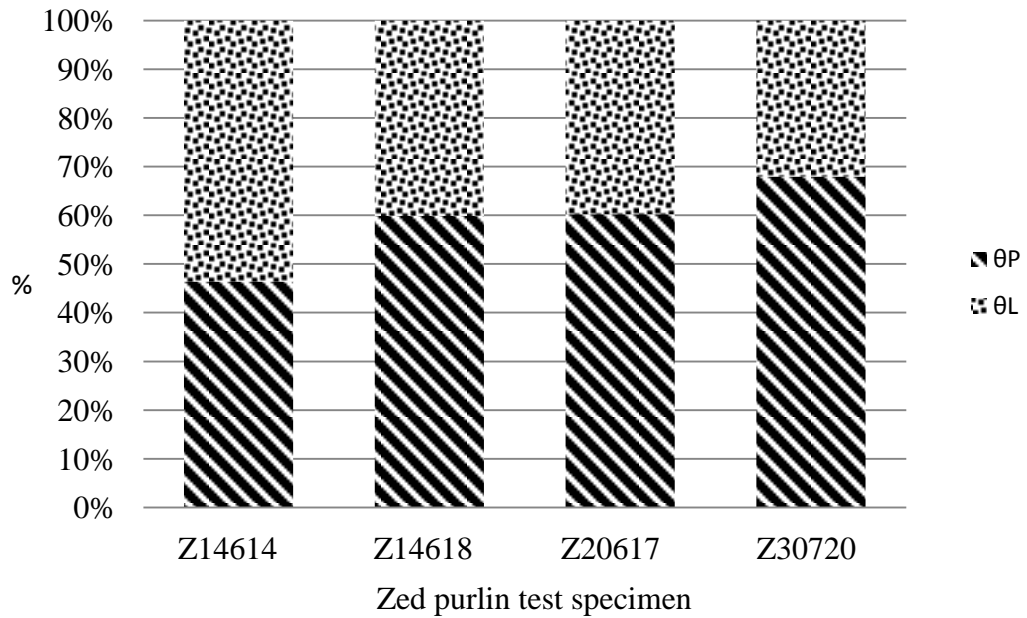
Figure 3-32: Proportion of θ_l and θ_p in overall rotation under FU for Z- sections

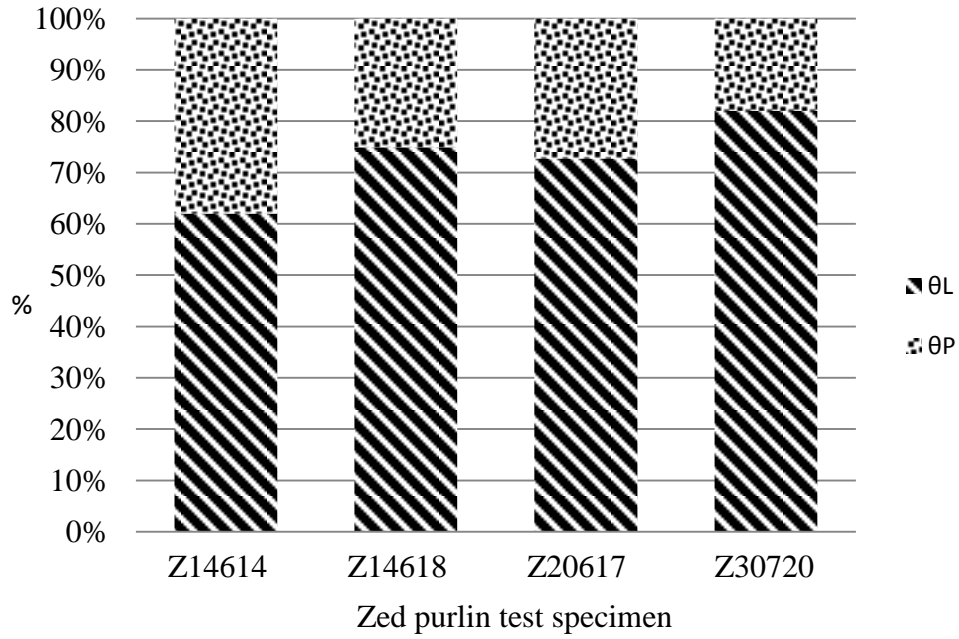The contribution of θ_l and θ_p to the overall rotation for Σ- sections is presented in Fig.3-29 and Fig.3-30, for the FD and FU conditions, respectively. In the FD condition, the proportion of θ_l ranges from 35% to 78% for 200 series sections, from 50% to 87% for 240 series sections and from 55% to 86% for 300 series sections. In the FU condition, this proportion has risen to 48%-88% for 200 series, 62%-92% for 240 series and 69%-96% for 300 series. In each series, this proportion will increase with the purlin thickness. This trend agrees with the fact that θ_l is due to the sheet deformation, while θ_p is due to the purlin flange panel deformation. The effect of flange width on the proportion of θ_l can also be observed from Figs.3-31 and 3-32. For instance, from section groups $\Sigma20025/\Sigma30025$ an $\Sigma24030/\Sigma30030$, the flange width rises from 62.5mm to 75mm, but the θ_l proportion in the FD condition varies from 79%/74% to 88%/86% and in the FU condition, from 88%/86% to 93%/95%. Therefore the effect of the flange width can be treated as insignificant.

3.5. Parametric study

The rotational stiffness of the purlin-sheet system depends on factors such as the thickness and profile of roof sheet, the cross-section of the purlin, the number of screws per unit length as well as the connection details (Katnam et al, 2007b). The analytical model developed in this paper has taken account of these factors, and it can therefore be used for parametric studies.

As discussed in the proceding section, θ_l and θ_p are related to the sheet thickness and purlin thickness, respectively. A group of Σ- sections with a depth 240mm and under the FD condition have been chosen as an example for parametric analysis. In Fig. 3-33, θ_l versus the sheet thickness curves for purlin sections of 3mm with various flange widths, ie. 62.5, 65, 75, 100 mm respectively, is presented. Similarly, Fig. 3-34 presents θ_p versus the purlin thickness curves for the same range of flange widths. On the basis of the results, the following observations can be made:

(1) θ_l declines with an increase in sheet thickness. The effect of sheet thickness on θ_l is more

90

notable for small t_s values, specifically, less than 0.6mm. The variation in θ_l caused by different flange widths C is inconclusive.

(2)   The effect of purlin thickness on θ_p has a similar trend to that of sheet thickness on θ_l. Additionally, when the purlin thickness is up to 1.5mm, this type of effect is particularly significant. The effect of flange width is only noticeable when the purlin thickness is rather small, e.g. up to 1.5mm.
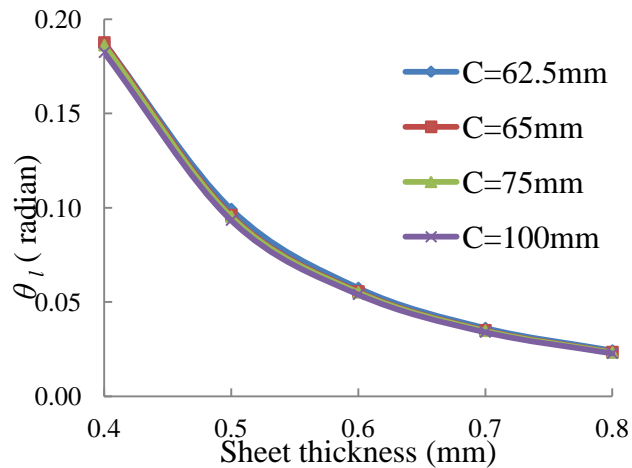

Figure 3-33: Relationship of θ_l with sheet thickness under different flange widths, C
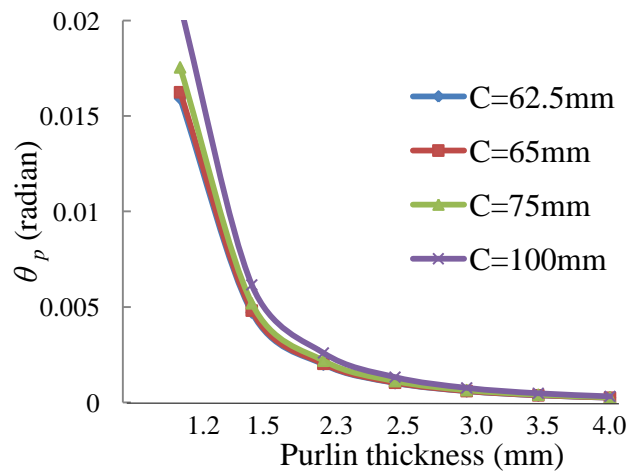
Figure 3-34: Relationship of θ_p with purlin thickness using different flange widths, C

3.6. Summary

An experimental programme to measure the rotational stiffness (F-test) was presented in this chapter. The test was adapted based on the EC3 specification and adjustments were made to measure the rotational stiffness at purlin-sheeting connection only. The test was carried out for a variety of geometries of Σ- and Z- sections and attached to a single sheet. The test was successfully conducted, and the corresponding rotational stiffness was derived from the moment-rotation curves at its linear range.

An analytical method to predict the rotational stiffness for cold-formed Z- and Σ-purlin/sheeting systems is developed and reported in this chapter. This new method considers the interactional effect at screw points as well as the effect of loading directions. The rotation in this method is divided into 4 components, namely: (1) θ_s, the rotation angle of the cantilever sheet under a row of concentrated moments generated at screw connection points; (2) θ_l, the rotation angle associated with the localised deformation of the sheet under the pulling force of each screw; (3) θ_k, the rotation angle due to the separation between the roof sheet and the purlin flange at the connection point; and(4) θ_p, the rotation angle due to the purlin flange bending. Whilst (3) is small enough to be assumed negligible, (1) is calculated based on cantilever beam theory (and then subtracted out from the result since it is irrelevant to the desired value); (2) is calculated on the basis of Levy's solution of single plate theory and (4) is calculated based on a slab bending theory.

It is found that the rotational stiffness is higher when the purlin is in contact with the sheet at the flange-web junction line than when the purlin touches the sheet at the flange-lip junction line. One of the reasons of this trend is that the latter case tends to have a shorter lever-arm, resulting in a high tensile force in the screws and hence a larger rotation. The method has been validated by a series of F-tests on both Z- and Σ- sections. A good agreement between the experimental and

analytical results (i.e., with an average difference of 4%) has been observed. The method provides a simplified means of predicting the rotational stiffness with high accuracy.

The main contribution from this chapter can be summarised as follows:

(a)   A set of F-tests have been conducted to measure the rotational stiffness of CFS purlin-sheeting system for both Z- and Σ- sections. The test is adapted based on EC3 specification, but with the use of dial gauges and inclinometers, this test can directly measure the rotational stiffness from moment/rotation relationship, instead of measuring the equivalent lateral stiffness K. By doing so to avoid unnecessary errors during the test process and thus provide a more accurate result.

(b)   The calculation model in EC3 is explained and adopted to predict the rotational stiffness. It has been verified with test results that the EC3 model lacks accuracy and can be either unsafe or over-conservative when use for design purposes.

(c)   In order to resolve this problem, a pure analytical method is proposed to predict the rotational stiffness of purlin-sheeting system at connection. The method can be applied to a wide range of CFS purlin with single sheet, regardless of the purlin geometry, sheet geometry and connection type and detail. The method simplified these factors into 4 components of rotations, and by working out the rotations of these components; the method is able to provide satisfactory results after test validation. This method also solves the problem of load direction by simplification and allowing for either way of purlin-sheeting contact.

Chapter 4: Verification and parametric studies of rotational stiffness prediction using Finite Element Method

4.1. Introduction

From Chapter 2 and Chapter 3, it is discovered that the rotational stiffness is an important parameter for the determination of the behaviour of CFS purlin-sheeting system. While conventional methods of predicting this value including experimental and analytical methods have shown a good level of accuracy, their limitations are unavoidable, such as its time-consuming progress or when the specimen does not meet analytical assumptions.

In this chapter, a FE model is established to investigate the rotational stiffness of cold-formed purlin-sheeting connection. The FE model is based on the F-test described in Chapter 3, with the presence of both purlin and sheeting sections. The screw at connection is represented with coupled nodes. The analyses performed include both geometric and material nonlinearities, and the relationship of moment-rotation are derived and compared with test data and analytical prediction introduced earlier.

In addition, parametric studies are carried out to further investigate the effect of roof sheeting on the integrated system. A new type of roof sheets with bulges, which is commonly used in the industry, is introduced and the effect of the sheet thickness is investigated. The results of rotational stiffness, localised displacement and stress distribution are compared with that of the ordinary sheet.

The numerical model provided in this chapter is believed to be a versatile option for engineers to attain more complete data information and results of higher accuracy. In addition, the chapter reveals convincing evidence on the significance of the roof sheet to purlin-sheeting system and can

have beneficial implications for the users on the selection of appropriate roof sheet.

This chapter consists of the following sub-sections: 4.2 introduce a FE model to replicate the experimental F-test. Detail of the model including element, material property, load and boundary conditions are explained, results are compared with test; 4.3 carries out a series of parametric study based on the existing FE model with regard to different sheeting profiles and thicknesses, results are summarised and compared with ordinary sheet; 4.4 summarises the findings of this chapter. This chapter is relatively short when compared to others, however the included findings are very practical and beneficial, and can be adopted directly to solve engineering problems.

4.2. Numerical modelling

Cold-formed steel section usually has very high width to thickness ratio, and hence is susceptible to buckling deformations. Shell element is the preferred option in analysing thin-walled structures because the membrane and bending deformations are of primary consideration for studying CFS members. A FE model is produced using ANSYS 13.0 Program (2007). The model is studied through the following stages: (i) the geometric model generation and discretisation into meshes; (ii) assigning the material properties and the loading characteristics; (iii) applying the end support boundary conditions and the contact details around the connection point and; (iv) the solutions schemes employed to derive non-linear behaviour of the structure.

4.2.1.   *Element type and meshing*

The aim of the establishment of this FE model is to replicate the F-test described in Chapter 3. For details of the test set-up and specimen properties one can refer to *Section 3.2.1* and *Section 3.2.2*. The general arrangement of the F-test is illustrated in Fig.4-1. The purlin is connected to trapezoidal sheet at every mid-trough. A multiple-point load is applied at the free purlin flange to

initiate an instant torsion. Both the purlin and the sheet are modeled using element SHELL181. The element is defined by 4 nodes, each having 6 degrees of freedom (i.e. 3 in translational directions and 3 in rotational directions). This type of element has been reported to provide good results in modelling cold-formed steel members with both material and geometry nonlinearity (ANSYS, 2007). Since the purlin-sheeting structure includes a repeated-wave sheet with identical geometry of every sheet trough and crest, as well as a purlin with consistent cross section geometry, the structure can be assumed under a uniform load and constant rotation along the length (the imperfection and the difference at screw point is assumed negligible). Therefore a cyclic model is used in the FE analysis instead of the complete structure (Fig.4-2). The cyclic model consists of a half wave-length sheet profile (that is the distance of mid-line between crest and trough due to the screw position) and the same width of purlin, symmetric boundary condition is applied for cross sections on both sides. This model arrangement has been verified with good accuracy yet greatly saved computational time (Katnam et al. 2007a and 2007b). Depending on the geometry and dimensions of purlin and sheet, different mesh densities are chosen through extensive trial-and-improvement process. The most satisfactory result was achieved using the following discretisation pattern for most sections: 6 elements in the purlin flange, 2 elements in the lip, 4 elements in the outer web, 10 elements in the inner-web, 1 element in all the corner except for where the interaction occurs between purlin and the sheet, 4 elements are applied to the corners to reduce stress concentration. A uniform mesh of 15 is used for the sheet area, as seen in Fig.4-2. For the screw point, finer mesh is applied at the screw position (Fig. 4-3) to avoid unnecessary convergency difficulties. The size of the half circle has the same diameter as the neoprene washer used in the test. The outer ring represents the size of neoprene washer and the inner ring represents the size of the thread. After meshing, any nodes

96

within the inner ring are coupled in all directions between purlin and sheet to simulate the effect

of screw; whereas the outer ring has no restraints applied.

Figure 4-1: General arrangement of F-test
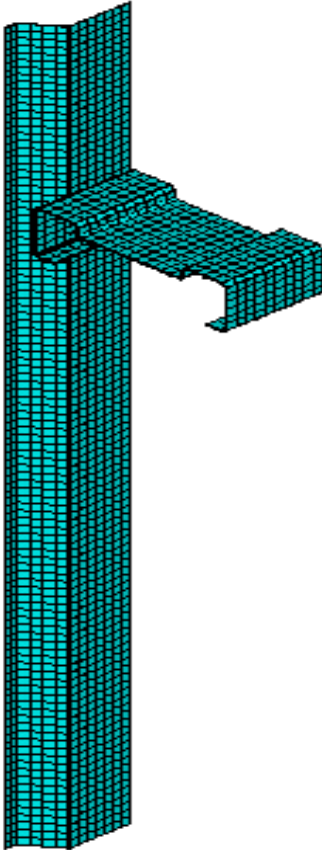
Figure 4-2: FE model and mesh pattern of F-test
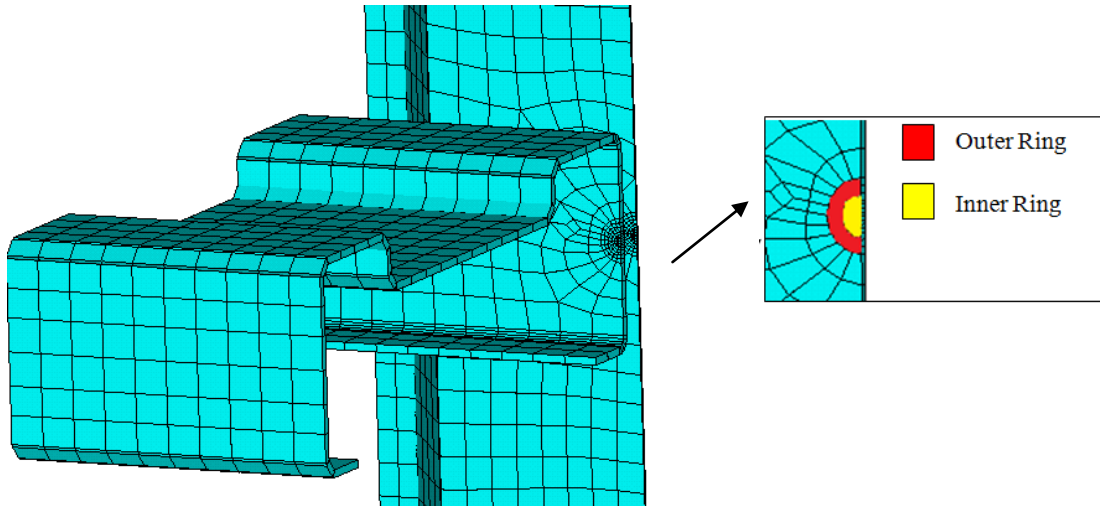
Figure 4-3: Mesh pattern at the screw connection

4.2.2. *Material property*

Both sheet and purlin are modeled as non-linear materials. For sheet, a linear elastic-plastic model was applied with Young's Modulus and Poisson's ratio was assumed as 2.1×10^5 N/mm^2 and 0.3, respectively. An idealised stress-strain curve with the yield strength 235N/mm^2 of the sheet and an elastic-perfectly plastic behaviour is assumed for the material.

For purlin, the same Poisson's ratio 0.3 is applied. The Young's Modulus and the nonlinear stress-strain curve were derived from a steel coupon test, and true stress-strain curve is modeled using a multi-linear isotropic hardening scheme with Von-Mises yield criterion. A typical curve of the stress-strain is provided in Fig.4-4. It is to note that the tensile tests were originally conducted by Liu (2012). The rest of the test curves can be found both in his PhD thesis and author's reference in section Appendix A-1, Chapter 3.
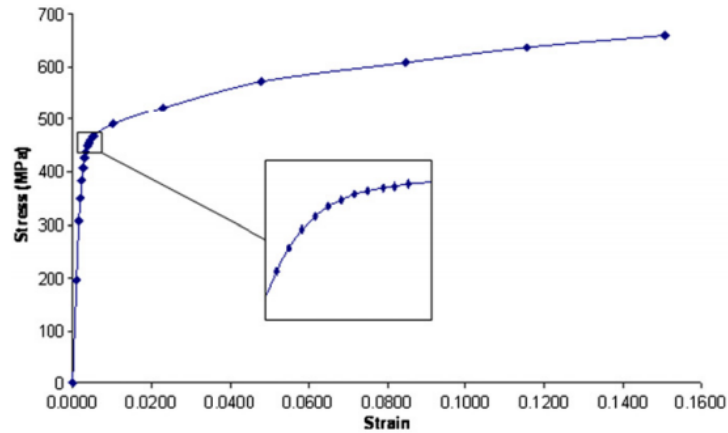
Figure 4-4: A typical stress-strain curve for thin-walled purlin section

4.2.3.   *Loading and boundary conditions*

The afore-mentioned symmetric boundary condition is applied for the cyclic model as shown in Fig. 4-5. The nodes along the boundaries of both sheet and purlin cross sections are constrained such that the displacement to the Z-axis and rotations to about the X-axis and Y-axis are zero. At the bottom of the sheet, a line of nodes where the bolts positioned were fully restrained along the width of sheet trough to achieve a rigid support. A point load is applied at the mid-flange of the purlin's free end.

At the contact line, the purlin and sheets are constrained at their matching nodes in all but vertical directions at the purlin's corner wherever it touches the sheet trough, i.e. flange-lip corner when purlin is facing downwards; and flange-web corner when purlin is facing upwards. In this way, the purlin cannot penetrate into the sheet but free to slide. This restraint is to ensure that no relative movement between purlin and sheeting, apart from vertical Y-Y direction, occurs during loading, since restrained purlin flange would shift upwards due to the rotation initiated by the free end load (amplified image in Fig.4-5).
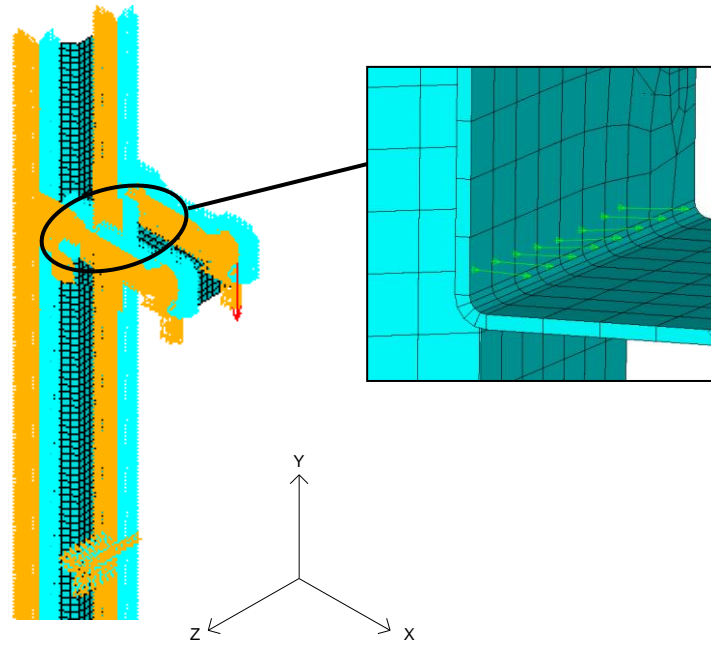
Figure 4-5: Boundary condition for the FE model

At the screw point, the hole has a radius of 2.75mm and the neoprene washer has a radius of 6.5mm. After meshing, any nodes within the inner ring are coupled in all directions between purlin and sheet to simulate the effect of screw.

4.2.4. Solution scheme

Since the concentrated load is applied at the free purlin flange, a deformation can be initiated immediately from the first sub-step of loading. This indicates that there is no need of a linear stability analysis using Eigen-value analysis and thus no imperfection would be included in this case.

A numerical incremental-iterative technique, Newton–Raphson's method was adopted because no convergency are to be considered at this stage and the cyclic integrated model presented in this case is relatively simple and stable; load control is used to monitor the load-displacement relationship..

4.2.5.   Results and discussion

The results were validated with experimental data and a comparison of rotational stiffness is summarised in Table 4-1 with details. The results are derived as moment-rotation relationships and $C_{D,A}$ values are determined when the applied load causes a free purlin lateral displacement equals to *1/10* of the purlin web depth. To replicate the F-test, rotations are measured at both ends of the purlin's web so that the difference between the two can exclude the effect of purlin web distortion. Rotation caused by sheet cantilever deflection is also eliminated from the overall rotation for ease of data comparison.

In Table 4-1, $C_{D,A}$ values derived from F-test data, analytical prediction as well as FE model are summarised for both Σ- and Z- sections. Numerical method is used as a validation for both the experimental and analytical method, along with the comparison ratios. An obvious increasing pattern can be observed for $C_{D,A}$ value with the increase of purlin thickness. A good agreement is generally obtained from all three depth series for the Σ- group, the standard deviation between test/numerical ratio and prediction/numerical on all cases are 0.045 and 0.062, respectively. The ratio, however at close inspection, did tend to differ when purlin geometry increases in terms of both flange width and thickness, i.e. for Σ- section 20025FD and 30025FD, the numerical/prediction ratio increases from 1.04 to 1.12. The average standard deviation for 300 series is 0.05 for test/prediction ratio and 0.08 for numerical/prediction ratio, both are larger than those of smaller sections. The same pattern is also observed for Z-sections. One reason for this discrepancy is caused by neglecting the rotation caused by purlin-sheeting separation at connection point, which may underestimate the overall rotation and result in a larger $C_{D,A}$. Another reason is the negligence of steel and neoprene washer in the numerical model. The purpose of using washers with the screw is to prevent possible leaking from the roof as well as

avoid local failure by reducing regional stress concentration around the screw point. Without this, a more severe local deformation may cause excessive rotation and result a smaller $C_{D,A}$. Therefore the ratio value would swing either way about 1.0 depending on the whichever dominating effect on the overall rotation.

The structural deformation of purlin-sheeting FE model is provided in Fig.4-6 and the von Mises stress distribution is presented in Fig.4-7a. As can be seen, maximum stress occurs around the connection point. Severe plastic deformation of the sheet near the screw point is observed, the stress reduced gradually around this point. At the crest of the sheet, the stress is small when compared to the sheet trough as seen on the colour histogram (Fig.4-7b). For the ease of illustration, these stress distributions are measured when the applied load leads to nonlinear deformation of the structure, however similar pattern can be found at all loading levels. The stress distribution in the purlin shows a uniform patter along the width and the length (x-x direction) of the purlin, suggesting that purlin is under distributed bending moment. Purlin flange-web corner is under relatively high stress but no sign of yielding. All these observations suggest that the stress, and thus the strength of purlin sheeting system can be affected by: (a) connection details; (b) sheet yield strength and geometry; and (c) purlin yield strength and geometry (of restrained flange). It is to note that no difference in rotational stiffness is observed for Σ- and Z- section unless for the above-stated factors since the varied web stiffeners are not considered in this chapter. However due to its nature of different geometry, Σ- and Z- sections may have a diverse behaviour under external load (Fig.4-8). The users should determine the way of contact under different loading directions prior to any analysis. For example, when under gravity load, Σ- purlins is in contact with sheet at its flange-web corner, whilst Z- section may contact with the sheet in either way depending on screw position, purlin geometry and the loading magnitude.

A complete comparison of moment-rotation in the linear range for all specimens is presented in Appendix A-3.

With the use of FE model, a detailed comparison to analytical method for each components of the rotation can be carried out. An example of Σ-20025FD is provided in the Appendix A.4.
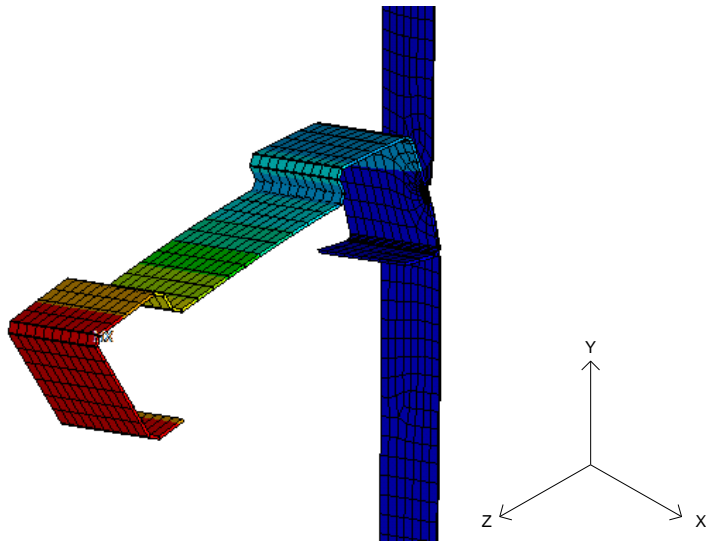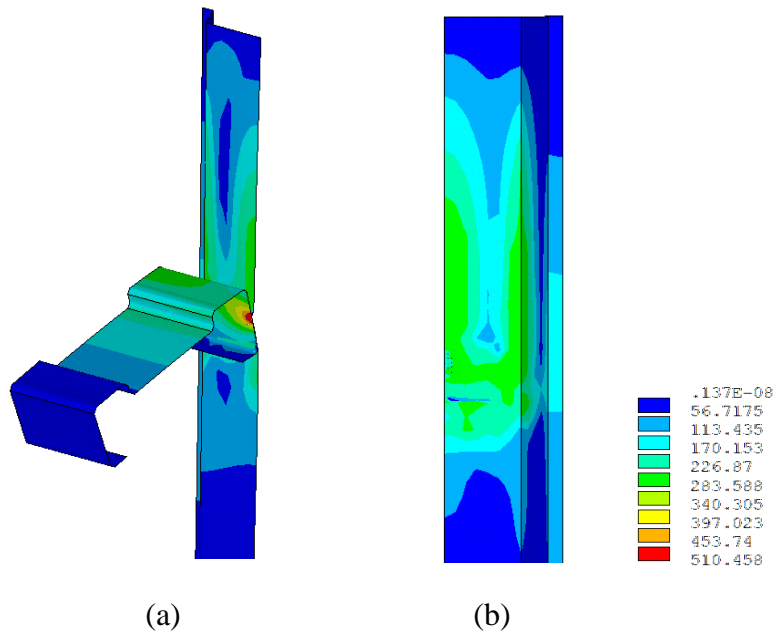

Figure 4-6: Structural deformation in the FE model

(a)   (b)

Figure 4-7: von Mises stress distribution in the FE model

Table 4-1: Comparison of rotational stiffness $C_{D,A}$ values

Specimen Name	Web depth mm	Flange width Mm	Thickness mm	$C_{D,A}$ Test Nmm/rad/mm	$C_{D,A}$ Prediction Nmm/rad/mm	$C_{D,A}$ Numerical, Nmm/rad/mm	Numerical /Test ratio	Numerical /Prediction ratio
Σ20012 FD	200	62.5	1.26	394	403	413	1.05	1.02
Σ20012 FU	200	62.5	1.26	508	502	503	0.99	1.00
Σ20016 FD	200	62.5	1.58	622	607	590	0.95	0.97
Σ20016 FU	200	62.5	1.58	691	772	712	1.03	0.92
Σ20025 FD	200	62.5	2.42	895	930	931	1.04	1.00
Σ20025 FU	200	62.5	2.42	1024	1048	1091	1.07	1.04
Σ24015 FD	240	62.5	1.50	593	588	612	1.03	1.04
Σ24015 FU	240	62.5	1.50	696	731	716	1.03	0.98
Σ24023 FD	240	62.5	2.24	848	860	857	1.01	1.00
Σ24023 FU	240	62.5	2.24	1009	987	967	0.96	0.98
Σ24030 FD	240	62.5	2.97	909	939	950	1.04	1.01
Σ24030 FU	240	62.5	2.97	1047	1090	1031	0.98	0.95
Σ30018 FD	300	75	1.80	735	672	684	0.93	1.02
Σ30018 FU	300	75	1.80	753	805	760	1.01	0.94
Σ30025 FD	300	75	2.32	921	883	992	1.08	1.12
Σ30025 FU	300	75	2.32	1078	1002	1064	0.99	1.06
Σ30030 FD	300	75	2.99	977	1023	985	1.01	0.96
Σ30030 FU	300	75	2.99	1191	1108	1261	1.06	1.14

Z14614 FD	145	62.5	1.56	512	557	511	1.00	0.92
Z14614 FU	145	62.5	1.54	762	717	766	1.01	1.07
Z14618 FD	145	62.5	1.78	730	723	727	1.00	1.01
Z14618 FU	145	62.5	1.78	820	889	805	0.98	0.91
Z20617 FD	200	65	1.78	680	674	658	0.97	0.98
Z20617 FU	200	65	1.71	876	868	819	0.93	0.94
Z30720 FD	300	75	2.08	940	810	843	0.90	1.04
Z30720 FU	300	75	2.08	1184	958	1031	0.87	1.08

* Σ represents sigma shaped purlin section, FD and FU represents the Facing Downwards and Facing Upwards of the purlin position when connected to sheet.

** $C_{D,A}$ value was derived from moment-rotation curve for Test and Numerical data where the load causes a purlin free flange deformation of 1/10 of web depth.
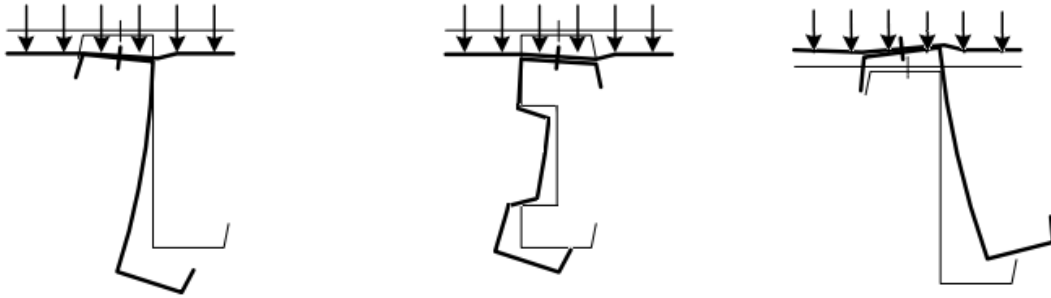
Figure 4-8: Deformation of Z- and Σ-sections under gravity load (adapted based on EC3

1993-1-3:2006)

4.3. Effect of sheet on the rotational stiffness of purlin-sheeting system

4.3.1. Introduction

Following the satisfactory validation of the above-mentioned numerical modelling, this FE model is then extended to cases where analytical and experimental methods have limitations. In this section extensive parametric studies are carried out to investigate the effect of sheeting on the overall performance of cold-formed purlin-sheeting system based on the similar results derived in the previous section between Σ- and Z- sections, only Σ- purlins are studied herein. The aim of presenting this database is to show that: (1) numerical method, once been validated by experimental results, can be used independently to predict the rotational restraint of CFS purlin system with single sheets and; (2) the effect of sheeting on the purlin system is significant, $C_{D,A}$ value can be sensitive to roof sheet shape and thickness.

By using FE model to select appropriate sheet type and thickness in engineering applications, users can be benefited greatly in terms of labour, material consumption as well as construction duration.

4.3.2. Different sheet profiles

It has been confirmed that sheet profile and geometry have an impact on the performance of purlin-sheeting system. For most analytical method, only first generation roof sheet with

regular profile can be used in the calculation model. However with further industrial development, sheet with more intermediate stiffeners and complex profile have become popular as it can provide a higher strength compare to conventional members. In this particular case it is the sheet that has a plurality of upwardly protrusive bulges (Fig.4-9). The bulges, when fastened with self-drilling screws, cannot come into full contact with the purlin along the width and therefore it is not practical to adopt ordinary analytical formulae when predicting the rotational stiffness and overall strength.
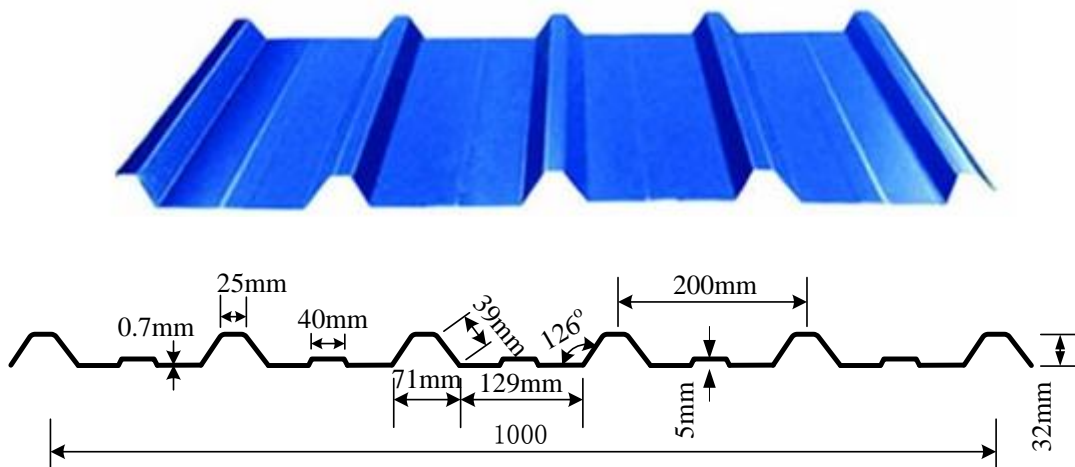

Figure 4-9: Profile of the sheet with bulges (type 2)

If the ordinary flat sheet is type 1 and the sheet with bulges is type 2, then FE model used for type 1 sheet is used for type 2 only with a change of the sheet profile with all the other conditions remain the same as seen from Fig. 4-10.
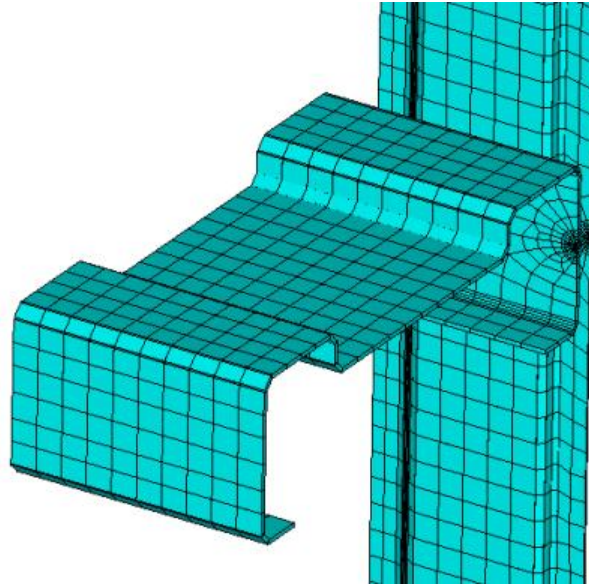
Figure 4-10: Rotational restraint test FE model for type 2 sheet (with a bulge in the mid-trough)

4.3.3.   Various sheet thicknesses

With more complicated profile, the trend in the industry is to save more material by reducing the roof sheet thickness while maintaining the strength level. Variation of the trapezoidal sheet thickness can be another factor that could affect the rotational stiffness of sheet purlin. In this section, a FE model, based on the above cyclic purlin-sheeting model, was established with a different sheeting profile. Three different sheet thicknesses, i.e. 0.5mm, 0.6mm and 0.7mm are parametrically investigated.

### 4.3.4.   Results and discussion

As Table 4-3 indicates, when using type 2 sheet, rotational stiffness $C_{D,A}$ reveals a noticeable increase when compared to normal trapezoidal (type 1) sheet. This is because the stiffening effect presented in type 2 sheet. The additional folds increases the rotational restraint, and thus the overall strength of the structure by an interaction of bending moment and its reaction that causes a stress combination in the sheeting. A comparison of at same loading level of both sheet types is presented in Fig. 4-11 below with von Mises stress distribution for sheet thicknesses of 0.7mm, 0.6mm and 0.5mm.   It is clear that under same loading level, type 2 has

experienced a less stress around the connection area, which tends to fade away dramatically at the place where the folds are presented; whilst type 1 has a much larger affected area. With using different thicknesses, type 2 sheet does not show a noticeable difference in the stress distribution; the change stays within a local area around the screw. Type 1, however, has an obvious increasing stress pattern with the reduced of sheet thickness. A simple comparison of the maximum localised deformation at screw point of both sheets is provided in Table 4-2 below.
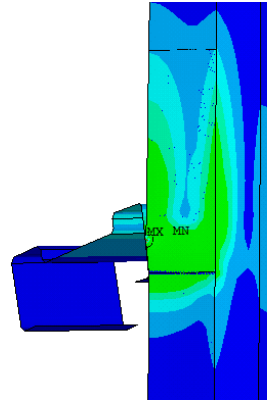
In terms of the $C_{D,A}$ values, it can be learnt from Table 4-3 that $C_{D,A}$ value of type 2 sheet at 0.5mm is similar or even higher than that of type 1 sheet at 0.6mm, which indicates a roof sheet with extra folds can use less material than a first generation sheet yet still achieve equivalent strength. This finding can have beneficial meanings for practical use. Also from the numerical analysis, it was found that type 2 sheet could provide the purlin with a 50% higher strength than that of type 1 sheet. This comparison will be carried out in the next chapter where full-scale purlin-sheeting system is to be investigated.

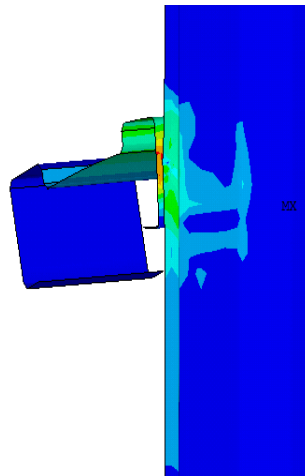Table 4-2: A comparison of sheet localised deformations at screw point

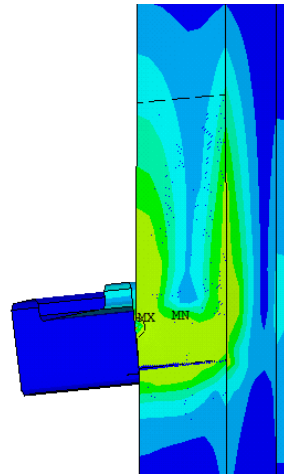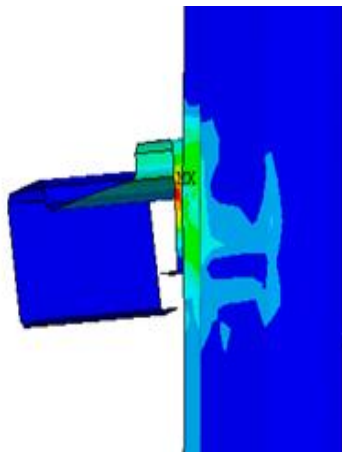| Sheet thicknesses	Type 1 (mm)	Type 2 (mm)	Type 1/Type 2 ratio
0.7mm	2.2	4.2	1.9
0.6mm	2.4	5.6	2.3
0.5mm	3.0	6.4	2.1
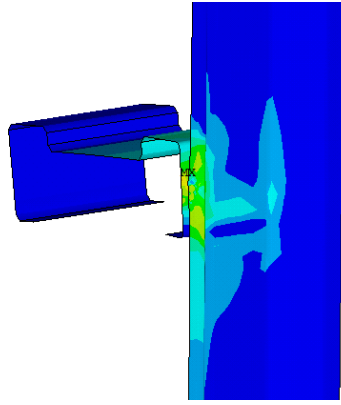
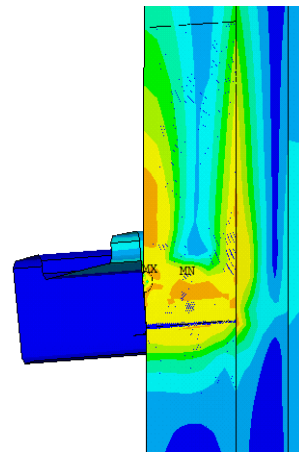(a) 20025 type 2 sheet 0.7mm   20025 type 1 sheet 0.7mm

(b) 20025 type 2 0.6mm   20025 type 1 0.6mm

(c) 20025 type 2 0.5mm   20025 type 0.5mm

Figure 4-11: A comparison of von Mises stress distributions of different sheet profiles under

same loading level

Table 4-3: Rotational stiffness at purlin-sheeting connection with various sheet type and thicknesses

Section	Type 2 sheet 0.5mm	Type 2 sheet 0.6mm	Type 2 sheet 0.7mm	Type 1 sheet 0.5mm	Type 1 sheet 0.6mm	Type 1 sheet 0.7mm	Type2/ Type 1 0.5mm	Type2/ Type 1 0.6mm	Type2/ Type 1 0.7mm
20012FD	380	419	462	315	387	413	1.21	1.08	1.12
20012FU	537	621	683	401	463	503	1.34	1.34	1.36
20016FD	556	688	812	406	458	590	1.37	1.50	1.38
20016FU	725	937	1160	425	557	712	1.71	1.68	1.63
20025FD	738	955	1210	561	736	931	1.32	1.30	1.30
20025FU	895	1160	1465	678	893	1091	1.32	1.30	1.34
24015FD	574	692	774	436	551	612	1.32	1.26	1.26
24015FU	721	913	1081	465	612	716	1.55	1.49	1.51
24023FD	855	1072	1319	558	703	857	1.53	1.52	1.54
24023FU	950	1172	1462	631	775	967	1.51	1.51	1.51
24030FD	916	1191	1476	572	774	950	1.60	1.54	1.55
24030FU	936	1217	1549	615	801	1031	1.52	1.52	1.50
30018FD	762	918	1050	499	592	684	1.53	1.55	1.54
30018FU	985	1246	1503	502	638	760	1.96	1.95	1.98
30025FD	1026	1286	1567	649	815	992	1.58	1.58	1.58
30025FU	1192	1521	1850	674	836	1064	1.77	1.82	1.74
30030FD	1098	1398	1732	625	786	985	1.76	1.78	1.76
30030FU	1228	1597	1968	786	1035	1261	1.56	1.54	1.56

4.4. Summary

A FE model is established to replicate the rotational restraint test described in Chapter 3. The model is generated using ANSYS program, both purlin and sheeting are modelled using shell element. The effect of screw is substituted by using lateral spring elements. The results of rotational stiffness are compared with test value and analytical prediction, a close agreement was found among them for both Σ- and Z- section.

Follow the satisfactory results of numerical simulation; the model is used to carry out parametric studies to investigate the effect of roof sheet on the rotational stiffness value. A special sheet profile with bulges is presented with 3 different thicknesses, 0.5mm, 0.6mm and 0.7mm. Results of $C_{D,A}$ values are given in relative sections, discussions of the sheet effect on rotational stiffness, stress distribution as well as localised deformation are provided.

With the findings from this chapter, the following conclusions can be made:

5. The numerical model is a useful tool in predicting rotational stiffness of purlin-sheeting system. As long as the geometry and material properties of the specimens are known, FE model can provide very close results when compared to test data, and can also provide a guidance for some cases where test and analytical method cannot be used;

6. The numerical model can provide a very detailed and visual presentation to studying the interactional behaviour of CFS purlin-sheeting system. Because the FE model only looks at the rotational restraint at screw point, it has no difference in terms of the purlin geometry (i.e. Σ- and Z- sections). Further studies can be carried out based on this FE model, such as to look at the rotational stiffness when considering purlin web-distortion (obviously in this case purlin geometry would have an impact on the rotational stiffness), ultimate load and post-failure behaviour of the screw point as well as the entire system, etc.

7. The sheet geometry and thicknesses have a significant impact on the rotational stiffness of purlin-sheeting system. More stiffeners provided in the sheet profile would achieve a higher rotational stiffness and vice versa; thicker sheet would also achieve a higher rotational stiffness and vice versa. Therefore with the use of complicated-profiled sheet, a thinner sheet can be adopted to achieve similar strength to that of a thicker, ordinary sheet. This model can be used by users to select the appropriate combinations of the roof sheeting so that an optimum solution can be provided.

The sheet would also have an impact on the purlin's load-carrying capacity; this will be compared and discussed in Chapter 4 for full-scaled systems.

Chapter 5: Load-carrying capacity of CFS purlin-sheeting system

5.1. Introduction

In this chapter, the load-carrying behaviour of CFS purlin-sheeting system is investigated via experimental and numerical approaches. The investigation is divided into three parts: firstly, a four-point bending test of Z- section with discontinuous sheet attachment. The test was carried out to examine the load-carrying capacity of Z purlin when partial (or insufficient) restraint was applied and distortional buckling may be the initiated buckling mode; Secondly, a UDL transverse loading test of Σ- purlins with continuous sheet attachment. The test was carried out to examine the load-carrying capacity of Σ- purlin when full (or sufficient) restraint was applied to the structure; finally finite element method was used to create a simulation to both of the experiments. In these FE models, the effect of sheet was either modelled using shell element (full model) or replaced by spring element (simplified model) with the rotational stiffness $C_{D,A}$ derived in section 3.2.5. The differences between full model and simplified model are studied in term of the stiffness of the structure, load-carrying capacity, buckling behaviour and failure modes. The validated FE model was then used to conduct parametric studies with various rotational stiffness and purlin spans.

The key research findings in this chapter are:

(a) When a purlin is inadequately restrained (i.e. unrestrained at constant moment span) under transverse bending, distortional buckling is likely to initiate structural instability, causing a significant reduction to the load-carrying capacity of the structure. It is found that EC3 does not provide an appropriate calculation for this particular situation, leading to an unsafe prediction when considering it as a single purlin or an over-conservative prediction when considering it as a purlin-sheeting system. A more suitable design method is required;

(b)When a purlin is restrained by continuous sheet attachment, local buckling is the primary buckling mode, followed by distortional buckling.

(c) FE models are able to produce and replicate test results for both test conditions with a high level of accuracy. A close agreement of ultimate load is found between the test and the simplified model. However for predicting member flexural stiffness and buckling modes, the simplified model is less satisfactory than the full model but can still provide design guidance for practical application;

(d) When carrying out parametric studies using existing FE models, it is found that rotational stiffness has a significant impact on the load-carrying capacity of the purlin-sheeting system. In addition, for studying double span purlin-sheeting systems, the FE simplified model can be used as a reliable guidance for strength prediction.

The chapter consists of following sections: 5.2 presents a series of four-point tests of Z-purlin with discontinuous sheeting, results are derived and compared with EC3; 5.3 generates a validated FE model based on the Z-test; 5.4 presents a series of UDL load test of Σ-purlin with continuous sheeting, results are derived and compared with a similar programme conducted by Yang and Liu (2012); 5.5 provides a validated FE model based on Σ- test with both simplified and full models, comparisons are made and more parametric studies based on these findings are given in 5.6. Summaries and findings are listed in 5.7.

5.2. Z- Purlin section with discontinuous sheet attachment

5.2.1. Introduction

Trapezoidal sheeting is usually applied to roof purlins to provide both lateral and rotational restraint through self-drilling or self-tapping screw connections. However in building engineering practice, where a full restraint to the purlins cannot be provided (for instance, due to the inadequate local stiffness of roof sheeting), a possibility of local,

lateral-torsional, distortional buckling or a combination of them would still take place under the external loading. In the EC3 design code, it allows the interaction between the local and distortional buckling, which is the most common failure mode for flexural members under bending. However when it is fastened with roof sheet, the buckling mode of purlin can be very different due to the interacting behaviour of purlin and sheeting at connections. This may change the buckling behaviour of the purlin and thus affect its load-carrying capacity. In most cases, full restraint is unlikely to take place so purlins are under a partial restraint instead. In some cases, distortional buckling can occur prior to local buckling, become the predominant buckling mode when the purlin is partially restrained by sheeting. Distortional buckling can lead to a significant lowering of the elastic critical load for cross sections such as Σ- members (Roberts and Jhita, 1983).

In order to replicate this condition, a series of single span, four-point bending tests of Z-purlins with restrained sheeting were carried out, after a similar study by Yu and Schafer (2007). The significance of this experiment is that the purlin is only restrained at its shear span, where distortional buckling is encouraged to occur within constant bending zone. A combined effect of local and distortional buckling is expected and the resulting loading capacities are compared with EC3 prediction. In addition, numerical simulations are established to simulate the test, with the use of rotational springs to replace the sheeting effect on purlin. Both the load-carrying capacity and failure buckling mode of the purlin-sheeting system under gravity loading are studied.

5.2.2. *Test Specimens and apparatus*

Four common sizes of CFS Z- sections are used in the tests. The geometry details of each test specimen is summarised in Table 5-1.

Table 5-1: Properties of test specimens: Z- sections
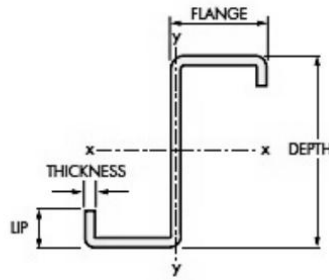
Specimens:	Depth (mm)	Flange (mm)	Lips (mm)	Thickness (mm)	Area (cm^2)	Z_{xx} (cm^3)
Z14614	145	62.5	20	1.4	4.26	19.83
Z14618	145	62.5	20	1.8	5.45	25.21
Z20618	200	65	20	1.8	6.53	39.56
Z30718	300	75	20	1.8	8.69	74.51

The apparatus used in the test and their functions are listed as follows:

- 1x Grant data logger – to collect the obtained test data and sent to computer

- 6x LVDTs – max. range 25mm for measuring vertical and horizontal displacement

- 1x load cell – for load measurement, with maximum capacity of 100kN

- 1x loading jack – to apply load onto the samples

- 4x dial gauge – to measure vertical and horizontal displacements

- 2x anti-sag bars– for each sample to prevent lateral buckling occurring in the purlins

- 2x steel sheeting – for each sample

- 2x rectangular hollow section (RHS) 3"x6"

- 1x RHS 4"x6"

- 4x timber block – to fill the gap between the purlin and bracing

M10 bolts are used for Z14614 and Z14618 sections while for the Z20618 and Z30718 section M16 bolts are used.

5.2.3. Test set-up and procedure

The test arrangement is shown in Fig. 5-1. Vertical downward loads were applied on the roof system (purlin-sheeting) via loading machine at 1/3 and 2/3 points of the purlin span (Fig.5-2). As a result, a pure bending zone was created at the mid-span with zero shear force. Load was applied in increments until failure. Load-deflection graphs were recorded for each specimen.
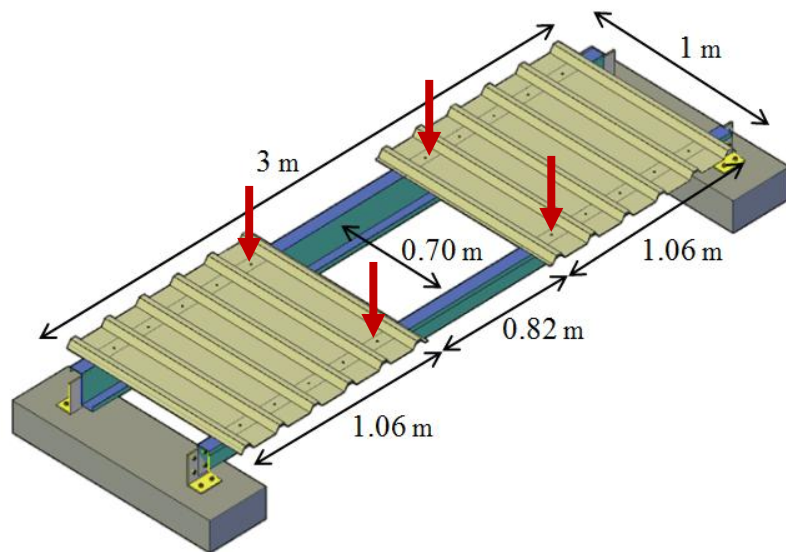

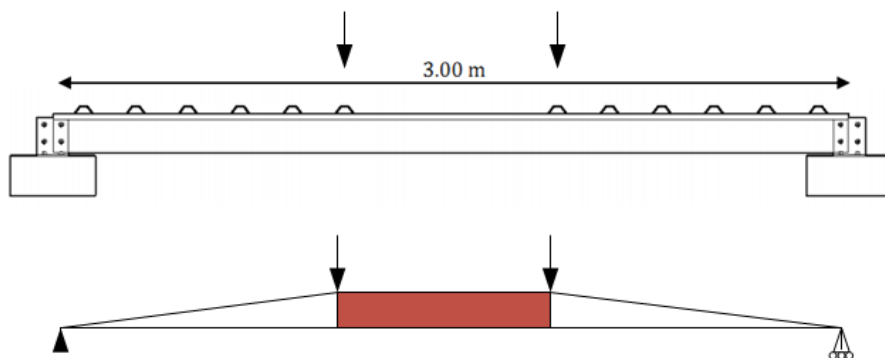Figure 5-1: An overview of the multi-point loading test arrangement

Figure 5-2: Elevation view and bending moment diagram of the test arrangement
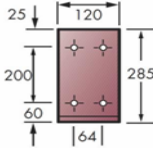
Figure 5-3: Anti-sag bars arrangement   Figure 5-4: Loading arrangement
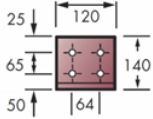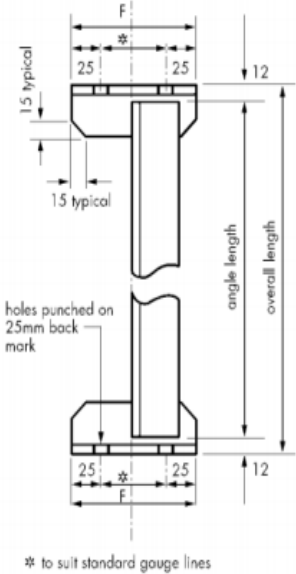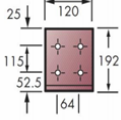
A pair of identical 3.0 metre Z purlins were positioned in parallel and facing each other, with a web-to-web distance of 0.66m. Purlins were fixed at both ends by using M10 bolts and cleats onto a concrete block to produce a simply support; purlins were connected to each other with a pair of anti-sag bars cross over below the loading points to provide sufficient lateral restraint (Fig.5-3); timber blocks were placed in the gap between purlin's web and the anti-sag bars to eliminate unwanted displacement and reduce possible stress concentration that may occur at the anti-sag bar connection point. In addition, distortional buckling instead of overall lateral buckling is likely to occur in sections where the lateral movement of the member is restrained by intermittent bracing and anti-sag bars (Ellifritt et al. 1998). The standard cleats and anti-sag bars for each size of purlins varied are provided in Table 5-2 below.

The same single skin corrugated sheets used in F-test in Chapter 3, i.e. 1070mm x 1000mm x 0.7mm were used in this case to partially connect the pair of purlins on their mid flange lines. As illustrated in Fig.5-4, the purlins are unrestrained in the constant moment span and are restrained on every trough of the sheet in the shear spans. In this way, distortional buckling and local buckling are allowed to occur only in the middle-span of the structure.

Table 5-2: Properties of cleats and anti-sag bars

Specimen Types	Cleat dimension (mm)	Anti-sag bar standard gauge line centres (mm)	Anti-sag bar head width, F(mm)	
Z146 series		65	115	
Z206 series		115	165	
Z307 series		200	250	

A direct downward loading transferred into four concentrated loading was applied by a loading jack onto the structure, the loading arrangement is shown in Fig.5-4. Six linear variable differential transformers (LVDTs) were used to monitor the deflection of the purlin-sheeting structures, four of which measured the vertical deflection of the purlins at the 1/3 and 2/3 of purlin span and the other two measured horizontal displacement of the web of purlin at its mid-span location. Incrementally increased loads were applied by the 60T Mand test machine and recorded by the load cell. All LVDTs and load cell were connected to the data logger and data were acquired by computers. Self-drilling screws were employed to fasten the mid-point of purlin's top flange with roof sheet by using one screw at every sheet trough (wider flange of the sheet).

The tensile yield and ultimate strength were determined for each steel coil samples. The tension test was conducted using the standard test procedure for metallic materials (BSI 2001). The test results and stress-strain curves are presented in Appendix A.1 of Chapter 3.

5.2.4. *Failure modes and test results*

Two different failure modes are observed from the tests. Type 1 features a local buckling near the inner edge of the roof sheets between the restrained and unrestrained purlin flange, where the lip plate buckled prior to the distortional buckling wave was observed (see Fig.5-5 and Fig.5-6). However, the purlin continued to carry loads until severe local buckling takes place at where the anti-sag bars are bolted to the purlin web, when the maximum load was reached (Fig.5-7). When unloaded, a permanent but reduced local deformation remains at the purlin flange (Fig.5-8). Type 1 failure was observed in sections Z14614.

Type 2 failure mode shows only the distortional buckling, as seen in Fig. 5-9. An evident distortional buckling wave was found on the restrained purlin flange. No local buckling curves were observed but the bracing anti-sag bars showed an obvious distortion under loading (Fig.5-10). When unloaded, a permanent local/distortional buckling type deformation remained at the purlin flange (Fig.5-11). Type 2 failure was observed in sections Z14618, Z20617 and Z30720.

In all tests, localised failure of sheet at the screw connection was observed. This does not necessarily initiate the failure of purlin but may reduce sheet restraining effect to purlin, and hence trigger the purlin to experience possible lateral and torsional movement, eventually leading to the purlin's failure. In addition, the use of the anti-sag bars has successfully prevented the purlin from lateral-torsional buckling but has caused local failure around its bolted connection. This deformation, again is not the direct cause of purlin failure, but may lead to local buckling in Type 1 mode.

The moment capacity of the purlin is provided in Table 5-3 together with EC3 predictions. The load-displacement curves are recorded and presented in section 5.3.6 to compare with numerical simulations, where the load was measured as per purlin section and the displacement was measured as the vertical deformation at the mid-span up to failure.

Figure 5-5: Distortional waves in flange-lip junction

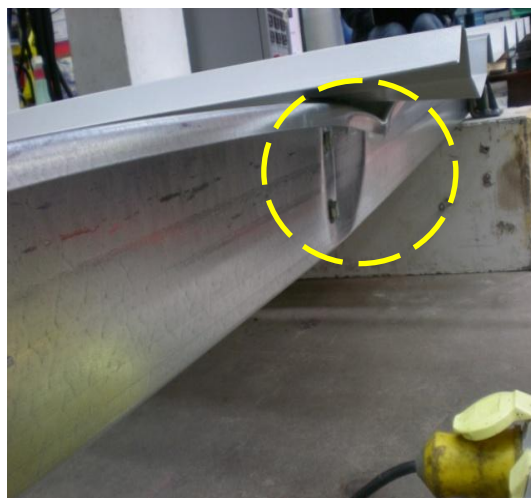Figure 5-6: Local buckling at flange and lip
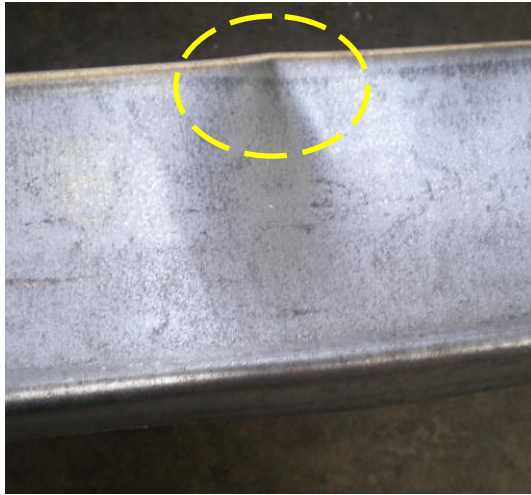

Figure 5-7: Localised deformation

Figure 5-8: Local buckling remaining as permanent deformation

Figure 5-9: Distortional buckling waves

Figure 5-10: Distortion of the anti-sag bars

Figure 5-11: Permanent distortional buckling deformation

5.2.5. *EC3 predictions*

EC3 does not consider purlin with partial sheet attachment, so the four-point bending test in this case can either be treated as a single beam under transverse loading or a purlin-sheeting system under vertical downward load.

In the former approach, the beam is considered with a combined effect of bending moment and local bearing action, due to concentrated loading. Anti-sag bars are provided so only local and distortional buckling is considered. By adopting analytical calculation according to EC3, the effect of shear is deem small enough to be neglected whilst the pure bending and local bearing should be considered by satisfy the following:

$$M_{Ed}/M_{c,Rd} \leq 1$$

$$F_{Ed}/R_{w,Rd} \leq 1$$

$$\frac{M_{Ed}}{M_{c,Rd}} + \frac{F_{Ed}}{R_{w,Rd}} \leq 1.25 \qquad \text{(Equation 5-1)}$$

where $M_{c,Rd}$ is the moment resistance of the cross-section given in EC3 (section 6.1.4) and $R_{w,Rd}$ is the appropriate value of the local transverse resistance of the web (from section 6.1.7). A working example is presented in the Appendix A-5.

For the latter case, the in-plane bending moment of a purlin section $M_{y,Ed}$ with attached sheet can be calculated using Eqn.5-2 for restraint purlins:

$$\alpha_{max,Ed} = \frac{M_{y,Ed}}{W_{eff,y}} + \frac{N_{Ed}}{A_{eff}} \leq f_y / \gamma_M \qquad \text{(Equation 5-2)}$$

where $N_{Ed}=0$ in this case.

A comparison of moment capacity are summarised in Table 5-3 and Fig.5-12. As indicated, when the sheet effect is not considered, EC3 prediction M_c is conservative for all cases, difference increases with the increase of specimen size, ranges from 7% to 25%. Whereas when considering full sheet effect, EC3 prediction $M_{y,Ed}$ are rather unsafe. Same increasing pattern is

found with the increase of specimen size, with a range from 3% to 26%. The standard deviation is 0.08 and 0.1, respectively.

Table 5-3: Ultimate moment capacities from tests compared with EC3 analysis

Specimens	EC3, M_c (kNm)	Test, M_t (kNm)	EC3 with sheet, $M_{y,Ed}$ (kNm)	M_t/M_c	$M_t/M_{y,Ed}$
Z14614	5.02	5.87	6.03	1.17	0.97
Z14618	7.39	7.87	8.96	1.07	0.88
Z20618	10.16	11.27	13.02	1.11	0.87
Z30718	13.70	17.07	23.02	1.25	0.74
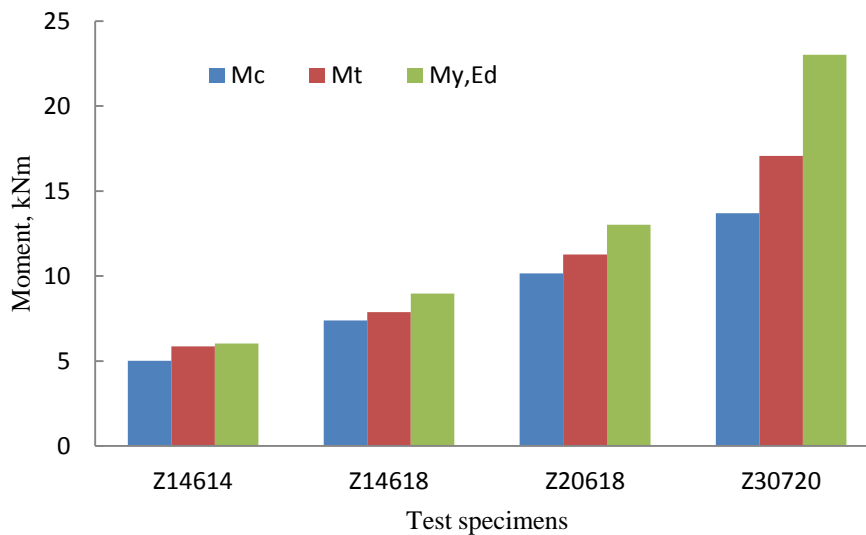
Figure 5-12: Comparison of test results and EC3 analysis

As seen, the difference between test results and EC3 predictions does not necessary increases with the increase of thickness but web depth. However the increase in thickness does seem to have an impact on the buckling failure mode, i.e. the members with higher thickness can avoid local buckling but failed in distortional buckling (Z14614 and Z14618). In addition, sections Z14614 has a closer moment to the prediction values than that of Z14618, Z20618 and Z30720, which all failed in distortional buckling. It can be suggested that the structure

experienced strength reductions when distortional buckling initiated the failure instead of local buckling (Yu 2006).

In this test, distortional buckling is allowed to take place; this is achieved by the removal of the sheet at constant bending moment zone. However the remaining sheet still provides the purlin with certain lateral and torsional restraint, which tends to elevate the bending moment capacity when compared with unsheeted members. This explained why M_c prediction is overly-conservative to use in this case since no sheet effect was considered.

When subjected to downward load, the top flange of Z- sections is under compression and can become unstable with both in- and out-plane deformation. With the attached sheet, the likelihood of distortional buckling is reduced, and hence elastic distortional buckling moment is increased. Whilst at the constant bending moment zone, the top purlin flange is unrestrained and can generate distortional buckling. In such a way, the purlin is only partially restrained by the sheet rather than under the full restraint. This explains why $M_{y,Ed}$ prediction is unsafe to use in this case since full restraint was assumed.

5.3. Finite element modelling of four-point bending test of Z- sections

5.3.1. Element type and meshing

An FE model using ANSYS is generated to simulate the test. SHELL181 is used to model the Z- purlin. Mesh size is shown in (Fig.5-13), i.e. there are 3 nodes in the lip stiffeners, 3 nodes in the flange-lip corner, 5 nodes in flanges and 11 nodes in web.
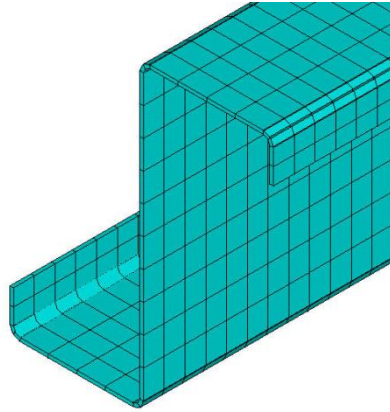
Figure 5-13: Mesh pattern of Z- section

The spring-damper element, i.e. COMBIN14, is selected to represent the rotational restraints provided by the sheet to purlin. COMBIN14 can be used as a pure rotational element with three degrees of freedom at each node (rotations in x, y, z axis). Based on the screwing detail in the test, this spring element is used to model the rotational restrain in z direction (Fig.5-14). Each element is created through two coincident nodes at the mid flange-web corner, one of which is isolated and the other is attached to purlin. The isolated node is fully restrained in all six degrees of freedom. The rotational stiffness value K is chosen from the F-test explained in Chapter 3.
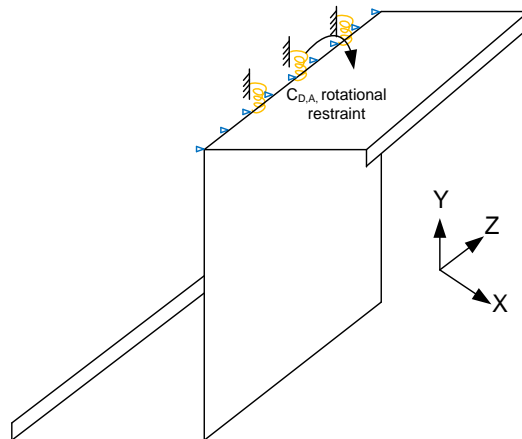
Figure 5-14: Illustration of spring configuration ini the FE model

5.3.2. *Loading and boundary conditions*

Concentrated force is applied on to element nodes at loading points as shown in Fig.5-15. The following boundary condition is applied to simulate the simple support and the restraints of the structure: purlin web is restrained in x (transverse) and y (vertical) directions at both two bolted position at one end and the top bolted position at the other end; whereas the bottom bolted point at the other end is restrained in x, y and z (longitudinal) directions (Fig.5-15). Transverse displacement in the plane of sheet is eliminated to achieve a lateral restraint provided by the attached sheet. The effect of anti-sag bars is represented with an area of transverse constraints.
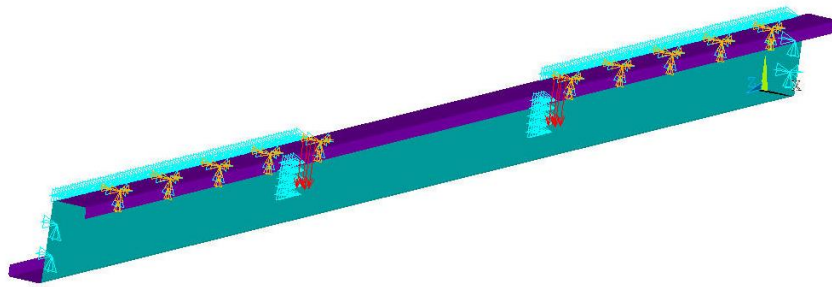
Figure 5-15: Overview of FE model for Z- four point bending test

5.3.3. *Material property and residual stress*

Material nonlinearity in the cold-formed steel beams was modelled with von Mises yield criteria and the isotropic hardening rule. The model was defined as elastic-perfect plasticity material, i.e. the tangent modulus being zero. All other components were modelled as elastic material, with elastic modulus $E = 2.1 \times 10^5 \, N/mm^2$ and passion ratio $v = 0.3$.

During the cold forming process, residual stress is introduced in the CFS sections. In the flat regions the bending residual stresses are found to be small. In the corner regions, the

bending residual stresses can be high. However it is also found that the strain hardening effect from cold-working effect during the forming process will counteract the effect of the residual stress. Therefore, in this study the stress-strain properties measured in the flat regions without membrane residual stresses are used for the entire Z- and Σ-section.

5.3.4. *Geometrical imperfections*

An eigen-value buckling analyses was performed to determine the possible shapes of the imperfection pattern in the form of basic linear buckling modes. In this case, local and distortional buckling modes were introduced into the model. Since the first occurrence of buckling mode is usually the critical one, the corresponding buckling shape with the lowest eigen-value was selected. The scale factor of the Eigen-modes is introduced based on the findings from Schafers and Pekoz (1998), i.e. a 25% percentile imperfection type was chosen, which is: half of the section thickness (t/2) for local buckling and the full thickness (t) for the distortional. The model was then updated with these imperfections modes for the non-linear analysis in following stage.

A typical shape of the local and distortional buckling is presented in Fig. 5-16 (a) and (b) below:
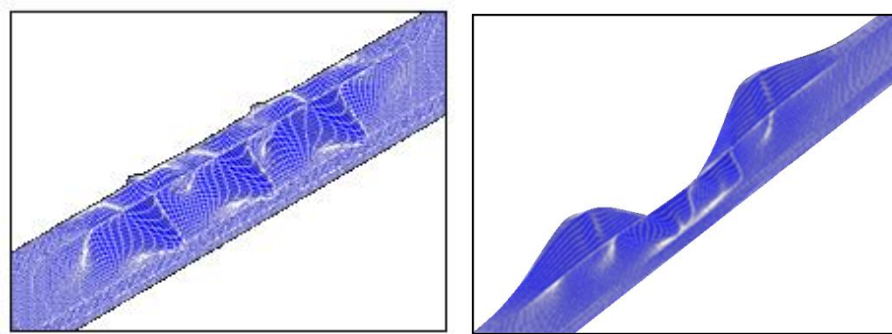
(a) Local buckling   (b) Distortional buckling

Figure 5-16: Local and distortional buckling from eigen-value buckling analysis

5.3.5. Solution scheme

The analysis was carried out in two phases, a linear eigen-value elastic buckling analysis followed by a nonlinear analysis.

The first stage involves using the sparse solver to carry out an eigen-value analysis, which produces the above-mentioned buckling modes which are used to update the geometric imperfection.

Once the model is geometrically updated, the structure consisted both of the material and geometric nonlinearities and was allowed to experience large deformation. In ANSYS Newton-Raphson (NR) method is adopted as the default method for solving non-linear analysis iteration. NR method can converge very fast since its convergence is in quadratic order, but due to the nature of the method the iteration process would become unstable, i.e. experience convergence difficulties when approaching failure point (Fig.5-17a), where the stiffness becomes zero. In these cases arc-length method can be used instead to overcome this problem as it allows both the displacement and the load to vary throughout time steps. The solution was set not to terminate until it fails to converge with the minimum arc-length radius (Fig. 5-17b)

| (a) Newton-Raphson method | (b) Arc-length method |
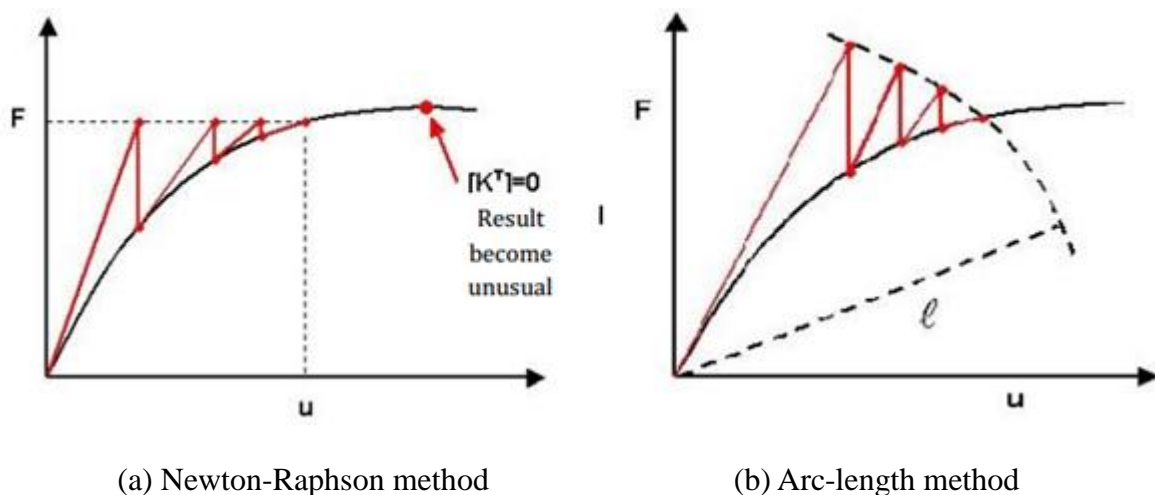
Figure 5-17: Comparison of two common nonlinear solving methods adopted in ANSYS

### 5.3.6. Results and discussion

In total, four purlin specimens have been tested in the experiment. The test results are used to verify the developed FE model with applied rotational stiffness from rotational restraint test. A comparison of load-deflection relationship of the three curves is presented in a Fig. 5-18, the ultimate load capacity is summarised in Table 5-4.

Table 5-4: Comparison of ultimate load of test and FEA results

Specimens	Ultimate load (kN)	
	Test	FEA
Z14614	10.2	10.5
Z14618	16.3	15.0
Z20618	22.9	20.8
Z30720	35.2	34.1

Z14614

Z14618

Z20618   Z30720
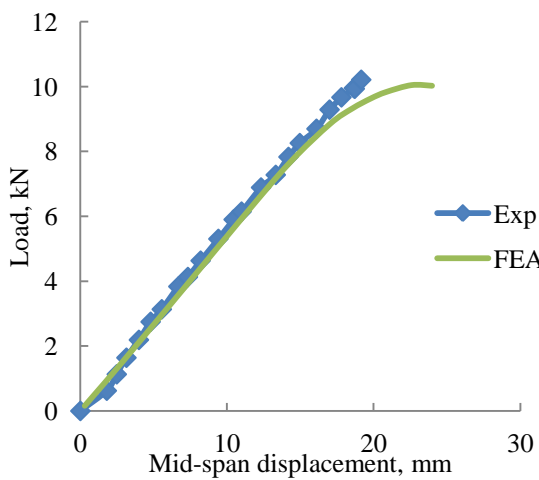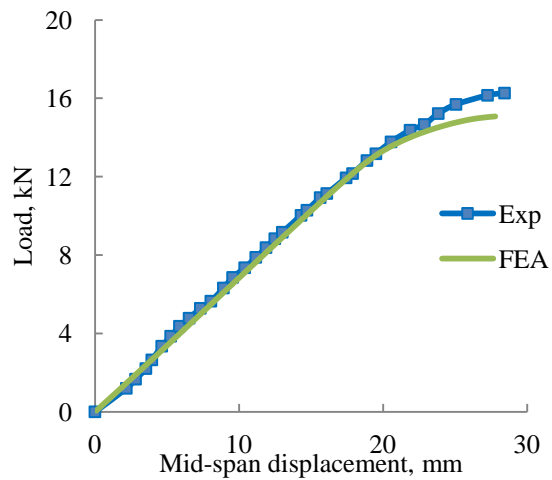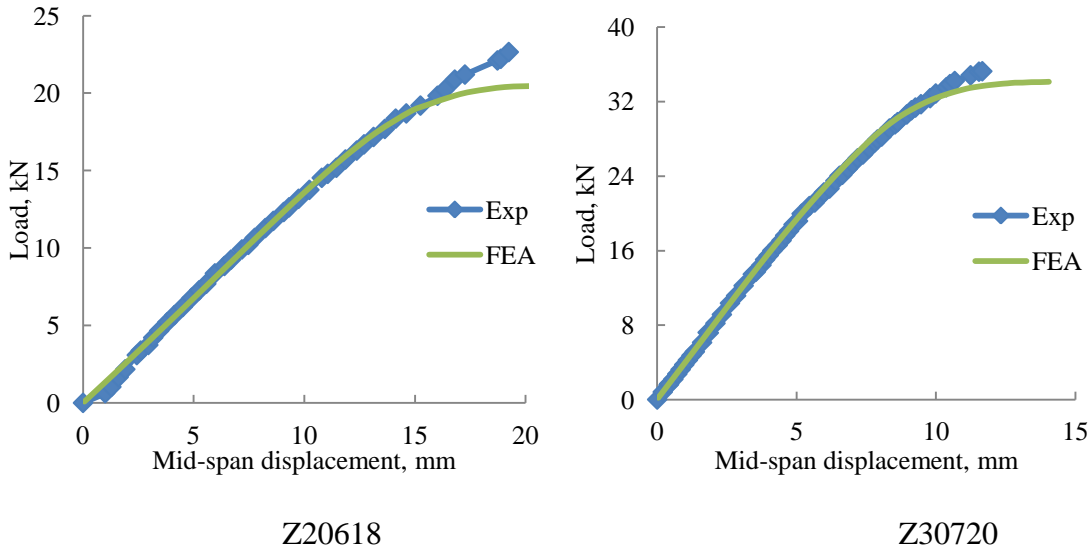
Figure 5-18: Load-displacement comparison of experimental and numerical results

As shown in Table 5-4, FE model has a close ultimate load compared to test results. The difference ranges from 3% to 10%. It is suggested that the distinction may be due to imperfection amplitude applied in the FE model and other experimental errors. The stiffness matches well between the test and FEA. Moment capacity is plotted in Fig.5-19 for the test and FEA simulation. It is seen that the difference is much smaller when compared to that of Fig. 5-12, suggesting that FE model provides a better prediction than EC3 models.
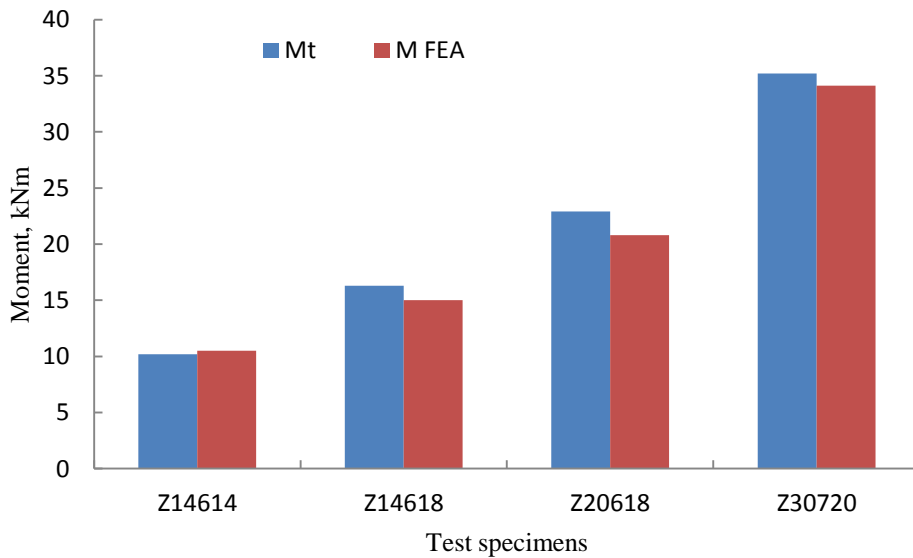
Figure 5-19: Comparison of test results and FEA analysis

For failure mode, the FE model is able to predict the local bearing occurred at the loading point and the distortional buckling wave at the constant bending moment zone (Fig.5-20). Maximum vertical displacement is found at the loading point. The von Mises stress distribution showed in Fig.5-21 indicates that high stress areas are at: (a) loading points, (b) anti-sag bar connection points and (c) supports. However numerical method is unable to reproduce type 1 failure mode of local/distortional interacting behaviour found in the test. This may be due to the absence of the sheet. For actual sheet presented in the FE model instead of spring element, a full model is provided in the later section with Σ- purlins in this chapter.
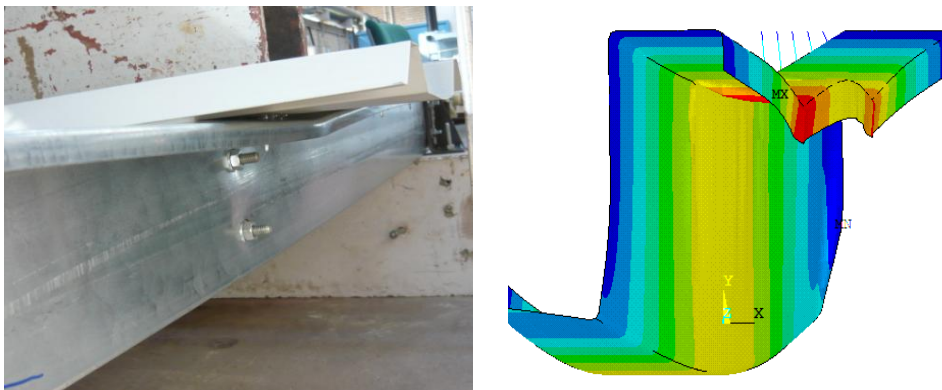
Figure 5-20: Comparison of the failure modes of Z-section 20618
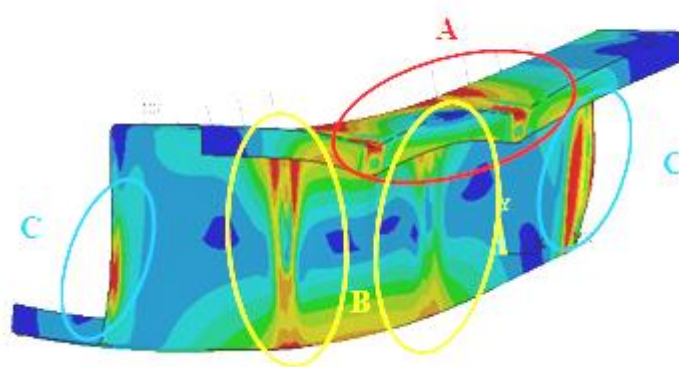
Figure 5-21: von Mises stress diagram of Z20618

5.3.7.   Conclusions

The behaviour of CFS Z purlin with single sheet attached under transverse loading was investigated via experimental, analytical (EC3) and numerical (FEA) approaches. The mid-span of the section was left unrestrained to allow distortional buckling to take place. Based on the findings, the following conclusions are to be drawn:

(1) The results and observation from four-point bending test has indicated that purlin was mostly likely to fail under a combined effect of distortional buckling and local bearing at the load point. One section was failed under local/distortional buckling interaction. None of the specimens failed under lateral-torsional buckling, due to the presence of sheeting and lateral anti-sag bars.

(2) In EC3 the partially restrained beam section is not specifically considered, so the prediction was either overly-conservative to apply (when being considered as a single beam under bending) or unsafe (when being considered as a full restrained purlin-sheeting system). Therefore a more appropriate design method should be developed.

(3) A non-linear FE model is established using ANSYS to replicate the test condition. The FE model has shown a close agreement to the test results in predicting ultimate moment capacity and load-displacement relationships. Difference in all cases is within 10%. The FE model has also successfully predicted the failure mode of distortional buckling and local bearing for most of the test specimens but could not predict local/distortional interaction. It is suggested due to absence of sheet element and imperfection applied onto the model.

(4) The validated FE model can be used for further investigation on the same matter. For example, due the limitation of the test machine, no post failure data was recorded.

With the help of the numerical tool, structural performance for post-failure, uplift loading case as well as other parametric studies can be directly generated.

5.4. Σ- purlin sections with continuous sheet attachment

5.4.1. *Introduction*

It is learnt from Chapter 3 that CFS Σ-profile has become a popular option for industrial use as the roof purlin, due to its additional stiffeners presented in the web. The stiffeners bring the shear centre closer to the web and hence reduce torsion introduced by applied load. Therefore Σ- purlins offer a higher load-carrying capacity when compared to conventional C-sections, and a larger torsional rigidity when compared to Z- sections, when the roof is flat or low pitched. As a result, Σ- section has been commonly used as purlins and side rails in modern industrial buildings as well as floor joists in residential buildings.

A bending test on Σ- sections with continuous roof sheet attachment has been conducted. In order to avoid the local bearing effect caused by concentrated loads in the previous test, a vacuum chamber is used to simulate uniform distributed load (UDL) condition. The reason that this is done is because when roof system experiences gravity load (i.e. snow, rainfall) and uplift load (i.e. wind), the structure is under an almost uniform load distribution.

In addition, considering the sheeted purlin may have a differing behaviour when under pure bending and UDL. One of the test results was compared with multi-point bending test conducted by Liu (2012), where the only difference between these two is the loading condition. The ultimate load and failure modes are compared and discussed in section 5.4.4.

FE model was established for simulation purpose with both the full model (where both purlin and sheet are represented) and the simplified model (with the use of rotational springs replacing the sheeting effect on purlin). Parametric studies are carried out to investigate the effect of loading (i.e. gravity and uplift), effect of screw spacing as well as various purlin spans.

5.4.2. *Test specimen and apparatus*

Nine common sizes of CFS Σ- sections are used in the tests. The geometry details of each specimen is summarised in Table 3-2 in the previous section.

The following apparatus are used in the testing programme:

- A vacuum chamber of 7000mm x 2000mm x760mm

- 9 purlin specimens. The bolted holes for the specimens are provided in Fig.5-22.

- LVDTs – 7 x (100-200mm in range) measurement for vertical and horizontal displacements

- 1 x pressure transducers

- 36x self drilling screw (5-5 x 30)– for each sample to connect the sheets and purlins

- 6x steel sheet – for each test, sheet profile is showed in Fig.3-13 in Chapter 3.

- steel stand at support

- 4x cleats – relevant size to act as supports

- M12mm bolts were used for 200 and 240 section and M16mm bolts were used for 300 section.
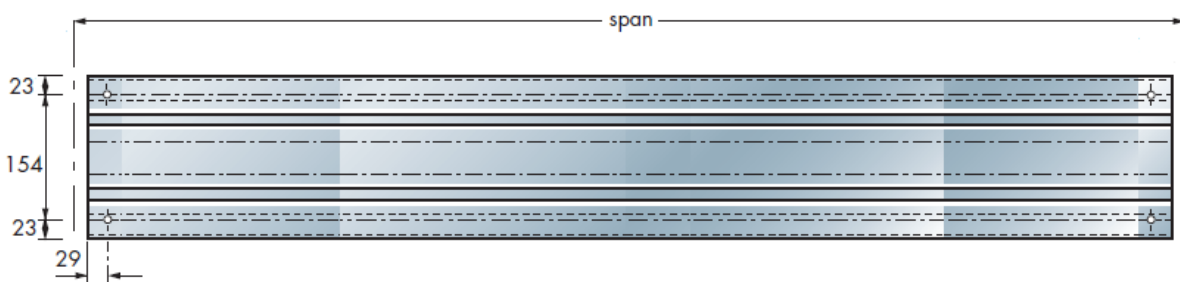
300 series
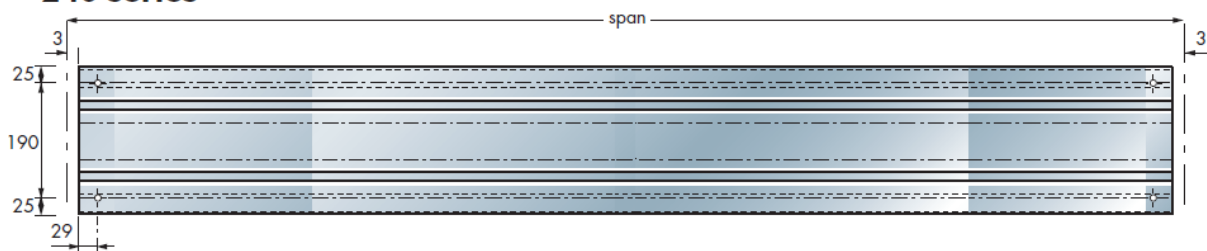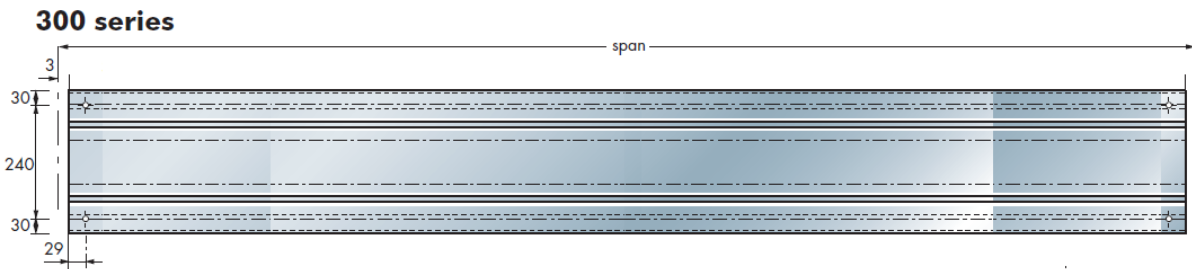
Note： M12mm bolts were use for 200 and 240 section and M16mm bolts were use for 300 section.

Figure 5-22: Bolt holes configuration for Σ- sections

5.4.3. Test set-up

An overview of the test assemblies is shown in Fig.5-23. A pair of simply-supported, identical Σ- purlins was positioned in an opposing with flanges pointing to each other. Roof sheeting was fixed to top flanges using self-drilling screws leaving the other flange free to move. At both ends the purlin sections are bolted onto a steel stand via cleats. The steel stand has a much higher strength than the purlin sections so deformation from the steel stand was eliminated. In all tests performed, the purlin is 6000mm in length; with a web to web distance of 660mm. After set-up, a membrane was applied on the top of the structure to seal the chamber. The membrane was bolted and sealed to the chamber edge as shown in Fig.5-24. The pressure is generated using a 1.5 kW vacuum pump with the maximum pressure of 26kPa. The pressure of chamber is controlled by an adjustable valve which provides a controlled leak. When applying loading, the pressure is generally increased in 0.2kPa per 5 min increments until the vicinity of failure occurs, where the increment is reduced to approximately 0.1kPa per 2 min. The pressure difference between the inside and outside of the chamber results in a UDL transverse load to the structure, which is measured by pressure transducers connected to computers (Fig.5-25).

Figure 5-23: Overview of vacuum chamber test set-up

Figure 5-24: Screw fastening arrangement for the membrane seal

Figure 5-25: Pressure transducer

5.4.4. Test results and discussion

Readings of pressure, displacement are taken at all increments. The ultimate load capacity is calculated using Pressure x Area (loaded sheeting under pressure). Moment capacity of the structure is derived by using $M=wL^2/8$, where w is the line load calculated from the pressure and L is the overall length of the purlin section.

The failure mode can be categorised into two types for the downward loading condition. Type 1 failure is associated with a local buckling occurred at the restrained purlin flange (Fig.5-26) along with the distortional buckling waves on the purlin flange-lip junction at the mid-span (Fig.5-27). This mostly occurs on sections with a relatively small thickness (i.e. 20012). Type 2 failure is associated with localised deformation at the sheet (near trough-crest junction) (Fig.5-28) with the distortional buckling waves on the purlin flange and lip at the mid-span, which is likely to occur on the sections with relatively large thickness (i.e. 30030). For both types, permanent distortion remained when it was unloaded and the sheet was

139

removed.

The reason for these two types to take place is that when the section has a small thickness, it tends to have a lower local buckling resistance than the distortional buckling. When the sections have larger thickness, their local buckling resistance increases, and the tendency of distortional buckling movement induces a large stress concentration and hence a localised deformation at the constraint points from the sheeting, resulting in a weakened restraint from the sheet to purlin. This may subsequently lower the distortional buckling resistance, leading the occurrence of distortional buckling ahead to local buckling or even completely replace it.

Figure 5-26: Local buckling of purlin Σ30030 FD

Figure 5-27: Local and distortional buckling of purlin Σ-30030 FD

Figure 5-28: Localised deformation at the trough-crest junction

A similar experiment on full restrained Σ- purlin-sheeting system was conducted by Liu and Yang (2012) where the only difference to this test was the loading condition. In their test, the structure was under multiple concentrated loads to simulate UDL condition, and the load direction is imitated by placing the structure in both ways, as shown in Fig.5-29. By comparing both experiments, similar failure modes were observed and the load-carrying capacities have

made a good agreement. A comparison of the load-displacement curves of 30030 FD is revealed in Fig.5-30. It is revealed that   there is no noticeable deviation on the stiffness of the specimens, by showing a difference on ultimate load of 8.5%.

The result of the comparison between two similar experiments suggests that: (a) the multiple load can be a good substitution to UDL when the test apparatus is limited; and (b) the vacuum chamber experiment is an on-going project so not all tests on purlin specimens are completed. With the validated test results from Yang and Liu (2012), its results can be used for further investigation on the numerical simulations in the following chapters.
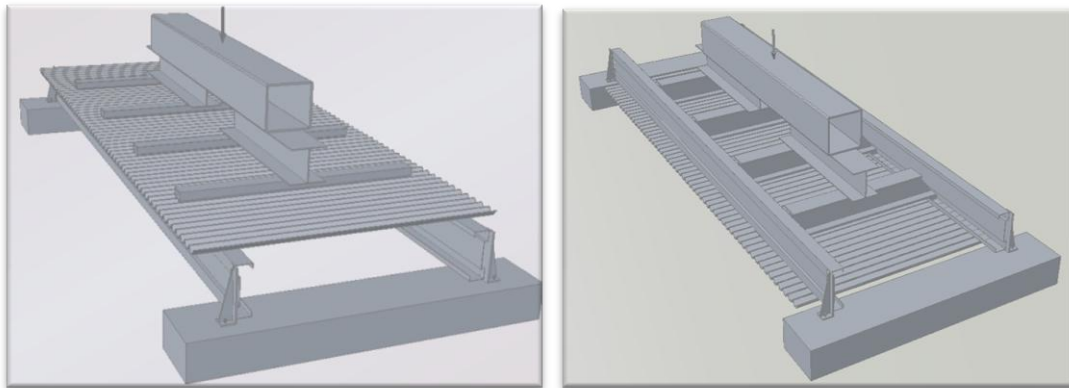
Figure 5-29: Gravity and uplift load conditions in Liu (2012)
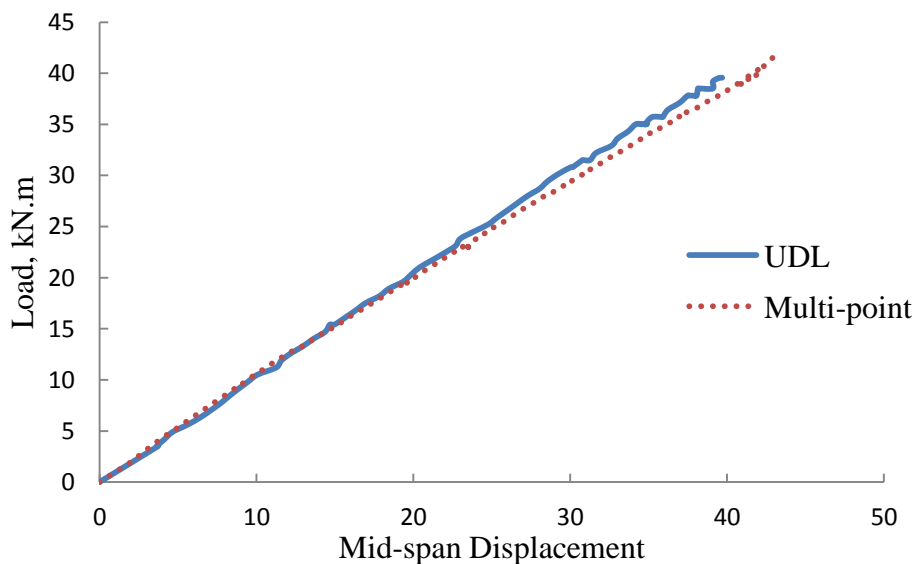
Figure 5-30: Load-displacement comparisons for Σ30030 FD

5.5. Finite element modelling using full model

5.5.1.   Element type and meshing

Previous researchers have rarely studied purlin-sheeting system using full model apart from Lucas (1997a and 1997b) and Yu and Schafer (2007) because of its complicated nature. In this section a full FE model of purlin-sheeting system under transverse loading is established and has been validated by experimental results with very satisfactory results. The experiment was originally conducted by Liu and Yang (2012). Since the pair of purlin sections is identical, the structure can be assumed as doubly symmetrical. SHELL 181 element is used for modelling both purlin and sheet section. The configuration is illustrated in Fig. 5-31. Mesh on the sheet is element size 10 and mesh on purlin is as follows: 2 elements on the lip stiffeners, 4 elements on flanges, 4 nodes on the out web, 8 elements on the inner web. For corners of restraint flange, 4 elements are used for each side. The reason of using finer mesh is to maintain the rounded corner effect and to achieve a better convergence for the contact between purlin and sheet. One element is used for all other corner and stiffeners.
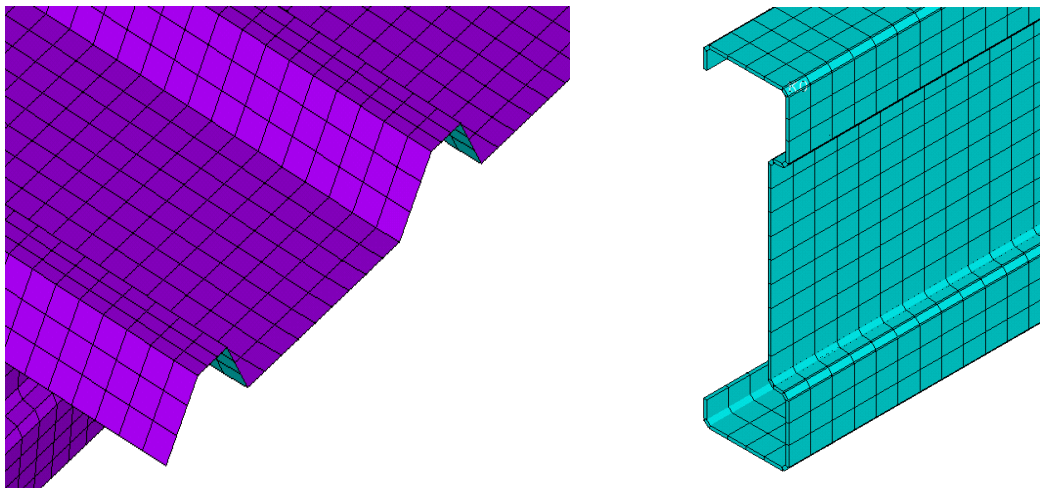
Figure 5-31: Configuration of full FE model of purlin-sheeting system

5.5.2.   Loading and boundary conditions

Flexible surface-to-surface contact pair is generated between the restrained purlin flange

and sheeting trough. Since purlin has a higher strength than the roof sheet, its restrained flange and two adjacent corners are assumed to be the target surface and the sheet troughs surfaces are assumed to be contact surface. This is because the assumption in ANSYS that contact surface cannot penetrate target surface. *Augmented Lagrange method* is used as contact algorithm, and the contact is detected on *Gauss points* and the behaviour of contact is *Standard,* therefore free sliding between the surfaces is allowed.

At supports, holes are created at each outer web of the purlin section, with the same edge clearance of the holes in the practical case. A finer mesh is used around the hole area to eliminate any possible stress concentration (Fig.5-32). The bolts are represented by using a 1/4 circular plate element with the radius of the element equals to that of a bolt. Thickness is assumed as 10mm so that the bolt is stiff enough to avoid any excessive distortion. At the centre, the node on the element is restrained in the vertical direction, and all other nodes are restrained in lateral direction. The nodes on the edge of the bolt hole and the outer arc surface of the plate were coupled together. This arrangement is to avoid any unwanted rotational restraints about the major bending axis while minimising the excessive local distortion near the bolt-beam interface.
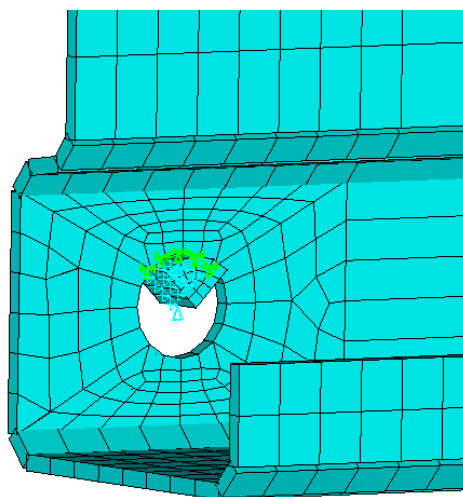
Figure 5-32: FE model arrangement detail at support

At screw point, node pair from purlin and sheet is fully coupled together. Symmetrical boundary condition is applied for cross section of both sheet and purlin so that: $w=\theta_x=\theta_y=0$. In the test the purlins are fixed onto a concrete block by using bolts and cleats. To simulate this in the FE model restraints are applied so that $u=v=0$ at mid point of purlin outer web, where bolts are placed (Fig.5-33).
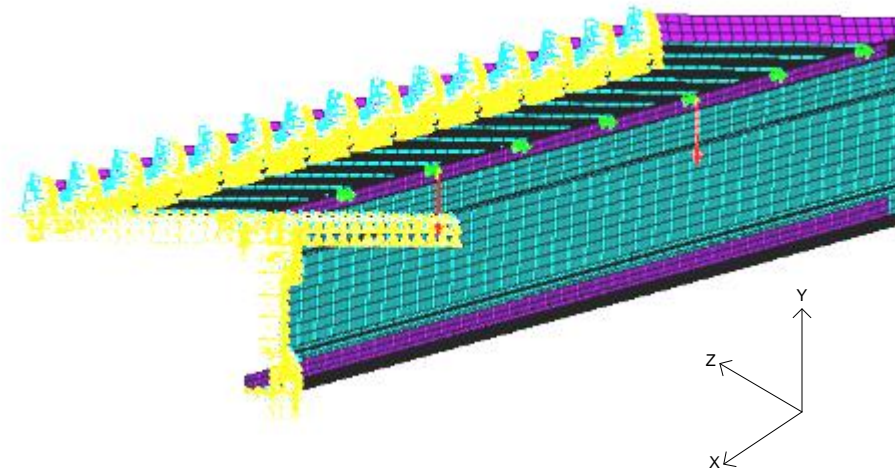

Figure 5-33: Boundary condition of the full FE model

5.5.3. *Material property*

Both sheeting and purlin is modelled including material non-linearity. For sheeting, a linear elastic-plastic model was applied with Young's Modulus and Poisson's ratio assumed to be as 2.1×10^5 N/mm^2 and 0.3, respectively. The bilinear isotropic hardening scheme is adopted for its plastic range, an idealised linear stress-strain curve is assumed with the yield strength of the sheet 235N/mm^2 and tangent modulus is zero.

For purlin, the same Poisson's ratio 0.3 is applied. The Young's Modulus and the nonlinear stress-strain curve were derived from a steel coupon test, and true stress-strain curve is modelled using a multi-linear isotropic hardening scheme with von-Mises yield criterion. The coupon test was conducted by Liu (2012), more detail of the results are provided in Chapter 3 as well.

5.5.4. Solution scheme

Solution scheme is the same to that of z purlin sections mentioned in previous section. However due to its additional nonlinearity generated from contact elements, convergency difficulty increases significantly. In order to overcome this problem, the radius and multiplier range of the arc-length method were specified to improve convergence. The initial value of arc-length radius was set as the first buckling load divided by the selected increment value. In this modelling, the value was normally taken as 200-250, which was large enough to reach the softening stage. The multiplier for the arc-length radius was set in a range between 1/1000 and 5. The arc-length radius was updated based on the number of iterations required in the previous load increment, and varies accordingly within the range of the specified limit. The solution ends when it fails to converge with the minimum arc-length radius.

5.5.5. FE model of simplified purlin-sheeting system

In previous researches there is a consensus that the effect of sheet can be simplified by using spring restraints. With the lateral restraint being mostly assumed as rigid, the rotational restraint can be replaced by a rotational spring element. Once the rotational stiffness $C_{D,A}$ value is derived, it can be used as an input for the FE model to monitor the behaviour of purlin-sheeting system under transverse loading. The above-mentioned model can be represented as a purlin only, with the effect of sheet simplified using spring elements. In this case the purlin is assumed to be laterally braced at the corner of contact, so at every node along the purlin section the displacement in X-X direction are assumed to be zero. Rotational restraints are applied by using spring element COMBIN 14, which is assumed to rotate about z-axis only. The rotational springs are positioned also at the corner of contact; the number and the distance between the springs are consistent with actual screws (Fig. 5-34). The spring element is created between two coincident nodes at restrained purlin flange-web junction line

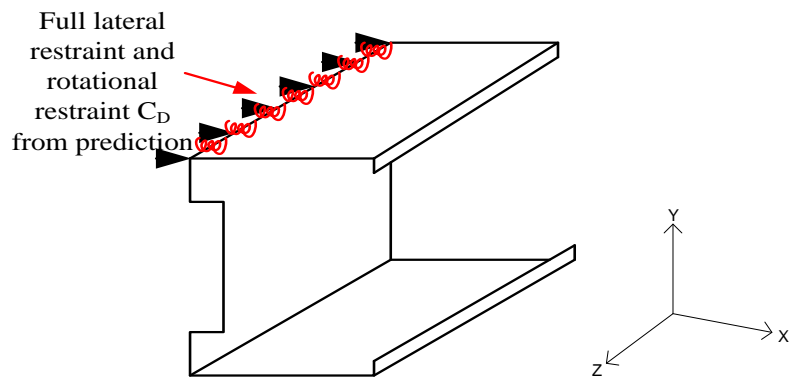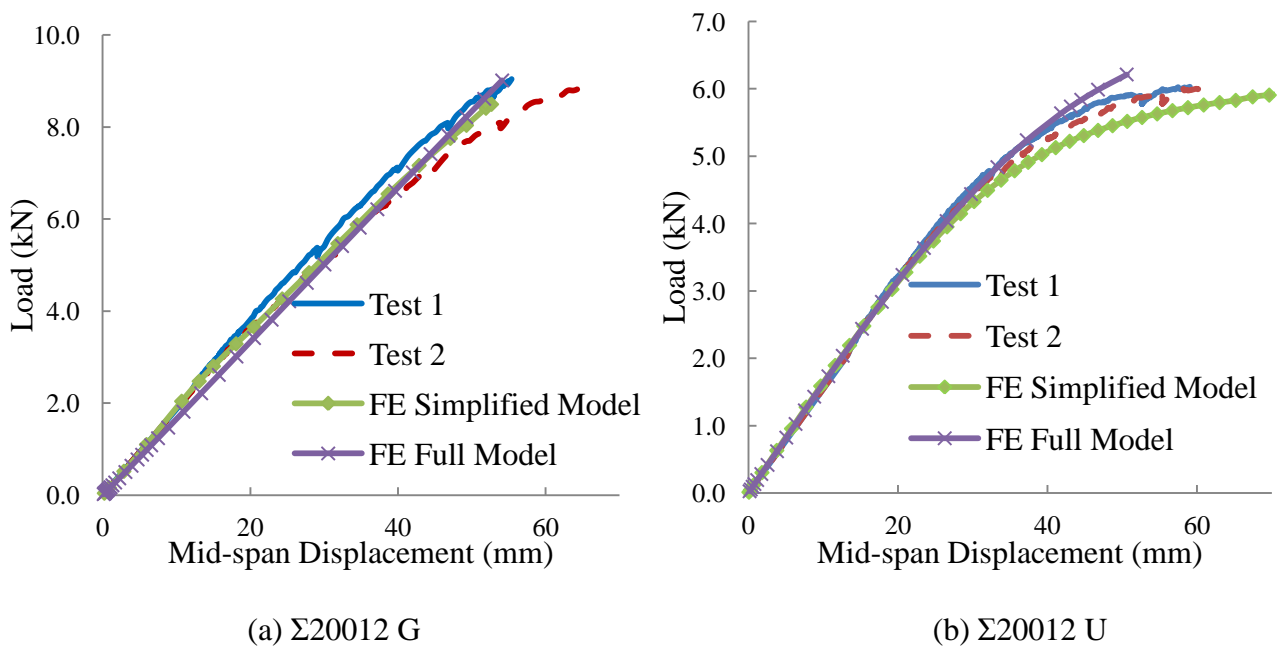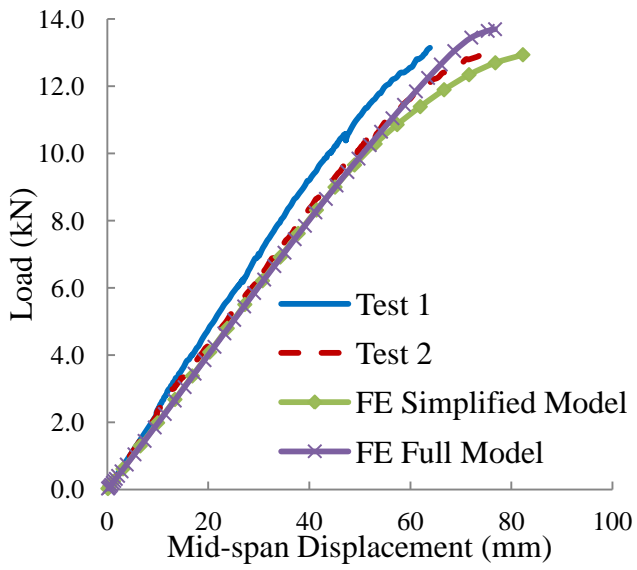with the isolated node being restrained in all six directions.

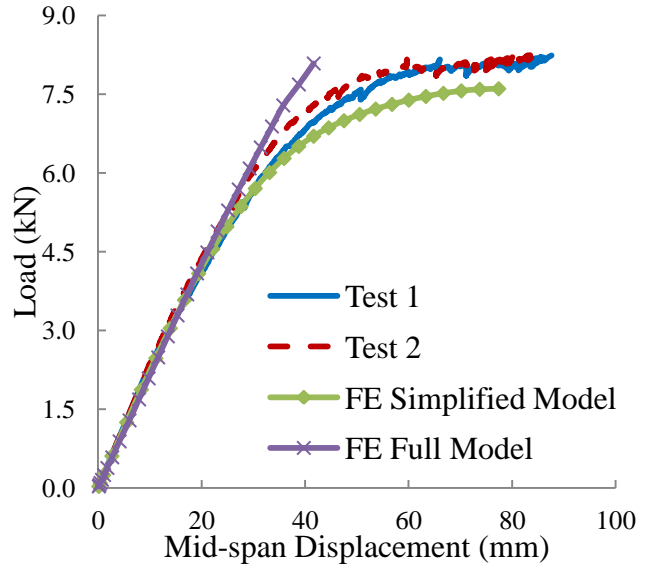Figure 5-34: Spring configurations in the simplified FE model

5.5.6. *Results and comparison*

In order to distinguish the test specimens used in F-test, Σ- sections are designated with a different suffix as 'G', representing gravity loading condition and 'U', representing uplift loading condition. Results of load-displacement curves are provided to compare the experiment, FE full model and FE simplified model in Figure 5-35 (a)-(r). Ultimate load of all three categories are summarised in Table 5-5.
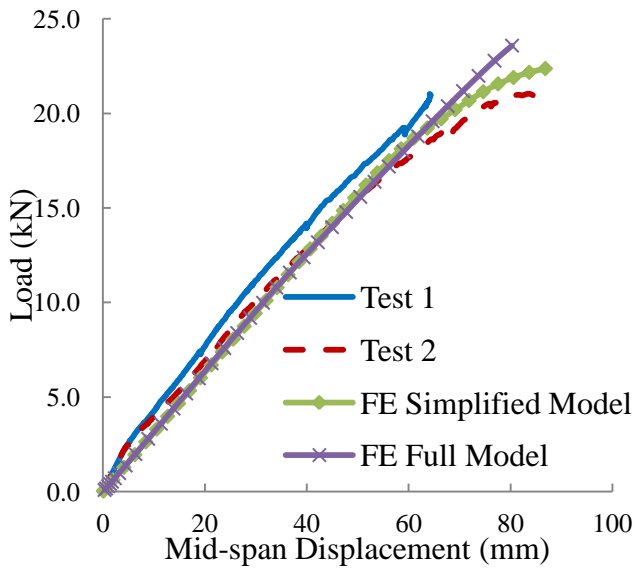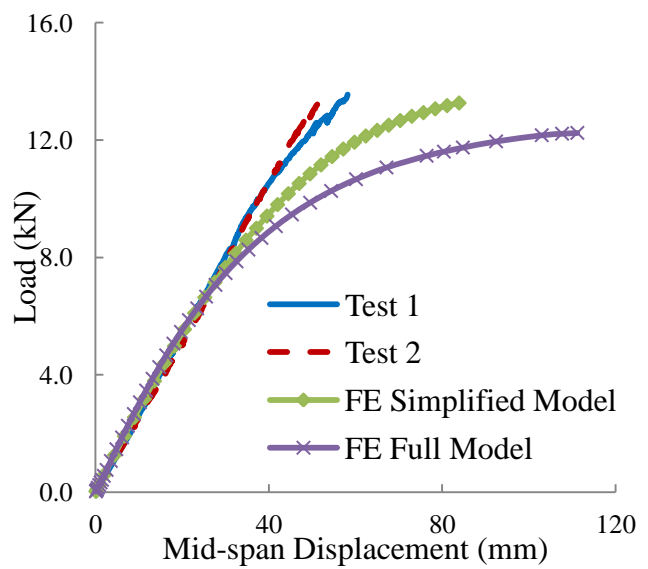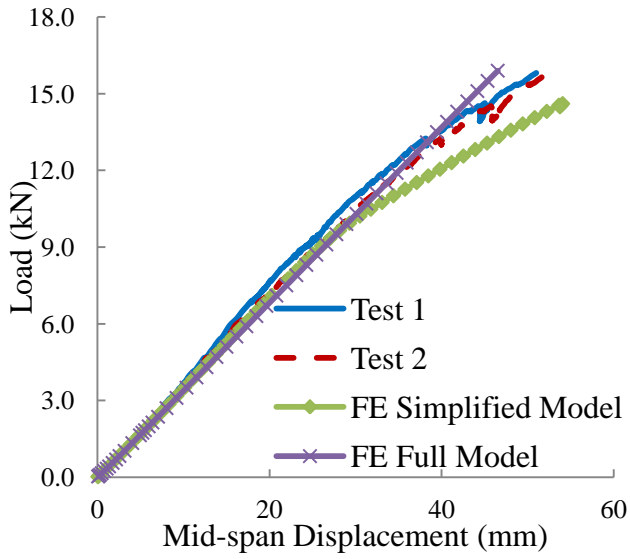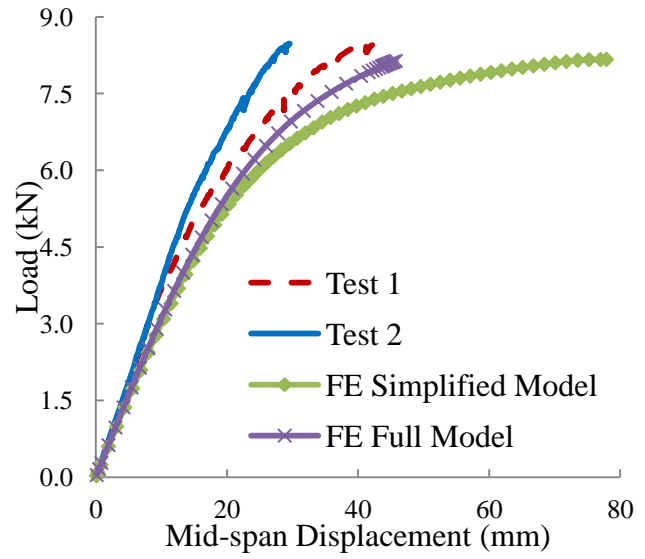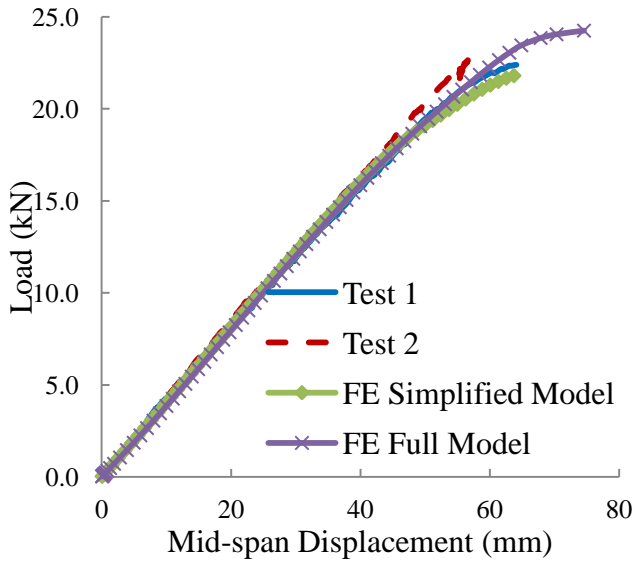
(a) Σ20012 G

(b) Σ20012 U

(c) Σ20016 G

(d) Σ20016 U

(e) Σ20025 G

(f) Σ20025 U

(g) Σ24015 G

(h) Σ24015 U

(i) Σ24023 G
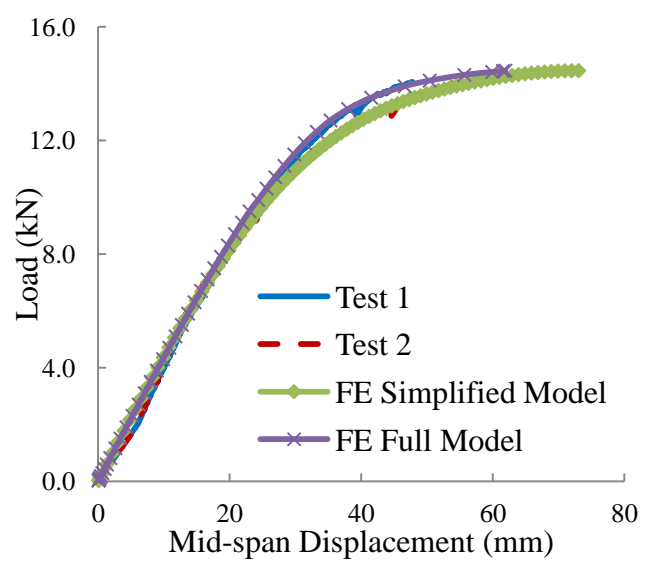
(j) Σ24023 U
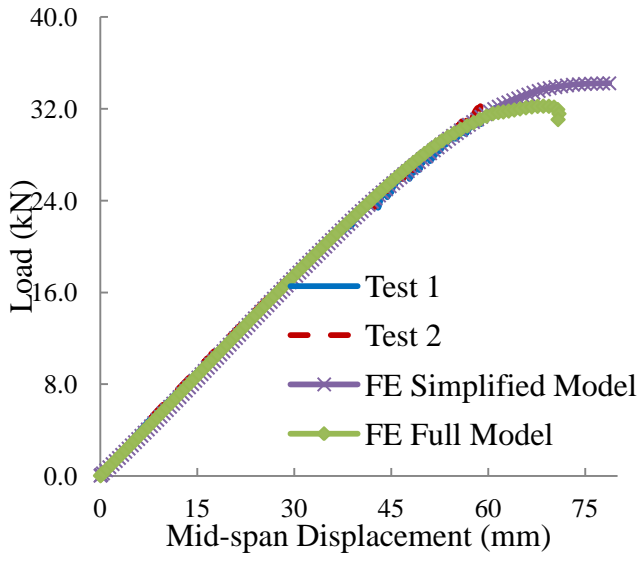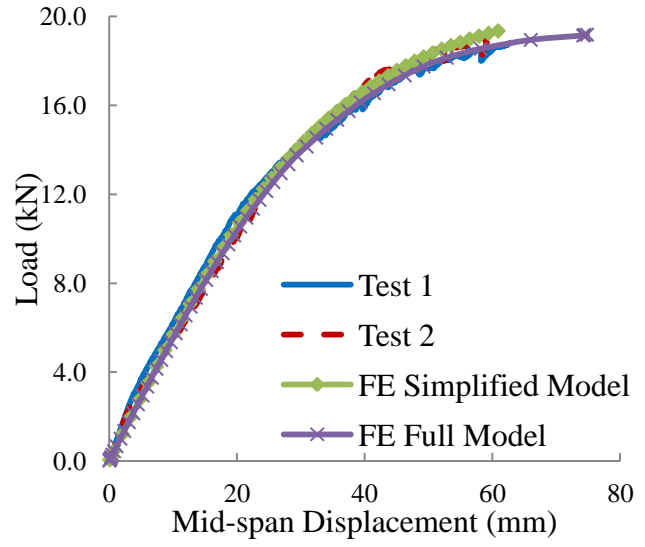
(k) Σ24030 G

(l) Σ24030 U
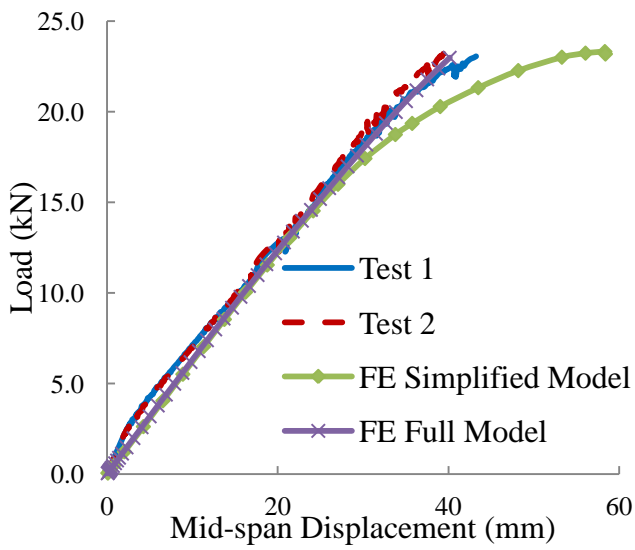
(m) Σ30018 G
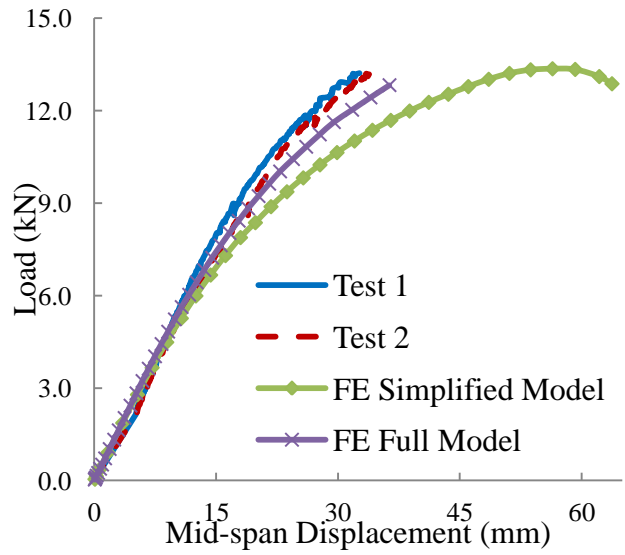
(n) Σ30018 U
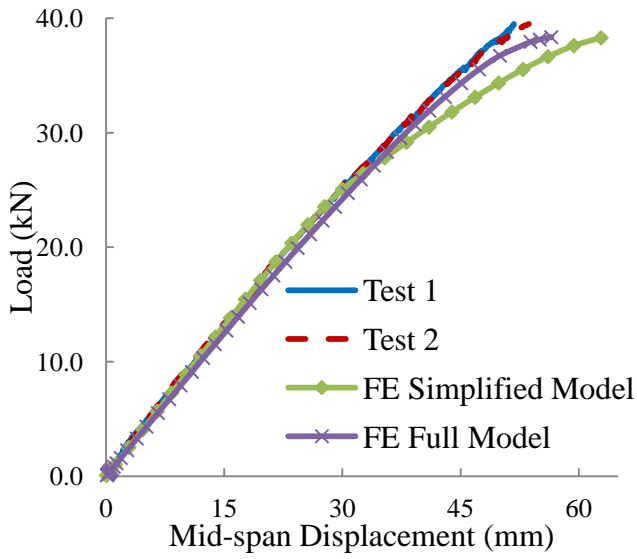
(o) Σ30025 G
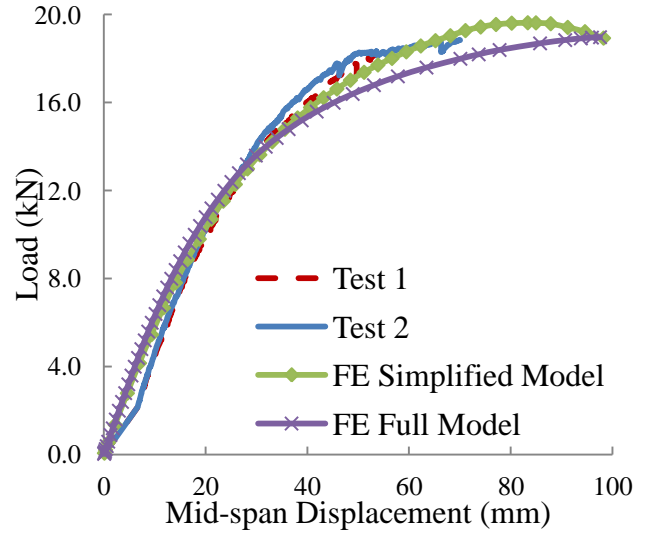
(p) Σ30025 U
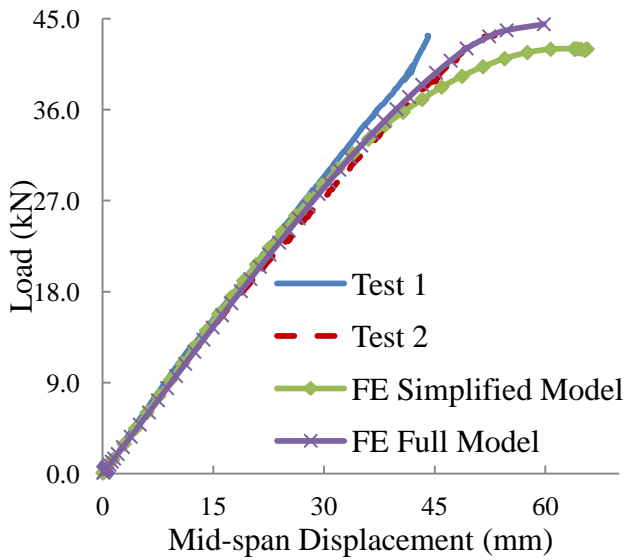
(q) Σ30030 G
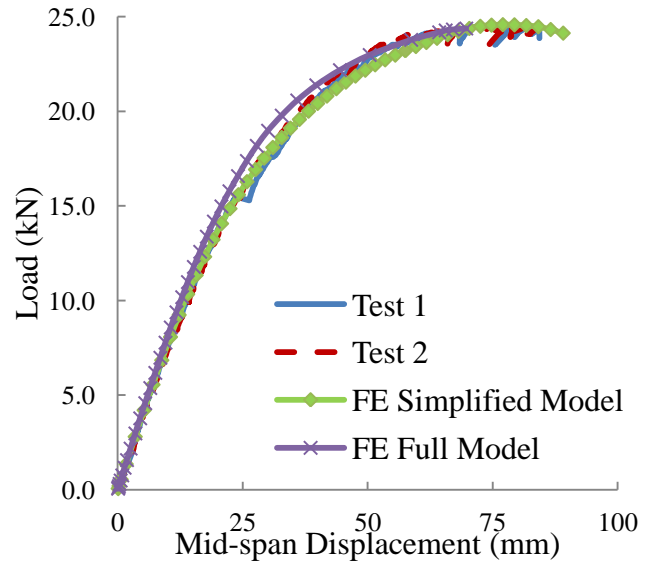
(r) Σ30030 U

Figure 5-35: Load-displacement curves comparison

151

Table 5-5: Ultimate load F_u comparison

Section	$F_{u,test}$ (kN)	$F_{u,FM}$(kN)	$F_{u,SM}$(kN)	$F_{u,FM}/F_{u,test}$	$F_{u,SM}/F_{u,test}$
20012G	9.0	9.01	8.52	1.00	0.94
20012U	6.0	6.21	6.06	1.03	1.01
20016G	13.1	13.7	12.9	1.05	0.98
20016U	8.2	8.1	7.6	0.99	0.93
20025G	20.8	23.6	22.7	1.13	1.09
20025U	13.5	12.2	14.0	0.90	0.99
24015G	15.8	16.3	14.5	1.03	0.92
24015U	8.5	8.1	8.2	0.95	0.96
24023G	22.2	24.3	21.8	1.09	0.98
24023U	14.2	14.4	14.5	1.01	1.02
24030G	32.5	34.2	32.2	1.05	0.99
24030U	18.2	19.2	19.4	1.05	1.07
30018G	23.1	23.0	23.2	1.00	1.00
30018U	13.2	12.8	13.4	0.97	1.02
30025G	39.5	38.3	38.3	0.97	0.97
30025U	18.9	19.0	19.6	1.01	1.04
30030G	43.3	44.4	42	1.03	0.97
30030U	24.4	24.4	24.6	1.00	1.01

It is shown in the load-displacement curves that both the FE models are able to predict the flexural stiffness and ultimate load with close agreement to the experimental results. Resulting curves from FE full model are closer to test than that of simplified model curves, since it considers the contact effect between purlin flange and sheet trough which enhances the member flexural stiffness. Some discrepancies were observed in test Σ20025U, Σ24015U and Σ30018U are suggested may due to the difference in initial imperfections. In these cases simplified models showed an excessive deformation than test and FEA full model, hence it is suggested that in uplift conditions the effect of sheet may be more significant due to the rotational restraint it provides to the purlin section.

Regarding the failure mode, a combination of localised buckling around loading point plus a distortional buckling wave was observed in the experiment. Comparisons between the FE models with von Mises stress distribution and test specimen are provided in Fig.5-36 and Fig.5-37, respectively. The areas in darker colour are under larger stress and hence show a tendency to buckling.

(a) FE full model   (b) Experiment (Gravity case)
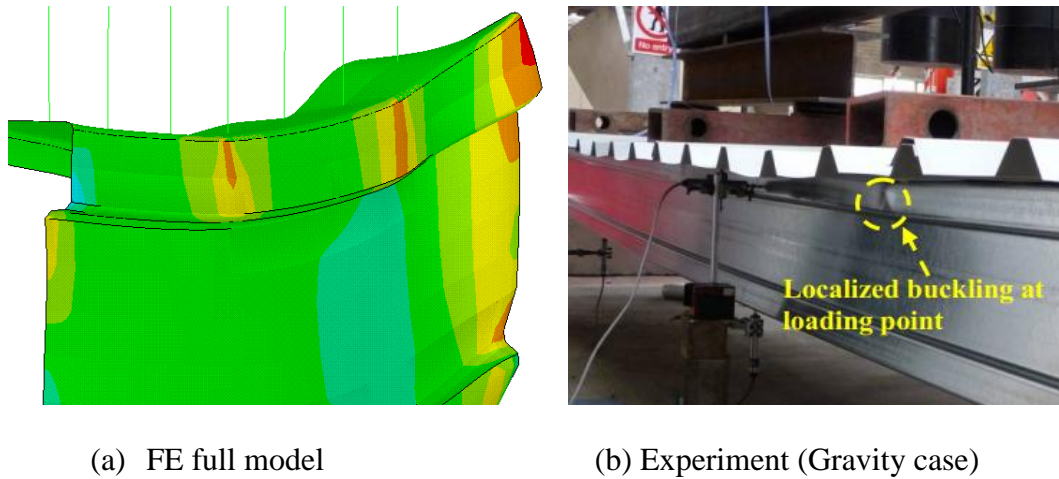
Figure 5-36: Observed local buckling comparison between FE model and test result

(a) FE full model   (b) Experiment (Gravity case)

Figure 5-37: A comparison of distortional buckling waves observed between FE full model and test

However for the FE simplified model, only local buckling is observed with the model. No sign of distortional buckling was seen. This suggests that the post-buckling strength of local buckling mode did not further develop into distortional buckling, instead the structure failed in

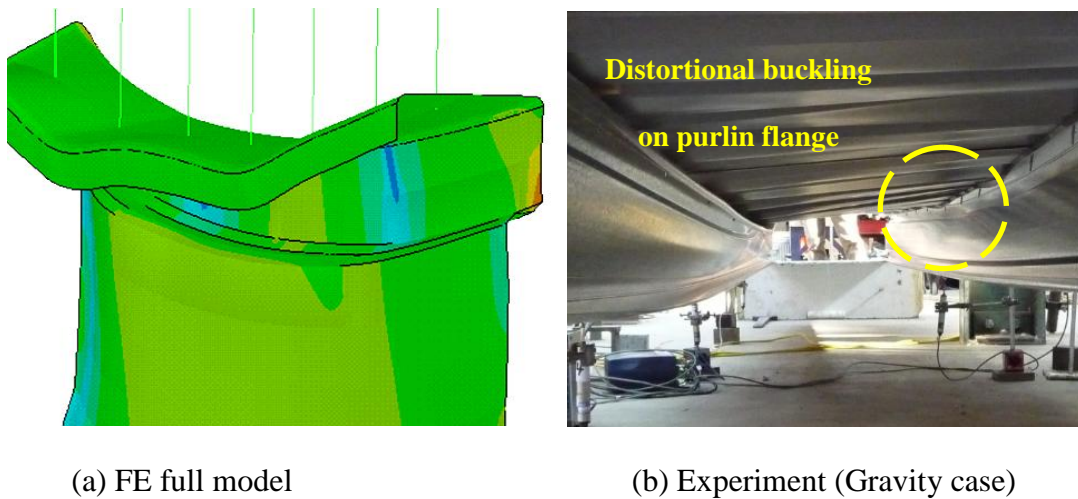local buckling. This can explain the reason why FE simplified model has a slight higher ultimate load than FE full model in some cases.

For the uplift loading case, combined local and lateral-torsional buckling was found as the typical failure mode (Fig.5-38 nd Fig.5-39). For simplified model, no local buckling was observed, which suggested that the structural failure was entirely due to lateral-torsional buckling. In addition, the failure model in simplified model shows a much larger lateral displacement than that in full model.
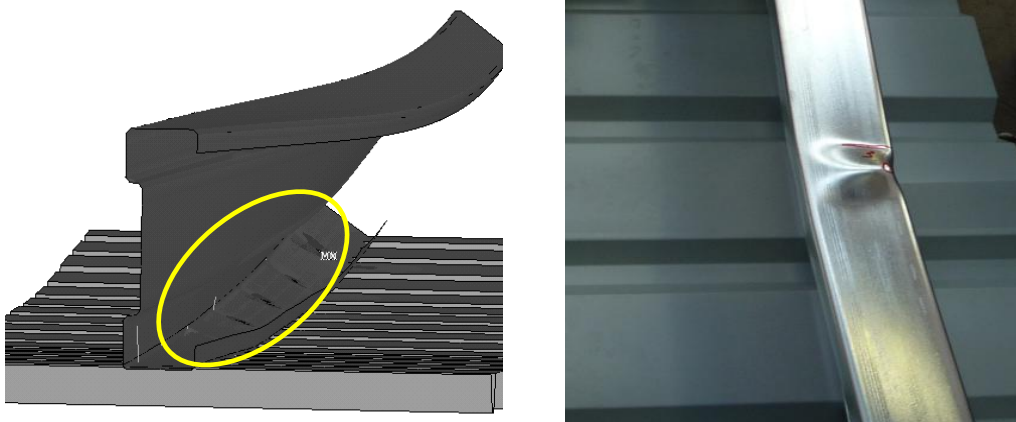

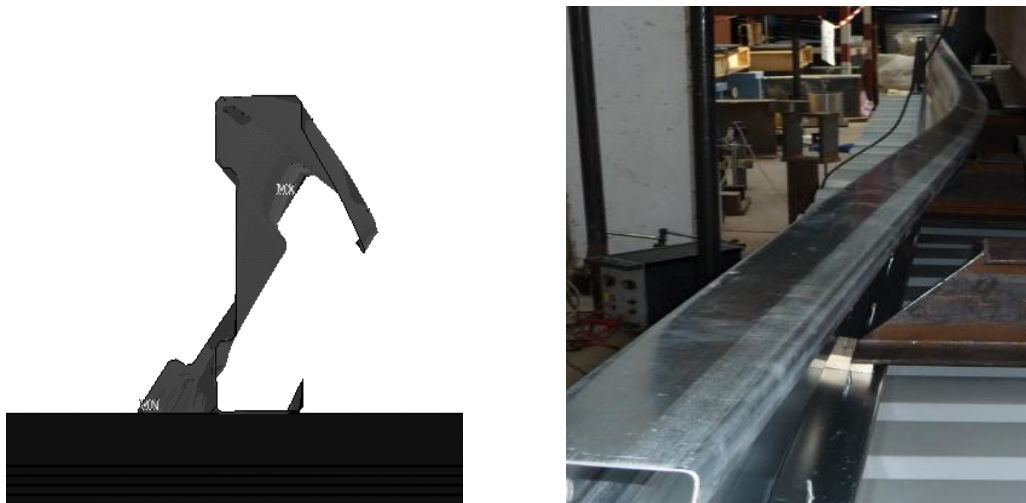Figure 5-38: Local buckling observed in FE full model and experiment (Uplift case)

Figure 5-39: LTB observed in FE full model and experiment (Uplift case)

All these findings suggest that FE simplified model can predict the purlin system ultimate load and initial flexural stiffness with a good level of accuracy. However for predicting model

deformation and failure buckling modes, the full model is a more reliable solution though establishing and analysing the model can be time-consuming.

5.6. Parametric studies on continuous purlin-sheeting system

5.6.1. *Different rotational stiffness*

In order to investigate the impact of rotational stiffness on the load carrying capacity of purlin-sheeting systems, a parametric study on the developed FE simplified model was carried out with rotational stiffness measured in the rotational restraint test and calculated by the EC3 specification (indicated as FEA and EC3, respectively). All other properties remain unchanged. A comparison of load-deflection relationship of these three curves is presented in Fig. 5-40 below with values summarised in Table 5-6.

Table 5-6: Comparison of the ultimate load of test, FE simulation and EC3 prediction

Specimens	Gravity load (kN)			Uplift load (kN)		
	Test	FEA	EC3	Test	FEA	EC3
20012	9.0	8.5	8.3	6.0	6.1	6.1
20016	13.1	12.9	15.0	8.2	7.6	7.4
20025	20.8	22.7	22.5	13.5	13.3	11.2
24015	15.8	14.6	14.5	8.5	8.2	7.4
24023	22.2	21.8	18.9	14.2	14.5	11.5
24030	32.5	32.2	30.8	18.2	19.4	16.4
30018	23.1	23.3	23.6	13.2	13.4	13.3
30025	39.5	38.3	37.4	18.9	18.7	17.1
30030	43.3	42.0	40.0	24.4	24.6	21.3
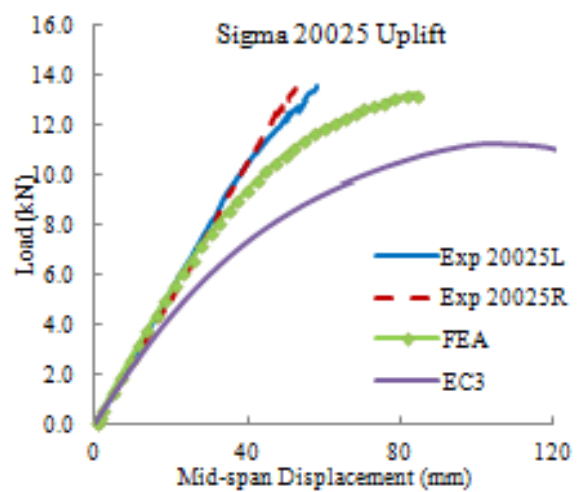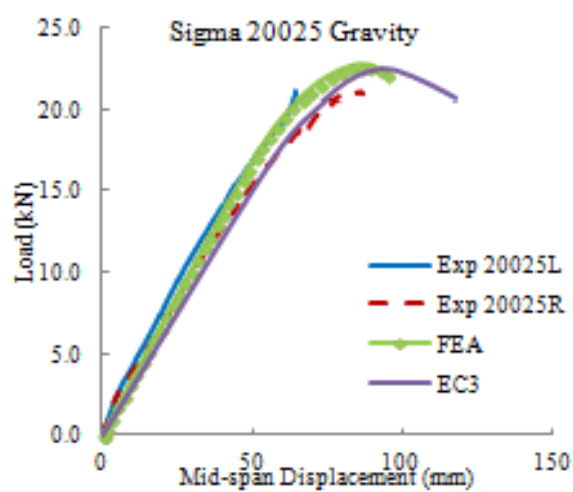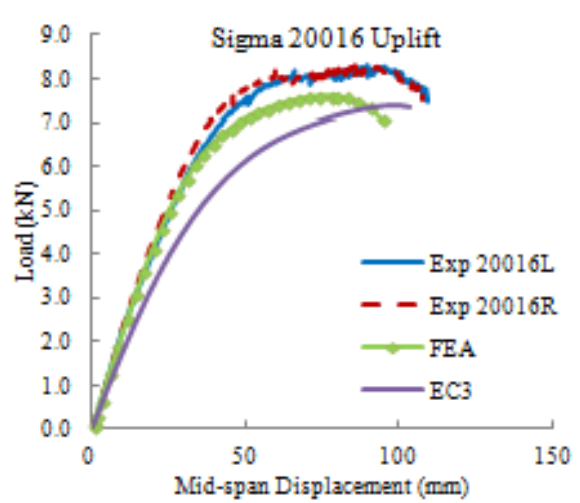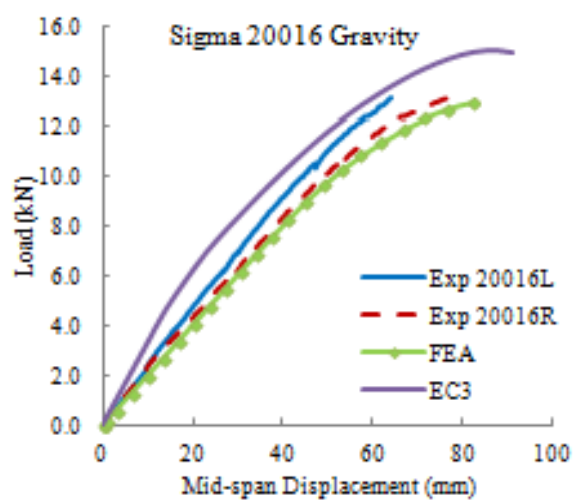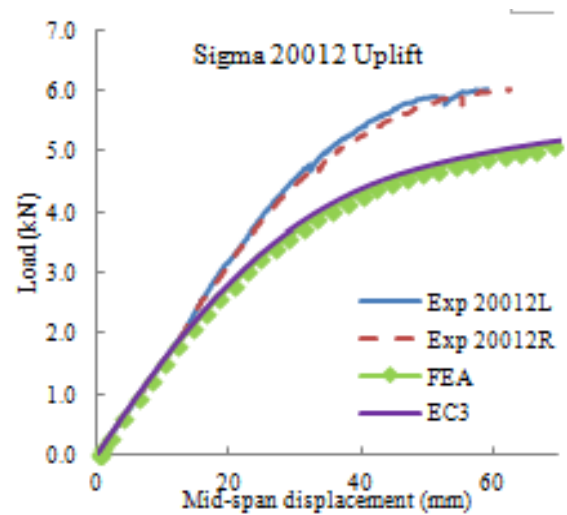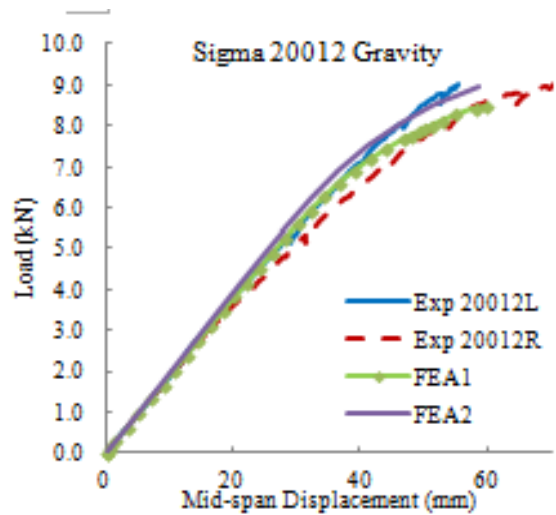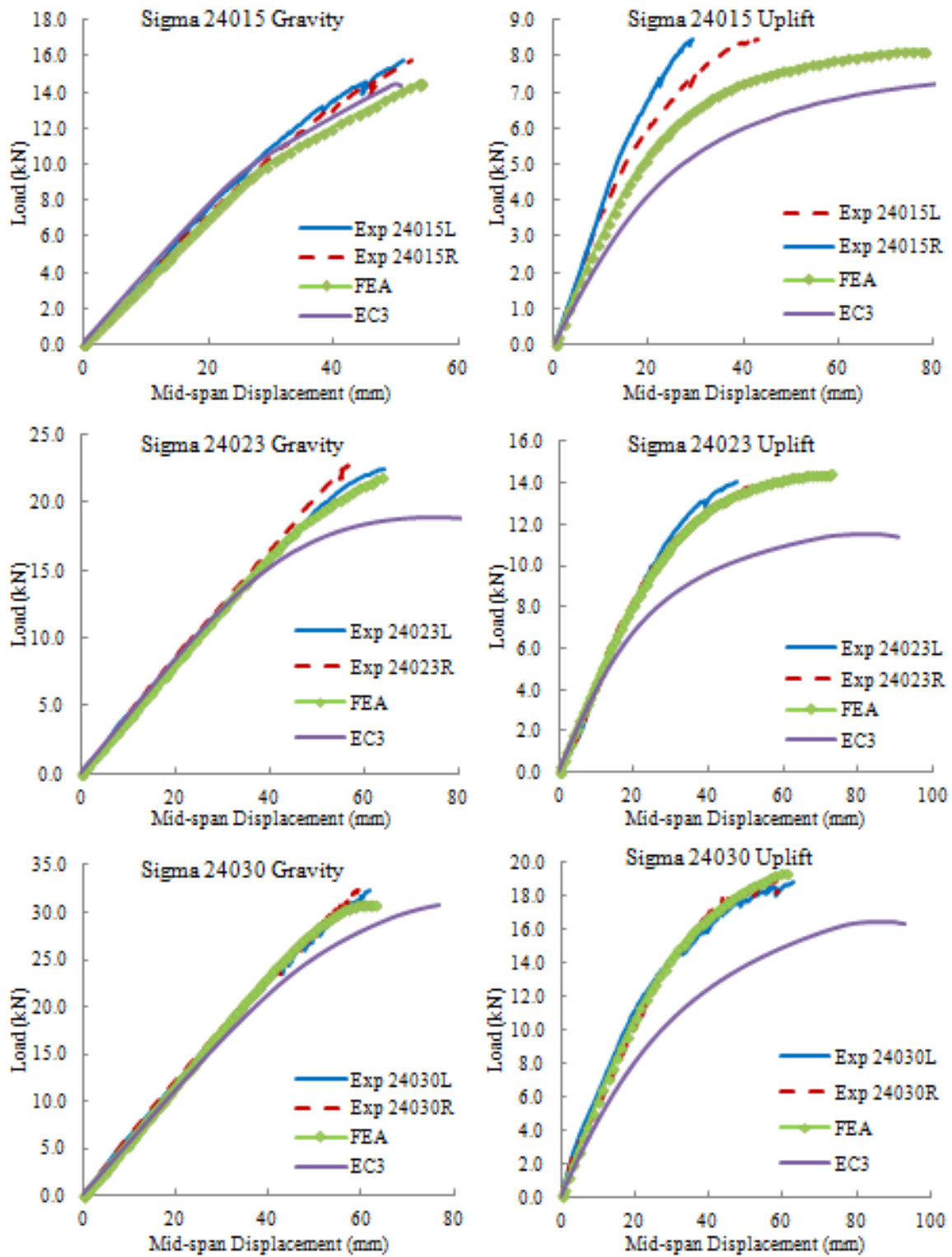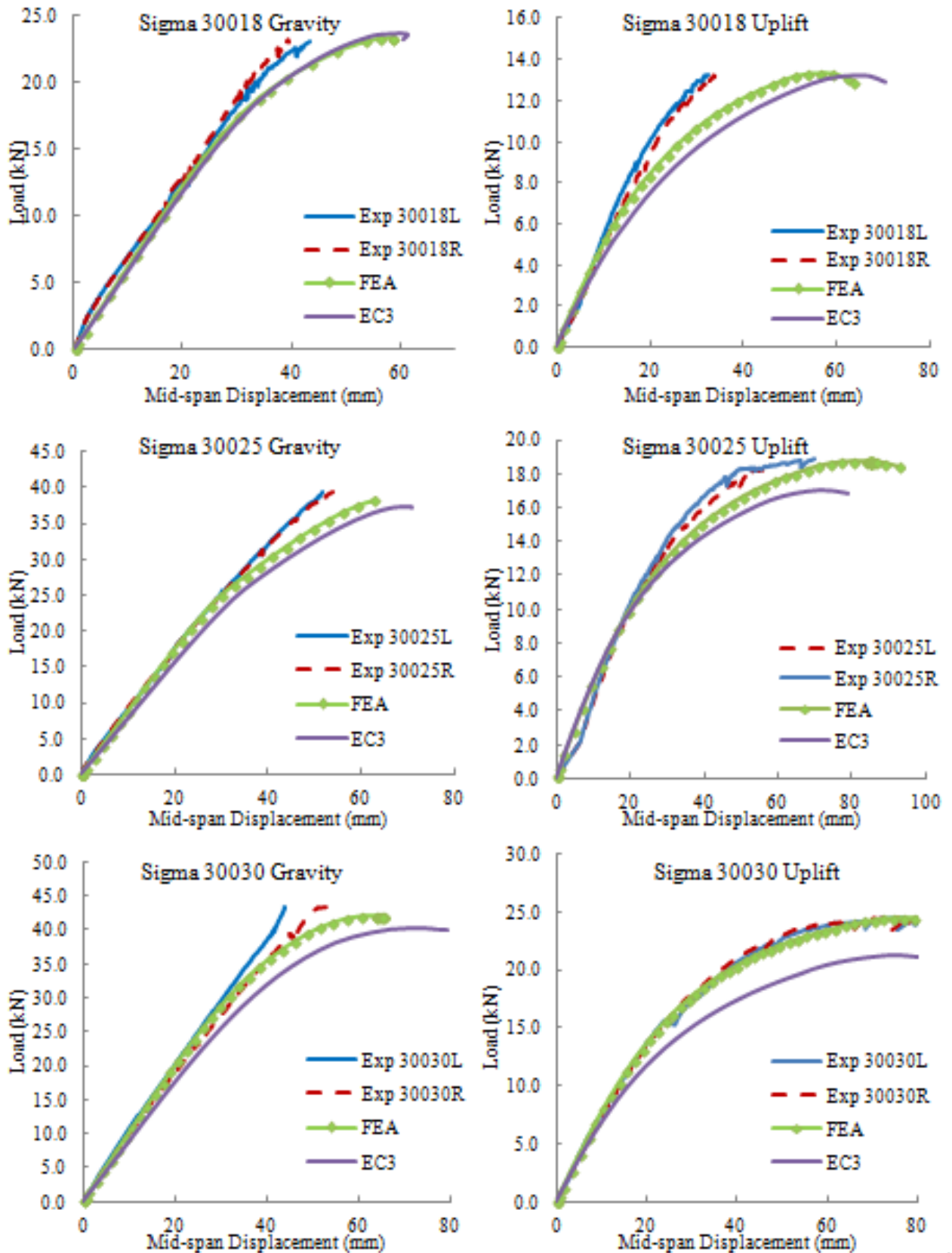
Figure 5-40: Load-displacement comparison curves of test, FEA and prediction

As shown in both figures and the table, the change in rotational stiffness can make a significant difference in load-carrying capacity of purlin-sheeting structure. Among all tested Σ- specimens, the discrepancy in ultimate load ranges from 1% to 8.4% when using test $C_{D,A}$ and from 1% to 23.5% when using EC3 $C_{D,A}$. Standard deviation is 0.043 and 0.088, respectively. It is suggested that when using $C_{D,A}$ values obtained from test, the derived load-carrying capacity is closer to tested values, proving that (a) the accuracy of test $C_{D,A}$ values; (b) the extent of conservatism of EC3 prediction on $C_{D,A}$ values and; (c) ultimate load is sensitive to rotational stiffness. These suggestions again verify the aims of this chapter as well as the thesis, that is, it is important to provide a design model with accurately predicted rotational stiffness, since it has an obvious impact on the strength and stiffness of the structure.

5.6.2. *Double span purlin-sheeting system*

The simplified FE model has provided good agreement with experimental results, and can substitute the full FE model with a satisfactory level of accuracy. This validation is important since full FE can be complex and time-consuming. An additional parametric study is carried out to study the performance of double span continuous purlin-sheeting system under bending using the simplified FE model. An illustration for a typical double span purlin-sheeting model from FEA is given in Fig. 5-41. The ultimate load is provided in Table 5-7 below for the same range of Σ- sections.

An example of $\Sigma24023$ under gravity load is compared with the full model for validation purpose only. The set-up is identical to one-span simplified and full FE model, apart from: (1) uniform distributed transverse load is used in this model to avoid localised deformation; (2) at the mid-span, a finer mesh is adopted for continuous connection to reduce possible stress concentration (Fig.5-42). After nonlinear analysis, the purlins in both cases are failed under a combination of local and distortional buckling at the middle connection, the same failure

modes are observed under gravity (Fig.5-43) and uplift loadings (Fig.5-44). The von Mises stress distribution contour indicates that maximum stress occurred at the mid-way of either side of the purlin section (red areas). The two models have a similar ultimate load, of 81.7kN of full model against 80.1kN of simplified model. Difference is less than 2%. However, the maximum displacement from the simplified model is still noticeably larger than that of the full model.
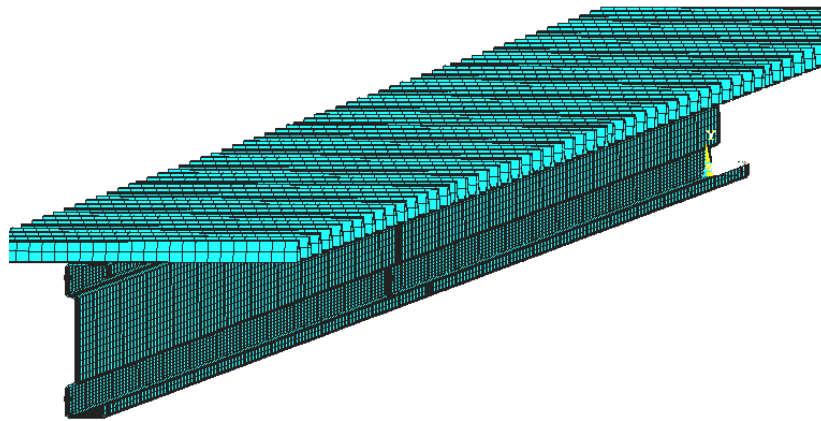

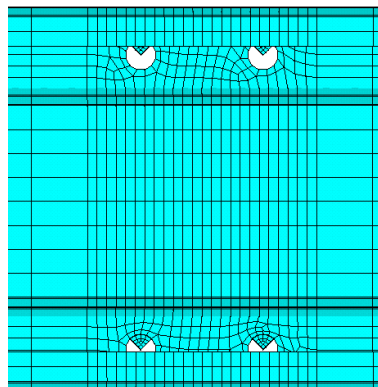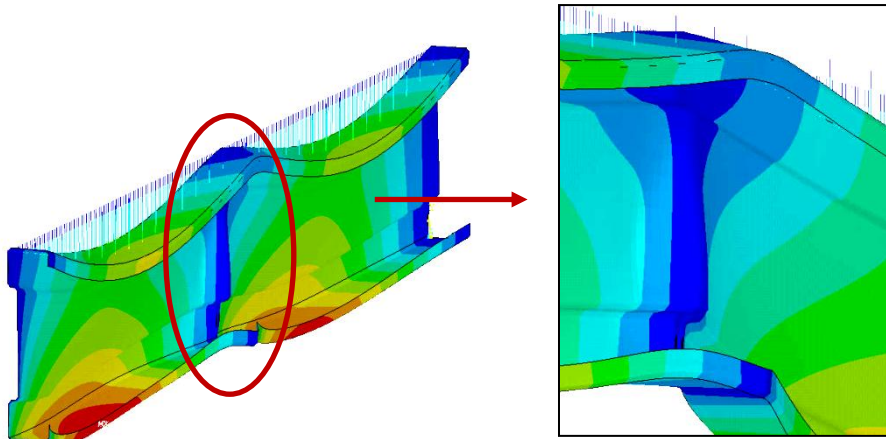Figure 5-41: FE model of a double span purlin-sheeting system

Figure 5-42: Continuous connection in double span FE model

(a) Simplified model
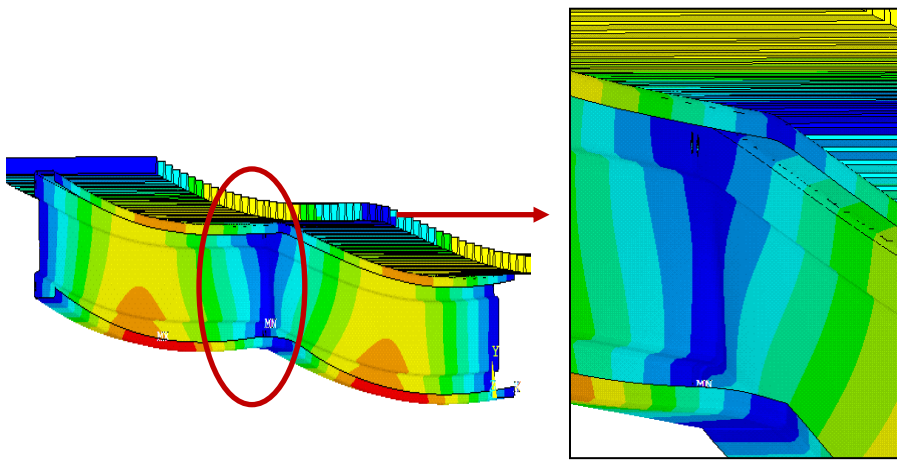
(b) Full model

Figure 5-43: Deformed shapes under gravity loading
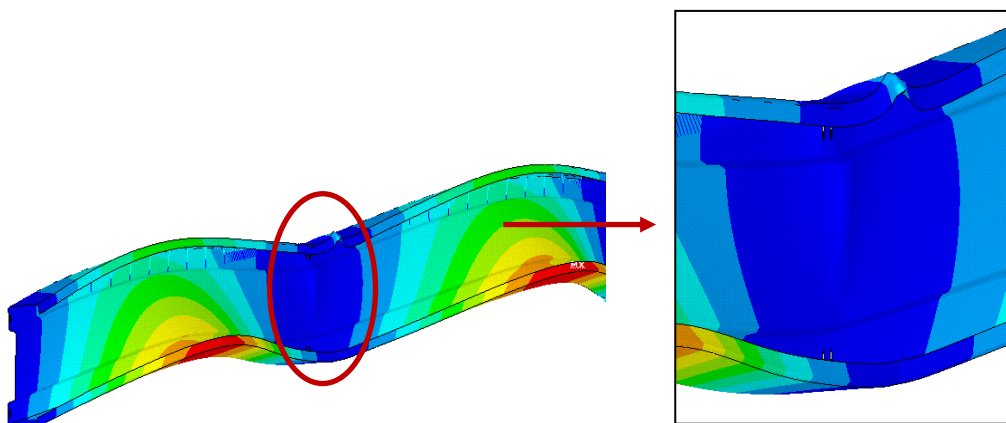
Figure 5-44: Deformed shape under uplift loading

Table 5-7: Ultimate load prediction of double-span Σ- purlin-sheeting system using simplified

FE model

Section ID	Ultimate load in gravity case, kN	Ultimate load in uplift case, kN
20012	23.3	22.4
20016	37.2	35.7
20025	71.7	68.7
24015	38.3	37.5
24023	74.2	71.6
24030	95.7	92.5
30018	50.1	47.8
30025	87.6	82.7
30030	113.1	107.4

5.7. Discussions and summary

In this chapter the load-carrying capacity of CFS purlin-sheeting system have been investigated. Two experiments were conducted to study single span Z- and Σ- purlin sections with either continuous or discontinuous single sheet attachment. Ultimate load, flexural stiffness as well as initial and failure buckling modes of the structures were studied in both cases. In the first experiment, test specimens were under concentrated loading and its results were compared with EC3 design methods; in the second experiment, test specimens were under uniformed distributed loading and its test results were compared with a similar multi-point loading test from Liu and Yang (2012). Numerical models were generated in ANSYS programme to replicate both tests before further developed to carry out additional parametric studies.

Based on the findings and discussion in this chapter, the following conclusions can be made:

(1) The results and observation from four-point bending test has indicated that purlin was mostly likely to fail under a combined effect of distortional buckling and local bearing at the

loading point. In EC3 the partially restrained beam section is not specifically considered, so the prediction was either not safe to apply (when consider it as a full restrained purlin-sheeting system) or overly-conservative (when consider it as a single beam under bending). Therefore a more appropriate design method should be developed;

(2) The results and observation from vacuum chamber test has indicated that purlin was mostly likely to fail under a combined local and distortional buckling mode. Lateral-torsional buckling can be eliminated as long as the sheet provides the purlin with sufficient lateral and rotational restraint under gravity loading. It can also conclude from the test results comparison between UDL and multi-point loading conducted by Liu and Yang (2012) that, when under a multi-point bending, if the number of loading point is sufficient enough to eliminate possible local bearing (i.e. stress concentration), similar results would be expected when compared to a counterpart test under UDL, thus multi-point load can be used as a substitute arrangement when UDL is difficult to achieve;

(3) In the four-bending test, FE models generated in ANSYS have successfully replicated the test condition with a close agreement in predicting ultimate moment capacity and load-displacement relationships. Difference in all cases is within 10%. The FE model has also successfully predicted the failure mode of distortional buckling and local bearing for most of the test specimens but could not predict local/distortional interaction. It is suggested due to the absence of sheet element and/or imperfection applied onto the model.

(4) In the multi-point bending test, FE model again has successfully simulated test conditions via both full model and simplified model. However for predicting member overall rotation especially at post-buckling stage, simplified model is less satisfactory than the full model;

(5) A series of parametric studies on existing FE model were established and it was found that: (a) rotational stiffness has a significant influence on the load-carrying capacity and a

noticeable impact on the structural stiffness, suggesting that it is important to determine $C_{D,A}$ value with a high level of accuracy; (b)For the study of double span or multi-span of purlin-sheeting system, the simplified FE model can be used as a guidance in predicting the ultimate load.

Overall, this chapter and the preceding two chapters have all revealed a concept that the numerical model can be used in the process for investigating the performance of cold-formed purlin-sheeting system ranging from its rotational stiffness, flexural stiffness to the bending behaviour and load-carrying capacity, without assistance of theoretical and experimental data.

Chapter 6: Conclusions

6.1. General

This thesis intends to investigate the structural performance of CFS purlin sections when used together with sheeting under external loads. This chapter provides a summary of the studies that have been carried out on the interactional performance of CFS purlin-sheeting system heretofore. The aims and objectives mentioned in the first chapter have so far been fulfilled by carrying out a series of experimental, numerical and analytical investigations.

The main contribution of the thesis is highlighted in section 6.2. Findings of each chapter are listed in 6.3-6.5 in the same writing order, respectively.

6.2. Main findings and contribution of this thesis

1. A series of rotational restraint test (F-test) has been conducted to measure the rotational stiffness of both cold-formed steel Z- and Σ- purlin sections when screw-fastened to single trapezoidal roof sheet. The test is adapted based on EC3 specifications and is able to measure the rotational stiffness directly.

2. An analytical method has been proposed to predict the rotational stiffness of CFS single skinned purlin-sheeting system. The method is:

   a) Pure analytical, i.e.: no empirical values or numerical calibration is required;

   b) Able to provide a highly accurate value when compared to test result and;

   c) Suitable to apply on a large range of purlin sections with regardless of its geometrical property.

3. A series of four-point bending test has been conducted on the CFS Z-purlin to derive its load-carrying capacity and failure modes when only the shear span was restrained by roof sheet. The test has realised a practical condition where purlin is not fully restrained by sheet and distortional buckling is likely to initiate prior to local buckling. Ultimate

loads are measured and compared to EC3. It is found that EC3 cannot provide an appropriate prediction for this specific condition.

4. A series of uniformly distributed load (UDL) bending test has been conducted on CFS Σ- purlin to derive its load-carrying capacity and failure modes when the section is continuously restrained by roof sheet. The test has realised a practical condition where medium-to-long span beams with no additional lateral restraint provided except the presence of roof sheet. It is found that only local and distortional buckling is likely to occur under gravity load. It is also found that when there are enough loading points to eliminate local stress concentration, multi-point load can be a fair substitution to uniformly distributed load without affecting the ultimate load and failure modes significantly.

5. A FE model has been established to successfully simulate the F-test, four-point bending test and multi-point test. A good agreement of ultimate load with the test results has been achieved. For multi-point test, full model, where sheet is modelled, can provide a more satisfactory result in modelling the member stiffness and failure mode than that of simplified model where sheet is replaced with laterally fixed BC with a rotational spring;

6. A series of parametric studies have been conducted based on the existing FE models to investigate the effect of sheet, i.e. different sheet profiles and thicknesses, the effect of connection i.e. different rotational stiffness as well as the effect of purlin sections on purlin-sheeting system i.e. different geometries and number of spans.

7. FEA models have been established to simulate the multi-point loading and the uniformly distributed loading tests. It has been proven to successfully replicate both test conditions. It was found that full model is able to achieve a better accuracy in

ultimate capacity and deformation of the structure, due to the presence of roof sheet elements.

Other major findings are listed below in different categories from 6.3 to 6.5.

6.3. Investigation on rotational stiffness of CFS purlin-sheeting system (experimental and analytical studies)

1. From F-test it is found that purlin thickness and sheet thickness has a significant impact on the rotational stiffness of purlin-sheeting system, little impact is observed with purlin depth and flange width. No difference due to purlin sections (Z- and Σ- member) if only the rotational stiffness at connection is considered.

2. It is found that loading direction can result a difference in the rotational stiffness due to different ways of purlin-sheet contact. The rotational stiffness is higher when the purlin is in contact with the sheet at the flange-web junction line than when the purlin only touches the sheet at the flange-lip junction line. One of the reasons causing this trend is that the latter case tends to have a shorter lever-arm, resulting in a high tensile force in the screws and hence a larger rotation.

3. EC3 model for predicting rotational stiffness is found lacking in accuracy, the result is either unsafe or overly-conservative when use for design purposes.

4. A pure analytical method is presented to predict the rotational stiffness of purlin-sheeting system at connection. The method is based on one-way slab theory and plate theory, which can apply to a wide range of CFS purlin with single sheet, regardless of the purlin geometry, sheet geometry and connection type and detail. The method is able to provide satisfactory results after test validation. This method also solves the problem of load direction by simplifying with either way of purlin-sheeting contact.

6.4. Investigation on rotational stiffness of CFS purlin-sheeting system (Numerical studies)

1. The result of the FE model is in close agreement to experimental results for predicting rotational stiffness at connection; in addition, the FE model has successfully predicted the rotation caused by each components assumed in analytical method, thus validated the analytical model.

2. The numerical model can provide a very detailed and visual presentation to studying the interacting behaviour of CFS purlin-sheeting system in terms of deformation and stress distribution, and it can be used as a guide for some cases where test and analytical method cannot be used or not available;

3. From the parametric studies, it was found that the sheet geometry and thicknesses have a significant impact on the rotational stiffness of purlin-sheeting system. More stiffeners provided in the sheet profile would achieve a higher rotational stiffness and vice versa; thicker sheet would also achieve a higher rotational stiffness and vice versa. Therefore with the use of complicated-profiled sheet, a thinner sheet can be adopted to achieve similar strength to that of a thicker, ordinary sheet. This model can be used by users to select the appropriate combinations of the roof sheeting so that an optimum solution can be provided.

6.5. Investigation on load-carrying capacity of CFS purlin-sheeting system

1. The results and observation from four-point bending test have indicated that purlin is mostly likely to fail under a combined effect of distortional buckling and local bearing at the load point. In EC3 the partially restrained beam section is not specifically considered, so the prediction was either overly-conservative, when consider it as a single beam under bending, or unsafe when consider it as a full restrained

purlin-sheeting system. Therefore a more appropriate design method should be developed;

2. The results and observation from UDL test have indicated that purlin is mostly likely to fail under a combined local and distortional buckling modes. Lateral-torsional buckling can be eliminated since the sheet provides the purlin with sufficient lateral and rotational restraint under gravity loading. It can also be concluded that, based on the test results comparison between UDL and multi-point loading conducted by Liu and Yang (2012), if the number of loading point is sufficient enough to eliminate possible local bearing (i.e. stress concentration), similar results can be expected when compare to a counterpart test under UDL, thus multi-point load can be used as a substitute arrangement when UDL is difficult to achieve;

3. In the four-point bending test, FE models generated in ANSYS have been successfully replicated the test condition with a close agreement in predicting ultimate moment capacity and load-displacement relationships. Difference in all cases is within 10%. The FE model has also successfully predicted the failure mode of distortional buckling and local bearing for most of the test specimens except for the local/distortional interaction in some of the tested specimens. It is suggested this is due to absence of sheet element and imperfection applied onto the model.

4. In the multi-point bending test, FE models once again have successfully simulated test conditions via both full model and simplified model. However for predicting structural deformation, the simplified model is equally good when compared to full model in predicting ultimate capacity, buckling modes and the general deformation of the structure. However in predicting overall rotation and stress distribution of the structure, full model is more satisfactory due the presence of the sheet.

5. A series of parametric studies on existing FE model have been established and it is found that:

    a) Rotational stiffness has a significant influence on the load-carrying capacity and a noticeable impact on the structural stiffness, proofing that it is important to determine $C_{D,A}$ value with a high level of accuracy;

    b) For studying double span or multi-span of purlin-sheeting system, the FE simplified model can be used as a liable guidance in predicting the ultimate load.

6. Most importantly, this chapter and the previous two chapters have together revealed a concept to use numerical model during the entire process for investigating the performance of cold-formed purlin-sheeting system from predicting its rotational stiffness, flexural stiffness, the bending behaviour and load-carrying capacity, without any theoretical and experimental assistance.

6.6. Limitations and future work

This thesis has addressed some important problems regarding the interactional performance of CFS purlin-sheeting system. However the results achieved so far only contribute to a small section of the entire research area and there are still many gaps waiting to be filled. This section is divided into two parts: first part involves the subjects related to the completion of current research work; second part involves other subjects related to the development of a research system of CFS purlin-sheeting performance.

6.6.1.   *The completion of current research work*

1. To complete the vacuum chamber test. The test is underway at Shanghai Jiao Tong University and is expected to be completed in the next two weeks. Once the test is

finished, all specimens are to be compared with multi-point loading test as well as FE model.

2. To establish a FE Full model for Z- purlin-sheeting system. In Z- purlin test, local/distortional buckling interaction was observed for small sections but was failed to be reproduced by FE model. Possible reasons include individual imperfection or because a full FE model was not used. It will be worthwhile to build a full model, to further investigate its performance, along with the use of various types of imperfections, and compare the result of its counterparts in Σ- sections.

3. To study the post buckling and post failure behaviour of purlin-sheeting system. In this thesis, the emphasis was on the rotational stiffness at connection and the impact of its interactional behaviour on the strength of purlin-sheeting system. Little has been done on the post buckling and post failure behaviour of purlin-sheeting system since it is difficult to achieve by any analytical method.   This can be realised by using FE model.

4. To investigate the other factors associated with rotational stiffness. When considering rotational stiffness only at connection, the purlin geometry does not make a difference. However when considering the overall rotational stiffness, it is obvious that purlin web distortion would contribute some rotations and thus results in a reduction on that value. Other factors such as different connection types, sheet with sandwich filling as well as different screw spans can be investigated in further studies.

6.6.2.   *To develop a research system for purlin-sheeting system*

1. With the validated FE model, a larger scale of purlin-sheeting system can be carried out for future study. Such as three or multi-span of purlins, double or multi-span of sheeting, since the interactional behaviour for multiple purlin-sheeting system may be very different.

2. In this thesis, only Z- and Σ- sections have been investigated. Other sections such as channel may be studied with different sectional geometries since they may have different buckling modes and structural behavior due to its various cross sections. In addition, the results can also be used to further validate the analytical method for predicting rotational stiffness.

3. In order to replicate real engineering conditions, the influence of dynamic loadings to purlin-sheeting system such as cyclic load (snow, wind, rain) and earthquake conditions, also the structural performance under elevated temperatures (in fire) can be further investigated based on the provided FE models.

REFERENCES

1. Adany S. and Schafer B.W. (2006a), "Buckling mode decomposition of single-branched open cross-section members via finite strip method: Derivation", *Thin-walled structures*, 44(5):563-584.

2. Adany S. and Schafer B.W. (2006b), "Buckling mode decomposition of single-branched open cross-section members via finite strip method: Application and examples", *Thin-walled structures*, 44(5):85-600.

3. AISI (2007), North American Specification for the Design of Cold-Formed Steel Structural Members. AISI S100-2007.

4. Alinia, M.M. and Moosavi, S.H. (2008), "A parametric study on the longitudinal stiffeners of web panels", *Thin-Walled Structures*, 46, 1213-1223.

5. AISC (2010), Specification for Structural Steel Buildings, ANSI/AISC 360-10

6. Bryan, G.H. (1891), "On the stability of a plane plate under thrusts in its own plane with applications to the buckling of the sides of a ship", *In: Proceedings of London Mathematics Society*, 22, 54–67.

7. Bailey C.G., Burgess I.W., and Plank R.J.(1996), "The lateral-torsional buckling of unrestrained steel beams in fire", *Journal of constructional steel research*, 36(2): 101-109

8. Bambach, M.R. (2009), "Photogrammetry measurements of buckling modes and interactions in channels with edge-stiffened flanges", *Thin-Walled Structures*, 47:5, 485-504.

9. Bambach, M.R. (2006), "Local buckling and post-local buckling redistribution of stress in slender plates and sections", *Thin-Walled Structures*, 44, 1118-1128.

10. Bambach, M.R. and Rasmussen, K.J.R. (2004), "Design provisions for sections containing unstiffened elements with stress gradient", *Journal of Structural Engineering*, 130(10), 1620–1628.

11. Batista, E.D.M. (2010), "Effective section method: A general direct method for the design of steel cold-formed members under local–global buckling interaction", *Thin-Walled Structures*, 48, 345-356.

12. Bebiano R., Pina P., Silvestre N. and Camotim D. (2008), "GBTUL 1.0β – Buckling and Vibration Analysis of Thin-Walled Members", *DE Civil/IST*, Technical University of Lisbon (http://www.civil.ist.utl.pt/gbt).

13. Beck, V.R. and Stevens, L.K. (1979), "Wind Loading Failures of Corrugated Roof Cladding", *Civil Eng. Trans.*, IEAust; 21(1): 45-56.

14. Bijlaard, P.P., and Fisher, G.P. (1953), "Column Strength of H-Sections and Square Tubes in Post-buckling Range of Component Plates", *N.A.C.A. Technical Note 2994*, Washington, D.C.

15. Bleich, M. (1952), "Buckling strength of metal structures". New York, N.Y: McGraw-Hill.

16. Boissonnade, N.and Somja H. (2012), "Influence of Imperfections in FEM Modelling of Lateral Torsional Buckling", *In: Proceeding of the annual stability conference*, Texas.

17. BSI (2001), "Metallic materials-Tensile testing-Part 1: Method of test at ambient temperature", BS EN 10002-1:2001.

18. BSI (2006a), "Design of Steel Structures–Plated Structural Elements.BS EN", 1993-1-5:2006.

19. BSI (2006b), "Design of Steel Structures–Cold Formed Structures. BS EN, 1993-1-3:2006".

20. Timoshenko, S.P. and Goodier J.N. (1970) "Theory of Elasticity", 3rd Edition, McGraw-Hill, New York, USA, ISBN: 0-07-07-2541-1.

21. Chan, S.L and Kitipornchai S. (1987), "Geometric nonlinear analysis of asymmetric thin-walled beam-columns", *Engineering Structures*; 9(4):243–54.

22. Chen, J.K.and Li, L.Y. (2010), "Distortional buckling of cold-formed steel sections subjected to uniformly distributed transverse loading", *International Journal of*

Structural Stability and Dynamics, 10(5), 1017-1030

23. Cheung, M.S. (1976), "Finite strip method in structural analysis", Oxford: Pergamon Press.

24. Chin, C.K., Al-Bermani, F.G.A. and Kitipornchai, S. (1993), "Finite element method for buckling analysis of plate structures",. *Journal of Structural Engineering ASCE*; 119:1048–68.

25. Chu, X.T., Ye, Z.M., Li, L.Y. and Kettle, R. (2006), "Local and distortional buckling of cold-formed zed-section beams", *International Journal of Mechanical Sciences,* 48, 378–388

26. Chu, X.T. Kettle, R. and Li, L.Y. (2004), "Lateral-torsion buckling analysis of partial laterally restrained thin-walled channel-section beams", *Journal of Constructional Steel Research*, 60, 1159-1175.

27. Chung, K.F and St.Quinton, D.(1996), "Structural performance of modern roofs with thick over-purlin insulation - Experimental investigation", *Journal of Constructional Steel Research*, 40(1) 17-38.

28. Cohen, J.M. and Pekoz, T. (1987), "Local buckling behavior of plate elements. Research Report", *Department of Structural Engineering*, Cornell University.

29. Davies, J. M. and Jiang, C. (1996a), "Design of thin-walled columns for distorsional

buckling, in: Rondal, J., Dubina, D., Gioncu, V. (Eds.)", *Coupled Instabilities in Metal Structures* – CIMS 96, London: Imperial College Press, pp. 165-172.

30. Davies, J. M. and Jiang, C. (1998), "Design for distortional buckling", *Journal of Constructional Steel Research*, 46, 1-3, Paper N. 104.

31. Davies, J.M. and Leach, P. (1994a), "First-order generalised beam theory", *Journal of Constructional Steel Research*, 31(2-3), 187-220.

32. Davies, J.M. Leach, P. and Heinz, D. (1994b), "Second-order generalised beam theory", *Journal of Constructional Steel Research*, 31(2-3), 221-241.

33. Dawe D.J.and Wang S (1996), "Finite strip large deflection and post-overall-buckling analysis of diaphragm-supported plate structures", *Computers and Structures,* 61(1): 155-170.

34. Dinis, P.B. and Camotim, D. (2010), "Local/distortional mode interaction in cold-formed steel lipped channel beams", *Thin-Walled Structures*, 48, 771-785.

35. Dinis, P.B. Camotim, D.and Silvestre, N. (2007), "FEM-based analysis of the local-plate/distortional mode interaction in cold-formed steel lipped channel columns", *Computers and Structures*, 85, 1461-1474.

36. Dubina, D. and Ungureanu, V. (2002), "Effect of imperfections on numerical simulation of instability behaviour of cold-formed steel members", *Thin-Walled*

Structures, 40, 239-262.

37. EI Damatty, A.A., Rahman, M. and Ragheb, O. (2003), "Component testing and finite element modelling of standing seam roofs", *Thin-walled structures*, 41(11), 1053-1072

38. Ellifrett, D.S., Glover, R.L., and Hren, J.D. (1998), "A simplified model for distortional buckling of channels and zees in Flexure", *Proceedings of the fourteenth international specialty conference on cold-formed steel structures*, St. Louis MO., October 15-16.

39. Fan L, Rondal J and Cescotto S. (1997), "Finite element modelling of single lap screw connections in steel sheeting under static shear", *Thin-Walled Structures*, 27(2), pp 165-185.

40. Galambos, T.V. (1968), "Structural Members and Frames", Prentice-Hall Inc., Englewood Cliffs,N.J.

41. Gao, T. and Moen, C. (2012), "Predicting rotational restraint provided to wall girts and roof purlins by through-fastened metal panels", *Thin-walled structures*, Volume 61, Pages 145-153.

42. Gebremedhin, K.G. and Price, J.W. (1999), "Tests of Post-frame building diaphragm", *Journal of Structural Engineering*, Vol. 125(10):1170-1178.

43. Gerard G. and Becker, H. (1957), "Handbook of Structural Stability Part I: Buckling of

Flat Plates", NACA TN 3781.

44. Hancock, G. J.(1978), "Local, Distortional, and Lateral Buckling of I-Beams", *ASCE J Struct Div*, v 104, n 11, p 1787-1798

45. Hancock, G.J. (1985), "Distortional buckling of steel storage rack columns", *Journal of Structural Engineering*, 111(12), 2770-2783.

46. Hancock, G.J. Murray, T.M. and Ellifritt, D.S. (2001), "Design of cold-formed steel structures to the AISI specification", New York: Marcel Dekker Inc.

47. Jiang, C. and Davies, J.M. (1997), "Design of thin-walled purlins for distortional buckling", *Thin-Walled Structures*, 29, 189-202.

48. Katnam, K.B., Van Impe, R., Lagae, G., and De Strycker, M. (2007a). "A theoretical numerical study of the rotational restraint in cold-formed steel single skin purlin-sheeting systems". *Computers & Structures*, 85(15-16): 1185-1193.

49. Katnam, K.B., Van Impe, R., Lagae, G., and De Strycker, M. (2007b). "Modelling of cold-formed steel sandwich purlin-sheeting systems to estimate the rotational restraint". *Thin-Walled Structures*, 45(6): 584-590.

50. Kavanagh, K. T., and Ellifritt, D. S. (1994). "Design strengths of coldformed channels in bending and torsion", *Journal of Structural Engineering*, ASCE, 120(5), 1599 – 1607.

51. Kip A.A, Toma A.W. (1986), "Research for the mechanical behaviour of cold-formed sections and drafting of design rules: Report of testing of diaphragm braced beams (3rd Edn)", TNO Building and Construction Research report, BI-86-54/63.5.5481.

52. Kirby, P. A. and Nethercot, D. A. (1979),. "Design of Structural Stability", Halsted Press, NY, NY.

53. Kwon, Y. B. and Hancock, G., J., (1992), "Tests of cold-formed channels with local and distortional buckling", *ASCE Journal of Structural Engineering*, Vol. 117, pp. 1786-1803.

54. LaBoube, R. A. (1990), "Estimating uplift capacity of light steel roof system", *J. Struct. Eng*, ASCE, 118 (3), 848-852

55. LaBoube, R. A. and Yu, W.W. (1982), "Bending Strength of Webs of Cold-Formed Steel Beams", *Journal of Structural Division*, ASCE, 108(ST7), pp1589-1604

56. Laine, M. and Tuomala, M. (1999), "Testing and design of gravity-loaded steel purlins restrained by sheeting", *Journal of Constructional Steel Research*, 49, 129-138.

57. Lau, S.C.W. and Hancock, G.J. (1989), "Inelastic buckling analysis of beam, columns and plates using the spline finite strip method", *Thin-Walled Structures* (7): 213-238.

58. Lau, S.C.W., and Hancock, G.J (1987), "Distortional Buckling Formulas for Channel

Columns", *Journal of Structural Engineering,ASCE*,1987, 113(5), pp 1063 – 1078.

59. Laudiero F, Zaccaria D (1988), "Finite element analysis of stability of thin-walled beams of open section", *International Journal of Mechanical Science* 30(8): 543–557

60. Lee, S.C. Davidson, J.S. and Yoo, C.H. (1996), "Shear buckling coefficients of plate girder web panels", *Computer and Structures*, 59(5), 789-7

61. Li, L.Y. (2004), "Lateral-torsional buckling of cold-formed zed-purlins partial laterally restrained by metal sheeting", *Thin-Walled Structures*, 42, 995-1011.

62. Li, L.Y. and Chen, J.K. (2008), "An analytical model for analyzing distortional buckling of cold-formed steel sections", *Thin-Walled Structures*, 46, 1430-1436.

63. Li, L.Y., Ren, C. and Yang, J. (2012), "Theoretical analysis of partially restrained zed-purlin beams subjected to up-lift loads", *Journal of Constructional Steel Research*, 70: 273-279.

64. Lindner, J. and Aschinger, R. (1994), "Load-carrying capacity of cold-formed beams subjected to overall lateral-torsional buckling and local plate buckling", *Journal of Constructional Steel Research*, 31, 267-287.

65. Lucas, R.M., F.G.A. AlBermani, and S. Kitipornchai (1997a), "Modelling of cold-formed purlin-sheeting systems .1. Full model", *Thin-Walled Structures*, 27(3): 223-243.

66. Lucas, R.M., F.G.A. AlBermani, and S. Kitipornchai (1997b), "Modelling of cold-formed purlin-sheeting systems .2. Simplified model", *Thin-Walled Structures*, 27(4): 263-286.

67. Liu, Q. (2012), "Structural analysis and design of cold-formed steel sigma purlins", PhD thesis, the University of Birmingham.

68. Macdonald, M. Heiyantuduwa, M.A. and Rhodes, J. (2008), "Recent developments in the design of cold-formed steel members", *Thin-Walled Structures*, 46(7-9), 1047-1053.

69. Mahaarachchi D (2003), "Behaviour and design of profiled steel cladding system subject to pull-through failure", PhD thesis, Queensland university of technology.

70. Mahendran, M. and Tang, R. B. (1998), "Pull-out strength of steel roof and wall cladding systems", *Journal of Structural Engineering*, *124*(10), pp. 1192-1201.

71. Mahendran, M. (1990b), "Static Behaviour of Corrugated Roofing under Simulated Wind Loading", *Civil Eng Trans*., IE Aust; 32(4): 211-218.

72. Mahendran, M. (1994), "Behaviour and Design of Crest Fixed Profiled Steel Roof Claddings Under High Wind Forces", *Eng Struct*; 16(5): 368-376.

73. Martin, L. H. and J. A. Purkiss (2007), "Structural design of steelwork to EN 1993 and

EN 1994", Burlington, Elsevier.

74. Michell, A.G.M (1899), "Elastic stability of long beams under trasnverse forces", *Philosophic magazine*, Vol.48,298

75. Misiek T, Kruger H, Ummenhofer T, and Kathage K.(2010), "Buckling of stiffeners for stainless steel trapezoidal sheeting", *Steel Construction* 3(4), 225-230, Wiley-VCH Verlag.

76. Mohri F, Damil N, and Potier-Ferry M (2008), "Large torsion finite element model for thin-walled beams", *Comput Struct* 86:671–683

77. Moore, D.B. and Sims, P.A.C. (1988a), "Load tests on full-scale cold formed steel roofs. Part 1: Sigma purlin system (BRE Report BR122)", Building Research Establishment.

78. Kankanamge, N. D. and Mahendran M. (2011), "Mechanical Properties of Cold-Formed Steels at Elevated Temperatures," *Thin-Walled Structures*, Vol. 49, No. 1. pp. 26-44. doi:10.1016/j.tws.2010.08.004

79. Nandini, P and Kalyanaraman, V. (2010) "Strength of cold-formed lipped channel beams under interaction of local, distortional and lateral torsional buckling." *Thin-Walled Structures*. 48:10-11, 872-877.

80. Natalia Kutanova (2009), "Cross-sectional instability of aluminum extrusions with complex cross-sectional shapes", PhD thesis.

81. Pekӧz, T. (1987), "Development of a unified approach to the design of cold-formed steel members", American Iron and Steel Institute, Research Report CF87-1.

82. Pekӧz, T. and Soroushian, P. (1982), "Behaviour of C- and Z-purlins under wind uplift", *In: Proceedings of the 6th International Specialty Conference on Cold-formed Steel Structures*. St. Louis, MO, USA, 409-429.

83. Pham, C.H. and Hancock, G.J. (2009), "Direct strength design of cold-formed purlins", *Journal of Structural Engineering*, 135(3), 229-238.

84. Pi, Y.L. Put, B.M. and Trahair, N.S. (1998), "Lateral buckling strengths of cold-formed channel section beams", *Journal of Structural Engineering*, 124, 1182-1191.

85. Pi, Y.L. Put, B.M. and Trahair, N.S. (1999), "Lateral buckling strengths of cold-formed Z-section beams", *Thin-Walled Structures*, 34, 65-93.

86. Prevatt, D. and Schiff, S. (1996), "Uplift Testing of Standing Seam Metal Roof Systems," Department of Civil Engineering, Clemson University, Clemson, SC, MBMA Report 9403, June 1996

87. Put, B.M. Pi, Y.L. and Trahair, N.S. (1999a), "Lateral buckling tests on cold-formed channel beams", *Journal of Structural Engineering*, 125, 532-539.

88. Put, B.M. Pi, Y.L. and Trahair, N.S. (1999b), "Lateral buckling tests on cold-formed Z

beams", *Journal of Structural Engineering*, 125, 1277-1283.

89. Barsoum, R.S. and Gallagher, R.H. (1970), "Finite element analysis of torsional and torsional-flexural stability problems", *International Journal for Numerical Methods in Engineering*, 2 (3), pp. 335–352

90. Ren, C., Li, L. Y. and Yang, J. (2012), "Bending analysis of partially restrained channel section purlins subjected to up-lift loadings", *Journal of Constructional Steel Research* 72. 254-260.

91. Robert, T.M. and Jhita, P.S. (1983), "Lateral, local and distortional buckling of I-beams", *Thin-Walled Structures*, 4(1), 289-308.

92. Ronagh, H.R., Bradford, M.A. and Attard, M.M. (2000), "Nonlinear analysis of thin-walled members of variable cross-section, Part I: theory", *Computer Structures* 77:285–299

93. Rousch, C.J. and Hancock, G.J. (1997), "Comparison of tests of bridged and unbridged purlins with a non-linear analysis model", *Journal of Constructional Steel Research*, 44, 197-220.

94. Salvadori, M. G. (1955), "Lateral Buckling of I-beams", *ASCE Transactions*, American Society of Civil Engineers, 120, 1165-1177.

95. Schafer B.W., and Adany S. (2006), "Buckling analysis of cold-formed steel members using CUFSM: conventional and constrained finite strip methods", *18th International*

Specialty Conference on Cold-Formed Steel Structures, October 26-27, 2006, Orlando, Florida

96. Schafer, B.W. and Adany, S (2006), "Buckling analysis of cold-formed steel members using CUFSM: conventional and constrained finite strip methods", *18th international specialty conference on Cold-formed steel structures*, Orlando, Florida.

97. Schafer, B. W. (2008), "Review: The Direct Strength Method of cold-formed steel member design", *Journal of Constructional Steel Research*, 64(7-8): 766-778.

98. Schafer, B. W., and Pekӧz, T. (1999), "Laterally braced cold-formed steel flexural members with edge stiffened flanges", *J. Struct. Eng.* 1252, 118–127

99. Schafer, B.W. (2008), "Review: The Direct Strength Method of cold-formed steel member design", *Journal of Constructional Steel Research*, 64, 766-778.

100. Schafer, B.W. and Pekӧz, T. (1998), "Direct strength prediction of cold-formed steel members using numerical elastic buckling solutions", In: Shanmugam NE, et al., editors. *Thin-walled structures*. Amsterdam: Elsevier.

101. Schardt, R. (1983), "The generalised beam theory", *In: Proceedings of the M.R. Horne Conference*, University of Manchester, Granada, London, 469-475.

102. Seif, M. and Schafer, B.W. (2010), "Local Buckling of Structural Steel Shapes", Elsevier, *Journal of Constructional Steel Research*. 66 (10) 1232-1247.

103. Serna, M.A., Lopez, A., Puente, I., and Yong, D. J. (2006), "Equivalent Uniform Moment Factors and Lateral Torsional Buckling of Steel Members", *Journal of Constructional Steel Research*, 62(6), 566-580.

104. Silvestre, N. and Camotim, D. (2004a), "Distortional buckling formulae for cold-formed steel C and Z-section members Part I-derivation", *Thin-Walled Structures*, 42(11), 1567-1597.

105. Silvestre, N. and Camotim, D. (2004b), "Distortional buckling formulae for cold-formed steel C and Z-section members Part II-Validation and application", *Thin-Walled Structures*, 42(11), 1599-1629.

106. Sokol, L. (1996), "Stability of cold-formed purlins braced by steel sheeting", *Thin-Walled Structures*, 25(4), 247-268.

107. Sridharan, S., (1982), "A semi-analytical method for the post-local-torsional buckling analysis of prismatic plate structures", *International Journal of Numerical Methods for Engineering*, Vol. 18, pp. 1685-1697

108. Standards Australia (2006), "Cold-Formed Steel Structures", AS/NZS 4600:2005. Standards Australia/Standards New Zealand.

109. Timoshenko, S.P. (1910), "Einige Stabilitatsrobleme der Elastiz~.tstheorie", *Z Math Phys 58*, 337-357.

110. Timoshenko, S.P. and Gere, J.M. (1961), "Theory of elastic stability", 2nd ed.New York: McGraw-Hill Book Co. Inc.

111. Timoshenko, S.P. (1945), "Theory of Bending, Torsion and Buckling of thin-walled Members of open sections", *Journal of the Franklin Institute*, March, April and May

112. Timoshenko. S.P. (1953), "Einige stabilitats probleme der Elastizitatstheorie, collected papers of Stephen Timoshenko", New York, N.Y.: McGraw-Hill, Book Co.

113. Tomà, T. and Wittemann, K. (1994), "Design of cold-formed purlins and rails restrained by sheeting", *Journal of Constructional Steel Research*, 31, 149-168.

114. Trahair N.S. (1993), "Flexural-torsional buckling of structures", London. E&FN Spon.

115. Trahair, N.S. (1994), "Lateral buckling strengths of unsheeted cold-formed beams", *Engineering Structures*, 16(5), 324-331.

116. Trahair, N.S. (2002), "Lateral buckling strengths of steel angle section beams", *research report No R812*, The university of Sydney.

117. Vacharajittiphan, P, Woolcock, S.T. and Trahair, N.S. (1974), "Effect of in-plane deformation on lateral buckling", *Journal of Structural Mechanics* 1974;3:29–60.

118. Vieira Jr, L. C. M., et al. (2010). "Simplified models for cross-section stress demands on C-section purlins in uplift", *Thin-Walled Structures*, 48(1): 33-41.

119. Vieira Jr, L. C. M., et al. (2010), "Simplified models for cross-section stress demands on C-section purlins in uplift", *Thin-Walled Structures*, 48(1): 33-41.

120. Vila Real PMM, Lopes N., Simoes da Silva L. and Franssen J.-M. (2004), "Lateral-torsional buckling of unrestrained steel beams under fire conditions: improvement of EC3 proposal", *Computers and structures*, 82: 1737-1744.

121. Vlasov V. Z. (1961), "Thin-Walled Elastic Beams", *Israel Program for Scientific Translations*, Jerusalem

122. Von Kármán, T. Sechler, E.E. and Donnell, L.H. (1932), "The strength of thin plates in compression", *ASME Transactions*, APM-54, 553–57.

123. Vrany, T. (2002), "Torsional restraint of cold-formed beams provided by corrugated sheeting for arbitrary input variables", *Eurosteel the 3rd European conference on steel structures*, Coimbra, Portugal.

124. Vrany, T. (2007), "Effect of loading on the rotational restraint of cold-formed purlins*"*, *Thin-Walled Structures*, 44(12): 1287-1292.

125. Winter, G. (1947), "Strength of thin steel compression flanges", *Transactions, ASCE*, 112, 527-576.

126. Xu, Y.L. and Reardon, G.F. (1993), "Test of Screw Fastened Profiled Roofing Sheets Subject to Simulated Wind Uplift", *Eng. Struct*; 15(6): 423-430.

127. Yang, D. and Hancock, G.J. (2004), "Compression tests of high strength steel channel columns with interaction between local and distortional buckling", *Journal of Structural Engineering*, 130(12), 1954-1963.

128. Yang, J. and Liu, Q. (2012), "An experimental study into flexural behaviour of sigma purlins attached with roof sheets", *Engineering Structures*, 45(0): 481-495.

129. Yap, D.C.Y, Hancock, G.J. (2006), "Interaction buckling and post-buckling in the distortional mode of thin-walled sections", *Research Report R870*, School of Civil Engineering, University of Sydney, Australia.

130. Ye, Z.M. Kettle, R.J. and Li, L.Y. (2004), "Analysis of cold-formed zed-purlins partially restrained by steel sheeting", *Computers and Structures*, 82, 731-739.

131. Ye, Z.M. Kettle, R.J. Li, L.Y. and Schafer, B.W. (2002), "Buckling behaviour of cold-formed zed-purlins partially restrained by steel sheeting", *Thin-Walled Structures*, 40, 853-864.

132. Yu, C. (2005), "Distortional buckling of cold-formed steel members in bending", PhD thesis, John Hopkins University.

133. Yu, C. and Schafer, B.W. (2003), "Local buckling tests on cold formed steel beams", *Journal of Structural Engineering*, 129, 1596-1606.

134. Yu, C. and Schafer, B.W. (2006), "Distortional buckling tests on cold-formed steel beams", *Journal of Structural Engineering*, 132, 515-528.

135. Yu, C. and Schafer, B.W. (2007), "Simulation of cold-formed steel beams in local and distortional buckling with applications to the direct strength method", *Journal of Constructional Steel Research*, 63, 581-590.

136. Yu, C. and Schafer, B.W.(2007), "Simulation of cold-formed steel beams in local and distortional buckling with applications to the direct strength method", *Journal of Constructional Steel Research*, 63(5), 581-590

137. Yu, W.W. (2000), "Cold-formed steel design", 3rd Edition. New York: John Wiley and Sons Inc.

138. Zhang, L. and Tong, G.S. (2008), "Moment resistance and flexural rigidity of lapped connections in multi-span cold-formed Z purlin systems*", Thin-Walled Structures*, 46, 551-560.

139. Zhao X.L., Hancock, G.J. and Trahair N.S. (1995), "Lateral buckling tests of cold-formed RHS beams, *Journal of structural engineering ASCE*, Vol. 121, No. 11, pp.1565-73.

140. Zhao C.X., Yang J. Wang F.L. Chan A.H.C (2014), "Rotational stiffness of cold-formed steel roof purlin-sheeting connections", *Engineering structures*, (59) 284-297

141. Ziemian R.D (2010), "The guide to stability design criteria for metal structures", 6th edition, Wiley.

142. Hancock, G.J (1997), "Design of distortional buckling of flexural member", *Thin-walled structures*, 20,3-12.

APPENDICES

Appendix A.1: Material coupon test

True stress-strain relationship is derived from material coupon test. The tension test conducted followed standard test procedure of tension testing of metallic materials in(BSI 2001). By using this stress-strain curve, 0.2% proof yield stress, ultimate stress and young's modulus can be determined.

For Z- sections, testing samples were cut by the manufacturer in form of flat steel sheets (coupons). Three coupon samples of each specimen were tested using Danison testing machine (Fig.A.1.1). Coupon sample was fully clamped at both ends by using the jaws of the machine, leaving 50mm clear distance in the middle section to measure the elongation under tension. Extensometer was applied to record the extension (Fig.A.1.2). Coupon dimensions and their corresponding 0.2% stress, ultimate stress and young's modulus are presented in Table A.1-I and Fig.A.1.3 for Z-section, Table A.1-II and Fig.A.1.4 for Σ- section. It is certified that material coupon test for Σ- section is conducted by Liu (2012).

Figure A.1.1: Tensile testing machine Figure A.1.2: Sample steel coupon under testing

Table A.1-I: Coupon sample geometry and results for Z-section

Section	Specimen name	Width (mm)	Thickness	0.2% proof stress	Ultimate load	Young's modulus
Z14614	Z146.14-t1	21.67	1.44	432	562	217859
Z14614	Z146.14-t2	21.68	1.43	433	569	211597
Z14614	Z146.14-t3	21.88	1.36	450	592	210914
Z14618	Z146.18-t1	25.28	1.67	450	595	218569
Z14618	Z146.18-t2	25.4	1.69	451	577	202778
Z14618	Z146.18-t3	25.5	1.66	452	577	205653
Z20618	Z206.18-t1	23.58	1.7	531	592	218827
Z20618	Z206.18-t2	22.79	1.68	554	599	219482
Z20618	Z206.18-t3	23.96	1.68	526	607	210534
Z30718	Z307.20-t1	25.23	2.00	505	623	215410
Z30718	Z307.20-t2	25.18	1.97	418	554	199402
Z30718	Z307.20-t3	25.18	1.97	387	520	211759
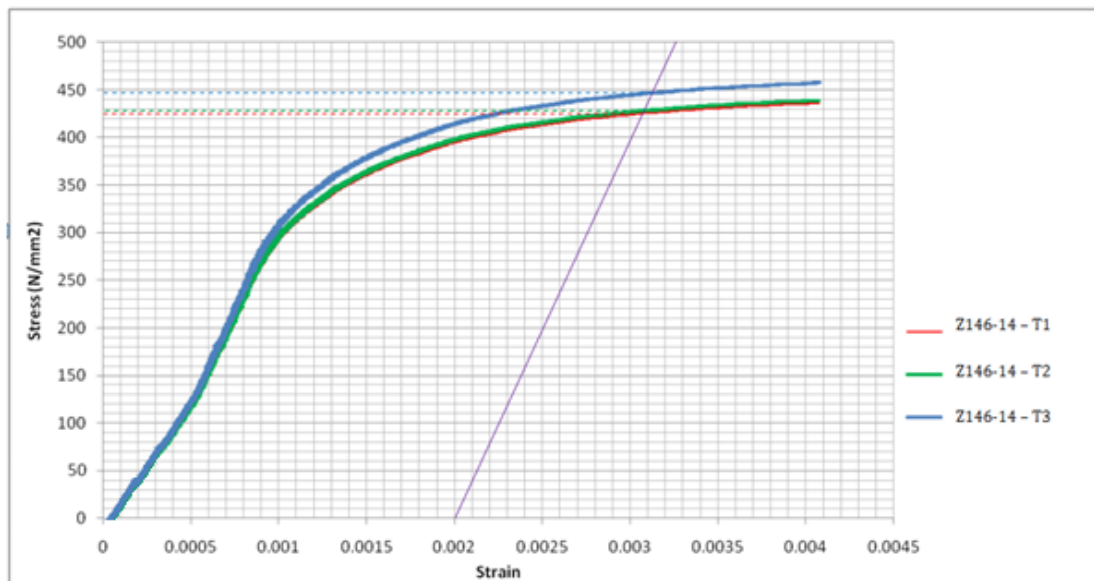
Z-14614
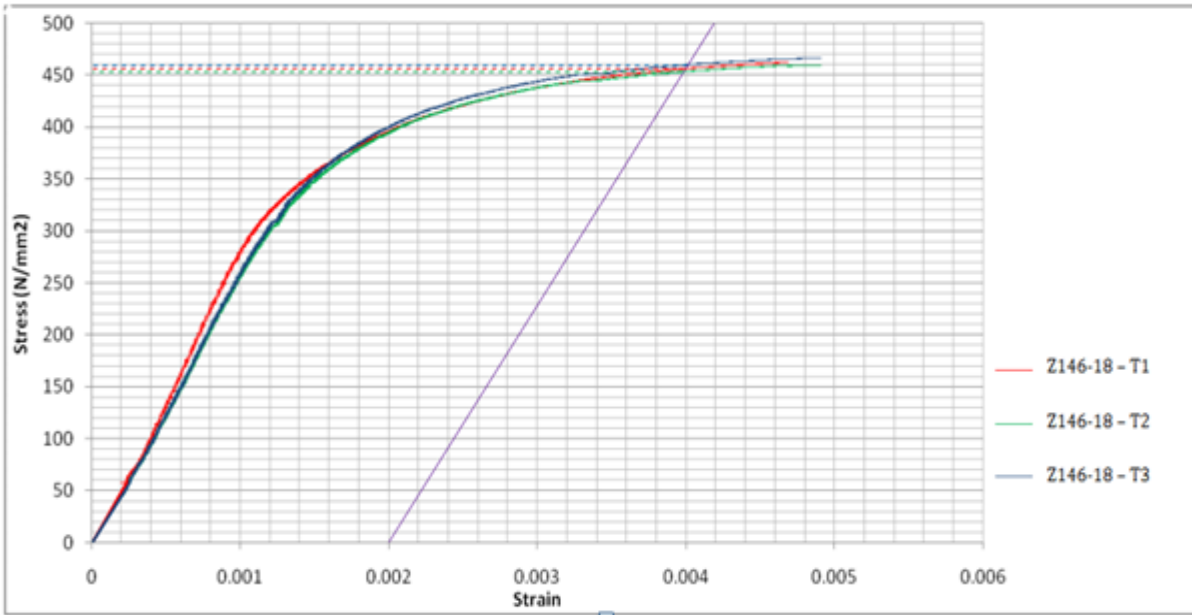
Z-14618
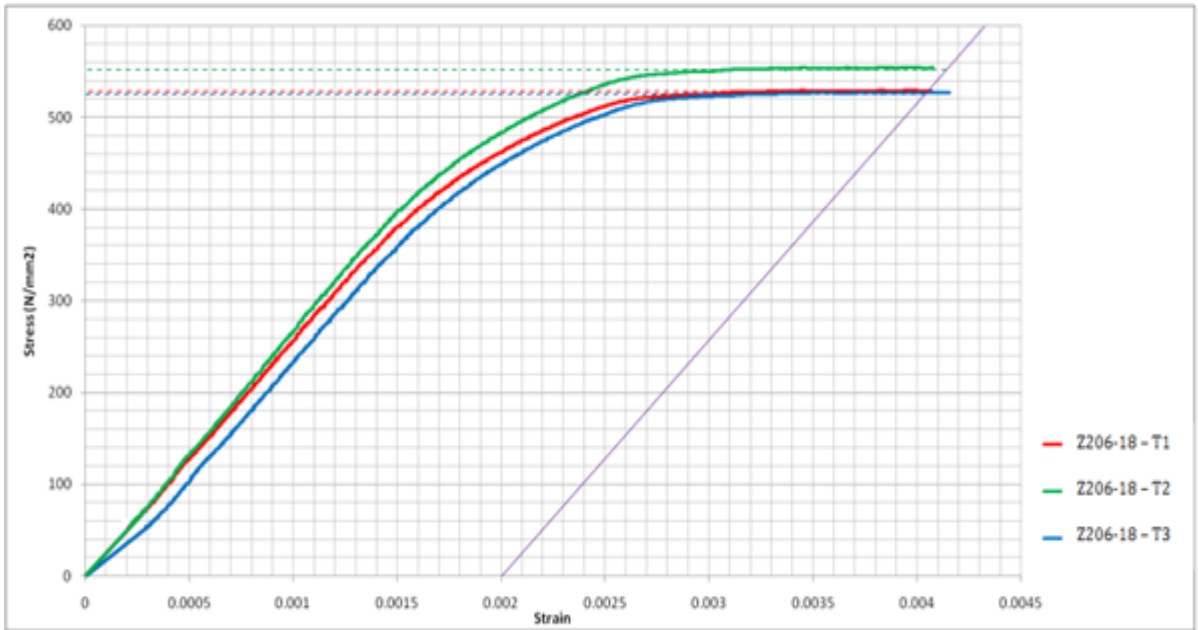
Z-20617
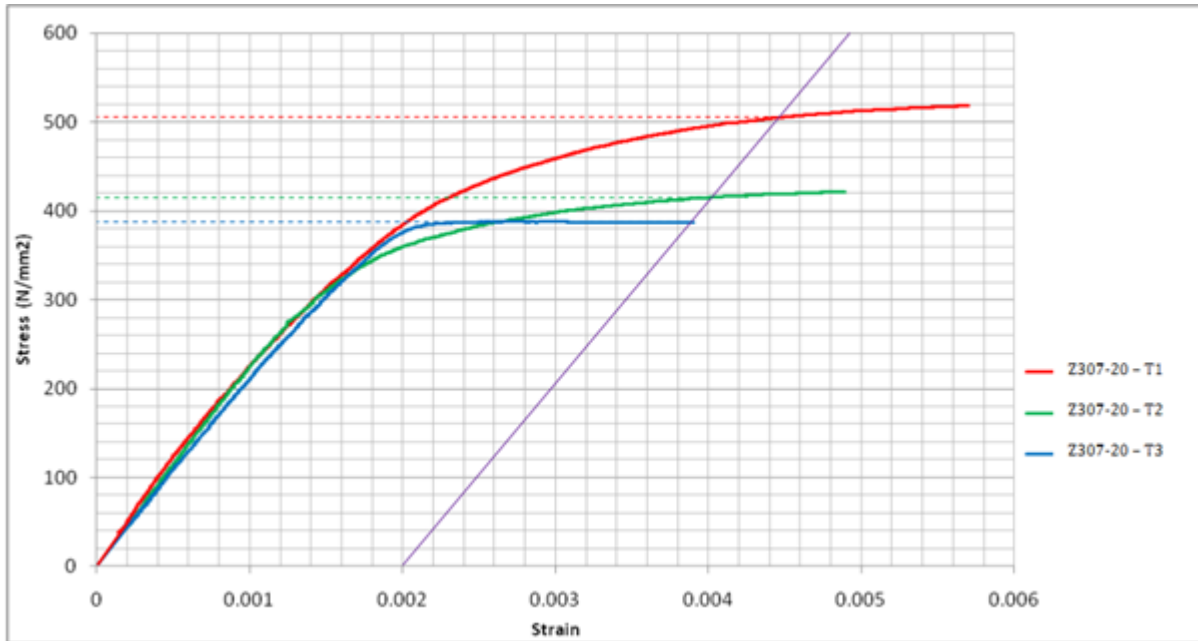
Z-30720

Figure A.1.3: Stress-strain Curves for Z-section

Tabl3 A.1-II:Coupon sample geometry and results for Σ-section

Coil ID	Measured width and thickness (mm)	Young's Modulus (N/mm²)	0.2% proof stress (N/mm²)	Ultimate tensile stress (N/mm²)	Associated sections
N281	w:19.70, t:1.23	205903	471	634	20012
N279	w:19.68, t:1.54	213645	433	609	20016
M3569	w:20.94, t:2.44	207284	447	646	20025 *20025 *24025 30025
N454	w:21.01, t:1.51	208220	507	603	24015
M3501	w:20.88, t:2.28	205465	456	660	24023
N070	w:21.07, t:3.07	217340	453	575	*20030 *24030 24030
N452	w:19.45, t:1.80	206663	455	666	30018
N456	w:20.75, t:3.05	207631	417	516	30030 *30030
N465	w: 20.87, t: 2.03	223549	518	655	*20020

* sections used as sleeves in the sleeved internal support tests

196

Figure A.1.4: Stress-strain curve for Σ- specimens

Coil ID: N281

Coil: N279

Coil: M3569

Coil: N454

Test ◆ Simulation

Coil: M3501

Test ◆ Simulation

Coil: N070

Test ◆ Simulation

198

Coil: N452

Coil: N456

Coil: N465

199
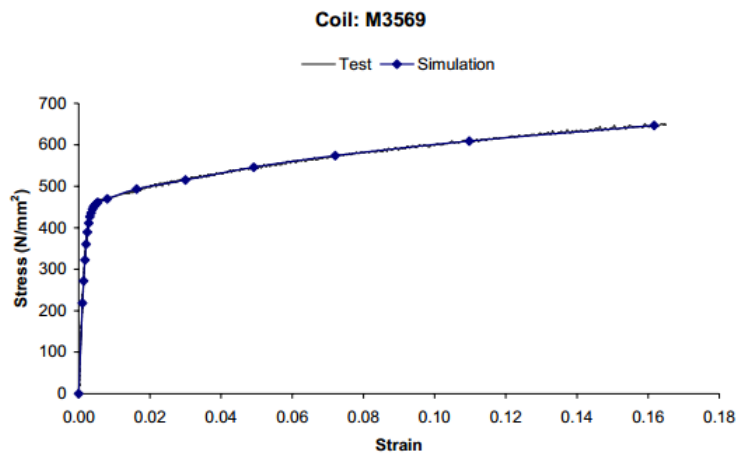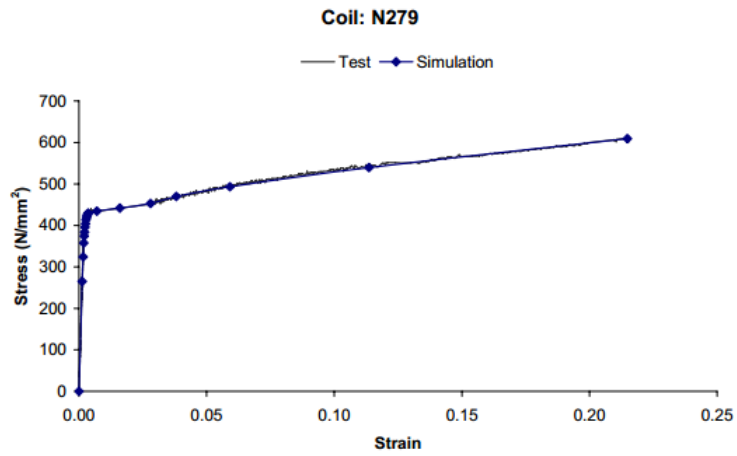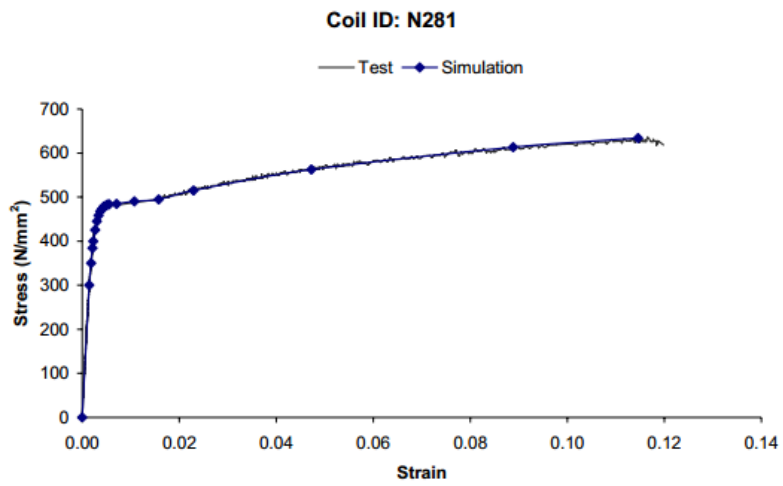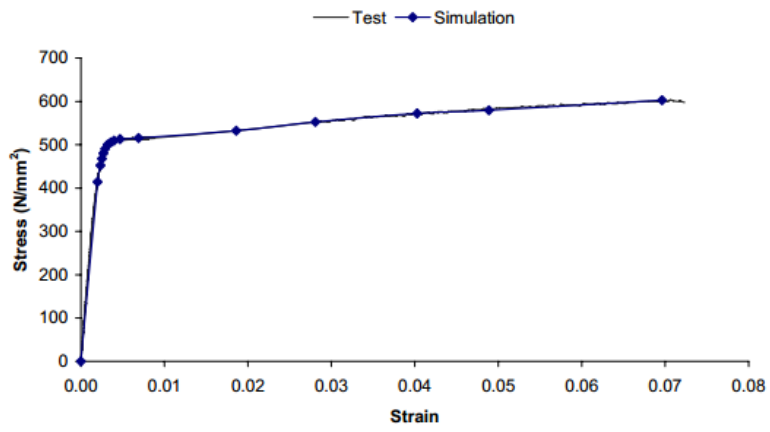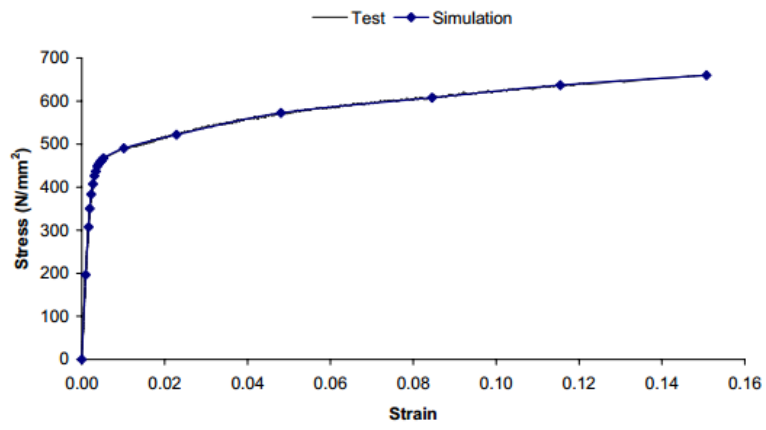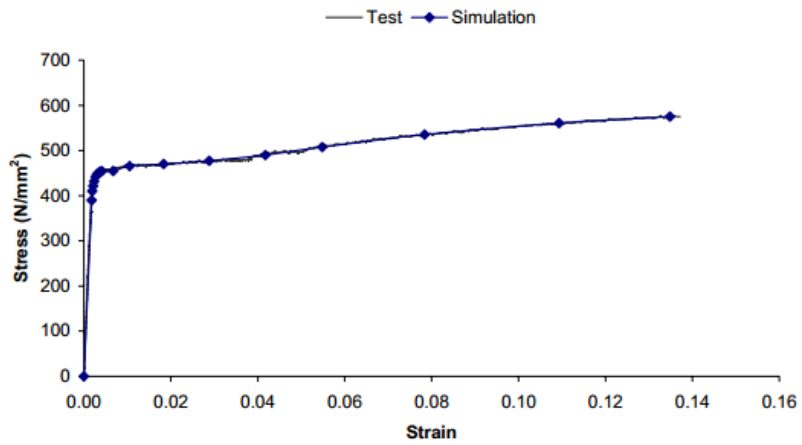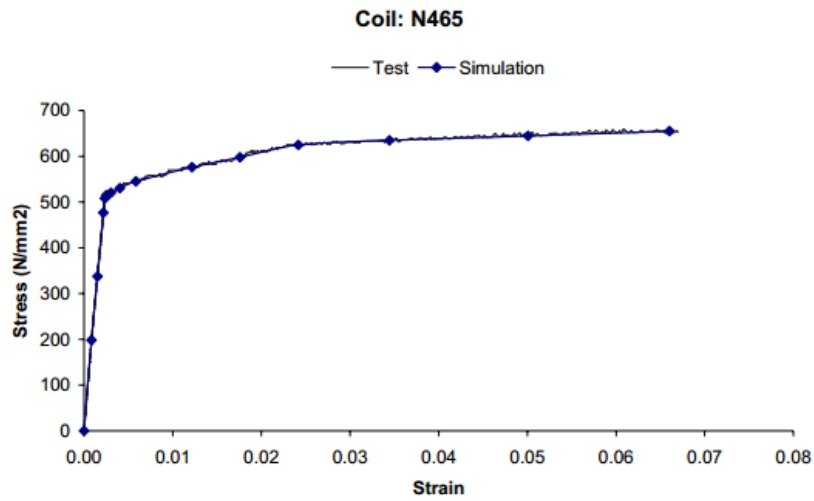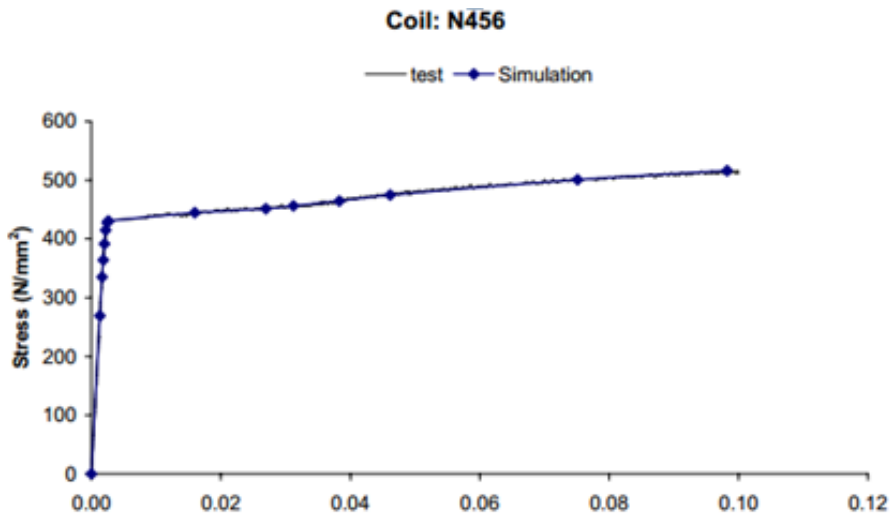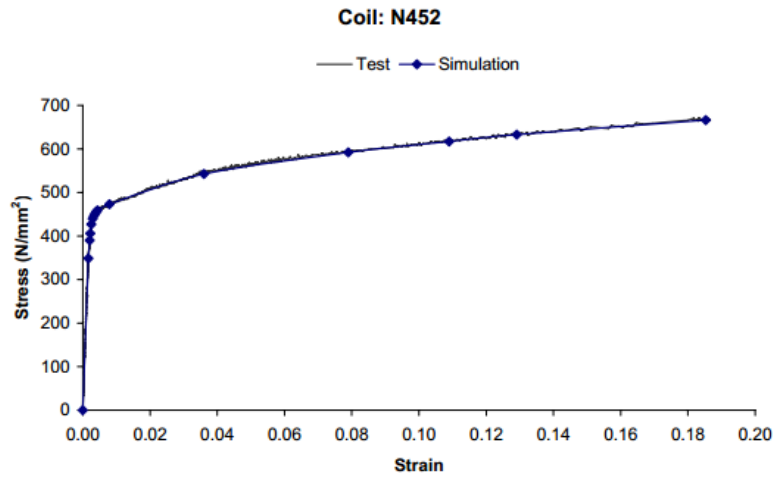
Appendix A.2: Working example of EC3 method

Details of the calculation can be referred to section 3.2.2 or BS EN 1993-1-3-2006: Section 10.1.5.2. Take test specimen Σ24030FD as a work example to demonstrate the EC3 calculation procedure. Sheet thickness=0.7mm, b_R=200mm, b_T=130mm.

Since FD test are equivalent to member under uplift load, therefore

$C_{100} = 2.6$ kNm/m and $b_{T,max}$=40 mm according to Table 10.3 (Fig.3-19).

b_a=flang width=62.5, then k_{ba}=(62.5/100)^2 as b_a<125mm, then k_{ba}=0.391.

k_t=(t_{nom}/0.75)$^{1.5}$=(0.7/0.75)$^{1.5}$=0.902, since t_{nom} of sheet <0.75mm.

k_{bR}=185/b_R=185/200=0.925.

k_A=1.0 for uplift load.

$k_{bT} = \sqrt{b_{T,max}/b_T} = \sqrt{40/130} = 0.555$

So $\qquad C_{D,A} = C_{100} \cdot k_{ba} \cdot k_t \cdot k_{bR} \cdot k_A \cdot k_{bT} = 2.6 \cdot 0.391 \cdot 0.902 \cdot 0.925 \cdot 1.0 \cdot 0.555 = 0.471$

kNm/rad/m =0.471 Nm/rad/mm. For a purlin length=1000mm, the overall

$C_{D,A}$=0.471*1000=471 Nm/rad/mm

Table 3-6: Summary of geometrical details of Σ24030FD specimen and sheeting

Purlin Section	Web depth mm	Flange width mm	t_s mm	t_p mm	a mm	b mm	b_T mm	h_T mm	S mm	L mm
Σ24030	240	62.5	0.7	2.99	31.25	31.25	130	65	200	1000

Appendix A.3: Working example of analytical method

Take test specimen Σ24030 FD as a worked example to demonstrate the application of the above-developed model. For the ease of reference, the geometrical details of both purlin and sheeting are listed in Table 3-6.The Young's modulus for both purlin and sheeting is $E = 210$ GPaand the Possion ratio $v = 0.3$. Five screws are used within a length of 1m, i.e. $n = 5$.

The second moment of area of purlin $I_p = Lt_p^3 \big/ 12\left(1 - v^2\right)$

$= 1000 \times 2.99^3 \big/ 12\left(1 - 0.3^2\right) = 2448\,\text{mm}^4$; coefficient β for screw at the mid-point of sheeting trough:$\beta = 0.078$. Therefore,the rotational stiffness is:

$$C_D = \cfrac{E}{\left(\cfrac{\beta h_T^2}{nt_s^3 a^2} + \cfrac{a}{3I_p} + \cfrac{b}{I_p}\right)} = \cfrac{2.1 \times 10^5}{\left(\cfrac{0.078 \times 62.5^2}{5 \times 0.7^3 \times 31.25^2} + \cfrac{31.25}{3 \times 2448} + \cfrac{31.25}{2448}\right)}$$

$$= 1055569\,\text{Nmm/rad/mm} = 1056\text{Nm/rad/mm}$$

Appendix A.4: A complete moment-rotation curves for all specimens
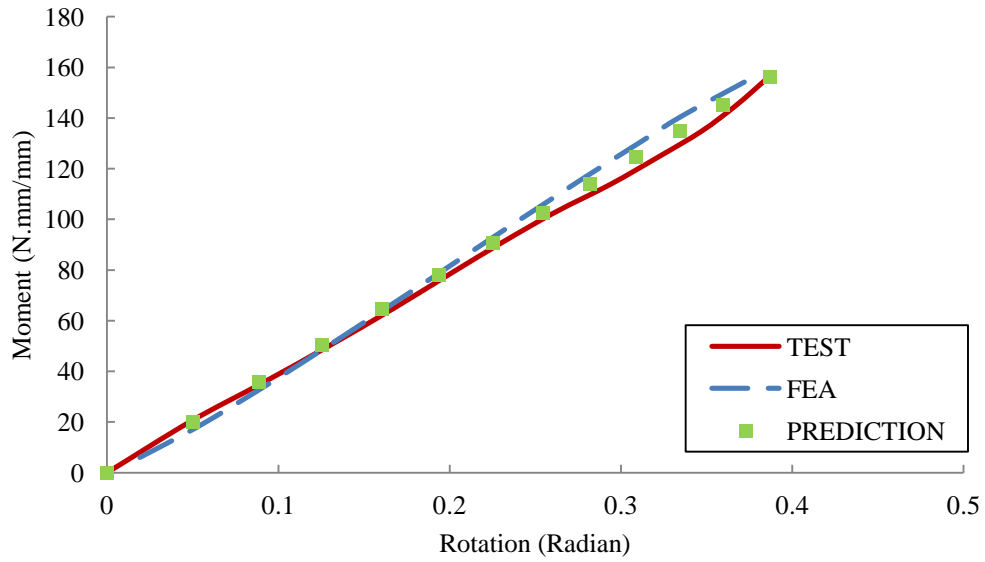
(a) 20012FD
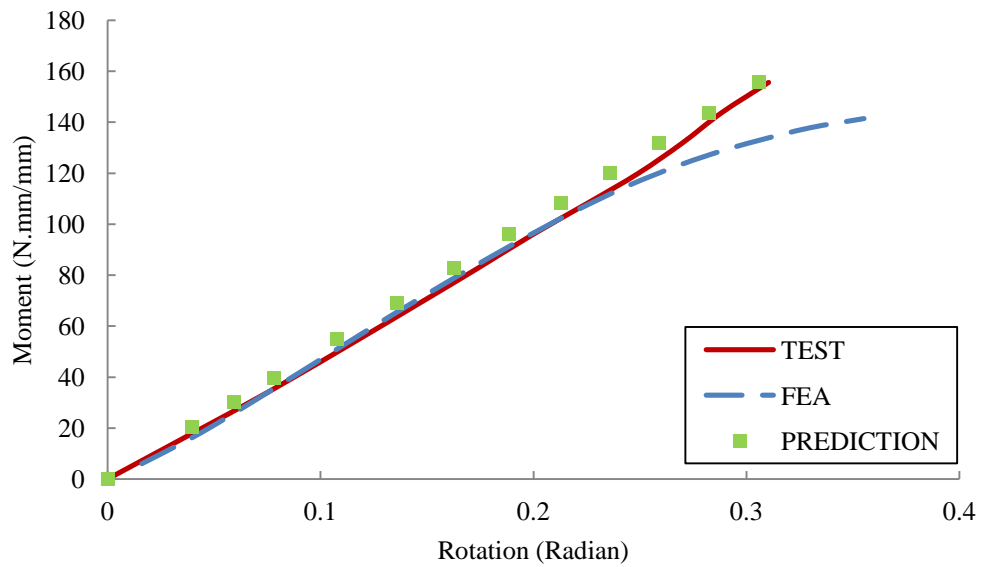
(b) 20012FU
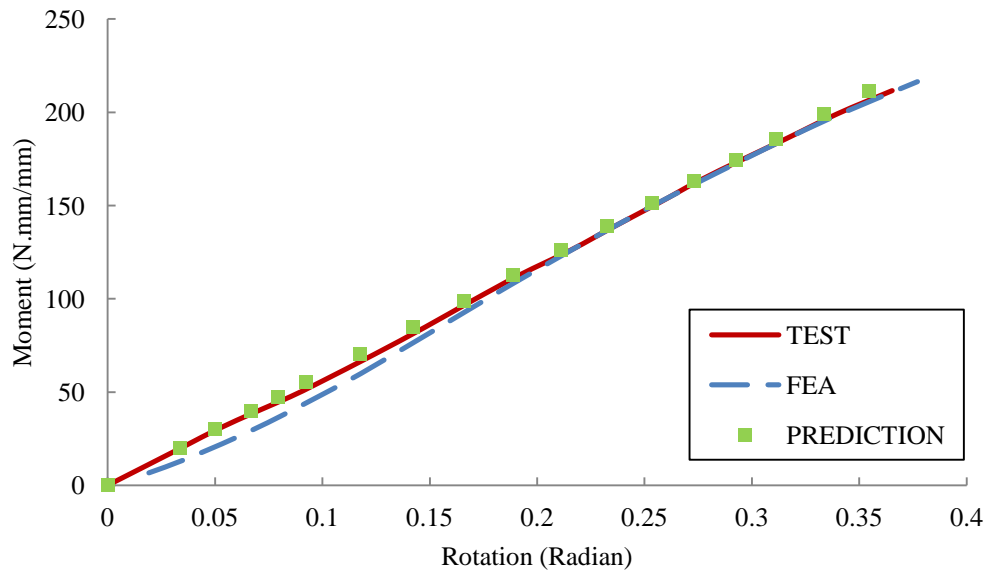
(c) 20016FD
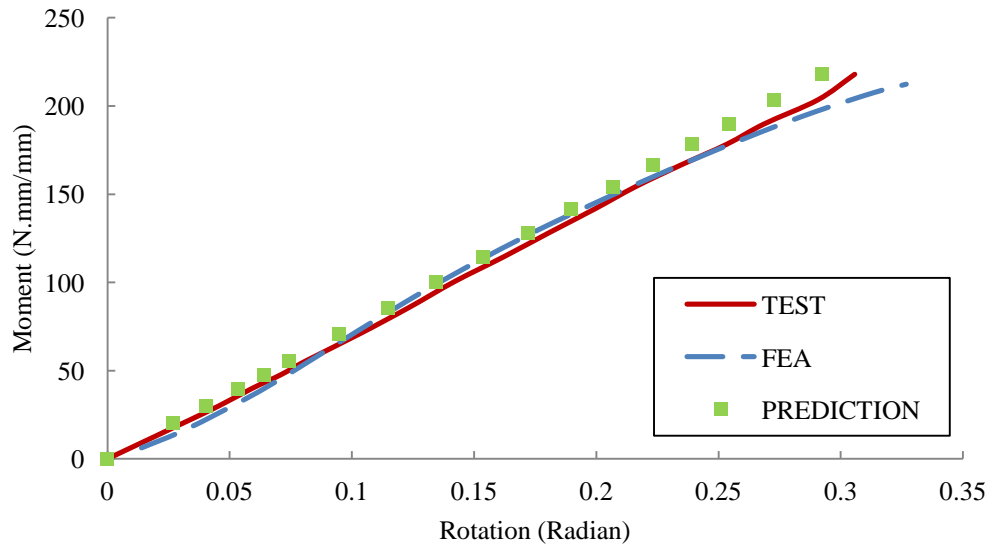
(d) 20016FU
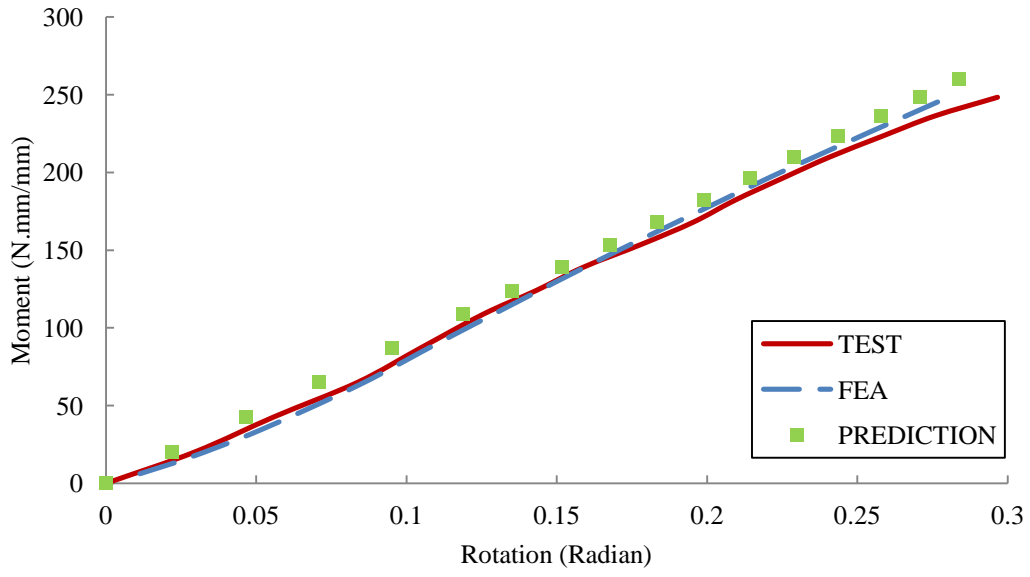
(e) 20025 FD
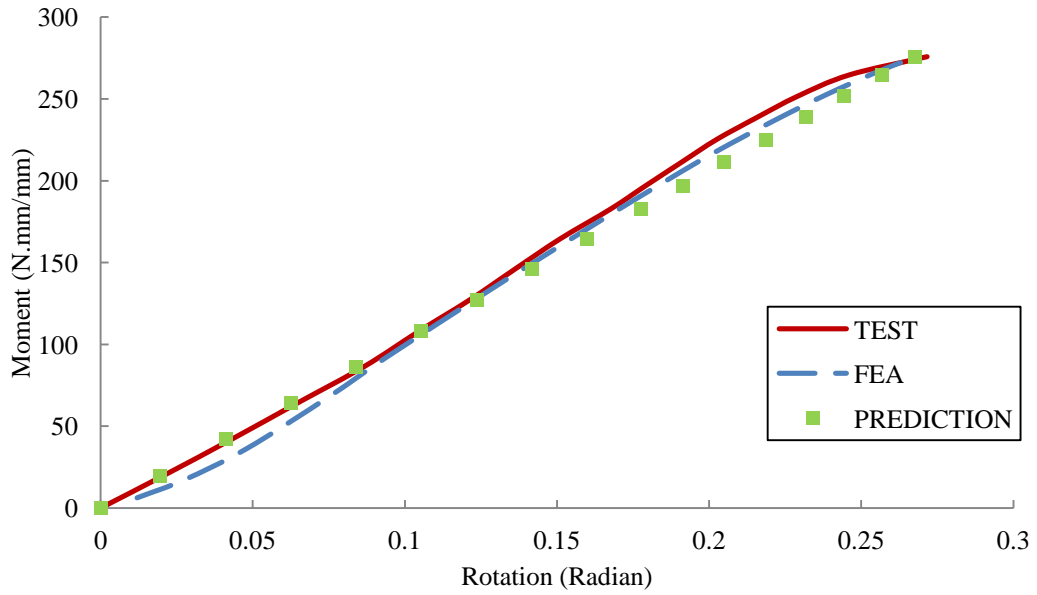
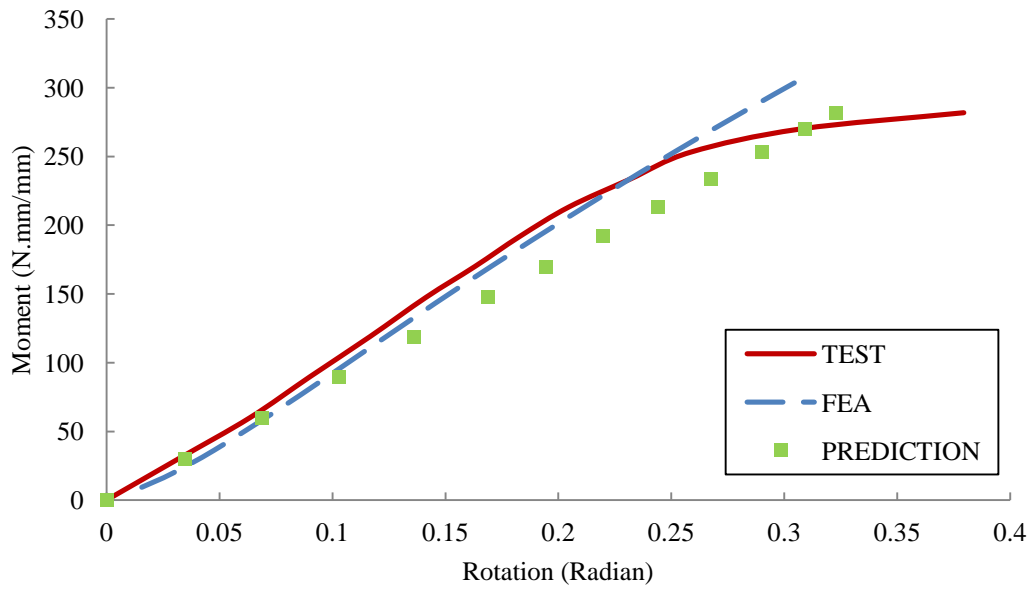(f) 20025FU
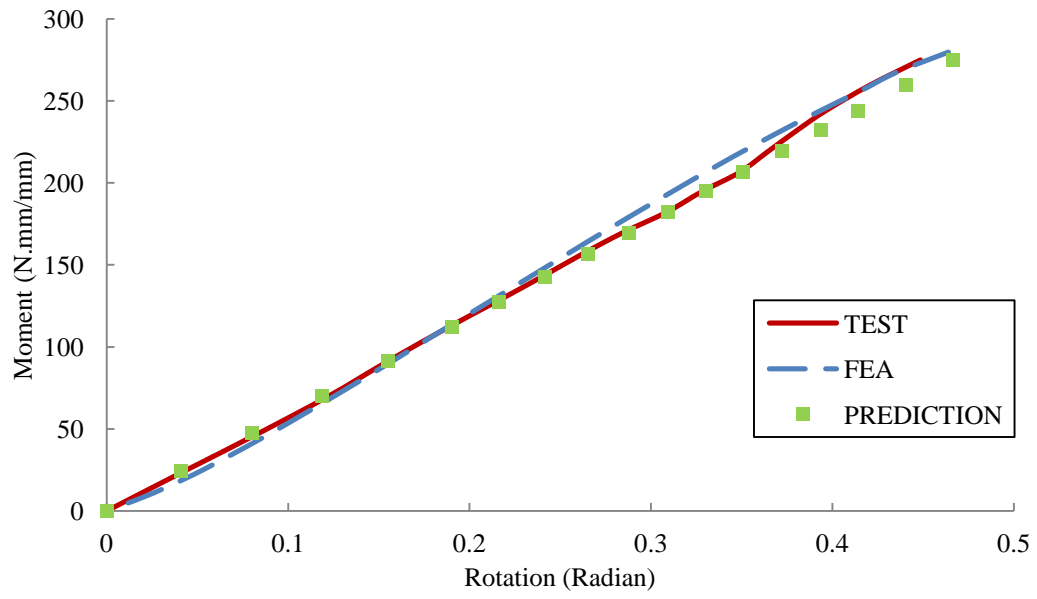
(g) 24015FD
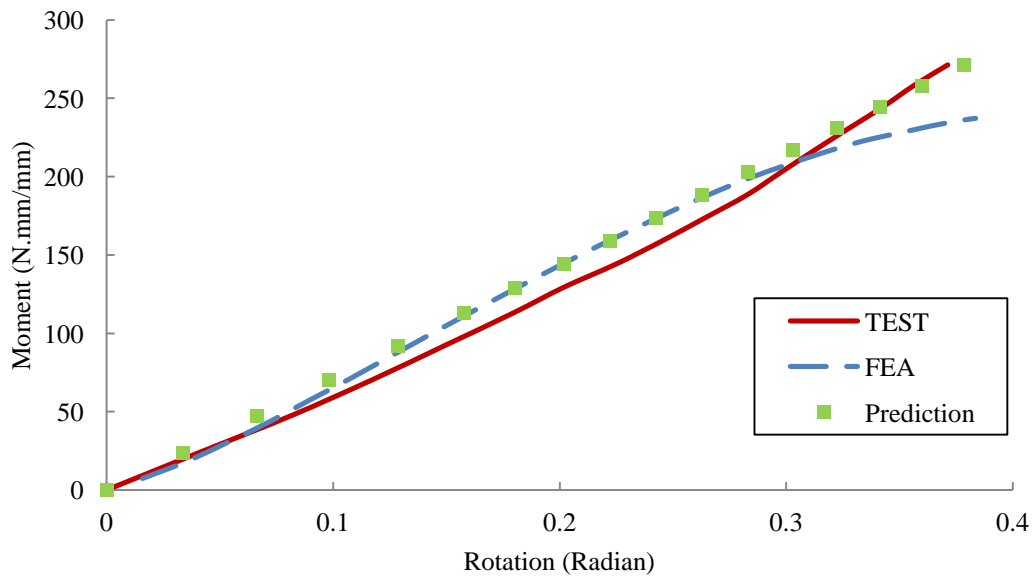
(h) 24015FU
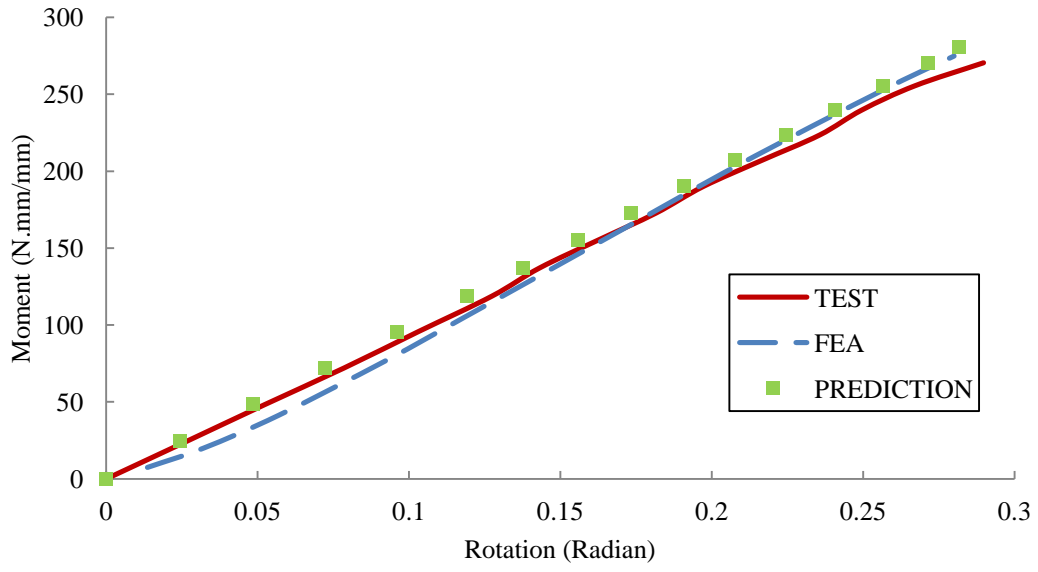
(i) 24023FD
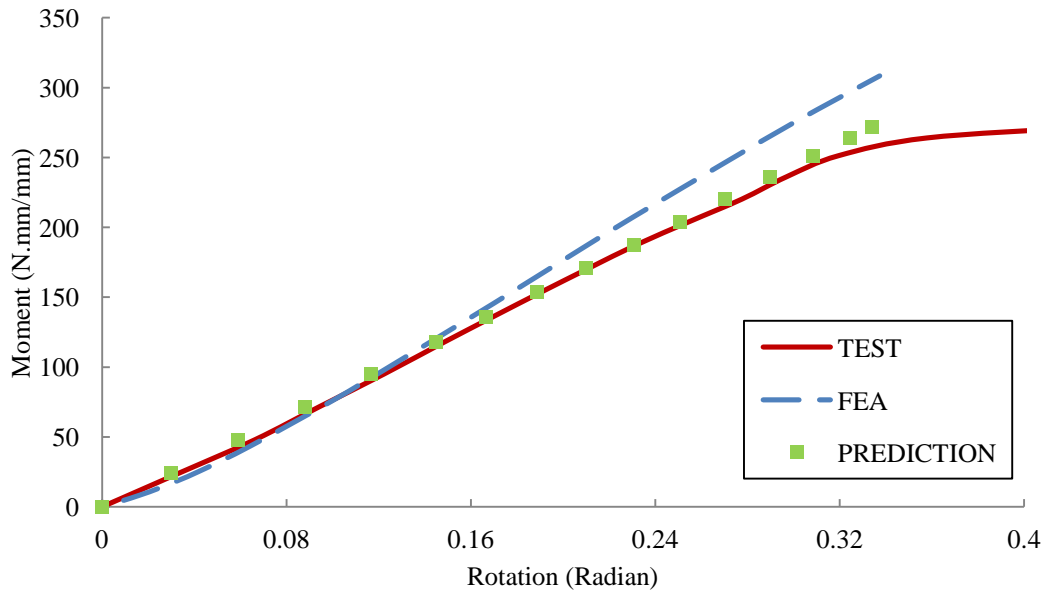
(j) 24023FU
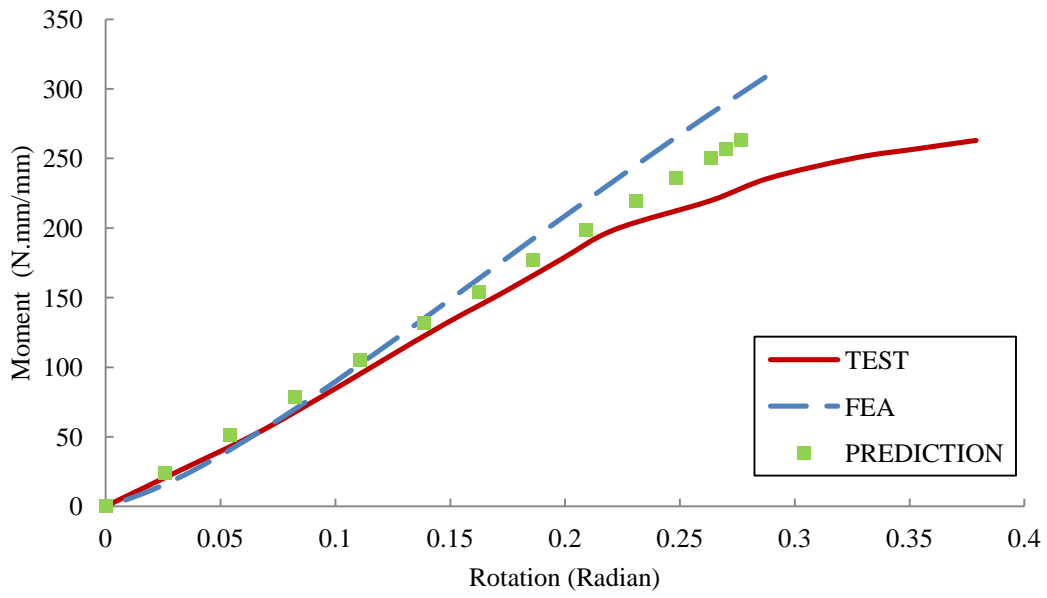
(k) 24030FD
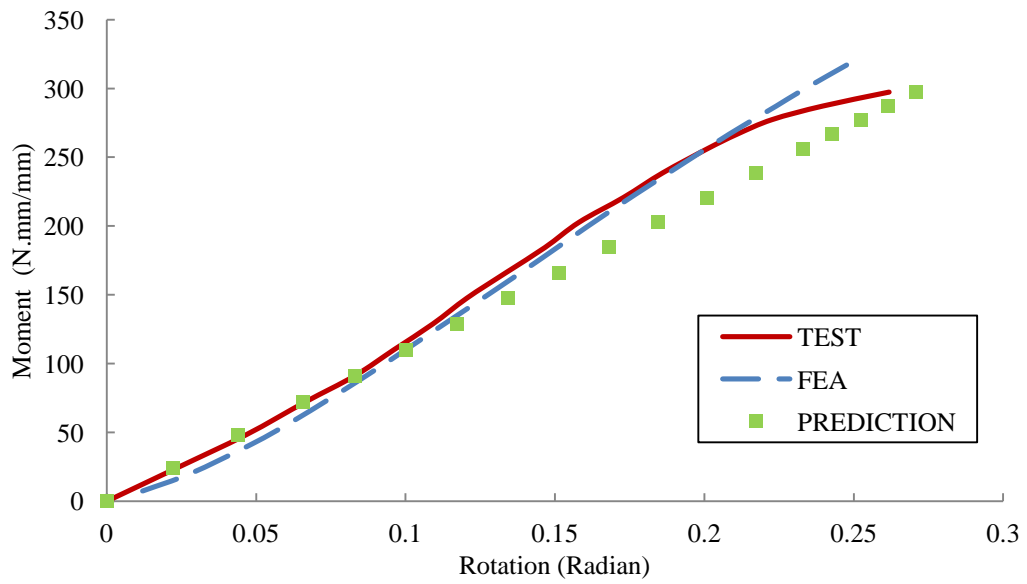
(l) 24030FU
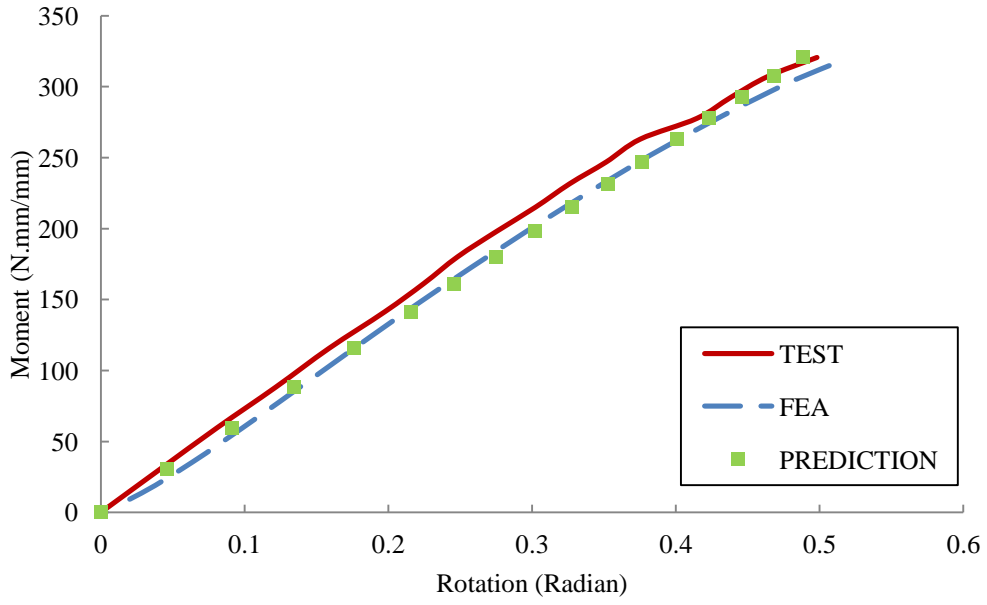
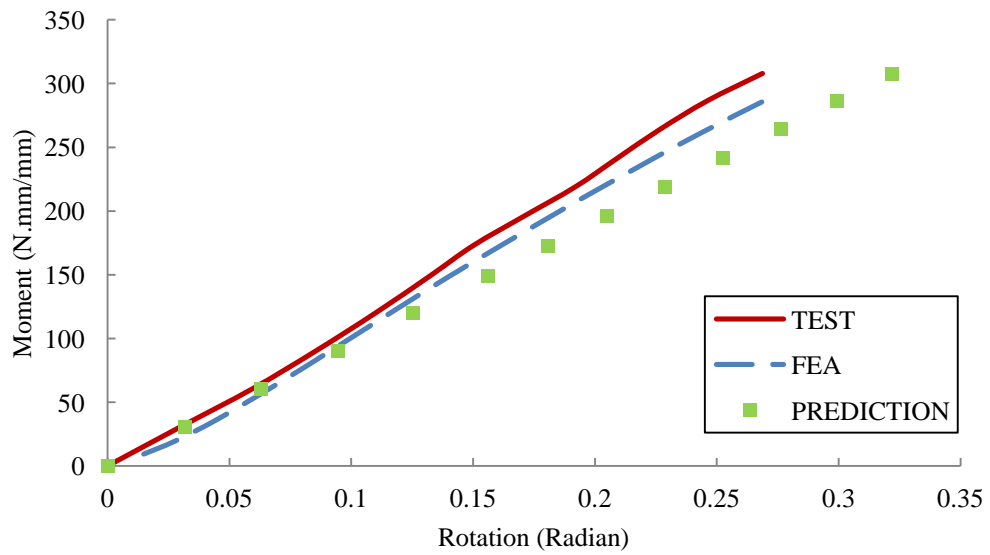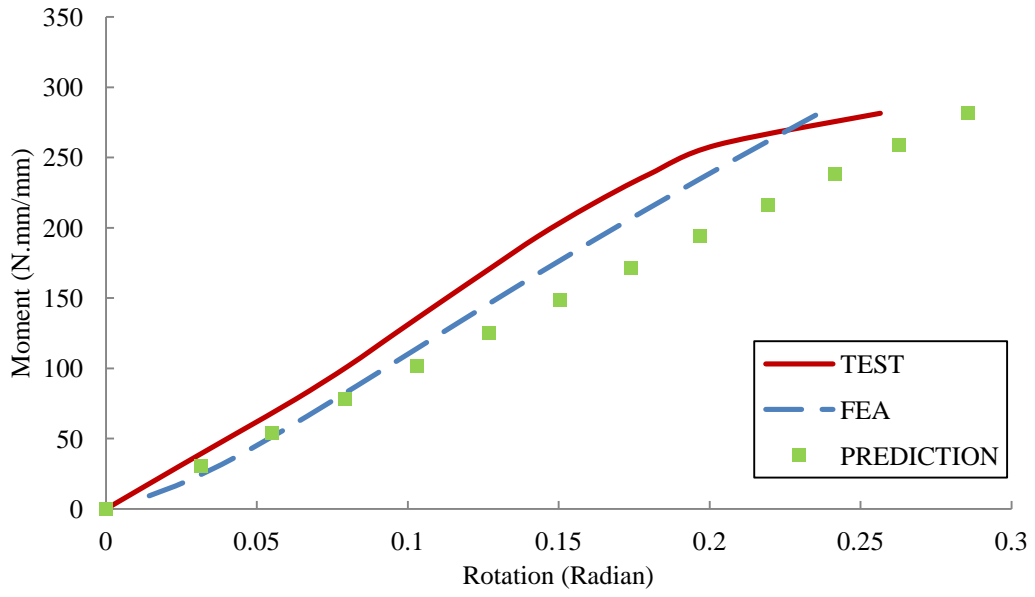(m)30018FD
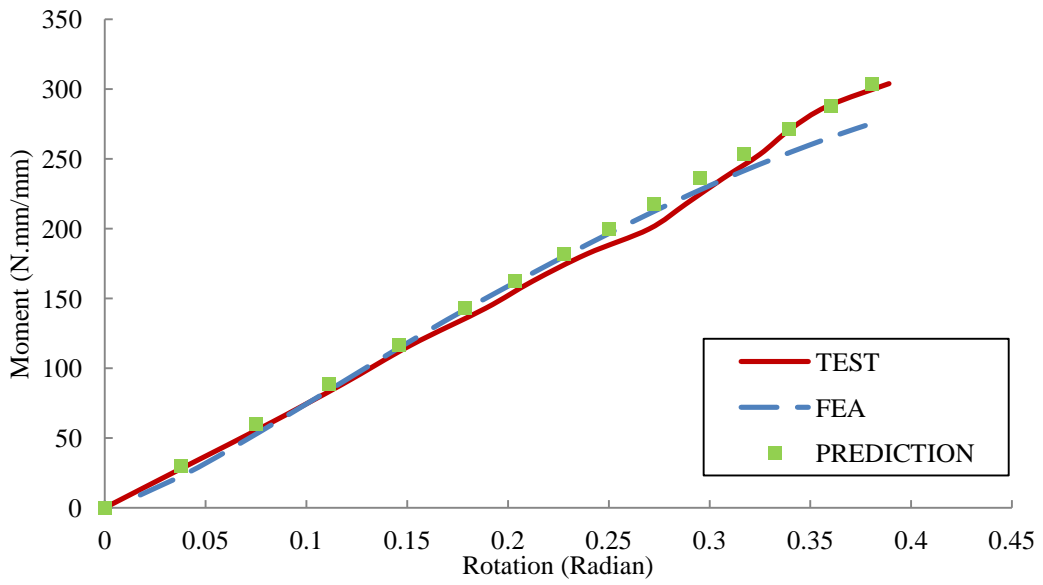
(n) 30018FU

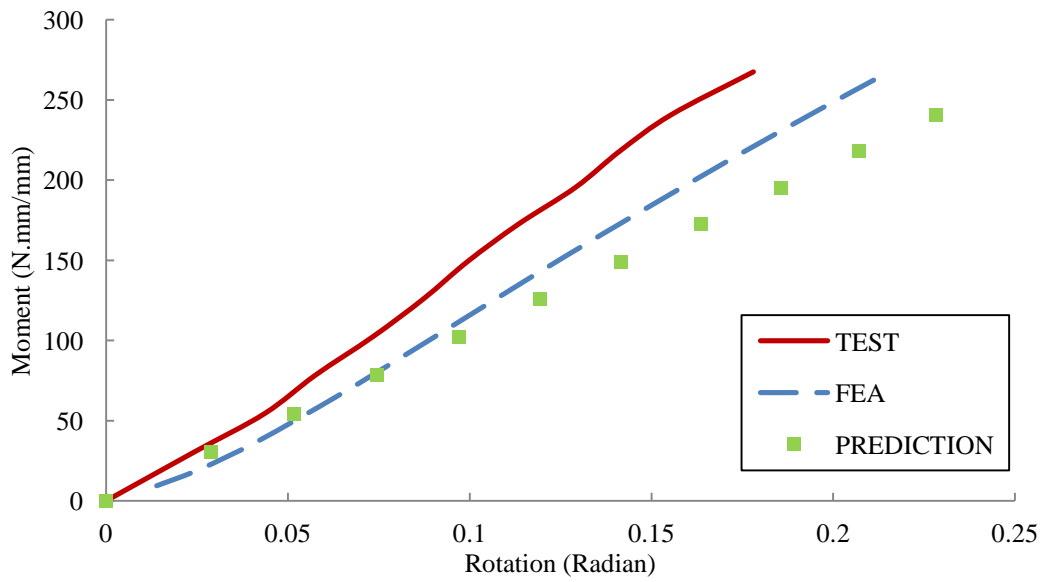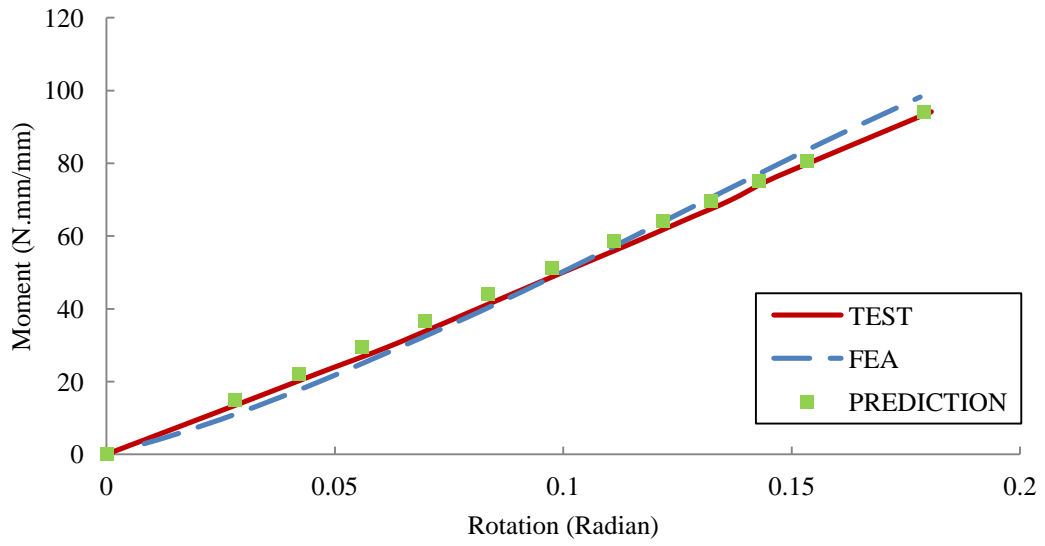(o) 30025FD

(p) 30025FU
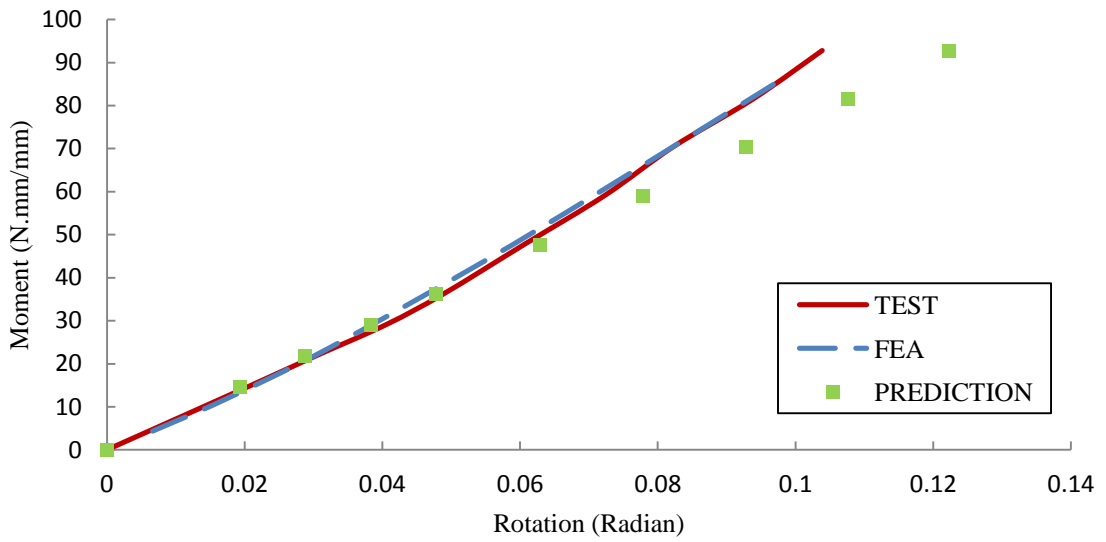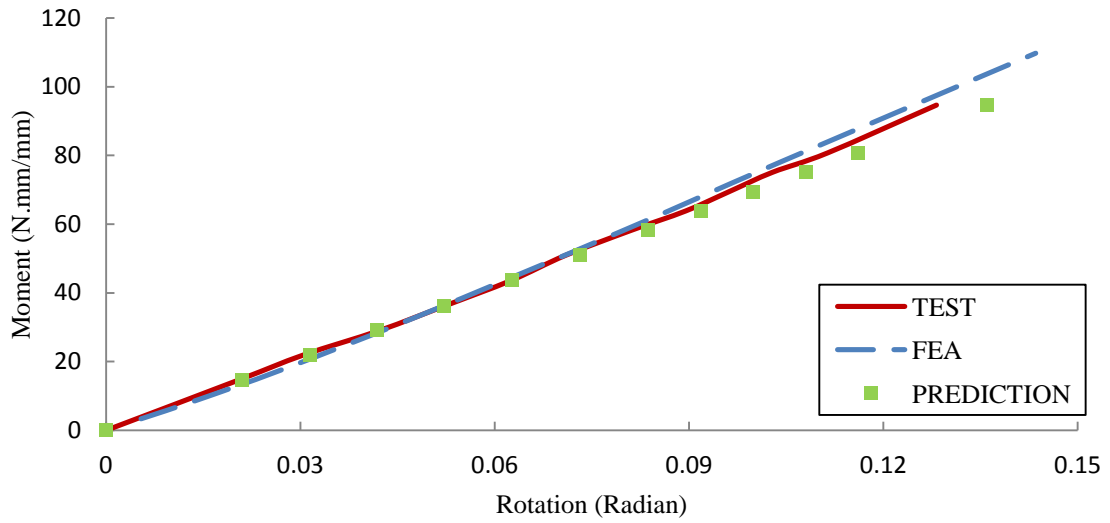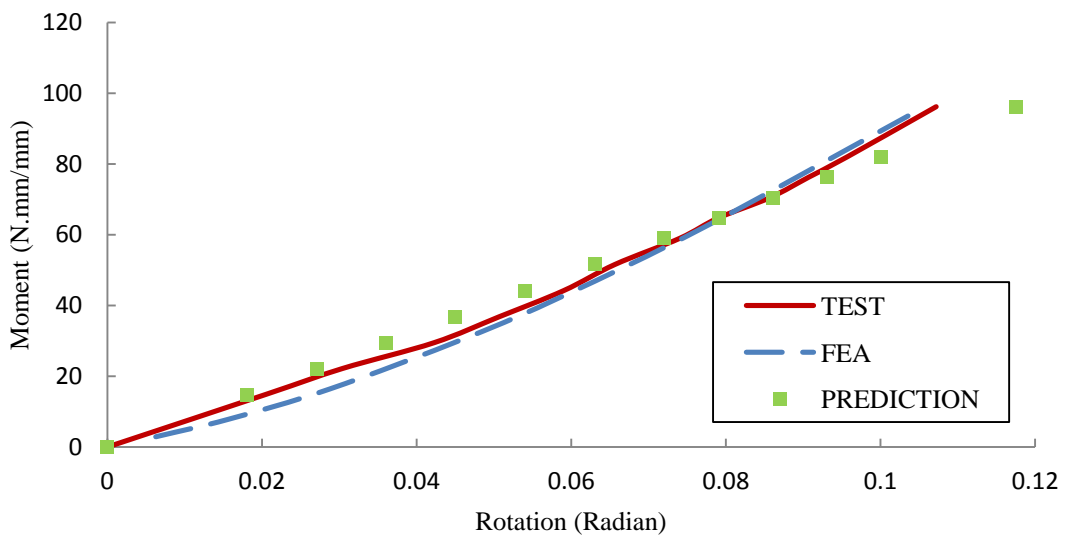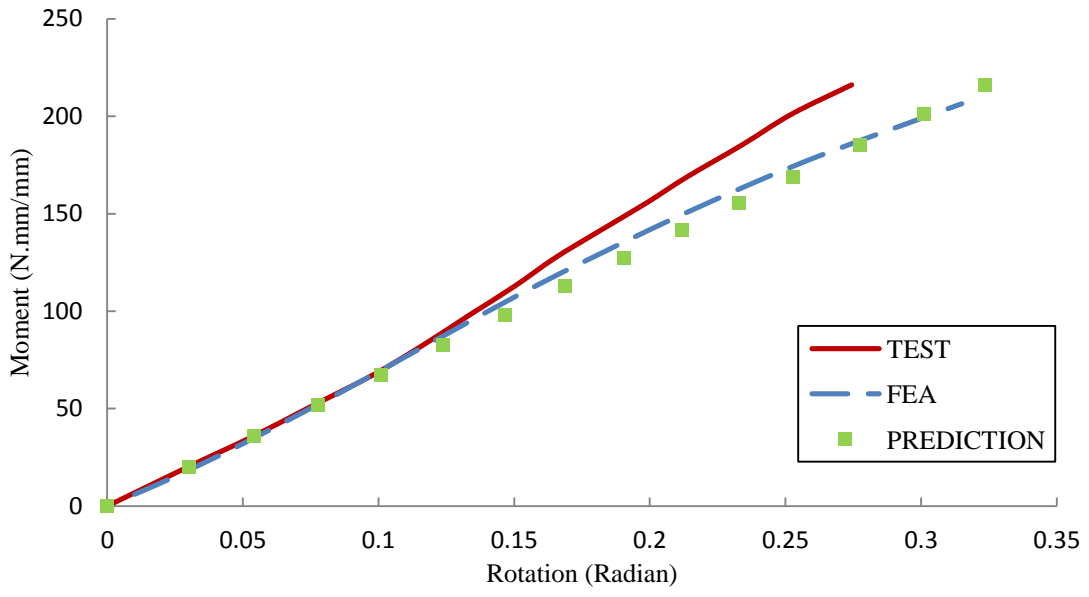
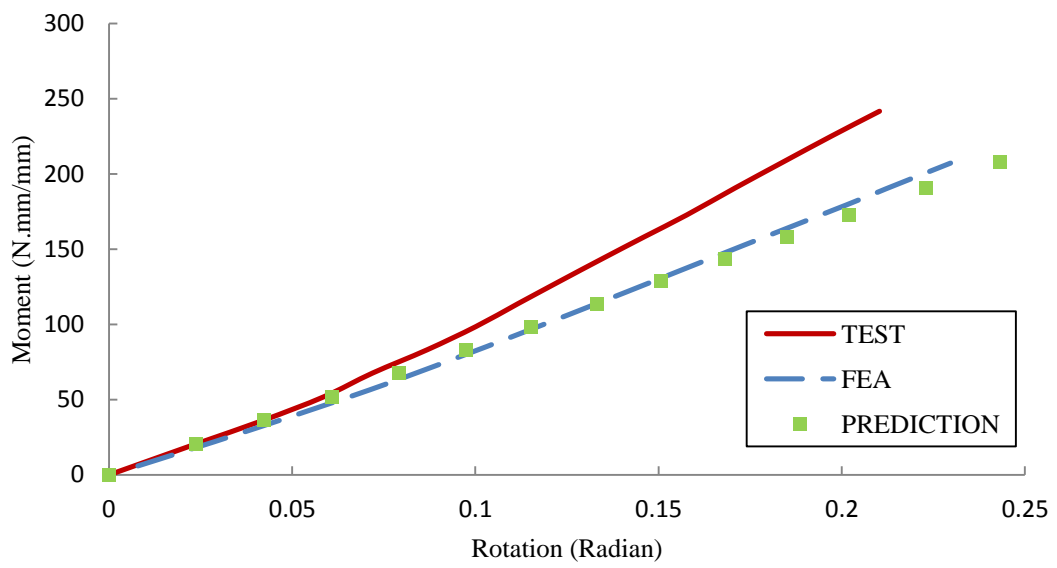(q) 30030FD

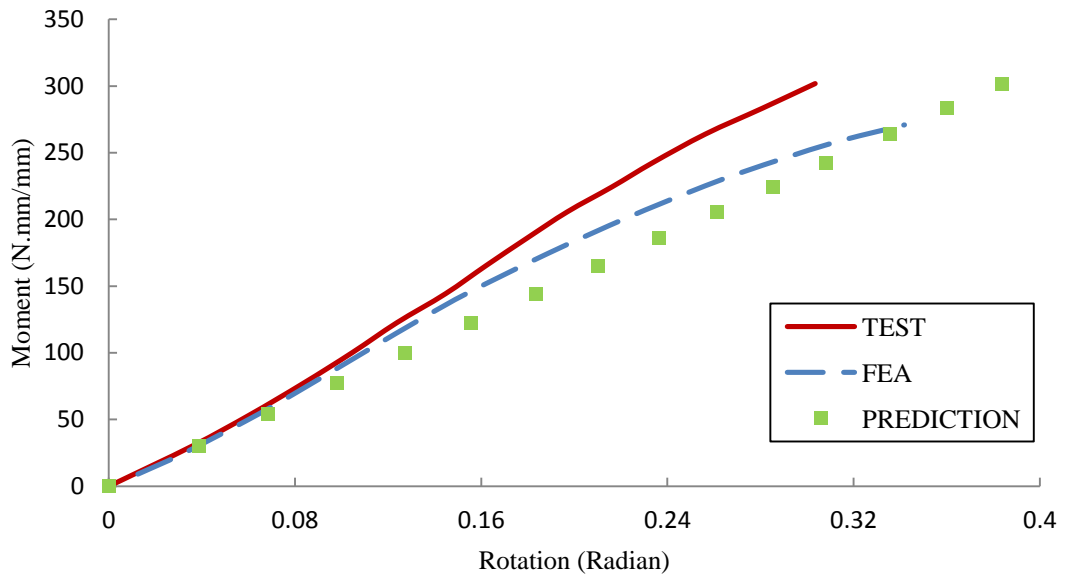(r) 30030FU

(s) Z14614 FD

(t) Z14614 FU

(u) Z14618 FD

(v) Z16418 FU
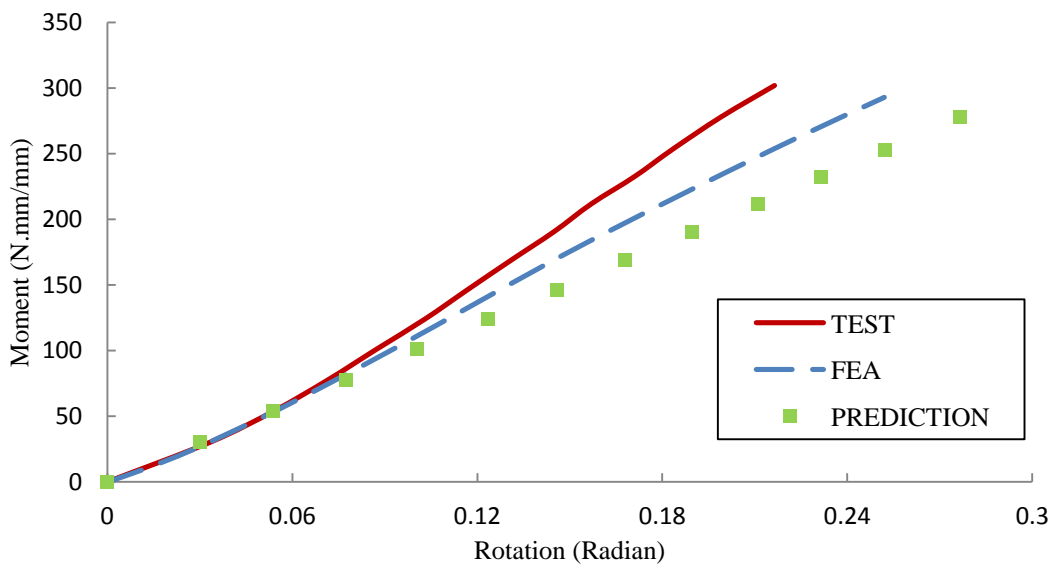
(w) Z20618 FD

(x) Z20618 FU

(y) Z30720 FD

(z) Z30720 FU

Appendix A.5: A comparison of numerical and analytical model: Σ20025 FD

As stated in the analytical method, rotation are contributed from three ways: (1) Rotation angle of the cantilever sheet, θ_s; (2) Rotation angle caused by the sheet local deformation at connection, θ_l and; (3) Rotation angle caused by the deformation of purlin flange, θ_p (The rotation caused by the separation θ_k is assumed negligible in analytical model and zero in FE model, which is not discussed in this case).

Take purlin sectionΣ20025 FD as an example, the θ_s is calculated using: $\theta_s = ML_1 / D$ where L_1 is the vertical distance between the fixed support and the point A, and $D = Et_s^3/12(1-v^2)$ is the flexural rigidity of the sheet. Whilst in FE model, rotation at the arrow point is measured. The moment-rotation comparison of θ_s is given in Fig. A 4.1.
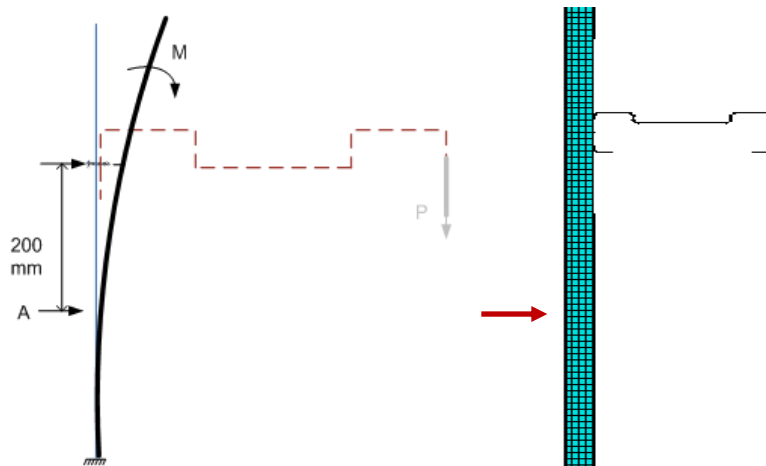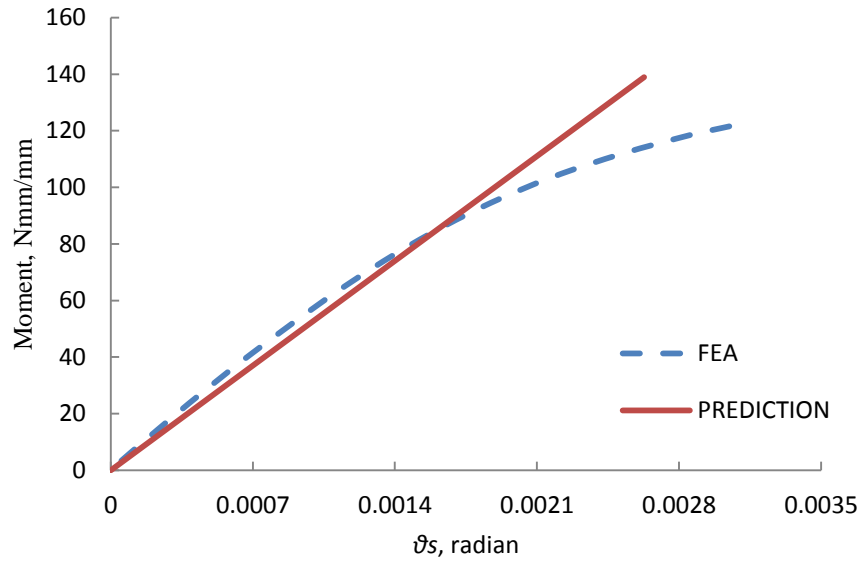
Figure A4.1: Moment-rotation comparison for θ_s

θ_l in the analytical model is calculated using plate theory with a simplified equation:

$$\theta_l = \frac{w}{a} = \frac{\beta F h_T^2}{E t_s^3 a} = \frac{\beta M h_T^2}{n E t_s^3 a^2}$$ where M is the applied moment. The coefficient β depends on the

b_T/h_T ratio and the location of crew in relation to the trough panels. β in this case is 0.078. In FE

model, difference of the lateral displacement at purlin contact line and the lateral displacement

at purlin screw point is taken, thus the comparison is shown in Fig. A4.2.
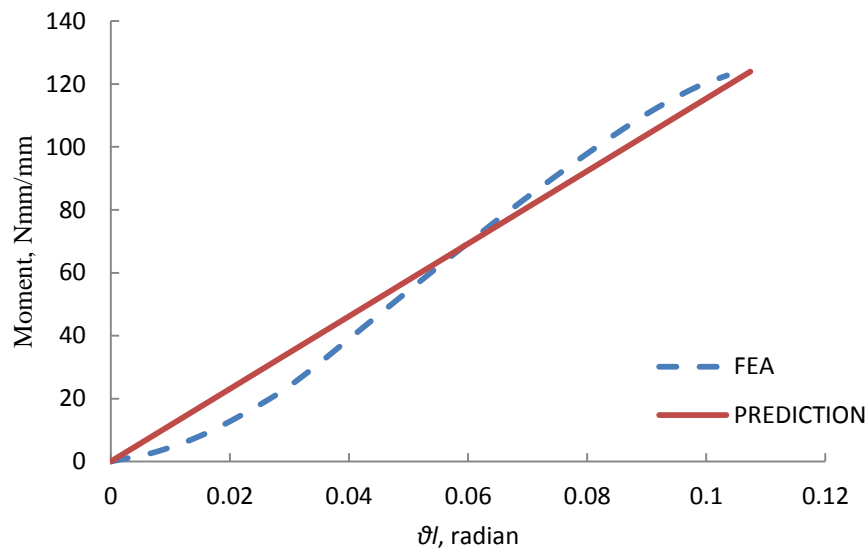
Figure A4.2: Moment-rotation comparison for θ_l

θ_p in the analytical model is calculated using one-way slab theory, using the equation of

$\theta_P = \dfrac{Ma}{3D}$ where a is the vertical distance between the screw point and the line of contact, and

D is the flexural rigidity of purlin flange panel. In FE model, difference in the rotation along the

length of the purlin between purlin screw point to the purlin corner is measured. A comparison

is shown in Fig. A4.3.
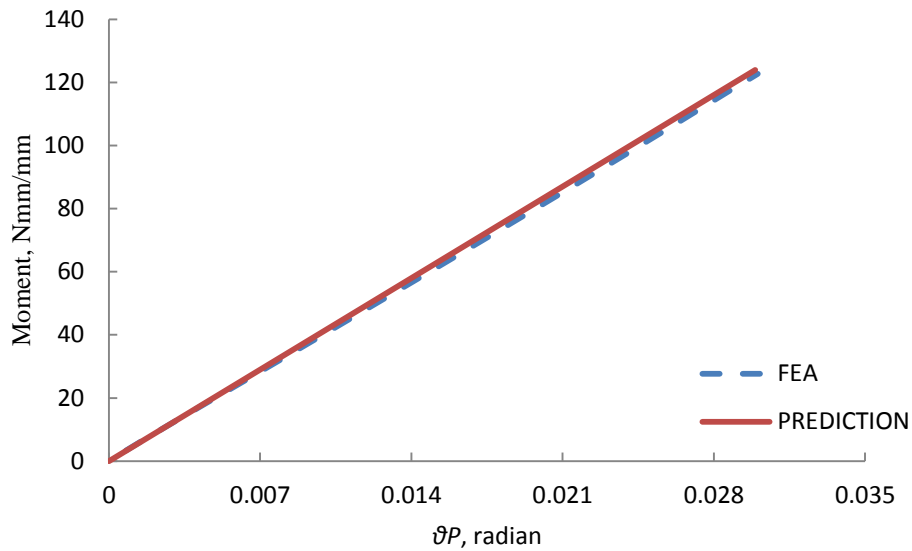
As seen in the above comparison curves, rotation of all components have made a close

match between the FE and analytical model.

Appendix A.6: Tensile strength of Z- section according to EC3

The calculation is based on the method recommended in EN 1993-1-3 (2006). Take an example of Z20617.
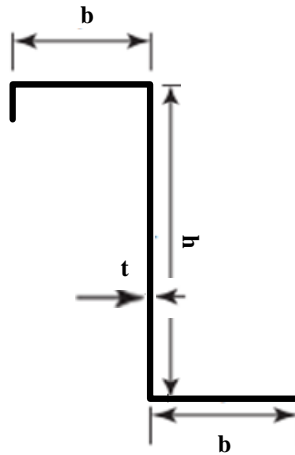
The dimensions of the cross-section are (where the influence of rounding of the corners is neglected):

Depth of web $h = 200$ mm

Width of flange in compression $b_c = 65$ mm

Width of flange in tension $b_t = 65$ mm

Length of lip $c = 20$ mm

Thickness $t = 1.7$mm

The material properties of the section are:

Modulus of elasticity $E = 210\,000$ N/mm^2

Poisson's ratio $v = 0,3$

Basic yield strength $f_{yb} = 450$ N/mm^2

Partial factor $\gamma_{M0}= 1,00$

Checking of geometrical proportions

The design method of EN 1993-1-3 (2006) can be applied if the following conditions

are satisfied (Section 5.2):

$b/t \leq 60$ $b_c/t = 65/1.7 = 38.2 < 60 \rightarrow$ok

                      $b_t/t = 65/1.7 = 38.2 < 60 \rightarrow$ok

$c/t \leq 50$ $c/t = 20/1.7 = 11.76 < 50 \rightarrow$ok

$h/t \leq 500$ $h/t = 200 /1.7 = 118 < 500 \rightarrow$ok

In order to provide sufficient stiffness and avoid primary buckling of the stiffener

itself,the size of stiffener should be within the following range (Section 5.2 in EN

1993-1-3(2006)):

$0,2 \leq c/b \leq 0,6$ $c/b_c = 20/65 = 0,31 \rightarrow$ok

                          $c/b_t = 20/65 = 0,31 \rightarrow$ok

For cold-formed steel sections the section properties are usually calculated based on the

dimensions of the section centre line as follows:

Depth of web $h_p = h - t = 200 - 1.7 = 198.3$ mm

Width of flange in compression $b_{p1} = b_c - t = 65 - 1.7 = 63.3$ mm

Width of flange in tension $b_{p2} = b_t - t = 65 - 1.7 = 63.3$ mm

Length of lip $c_p = c - t /2 = 20 - 1.7 /2 = 19.15$ mm

Calculation of gross section properties

Gross cross-section area:

$$A = t\,(2\,c_p + b_{p1} + b_{p2} + h_p) = 1.7 \times (2 \times 19.15 + 63.3 + 63.3 + 198.3) = 617.44\ \text{mm}^2$$

Position of the neutral axis with regard to the flange in compression:

$$z_c = h_p/2 = 198.3/2 = 99.15\ \text{mm}$$

Position of the neutral axis with regard to the flange in tension:

$$z_t = h_p - z_c = 198.3 - 99.15 = 99.15\ \text{mm}$$

Second moment of the gross cross-sectional area:

$$I_y = \left(h_p^3 + 2\,c_p^3\right)t/12 + \left(b_{p1} + b_{p2}\right)t^3/12 + z_c^2 b_{p1}t + z_t^2 b_{p2}t + c_p t(z_c - c_p/2)^2 + c_p t(z_t - c_p/2)^2$$
$$= 3745000\ \text{mm}^4$$

Gross section modulus with regard to the flange in compression:

$$W_{y,c} = I_y/z_c = 3745000/99.15 = 37771\ \text{mm}^3$$

Gross section modulus with regard to the flange in tension:

$$W_{y,t} = I_y/z_t = 3745000/99.15 = 37771\ \text{mm}^3$$

Calculation of effective section properties

The general (iterative) procedure is applied to calculate the effective properties of the compression flange and the lip (plane element with edge stiffener). The calculation should be carried out in three steps:

Step 1 Obtain an initial effective cross-section for the stiffener using effective widths of the flange and lip determined by assuming that the compression flange is doubly supported, the

stiffener gives full restraint (K =∞) and that the design strength is not reduced, that is, $\sigma_{com,Ed}=$ f_{yb}/γ_{M0}.

Effective width of the compressed flange

For the internal compression flange the stress ratio $\psi = 1$ (uniform compression),so the buckling coefficient is taken as $k_\sigma = 4$. The relative slenderness thus is:

$$\overline{\lambda}_{b,red} = \overline{\lambda}_b = \sqrt{\frac{f_{yb}}{\sigma_{cr,b}}} = \sqrt{\frac{450}{547}} = 0.907$$

where $\sigma_{cr,b} = \dfrac{\pi^2 E}{12(1-v^2)}\dfrac{k_\sigma}{\left(\dfrac{b_{p1}}{t}\right)^2} = \dfrac{3.14^2 \cdot 210000}{12(1-0.3^2)}\dfrac{4}{\left(\dfrac{63.3}{1.7}\right)^2} = 547 \text{ N/mm}^2$

Since $\overline{\lambda}_{b,red} > 0.673$, the width reduction factor for the doubly supported compression element is calculated by:

$$\rho = \frac{\overline{\lambda}_{b,red} - 0.055(3+\psi)}{\overline{\lambda}_{b,red}^2} = \frac{0.907 - 0.055(3+1)}{0.907^2} = 0.835$$

The effective width of the compressed flange thus is:

$b_{eff} = \rho \, b_{p1} = 0{,}835 \text{x} 63.3 = 52.9 \text{ mm}$

$b_{e1} = b_{e2} = 0{,}5 b_{eff} = 0{,}5 \times 52.9 = 26.4 \text{ mm}$

Effective length of the lip

For the compression lip, the buckling coefficient should be taken as follows:

$k_\sigma = 0{,}5$ if $c_p/b_{p1} \leq 0{,}35$

$k_\sigma = 0,5 + 0,83(c_p/b_{p1} - 0,35)^{2/3}$ if $0,35 \le cp/bp1 \le 0,6$

For $c_p/b_{p1} = 19.15/63.3 = 0,303 < 0,35$ $k_\sigma = 0,5$.

The relative slenderness is:

$$\bar{\lambda}_{c,red} = \bar{\lambda}_c = \sqrt{\frac{f_{yb}}{\sigma_{cr,c}}} = \sqrt{\frac{450}{747}} = 0.776$$

where $\sigma_{cr,c} = \frac{\pi^2 E}{12(1-v^2)} \frac{k_\sigma}{\left(\dfrac{c_p}{t}\right)^2} = \frac{3.14^2 \cdot 210000}{12(1-0.3^2)} \frac{0.5}{\left(\dfrac{19.15}{1.7}\right)^2} = 747 \text{ N/mm}^2$

Since $\bar{\lambda}_{c,red} = 0,776 > 0.748$, the width reduction factor for outstand compression element

thus is given by:

$$\rho = \frac{\bar{\lambda}_{c,red} - 0.188}{\bar{\lambda}^2_{b,red}} = \frac{0.776 - 0.188}{0.776^2} = 0.976$$

The effective length of the compression lip thus is:

$c_{eff} = \rho c_p = 0.976 \times 19.15 = 18.69$ mm

The corresponding effective area of the edge stiffener is:

$A_s = t (b_{e2} + c_{eff}) = 1.7 \times (26.4 + 18.69) = 76.7 \text{ mm}^2$

Step 2 Use the initial effective cross-section of the stiffener to determine the reduction factor, allowing for the effects of the distortional buckling. The elastic critical stress of the distortional buckling for the edge stiffener is:

$$\sigma_{cr,d} = \frac{2\sqrt{KEI_s}}{A_s} = \frac{2\sqrt{0.362 \cdot 210000 \cdot 2563}}{76.7} = 364 \text{ N/mm}^2$$

where $K = \frac{Et^3}{4(1-v^2)(b_1^2 h_p + b_1^3)} = \frac{210000 \cdot 1.7^3}{4 \cdot (1-0.3^2)(55.56^2 \cdot 198.3 + 55.56^3)} = 0.362$

$$b_1 = b_{p1} - \frac{b_{c2}^2}{2(b_{c2} + c_{eff})} = 63.3 - \frac{26.40^2}{2(26.40 + 18.69)} = 55.56 \, \text{mm}$$

$$I_s = \frac{b_{e2}t^3}{12} + \frac{c_{eff}^3 t}{12} + b_{e2}t\left[\frac{c_{eff}^2}{2(b_{e2} + c_{eff})}\right]^2 + c_{eff}t\left[\frac{c_{eff}}{2} - \frac{c_{eff}^2}{2(b_{e2} + c_{eff})}\right]^2 = 2563 \, \text{mm}^4$$

Thickness reduction factor for the edge stiffener is calculated based on the relative slenderness of the edge stiffener as follows:

$$\overline{\lambda}_d = \sqrt{\frac{f_{yb}}{\sigma_{cr,d}}} = \sqrt{\frac{450}{411}} = 1.046$$

$\chi_d = 1{,}0$ if $\lambda_d \leq 0{,}65$

$\chi_d = 1{,}47 - 0{,}723\lambda_d$ if $0{,}65 < \lambda_d < 1{,}38$

$\chi_d = 0{,}66 / \lambda_d$ if $\lambda_d \geq 1{,}38$

$0{,}65 < \overline{\lambda}_d < 1{,}38$ so$\chi_d = 1{,}47 - 0{,}723\lambda_d = 0{,}666$

Step 3 As the reduction factor for the buckling of the stiffener is$\chi_d = 0{,}666 < 1$, iterations are required to refine the value of the reduction factor. The iterations are carried out based on the reduced design strength, $\sigma_{com,Ed,i} = \chi_{d,i-1} f_{yb} / \gamma_{M0}$to obtain new effective widths of the lip and flange in the stiffener and recalculate the critical stress of distortional buckling of the stiffener and thus to obtain new reduction factor. The iteration stops when the reduction factor χ_d converges. The final values obtained after iterations are $b_{e2} = 30{,}1$,$c_{eff} = 19{,}15$ and $\chi_d = 0{,}663$.

Effective width of the web

The position of the initial neutral axis (web is assumed as fully effective) with regard to the flange in compression is given by:

$$h_c = \frac{c_p\left(\dfrac{h_p-c_p}{2}\right)+b_{p2}h_p+\dfrac{h_p^2}{2}+\dfrac{c_{eff}^2\,\chi_d}{2}}{c_p+b_{p2}+h_p+b_{e1}+\left(b_{e2}+c_{eff}\right)\chi_d}=105.8 \text{ mm}$$

The stress ratio thus is:

$\psi = -(hp - hc)/hc = -(198.3 - 105.8)/105.8 = -0{,}874$

The corresponding buckling coefficient is calculated by

$k\sigma = 7{,}81 - 6{,}29\,\psi + 9{,}78\,\psi^2 = 20.78$

The relative slenderness thus is:

$$\bar{\lambda}_{h,red} = \bar{\lambda}_h = \sqrt{\frac{f_{yb}}{\sigma_{cr,h}}} = \sqrt{\frac{450}{411}} = 1.247$$

where $\sigma_{cr,h} = \dfrac{\pi^2 E}{12(1-v^2)}\dfrac{k_\sigma}{\left(\dfrac{h_p}{t}\right)^2} = \dfrac{3.14^2 \cdot 210000}{12(1-0.3^2)}\dfrac{20.78}{\left(\dfrac{198.3}{1.7}\right)^2} = 289.5 \text{ N/mm}^2$

The width reduction factor thus is:

$$\rho = \frac{\bar{\lambda}_{h,red}-0.055(3+\psi)}{\bar{\lambda}_{h,red}^2} = \frac{1.247-0.055(3-0.874)}{1.247^2} = 0.727$$

The effective width of the zone in compression of the web is:

$h_{eff} = \rho h_c = 0{,}727 \times 105.8 = 76.9 \text{ mm}$

Part of the effective width near the flange is:

$h_{e1} = 0{,}4h_{eff} = 0{,}4 \times 76.9 = 30.8 \text{ mm}$

Part of the effective width near the neutral axis is:

$$h_{e2} = 0,6h_{eff} = 0,6 \times 76.9 = 46.1 \text{ mm}$$

Thus, $h_1 = h_{e1} = 30.8$ mm

$$h_2 = (h_p - h_c) + h_{e2} = (198.3 - 105.8) + 46.1 = 138.6 \text{ mm}$$

The effective widths of the web obtained above are based on the position of the initial neutral axis (web is assumed as fully effective). To refine the result iterations are required which is based on the newly obtained effective widths, h_{e1} and h_{e2}, to determine the new position of the neutral axis. The stress ratio, buckling coefficient, relative slenderness, width reduction factor and effective widths of the web thus are re-calculated according to the new position of the neutral axis. Iteration continues until it converges. The final values obtained after iterations are $h_{e1} = 30.76$ mm, $h_{e2} = 46.14$ mm and $h_2 = 138.6$ mm (see Fig. A5-1).
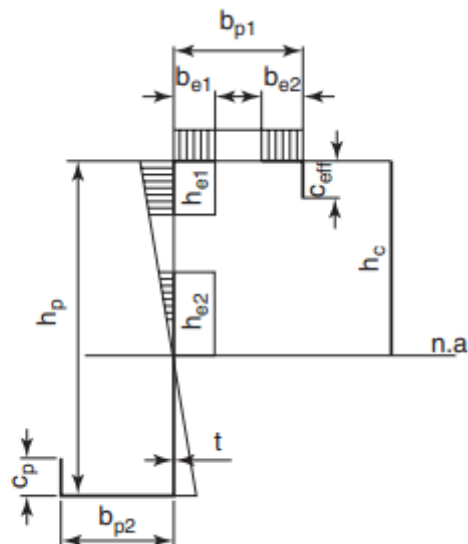

Figure A5-1: Symbols used for representing the dimensions of the effective cross-section

(Martin and Purkiss, 2008)

Position of the neutral axis with regard to the flange in compression:

$$z_c = \frac{t\left[c_p\left(\dfrac{h_p - c_p}{2}\right)+b_{p2}h_p+h_2\left(\dfrac{h_p-h_2}{2}\right)+\dfrac{h_1^2}{2}+\dfrac{c_{eff}^2\,\chi_d}{2}\right]}{A_{eff}} = 111.42 \text{ mm}$$

Position of the neutral axis with regard to the flange in tension:

$z_t = h_p - z_c = 86.88$ mm

Second moment of the effective sectional area:

$$I_{eff,y} = \frac{t\left(h_1^3+h_2^3+c_p^3+\chi_d c_{eff}^3\right)}{12}+\frac{t\left(b_{p2}+b_{e1}+b_{e2}\chi_d^3\right)}{12}+c_{pt}\left(z_t-\frac{c_p}{2}\right)^2+b_{p2}tz_t^2+h_2t\left(z_t-\frac{h_2}{2}\right)^2+$$

$$h_1t\left(z_c-\frac{h_1}{2}\right)^2+b_{e1}tz_c^2+b_{e2}\left(\chi_d t\right)z_c^2+c_{eff}\left(\chi_d t\right)\left(z_c-\frac{c_{eff}}{2}\right)^2 = 3147658 \ mm^4$$

Effective section modulus with regard to the flange in compression:

$W_{eff,y,c} = I_{eff,y}/z_c = 3147658/111.42 = 28250$ mm^3

Effective section modulus with regard to the flange in tension:

$W_{eff,y,t} = I_{eff,y}/z_t = 3147658/86.88 = 36230$ mm^3

The design value of the resistance of the section to bending moment about the y-axis due to local and distortional buckling is:

$M_{Ed} = f_{yb}W_{eff,y,c}/\gamma_{M0} = 450 \times 28250/1.0/1000000 = 12.7$kNm

For a beam under combined bending and local bearing, the moment resistance should

226

satisfy the following:

$$\frac{M_{Ed}}{M_{c,Rd}} + \frac{F_{Ed}}{R_{w,Rd}} \leq 1.25 \text{; thus } M_{c,Rd} = 12.7/1.25 = 10.16 \ kNm$$